Experimental and Modeling Analysis of the Dynamic Response of Bio-Based Sandwich Structures

by

Claudia Sergi

A dissertation submitted by in partial fulfillment of the requirements for the degree of Doctor of Philosophy in

Electrical, Material and Nanotechnology Engineering
Sapienza Università di Roma

&

Mechanical Engineering and Industrial Organization
Universidad Carlos III de Madrid

Advisor(s):

Jacopo Tirillò

Enrique Barbero Pozuelo

Sonia Sanchez Saez

December 2020

"The choice of a young man depends on his inclination, but also on the luck of meeting a great mentor".

I want to take advantage of the wise words pronounced by the Nobel Prize Rita Levi-Montalcini, woman and compatriot, to dedicate this research work to my mentors. Not only I had the luck of meeting a great mentor, I had the honor of meeting two. The Greek philosopher Socrate said that a good professor explains and demonstrates, but only a mentor inspires and the Libanese artist Khalil Gibran said that a mentor guides you to the threshold of your mind. I want to dedicate this work to the people who followed me in my PhD course not from above as chiefs, but by my side as leaders, pushing me always a step forward to overcome my limits and helping me to improve as a researcher and as a person.

ACKNOWLEDGEMENTS

PUBLISHED AND SUBMITTED CONTENT

➤ *"Quasi-static and low-velocity impact behavior of intraply hybrid flax/basalt composites"* Fabrizio Sarasini, Jacopo Tirillò, Luca Ferrante, Claudia Sergi, Pietro Russo, Giorgio Simeoli, Francesca Cimino, Maria Rosaria Ricciardi, Vincenza Antonucci, Fibers 2019, 7, 26, doi:10.3390/fib7030026
Author Contributions: Conceptualization, F.S., J.T., C.S. and P.R.; methodology, F.S. and L.F.; formal analysis, F.S., J.T. and C.S.; investigation, L.F., G.S., F.C., M.R.R. and V.A.; writing—original draft preparation, F.S.; writing—review and editing, F.S., P.R., M.R.R., V.A. and J.T.; supervision, F.S. and J.T.

The material from this source included in this thesis is not singled out with typographic means and references and is included in Chapters 2 and 4.

➤ *"Cork core sandwich structures: static and dynamic response"* Claudia Sergi, Jacopo Tirillò, Fabrizio Sarasini, Pietro Russo, Enrique Barbero Pozuelo, Sonia Sanchez-Saez, Proceeding of the 2019 International Conference on Composite Materials (ICCM22), Melbourne, Australia, August 11-16, 2019
The material from this source included in this thesis is not singled out with typographic means and references and is included in Chapters 2, 3, 4 and 5.

➤ *"The Potential of Agglomerated Cork for Sandwich Structures: A Systematic Investigation of Physical, Thermal, and Mechanical Properties"* Claudia Sergi, Jacopo Tirillò, Fabrizio Sarasini, Enrique Barbero Pozuelo, Sonia Sanchez-Saez and Christoph Burgstaller, Polymers 2019, 11, 2118, doi:10.3390/polym11122118
Author Contributions: Conceptualization, F.S., J.T., E.B.P., and S.S.S.; validation, E.B.P., C.S., and S.S.S.; formal analysis, F.S., C.S., and J.T.; investigation, C.S. and C.B.; writing—original draft preparation, F.S. and C.S.; writing—review and editing, E.B.P., J.T., C.B., and S.S.S.; visualization, F.S. and C.S.; supervision, E.B.P. and J.T.

The material from this source included in this thesis is not singled out with typographic means and references and is included in Chapters 2 and 3.

➤ *"Temperature, strain rate and anisotropy effects on compressive response of natural and synthetic cellular core materials"* Claudia Sergi, Fabrizio Sarasini, Jacopo Tirillò, Enrique Barbero, Sonia Sanchez-Saez, Marco Sasso, Edoardo Mancini, Composite Structures 2021, 260, 113268, doi:10.1016/j.compstruct.2020.113268
Author Contributions: Claudia Sergi: Data curation, Formal analysis, Investigation, Methodology, Visualization, Writing - original draft. Fabrizio Sarasini: Methodology, Validation, Writing - review & editing. Jacopo Tirillò: Conceptualization, Formal analysis, Supervision, Validation, Writing - review & editing. Enrique Barbero: Conceptualization, Methodology, Supervision, Writing - review & editing. Sonia Sanchez-Saez: Conceptualization, Methodology, Supervision, Writing - review & editing. Marco Sasso: Investigation, Methodology, Validation, Writing - review & editing. Edoardo Mancini: Investigation, Methodology, Validation, Writing - review & editing

The material from this source included in this thesis is not singled out with typographic means and references and is included in Chapters 2 and 3.

➢ *"Assessment of agglomerated cork and PVC foams cores crashworthiness under multiple-impact events in different loading conditions"* Claudia Sergi, Fabrizio Sarasini, Enrique Barbero, Sonia Sanchez-Saez, Jacopo Tirillò, Polymer Tesing 2021, 96, 107061, doi:10.1016/j.polymertesting.2021.107061

Claudia Sergi: Data curation, Formal analysis, Investigation, Methodology, Visualization, Writing – Original draft. Fabrizio Sarasini: Methodology, Validation, Writing – Review & Editing. Enrique Barbero: Investigation, Conceptualization, Methodology, Supervision, Writing – Review & Editing. Sonia Sanchez-Saez: Conceptualization, Methodology, Supervision, Writing – Review & Editing. Jacopo Tirillò: Conceptualization, Formal analysis, Supervision, Validation, Writing – Review & Editing.

The material from this source included in this thesis is not singled out with typographic means and references and is included in Chapters 2 and 3.

Paper under consideration for publication in peer reviewed journals:

➢ *"The effects of water absorption and salt fog exposure on agglomerated cork compressive response"* Claudia Sergi, Fabrizio Sarasini, Vincenzo Fiore, Enrique Barbero, Sonia Sanchez-Saez, Jacopo Tirillò

The material from this source included in this thesis is not singled out with typographic means and references and is included in Chapters 2 and 3.

➢ *"Experimental and Finite Element Analysis of the impact response of agglomerated cork and its intraply hybrid flax/basalt sandwich structures"* Claudia Sergi, Simonetta Boria, Fabrizio Sarasini, Pietro Russo, Libera Vitiello, Enrique Barbero, Sonia Sanchez-Saez, Jacopo Tirillò

The material from this source included in this thesis is not singled out with typographic means and references and is included in Chapters 2, 3 and 5.

➢ *"Effect of temperature on the low-velocity impact response of environmentally friendly cork sandwich structures"* Claudia Sergi, Fabrizio Sarasini, Pietro Russo, Libera Vitiello, Enrique Barbero, Sonia Sanchez-Saez, Jacopo Tirillò

The material from this source included in this thesis is not singled out with typographic means and references and is included in Chapters 2, 3, 4 and 5.

➢ *"Experimental and numerical analysis of the ballistic response of agglomerated cork and its bio-based sandwich structures"* Claudia Sergi, Fabrizio Sarasini, Pietro Russo, Libera Vitiello, Enrique Barbero, Sonia Sanchez-Saez, Jacopo Tirillò

The material from this source included in this thesis is not singled out with typographic means and references and is included in Chapters 2, 3, 4 and 5.

OTHER RESEARCH MERITS

➤ *"Effect of basalt fibre hybridisation and sizing removal on mechanical and thermal properties of hemp fibre reinforced HDPE composites"* Fabrizio Sarasini, Jacopo Tirillò, Claudia Sergi, Maria Carolina Seghini, Luca Cozzarini, Nina Graupner, Composite Structures 2018, 188, 394-406, doi: 10.1016/j.compstruct.2018.01.046

➤ *"Durability of Basalt/Hemp Hybrid Thermoplastic Composites"* Claudia Sergi, Jacopo Tirillò, Maria Carolina Seghini, Fabrizio Sarasini, Vincenzo Fiore, Tommaso Scalici, Polymers 2019, 11, 603, doi:10.3390/polym11040603

➤ *"Effect of temperature and fiber type on impact behavior of thermoplastic fiber metal laminates"* Fabrizio Sarasini, Jacopo Tirillò, Luca Ferrante, Claudia Sergi, Francesca Sbardella, Pietro Russo, Giorgio Simeoli, David Mellier, Andrea Calzolari, Composite Structures 2019, 223, 110961, doi: 10.1016/j.compstruct.2019.110961

➤ *"Hybrid Cellulose–Basalt Polypropylene Composites with Enhanced Compatibility: The Role of coupling Agent"* Claudia Sergi, Francesca Sbardella, Matteo Lilli, Jacopo Tirillò, Andrea Calzolari, Fabrizio Sarasini, Molecules 2020, 25, 4384, doi:10.3390/molecules25194384

➤ *"Enhanced Infrared Sparse Pattern Extraction and Usage for Impact Evaluation of Basalt-Carbon Hybrid Composites by Pulsed Thermography"* Jue Hu, Hai Zhang, Stefano Sfarra, Claudia Sergi, Stefano Perilli, Clemente Ibarra-Castanedo, GuiYun Tian, Xavier Maldague, Sesnors 2020, 20, 7159, doi:10.3390/s20247159

➤ Book Chapter *"Recent Toughening strategies in carbon fiber reinforced composites"* Fabrizio Sarasini, Claudia Sergi, Francesca Sbardella, Jacopo Tirillò in *"Fiber reinforced Composites. Constituents, Compatibility, Perspectives and Applications"* K. Joseph, K. Oksman, G. George, R. Wilson & S. Appukuttan (pp. 405-438), Woodhead Publishing, 2021

➤ Book Chapter *"Visco-Elasto-Plastic characterization of PVC Foams"* Marco Sasso, Fabrizio Sarasini, Edoardo Mancini, Attilio Lattanzi, Jacopo Tirillò, Claudia Sergi, Emanuele Farotti, in *"Challenges in Mechanics of Time Dependent Materials, Volume 2"* Meredith Silberstein & Prof. Alireza Amirkhizi (Chapter 13), Springer International Publishing, 2021

LIST OF ABBREVIATIONS

Au	Gold
C	Carbon
CAI	Compression After Impact
Cl	Chloride
DIC	Damage Image Correlation
DMA	Dynamic Mechanical Analysis
DSC	Differential Scanning Calorimetry
DTG	Differential Thermogravimetry
EDS	Energy Dispersive Spectroscopy
EPP	Expanded Polypropylene
EPS	Expanded Polystyrene
FE-SEM	Field Emission - Scanning Electron Microscopy
FEA	Finite Element Analysis
HCl	Hydrochloric Acid
HDPE	High Density Polyethylene
IPPC	Integrated Pollution Prevention and Control
LDPE	Low Density Polyethylene
LOESS	Locally Estimated Scatterplot Smoothing
MA-g-PP	Maleic Anhydride grafted Polypropylene
MFI	Melt Flow Index
Na	Sodium
NaCl	Sodium Chloride
NFCs	Natural Fiber Composites
PC	Polycarbonate
PE	Polyethylene
PECVD	Plasma Enhanced Chemical Vapor Deposition
PET	Polyethylene terephthalate
PHA	Polyhydroxyalkanoate
PLA	Poly (lactic acid)
PMI	Polymethacrylimide
PMMA	Poly (methyl methacrylate)
PP	Polypropylene
PPC	Compatibilized polypropylene
PS	Polystyrene
PTFE	Polytetrafluoroethylene
PUR	Polyurethane
PVC	Polyvinyl chloride
SAN	Styrene-acrylonitrile
SHPB	Split Hopkinson Pressure Bar
Si	Silicon
TGA	Thermogravimetric Analysis
UV	Ultraviolet

TABLE OF CONTENTS

INDEX OF FIGURES

INDEX OF TABLES

Introducción

La Gran Isla de Basura del Pacifico, el cambio climático y el efecto invernadero son solamente algunas de las consecuencias negativas debidas a la explotación masiva y desconsiderada del petróleo para la producción de materiales sintéticos, como los plásticos. En muchos sectores industriales se emplean ampliamente materiales compuestos que utilizan polímeros sintéticos para la fabricación de matrices y fibras sintéticas, i.e. vidrio, carbono y polímeros, para la fabricación de refuerzos. La polución del aire, del agua y del suelo generadas por la dificultad asociada a la eliminación de estos materiales no biodegradables y la contaminación producida durante su fabricación ha llevado a muchos países a promulgar normativas más restrictivas en el tema de eliminación de la basura y de emisiones gases de efecto invernadero.

Existe una tendencia creciente hacia un modelo industrial eco-sostenible, destinada a frenar los efectos dañinos en el medio ambiente. Una de las opciones para alcanzar este modelo es la utilización de materiales de origen natural y de fuentes renovables. Esto tipo de materiales no solo reducen el impacto ambiental del proceso de producción las emisiones de CO_2, sino que también facilita la eliminación de los componentes al final de su vida útil gracias a una parcial o total biodegradabilidad. La presente Tesis Doctoral se integra en este contexto de respeto al medio ambiente proponiendo una estructura sándwich compuesta por un núcleo de corcho aglomerado y pieles fabricadas con un laminado de tejido hibrido de fibras de basalto y lino en una matriz de polipropileno.

La sustitución de las tradicionales espumas sintéticas, empleadas como núcleos de las estructuras sándwich, por corcho aglomerado permitiría utilizar un material biodegradable y de fuentes renovables. Este material se fabrica a partir de los desechos derivados de la producción de los tapones de corcho permitiendo así un máximo aprovechamiento de los recursos naturales cultivados. Se debe considerar que, además, el corcho aglomerado se caracteriza por poseer algunas propiedades extremadamente ventajosas como un buen aislamiento térmico y acústico, útil en el mundo de las construcciones para mejorar la eficiencia energética de los edificios. Además, este material presenta una impresionante recuperación dimensional, fundamental para asegurar una mayor estabilidad dimensional de la estructura sándwich.

Teniendo en cuenta que la optimización del peso y de las propiedades mecánicas es un aspecto fundamental en el diseño de un material sándwich para conseguir una estructura lo más eficiente posible, en este trabajo se ha analizado la influencia de la densidad del corcho aglomerado en las propiedades físicas, térmicas y mecánicas del núcleo y de la estructura sándwich completa estudiando tres corchos aglomerados con tres diferentes densidades. Adicionalmente, el mismo estudio realizado para el corcho fue realizado también para tres espumas de policloruro de vinilo (PVC) ampliamente usadas y de propiedades conocidas que sirven de referencia para resaltar las fortalezas y los puntos débiles del núcleo natural y para demostrar su idoneidad como núcleo en estructuras sándwich.

Para las pieles se ha elegido como refuerzo un tejido hibrido de fibras de basalto y lino para mantener lo máximo posible la naturaleza eco-sostenible de la estructura sándwich, evitando el empleo de fibras de vidrio, ampliamente usadas, y utilizando materiales de origen mineral y vegetal y de fuentes renovables. El empleo de la técnica de hibridación permite superar las desventajas relacionadas con el uso de un único tipo de fibra y mejorar la calidad de los laminados explotando el efecto sinérgico relacionado con las fortalezas de ambas fibras. Las fibras de basalto aseguran la consecución de propiedades mecánicas satisfactorias mientras que la presencia de las

fibras de lino permite reducir el peso del compuesto confiriéndole también una parcial biodegradabilidad.

Aunque las estructuras sándwich sean ampliamente usadas en muchas aplicaciones industriales gracias a sus excelentes propiedades a flexión y a su bajo peso derivados de su peculiar estructura, su vulnerabilidad a los fenómenos de impacto es una de sus limitaciones en aplicaciones estructurales. Por esta razón, el estudio del comportamiento a impacto de las estructuras sándwich, en particular la resistencia y la tolerancia al daño, es fundamental para el conocimiento de los diferentes mecanismos de daño que pueden ocurrir y como estos puedan afectar las prestaciones mecánicas y la capacidad resistente de las estructuras. Teniendo en cuenta esta carencia que afecta las estructuras sándwich, el segundo objetivo de esta tesis es disponer de un conocimiento adecuado del comportamiento a impacto de las estructuras sándwich propuestas, para asegurar su idoneidad en todas aquellas aplicaciones en que la resistencia a impacto tiene que estar incluida en los criterios principales del diseño.

Se ha estudiado el comportamiento a impacto de las estructuras sándwich seleccionadas en diferentes condiciones de impacto, en particular punzonamiento, impacto a baja velocidad con soporte CAI (*Compression After Impact*) e impacto balístico. Los ensayos de punzonamiento y los de impacto a baja velocidad con soporte CAI permitieron evaluar la influencia de las condiciones de contorno de la estructura y la modificación de los mecanismos de deformación y de disipación de la energía. La realización de ensayos de impacto de baja y alta velocidad permitió evaluar el efecto de la masa y la velocidad de impacto de las estructuras. Esta oportuno subrayar que dicho estudio no fue efectuado solamente sobre las estructuras sándwich completas sino también sobre los núcleos y las pieles de manera independiente, para comprender el comportamiento a impacto de las componentes individuales y evaluando la interacción entre ellos en la estructura sándwich completa.

Para completar el trabajo, se ha analizado la influencia de la densidad de los núcleos y la temperatura de servicio en la respuesta a impacto de la estructura y de sus diferentes componentes. Se ha realizado un análisis post impacto a través de técnicas no destructivas, como por ejemplo la perfilómetria, para cuantificar la extensión del daño.

En vista de la notable influencia ejercida de las cargas dinámicas sobre las estructuras sándwich y teniendo en cuenta las extraordinarias capacidades de recuperación dimensional del corcho y para profundizar en el conocimiento de su comportamiento a compresión, se han realizado ensayos de compresión dinámicas a diferentes velocidades de deformación sobre los núcleos, en torre de caída de peso y en barra Hopkinson, teniendo en cuenta el efecto de varios parámetros como la anisotropía, la temperatura y el número de impactos sucesivos. Este último parámetro es muy importante para conocer el efecto provocado por una acumulación del daño con el paso del tiempo y como resultado de la exposición a varios fenómenos de impacto de menor entidad respecto al efecto causado de un impacto individual de mayor entidad.

La elección del polipropileno como matriz polimérica en la fabricación de las pieles está estrechamente relacionada con los dos principales objetivos de la Tesis. Desde la perspectiva del impacto ambiental el polipropileno no es biodegradable, pero siendo un polímero termoplástico puede ser reprocesado y reciclado de manera sencilla al final de la vida útil del componente contrariamente a lo que ocurre con las matrices termoestables que se pueden eliminar solamente como residuos para explotar su valor calorífico. Desde la perspectiva de la resistencia a impacto y de la tolerancia al daño, el uso de una matriz termoplástica dúctil respecto a una termoestable, que es intrínsecamente frágil, permite explotar mecanismos adicionales de disipación de energía,

como por ejemplo la plasticidad de la matriz, que pueden prevenir un daño excesivo del componente o su rotura catastrófica.

Considerando la pésima adherencia en la interfaz entra las fibras naturales hidrófilas y la matriz hidrófoba y el efecto negativo que este fenómeno presenta en las propiedades mecánicas, se ha decidido estudiar el efecto de un agente de acoplamiento a base de anhídrido maleico sobre las propiedades mecánicas cuasi-estáticas y dinámicas de las pieles y de las estructuras sándwich. Se ha observado que, la mejora de la adhesión entre fibra y matriz resulta positivo para las propiedades cuasi-estáticas, produciendo un incremento en la rigidez y en la resistencia máxima. Sin embargo, la presencia del agente de acoplamiento empeora la respuesta frente a cargas de impacto estructura induciendo una fragilización del compuesto a causa de la inhibición de algunos mecanismos de disipación de la energía. En vista de esto se considera que, el uso del agente de acoplamiento tiene que ser evaluado de manera específica en función de la aplicación de la estructura sándwich.

Por último, se ha realizado a una modelización numérica empleando un código comercial de elementos finitos tanto del núcleo corcho como del núcleo de espuma de PVC. El objetivo con este modelo es demostrar que es posible utilizar modelos simples que permitan predecir la respuesta de las estructuras y aumentar así su utilización a escala industrial donde se prefiere el empleo de materiales conocidos para reducir potenciales contraindicaciones y donde la posibilidad de predecir el comportamiento de un material a través de una simulación numérica permite reducir considerablemente los costes de producción.

Introduzione

Il *Great Pacific Garbage Patch*, i cambiamenti climatici, l'effetto serra sono solo alcuni dei risvolti negativi dovuti allo sconsiderato sfruttamento del petrolio e dei prodotti chimici nella produzione di materiali sintetici, come le plastiche e le fibre di rinforzo dei materiali compositi, largamente impiegati nei più svariati settori industriali e nella produzione di massa. La contaminazione dell'aria, dell'acqua e del suolo risultante dalle ingenti emissioni di agenti inquinanti e dalle difficoltà connesse con lo smaltimento di questi materiali non biodegradabili, ha spinto molti paesi ad emanare normative sempre più restrittive in materia di smaltimento dei rifiuti ed emissioni. Questo orientamento *green*, volto a contrastare gli effetti dannosi sull'ambiente causati dalla produzione industriale, incoraggia lo sfruttamento di materiali provenienti da fonti rinnovabili al fine di ridurre le emissioni di CO_2 e, quindi, l'impatto ambientale del processo produttivo e di facilitare lo smaltimento del componente a fine ciclo vita grazie ad una parziale o totale biodegradabilità. Il seguente lavoro si inserisce in questo contesto ecosolidale proponendo una struttura sandwich *green* prodotta con *core* in sughero agglomerato e pelli in polipropilene rinforzato con tessuto ibrido basalto-lino.

La sostituzione delle tradizionali schiume sintetiche, impiegate come *core,* con il sughero agglomerato consentirebbe lo sfruttamento di un materiale biodegradabile e da fonte rinnovabile approfittando degli scarti provenienti dalla produzione dei tappi di sughero che altrimenti andrebbero persi consentendo, tra l'altro, il pieno utilizzo del materiale coltivato. È inoltre necessario considerare che il sughero agglomerato presenta alcune caratteristiche estremamente vantaggiose come un buon isolamento termico ed acustico, utili nel mondo dell'edilizia per migliorare l'efficienza energetica degli edifici, e un eccezionale recupero dimensionale fondamentale per assicurare una maggior stabilità dimensionale alla struttura sandwich con esso prodotta. Considerando che l'ottimizzazione del peso e delle proprietà meccaniche è un aspetto chiave nella progettazione dei compositi sandwich per ottenere la struttura più performante possibile, si è affrontata l'influenza esercitata dalla densità del sughero agglomerato sulle proprietà fisiche, termiche e meccaniche del solo *core* e della struttura complessiva attraverso lo studio di tre sugheri agglomerati caratterizzati per l'appunto da una diversa densità. In aggiunta, la stessa campagna sperimentale effettuata sul sughero è stata realizzata anche su tre schiume in polivinilcloruro (PVC) con caratteristiche note e consolidate in modo tale che fungessero da riferimento e consentissero di evidenziare i punti di forza e di debolezza del materiale naturale nonché di legittimarne l'idoneità come materiale *core*. Anche la selezione del tessuto ibrido basalto-lino come rinforzo per le pelli è da attribuire alla volontà di mantenere il più possibile la natura ecosolidale del composito sandwich evitando di ricorrere alle fibre di vetro, già massicciamente impiegate, e sfruttando materiale di origine minerale e vegetale e quindi da fonte rinnovabile. Peraltro, l'impiego della tecnica dell'ibridizzazione consente di superare gli svantaggi connessi con l'uso del singolo tipo di fibra e di migliorare la qualità del laminato sfruttando l'effetto sinergico connesso ai punti di forza di ambedue. Nel caso specifico le fibre di basalto assicurano il raggiungimento di proprietà meccaniche soddisfacenti mentre la presenza del lino consente di ridurre il peso del composito conferendogli anche una parziale biodegradabilità.

Nonostante i compositi sandwich risultino insostituibili in molte applicazioni industriali grazie alle incomparabili proprietà flessionali e il basso peso attribuibili alla loro peculiare struttura, la loro vulnerabilità ad eventi di impatto ne impedisce una diffusione su larga scala. La compromissione dell'integrità e della stabilità strutturale dovuta all'impatto e la conseguente

riduzione delle proprietà meccaniche residue tende a rendere queste strutture meno affidabili. Per tale ragione, lo studio del comportamento ad impatto dei compositi sandwich, e in particolare la loro resistenza e tolleranza al danno, risulta fondamentale per comprendere gli innumerevoli meccanismi di danneggiamento che possono intervenire e come gli stessi influenzino le prestazioni meccaniche e le capacità portante della struttura. In considerazione di questa carenza che affligge le strutture composite sandwich, il secondo scopo di questo lavoro è fornire un'accurata caratterizzazione del comportamento ad impatto dei nuovi biocompositi proposti per assicurarne l'idoneità in tutte quelle applicazioni industriali in cui la resistenza all'impatto deve essere inclusa tra i criteri principali di progetto.

Varie condizioni di impatto sono stata considerate, in particolare impatto *puncture*, impatto con supporto CAI (*Compression After Impact*) e impatto balistico, al fine di presentare una caratterizzazione più accurata possibile del comportamento ad impatto delle strutture composite in studio. L'esecuzione dei test di tipo *puncture* e di tipo CAI ha consentito di valutare l'influenza esercitata dalle condizioni a contorno del supporto e la conseguente alterazione dei meccanismi di deformazione e di dissipazione dell'energia da esso derivanti mentre i test di impatto balistico hanno consentito di valutare l'effetto della massa e della velocità di impatto passando dagli impatti a bassa velocità effettuati con masse pesanti a impatti più localizzati effettuati con elevate velocità e piccole masse. È opportuno evidenziare che la suddetta campagna sperimentale non è stata effettuata solamente sulle strutture sandwich complete, ma anche sui soli *core* e sulle sole pelli al fine di comprendere al meglio lo scenario di danneggiamento separando il comportamento ad impatto delle singole componenti e valutando solo in un secondo momento come esso evolve in conseguenza dell'assemblaggio del composito. Per completare soddisfacentemente il lavoro parametri quali la densità dei *core* e la temperatura di esercizio sono stati presi in considerazione, con lo scopo di valutare come questi modificassero la reazione all'impatto della struttura e delle sue componenti, ed è stata effettuata un'analisi post-impatto attraverso tecniche non distruttive, come ad esempio la profilometria, al fine di ottenere informazioni utili a supportare l'analisi dinamica della struttura e a quantificare l'estensione del danno. Alla luce della notevole influenza esercitata dai carichi dinamici sulle strutture sandwich e in considerazione delle straordinarie capacità di recupero dimensionale del sughero, ulteriori test dinamici, come compressioni dinamiche in torre a caduta di peso e test in barra Hopkinson, sono stati effettuati sui soli *core* al fine di approfondire lo studio relativo al loro comportamento a compressione prendendo in considerazione l'effetto di vari fattori come la velocità di deformazione, l'anisotropia, la temperatura e il numero di impatti. Quest'ultimo è di particolare importanza per conoscere l'effetto provocato dall'accumulazione del danno con il passare del tempo a seguito dell'esposizione del componente a vari eventi di impatto di minor entità rispetto all'effetto dannoso causato da un singolo impatto di maggior entità.

La scelta di impiegare il polipropilene come matrice polimerica per la produzione delle pelli è strettamente correlata con i due obiettivi della tesi. Dal punto di vista dell'impatto ambientale il polipropilene non è biodegradabile, ma essendo un polimero termoplastico può essere facilmente riprocessato e riciclato a fine ciclo vita al contrario delle matrici termoindurenti che possono essere solamente smaltite e termo-valorizzate per sfruttare il loro potere calorifico. Dal punto di vista della resistenza e della tolleranza al danno, l'uso di una matrice termoplastica duttile rispetto ad una termoindurente, che a causa della sua struttura a network 3D è intrinsecamente fragile, permette di sfruttare meccanismi addizionali di dissipazione dell'energia, come ad esempio la plasticizzazione della matrice, che possono prevenire un danneggiamento eccessivo del componente o una sua rottura catastrofica. Tenendo poi in considerazione le ingenti problematiche connesse con la pessima interfaccia che si viene a creare tra le fibre naturali idrofile

e la matrice polimerica idrofoba e le scarse proprietà meccaniche risultanti, si è deciso di studiare l'effetto di un agente accoppiante a base di anidride maleica, inserito nel master batch della matrice, sulle proprietà quasi statiche e dinamiche delle sole pelli e delle strutture sandwich complessive. Si è visto che se il miglioramento dell'adesione tra fibra e matrice risulta positivo per le proprietà quasi statiche determinando un aumento della rigidezza e della resistenza massima esso gioca un ruolo negativo nella risposta dinamica ad impatto della struttura inducendo un infragilimento del composito a causa dell'inibizione di alcuni meccanismi di dissipazione dell'energia. Alla luce di ciò, anche l'uso dell'agente accoppiante deve essere accuratamente valutato a seconda dell'applicazione del composito se si desidera ottenerne un'ottimizzazione delle prestazioni.

Infine, si è provveduto ad effettuare una modellizzazione agli elementi finiti sia del sughero che delle schiume in PVC con l'intento di standardizzare la modellizzazione di un materiale innovativo e relativamente nuovo come il sughero nella speranza di incoraggiare il suo utilizzo su scala industriale dove l'impiego di materiali consolidati è normalmente preferito per ridurre potenziali controindicazioni e dove la possibilità di predire il comportamento di un materiale attraverso una semplice simulazione numerica consente di ridurre notevolmente i costi di produzione.

Introduction

The Great Pacific Garbage Patch, the climate change, the greenhouse effect are only some of the implications of a thoughtless exploitation of crude oil and chemicals for the production of synthetic materials such as plastics and fibrous reinforcements which are extensively used in many industrial fields and in mass production. The resulting contamination of air, water and soil due to the huge emission of pollutants and to the complex disposal of these non-biodegradable materials, pushed many countries to promulgate more restrictive regulations in the field of waste disposal and emissions. This green tendency, intended to counteract the detrimental effect of industrial production on the environment, encourages the exploitation of bio-based materials from renewable resources with the aims of reducing the carbon footprint of the production process and facilitating the disposal of the component at the end of its life-cycle thanks to a partial or total biodegradability. The present work is part of this eco-friendly framework proposing a green sandwich structure made up with an agglomerated cork core and with polypropylene skins reinforced with a flax/basalt hybrid fabric.

The replacement of traditional synthetic foam cores with agglomerated cork would allow to exploit a biodegradable material from renewable resources taking advantage of the wastes derived from wine stopper production, which otherwise would be lost, thus ensuring a full exploitation of the harvested material. Moreover, agglomerated cork is characterized by favorable features like a good acoustic and thermal insulation capability useful to improve energy efficiency in buildings and construction and an outstanding dimensional recovery capacity beneficial to ensure an improved dimensional stability to the overall sandwich structure. Considering that the optimization of weight and mechanical properties is one of the key parameters in sandwich composites design in order to obtain the most performing structure, the influence of agglomerated cork density on the physical, thermal and mechanical properties of the sole core and of the overall sandwich structure was addressed investigating three agglomerated corks with different densities. Moreover, to point out the advantages and the drawbacks connected with agglomerated cork and to legitimate its feasibility as core material, three well established PVC foams with the same densities were subjected to the same experimental campaign carried out on cork in order to provide a good benchmark. The selection of a flax/basalt hybrid fabric as skin reinforcement is intended to preserve the eco-friendliness of the sandwich structure avoiding the massively employed glass fibers and exploiting materials from vegetable and mineral renewable resources. Moreover, the hybridization enables a synergistic exploitation of both fiber types. In particular, basalt fibers add satisfying mechanical performances while flax fibers provide a reduction of laminate weight and its partial biodegradability.

If sandwich structures are irreplaceable in many industrial applications thanks to the unique flexural properties together with a low weight that derive from the peculiar design, their high susceptibility to impact events prevents their massive widespread. The degradation of the structural integrity and stability resulting from these occurrences and the corresponding reduction of the residual mechanical properties can make them unreliable. For this reason, the investigation of the impact response of sandwich composites, i.e. damage resistance and damage tolerance, is essential to be aware of the several failure mechanisms that can intervene and how they affect the mechanical performances and the load bearing capabilities of the structure. Considering this flaw that vexes these structures, the second aim of this work is to provide an extensive characterization of the impact response of these novel bio-based composites in order to grant their feasibility in all those industrial fields where impact resistance needs to be included in the design criteria.

In order to present a thorough characterization of the impact response of the structures under study, different impact conditions were considered, i.e. puncture impact tests, impact tests with compression after impact (CAI) support and ballistic impact tests. The execution of puncture and CAI impact tests allows to evaluate the influence of different boundary conditions and a potential alteration of the deformation and energy dissipation mechanisms whereas the execution of ballistic impact tests permits to assess the effect of impact mass and velocity moving from low velocity impacts performed with a heavy mass to more localized high velocity impacts performed with a little mass. Moreover, this experimental campaign was carried out not only on the overall structures but also on the sole cores and skins in order to achieve a more accurate understanding of the damage scenario splitting up the impact behavior of the single components and evaluating only at a later time how it evolves as a consequence of composite ensemble. Various parameters such as core density and operating temperature were considered in order to evaluate how structure's response to impact modifies and a post-impact analysis through non-destructive technique such as profilometry was carried out to support the dynamic analysis of structures and to quantify damage extent. In light of the high importance played by dynamic loading on sandwich structures and of the peerless dimensional recovery of agglomerated cork, further impact investigations, i.e. drop weight tower dynamic compression tests and split Hopkinson pressure bar (SHPB) tests, were carried out on the sole core materials to examine the effect of strain rate, anisotropy, temperature and number of impacts. This latter parameter is of main importance to evaluate the effect of an accumulation of damage over time induced by minor impact events rather than the detrimental effect caused by a single impact.

The choice to use polypropylene as polymer matrix in skin manufacture is strictly correlated with the two main goals of the work. From the environmental point of view, polypropylene is not biodegradable, but being a thermoplastic polymer can be easily reprocessed and recycled at the end of its life cycle contrary to thermosetting matrices that can only be disposed and used to waste-to-energy to exploit their heating value. From the damage resistance and damage tolerance point of view, the use of a ductile thermoplastic matrix rather than a thermosetting one, which is intrinsically brittle due to its 3D network structure, allows to introduce additional energy dissipation mechanisms like matrix plasticization that can prevent an excessive damage and the catastrophic failure of the overall structure. Considering the relevant fiber/matrix interface issues between the hydrophilic natural fibers and the hydrophobic polymer matrices and hence the poor resulting mechanical properties, the effect of a maleic anhydride coupling agent, added to the matrix master batch, on the quasi-static and dynamic properties of the sole skins and of the overall sandwich structures was investigated. If the improved fiber/matrix adhesion plays a positive role on the quasi-static properties of both laminates and sandwich panels determining an increase in stiffness and maximum strength, it induces an embrittlement in dynamic impact conditions as some energy dissipation mechanisms are prevented. For this reason, the use or not of coupling agent is another aspect to evaluate carefully depending on composite application to optimize the performances.

Finally, a finite element modelling was performed on both agglomerated cork and PVC foam in order to standardize the modelling of an innovative and relatively new material as cork, encouraging its spread at an industrial level where the use of well-established materials is normally preferred to reduce the possibility of setbacks and where the possibility to predict the response of a material through numerical simulation allows to reduce the manufacturing costs.

Chapter 1: State of the Art

1.1 Sandwich Composite Structures

1.1.1 Basic principles

In 1907 the American chemist Leo Hendrik Baekeland produced the first synthetic resin, Bakelite, thus leading to the beginning of polymers era. The introduction of these innovative materials in the manufacturing market allowed the development of new technology and in particular the arrival of polymer matrix composite. This new class of materials enabled to reach mechanical performances similar to metals ones but with a much lower weight of the overall structure. This feature is of main importance in most industrial applications, such as transportations and buildings, and that is the reason why polymeric composite reinforced with glass, carbon or aramid fibers are widespread in automotive, civil, naval, aeronautical and aerospace industries.

Sandwich structures are a particular type of composite materials characterized by a high flexural stiffness to weight ratio that makes them suitable for structural purposes in all the fields previously cited [1,2]. They are designed taking advantage of the fundamental principle used to produce I-beams that states that when a structure is submitted to bending the outer surfaces are the ones that undergo the highest loading and that the higher is the distance between them and the neutral plane the stiffer is the structure [2–4]. To employ this concept sandwich composites are produced using two stiff face sheets, called skins, that are fixed to a low-density material that represents the core as schematized in Figure 1. The main goal of the core material is to ensure the spacing of the skins and thus increasing the flexural performances of the structure without increasing significantly its weight. In general, the skins carry the in-plane and bending loads whereas the core carries the transverse shear loads to which the composite is submitted [1].
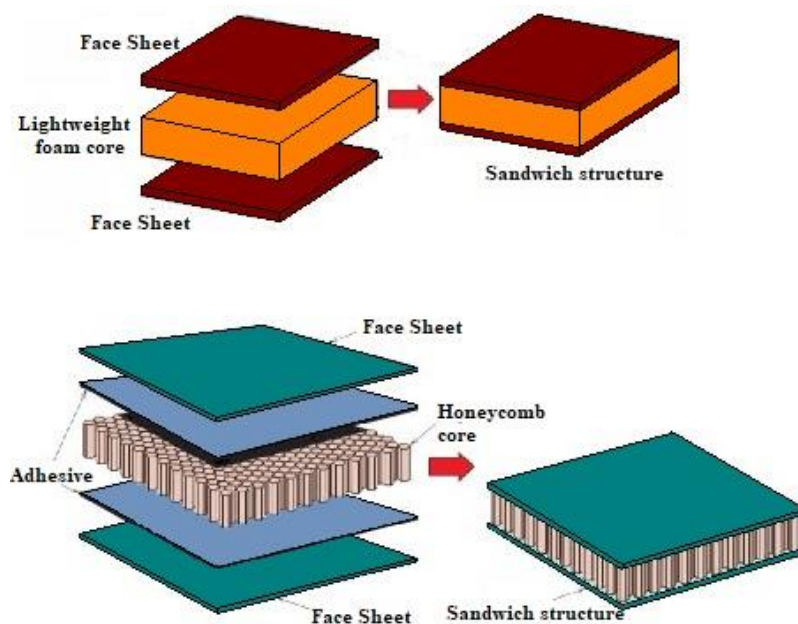
Figure 1: Sandwich composite structures schematization

In order to better understand the improvement in flexural performances given by the use of sandwich structures instead of monocoque ones, it is possible to compare the achievable results from a mathematical point of view [1]. The flexural stiffness of a monocoque construction of thickness $2t_f$ is:

$$D_{mon} = \frac{E_f (2t_f)^3}{12(1-v_f^2)} = \frac{2E_f t_f^3}{3(1-v_f^2)} \qquad (1.1)$$

where E_f is the modulus of elasticity and v_f the Poisson ratio. The flexural stiffness of a sandwich structure, constituted by a core material of thickness h_c and two skins of thickness t_f made up with the same material of the monocoque structure, is:

$$D_{sand} = \frac{2E_f t_f (\frac{h_c}{2})^2}{(1-v_f^2)} = \frac{E_f t_f h_c^2}{2(1-v_f^2)} \qquad (1.2)$$

where the contribute of the core to flexural stiffness was neglected and it was assumed $h_c \gg t_f$. Calculating the ratio of these two flexural stiffnesses the equation obtained is:

$$\frac{D_{sand}}{D_{mon}} = \frac{3}{4}\left(\frac{h_c}{t_f}\right)^2 \qquad (1.3)$$

This means that if the core has a thickness of 20 times higher than the ones of the skins, the sandwich flexural stiffness is 300 times higher than the one of the monocoque structure [1]. Similar conclusion can be drawn considering the maximum stress that is reached in the two structures when submitted to a bending moment, M. The maximum stress reached in the monocoque structure is:

$$\sigma_{mon} = \pm \frac{6M}{(2t_f)^2} = \pm \frac{3M}{2\,t_f^2} \qquad (1.4)$$

whereas the maximum stress reached in the sandwich structure is:

$$\sigma_{sand} = \pm \frac{M}{t_f h_c} \qquad (1.5)$$

Calculating the ratio of the bending stress reached in a face of the sandwich structure and the one reached in the monocoque structure the equation obtained is:

$$\frac{\sigma_{sand}}{\sigma_{mon}} = \frac{2t_f}{3h_c} \qquad (1.6)$$

This means that considering the previous instance where the core has a thickness of 20 times higher than the ones of the skins it is possible to conclude that the bending stress reached in the sandwich structure is 1/30 of the one reached in the monocoque structure that has approximately the same weight [1].

1.1.2 Core and skins material selection

A key point in the production of sandwich structures is the selection of the right core and skins materials in order to optimize the weight and the properties of the structure as a function of its application. Skins are always thin and must be characterized by high flexural stiffness, high tensile and compressive strength and good impact and wear resistance. Most of the times they consist of a single metallic layer or of a stiff and strong composite material but any structural material that can be shaped as a thin sheet can be used as a skin [2].

Core materials must be characterized by low density in order not to affect significantly the overall structure weight, by high shear stiffness and strength but also by a high out of plane stiffness in order to prevent core thickness decrease that would cause a high decrease of sandwich structure flexural performances [2]. The study and the design of core materials started in 1940 and is still proceeding in an effort to achieve a perfect balancing of weight and mechanical performances as a function of the application. Core can vary in both materials used and architecture but usually all the types can be grouped in four main classes: foam or solid core, honeycomb core, web core and corrugated or truss core as shown in Figure 2.
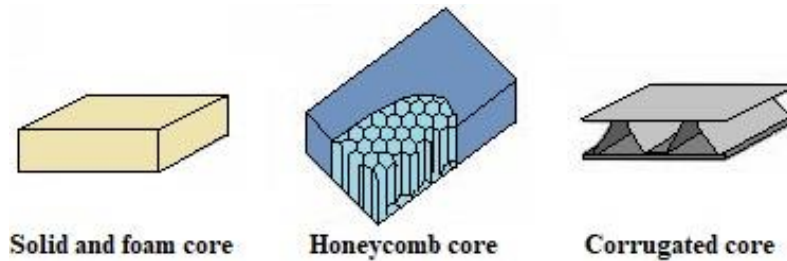
Figure 2: Schematization of different types of core materials [2]

In the class of solid and foam cores it is possible to find synthetic polymeric foams, such as PVC (polyvinyl chloride), PUR (polyurethane), PS (polystyrene), and metallic foams, such as Aluminum foams, in a wide range of densities, but also bio-inspired cores such as balsa wood. These types of core are largely used because they are relatively inexpensive and are able to lend thermal and acoustic insulating capabilities to the structures produced with them [1].

Honeycomb cores advent took place in the late 1940's and 1950's [2] and can be described as an array of vertical channels connected together by thin walls. The shape of the cells can vary as a function of the application but hexagon, square and circles are the most common geometry used. Honeycomb structures are able to ensure minimal density and high out of plan shear and compression properties [1]. Their main drawback is the high cost that make them suitable principally for aerospace applications [2].

Corrugated cores can be defined as prismatic structures that form open channels parallel to the facings. Over time these architectures have become more and more complex in order to tailor their properties as a function of their application. This aim was achieved for example through the introduction of hierarchical corrugated cores, of two way corrugated cores, of bi-directional corrugated-strip cores and so on [5].

1.1.3 Industrial applications

As previously mentioned, sandwich composite structures are widely used in many different industrial areas. They are massively used in transportation in order to reduce the weight of the

vehicles and consequently the emission of pollutants without compromising the structural integrity and the mechanical performances. Their employment in this industrial field also allows to take advantage of the thermal and acoustic insulating capacities that enable, for example, the transportation of cold goods with a lower waste of energy [2]. The optimization of heating and cooling processes is of main importance even in civil engineering where the shield to heat in summer and the block of heat losses in winter by the walls improves considerably buildings energy efficiency [2,6]. In naval industry sandwich structures are used in both ships and submarine applications. Even in this context the possibility to couple good mechanical properties with a low weight of the structure allows to beware of essential characteristics such as stability, payload, reduction of the fuel consumption and so on [2,7]. All of these features gain even more importance in the aeronautical and aerospace fields and that is why sandwich composites are widespread for both structural and semi-structural uses in these industrial sectors. Their employment allows to improve noise and vibrations damping and that is an added value in aircraft cabins design but also in wind turbine blades [8]. In the latter the high stiffness to weight ratio of sandwich structures is the guarantee to maximize the conversion of wind power in electrical energy in fact if the low weight is necessary to obtain a good efficiency the high stiffness allows to avoid phenomena such as buckling that could alter the air flow on the blade thus affecting negatively the conversion process [2,9]. At last sport industry has to be considered in fact many sport equipment such as snowboards, hockey hurleys, surfboards, helmets are produced taking advantage of sandwich structures design [10,11]. The evolution of materials throughout the years and the employment of lighter and high-performing furniture guaranteed a significant improvement of athletes performances.

1.1.4 Weaknesses and set of problems

Until now only the main advantages of sandwich structures were considered and discussed neglecting the weaknesses and the problems connected with the use of these types of composite.

The first concern is connected with the susceptibility to damage of these structures when subjected to impact loading. Impact events such as tool drops, runway debris, bird strikes, hailstones, etc. can occur in every-day life and can heavily affect sandwich structural integrity, stability and reliability inducing a reduction of the stiffness and of the load bearing capacities [12]. In sight of this, it appears evident the need to enhance the knowledge on sandwich composites impact behavior investigating both structure impact response and the residual properties after impact. The study of the impact response allows to address composite damage resistance and failure mechanisms whereas the study of residual properties allows to evaluate material damage tolerance. Damage resistance can be defined as the capacity of a structure to resist to damage when an impact event occurs whereas damage tolerance is the capability of a material to go on behaving satisfactorily from a mechanical point of view when damaged and without undergoing reparation [12].

The evaluation and identification of the failure mechanisms that can affect a sandwich composite during an impact are of main importance because the resulting damage scenario of these structures is much more complex than composite laminates one and many different failure modes can arise competing with one another. Composite laminates are characterized by three main damage mechanisms matrix cracking, fiber breakage and delamination. These mechanisms pertain also to sandwich structures and in particular to their face sheets, but core buckling, crushing, cracking and failure in shear must be also considered just as considerable indentation and core-face sheet

debonding [12,13]. Moreover core-skins bond induces stress concentrations causing a more local damage and a premature failure of the face sheet [13,14]. In light of this convoluted framework, the prediction of the residual properties and the validation of the feasibility of a sandwich structure for a certain industrial application require a detailed investigation.

The second problem connected with the use of sandwich structures is the massive use of synthetic materials that most of the times are not biodegradable, originate from crude oil and their production causes huge emissions with the consequent contamination of air, water and soil. The increasing problems related to environmental pollution, such as global warming, and to waste disposal, such as the formation of the Great Pacific Garbage Patch, pushed many countries to promulgate more restrictive regulations in order to face the environmental decay challenge. In 1990 the United States approved some amendments to the Clean Air Act and Clean Water Act in order to improve environmental protection [15]. In 2008 even the European Parliament dealt with this issue promulgating the directive 2008/1/EC in the field of Integrated Pollution Prevention and Control (IPPC) that replaced the previous directive 96/61/EC. In this new directive it is possible to find many regulations that address industrial emissions (2010/75/EU), waste management (2008/98/EC), packaging and packaging waste (94/62/EC), landfills (1999/31/EC), end of life vehicles (2000/53/EC) and so on. The common guideline tends to deter the use of landfills, to encourage activities such as reuse, recovery and recycling and to promote the use of biodegradable and composting materials. To reach this last aim a possible path is the exploitation of bio-based materials from renewable resources that most of the times are biodegradable and allows to reduce the carbon footprint and the use of chemicals in the production phase. Researchers accepted this new challenge trying to apply this eco-friendly trend to composite materials and to sandwich structures in order to make them more eco compatible.

1.2 Bio-Based Core Materials

The selection of the most appropriate core material is one of the key points in the design of a sandwich structure. In addition to the characteristics previously presented, such as low density and high out of plane stiffness, eco-friendliness has to be included nowadays in the design criteria. For this reason, the substitution of the traditional PVC, PUR and PS foams or of the polypropylene (PP) and Nomex honeycomb structures is a main goal to ensure performing sandwich structures that meet the new European IPPC directives. A possible way to reach this aim is the employment of bio-based core materials that permit to take advantage of natural renewable resources, to lower the emission of pollutants and greenhouse gases and to reduce the consumption of energy and chemicals in the production phase and to obtain a total or partial biodegradation of the composite at the end of its life cycle. Two materials of vegetal origin drew the attention of researchers and demonstrated a good potential as core materials in sandwich structures: balsa wood and cork.

1.2.1 Balsa Wood

Balsa wood, also known as Ochroma pyramidale, is a tropical hardwood that origins from an equatorial tree native in America and mainly cultivated in Ecuador [16,17]. It is characterized by a low density ascribable to the fast growth of the tree which can reach 20 m of height and 75 cm of diameter in 5-8 years. This feature together with satisfying mechanical properties makes it the lightest commercial timber available in fact, even if other types of wood are characterized by a

lower density, they do not have adequate mechanical properties to be suitable as core materials in industrial applications such as wind turbine blades, sports equipment, marine and aircrafts [16,18,19].

Balsa wood microstructure is shown in Figure 3 and in particular picture A represents a SEM micrograph of the axial section whereas picture B displays a schematization of a portion of the trunk. Three main directions characterize balsa microstructure: longitudinal (L), radial (R) and tangential (T). The longitudinal direction is the one that runs parallel to the axis of the trunk, the radial direction is the one that runs parallel to trunk radius and the tangential direction is the one perpendicular to the theoretical plane created by the previous two. The trunk is composed for 66-76 % of fibers, 20-25% of rays and 3-9% of vessels.

Fibers are also known as *Tracheids* and are prismatic cells with an elongated shape along the longitudinal direction and with a polygonal base that presents a hexagonal shape most of the times. Fibers are arranged in parallel to the longitudinal direction and are the load bearing components of the tree providing the mechanical support necessary to the plant to stand its own weight and to resist to external loads such as the one applied by the wind [16–18]. Fibers are characterized by an average length of 600-700 μm and by a diameter of 20-40 μm, cell wall thickness is the parameter that varies more depending on wood density and in particular can range between 0.8 and 3 μm. Rays are parenchyma cells characterized by a shorter length than fibers of about 30 μm and by a brick-like shape. They run along the radial direction and have the function to store the nutrients and the sugars until they are consumed by the plant. Vessels are long channels with an elliptical shape and a diameter between 150 and 350 μm which run along the longitudinal direction as the fibers. They play the major role to transfer the fluid mineral solutions absorbed by the roots to the upper part of the plant [16–18,20].

The high complexity of balsa wood microstructure leads inevitably to a strong anisotropy in material properties and from a mechanical point of view it can be considered as an orthotropic material along the longitudinal, radial and tangential axes. The better mechanical performances in terms of strength and stiffness are reached along the longitudinal direction thanks to the orientation of the fibers whereas the material proves to be weaker and more flexible along the other two directions [16,17].
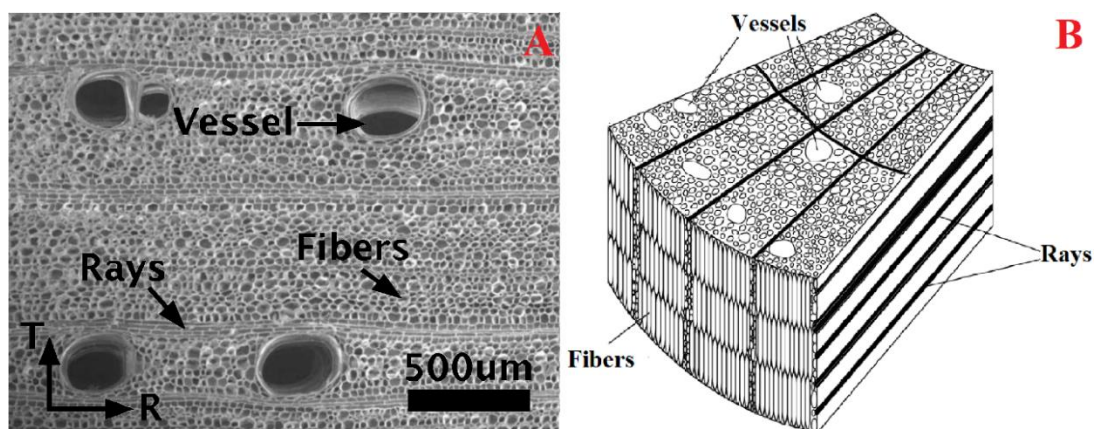
Figure 3: SEM image of an axial section of balsa wood (A) [16] and schematization of a sector of balsa wood (B) [17]

Another parameter that strongly influences balsa wood mechanical properties and more in general bio-based materials properties is the chemical composition. Cellulose, hemicellulose and lignin are the main constituents of balsa wood and of all natural vegetable fibers, such as flax, hemp, etc. In particular, balsa wood chemical composition consist of 40-45 % of cellulose, 25-30 % of hemicellulose and 20-25 % of lignin [18].

Cellulose is a polysaccharide that is a linear polymer composed by glucose units connected one another by β-1,4-glycosidic bonds as shown in Figure 4. The linearity of cellulose molecules strongly influences the supramolecular structure in fact cellulose macromolecules organize themselves in microfibrils that are the fundamental structural unit of the cell walls. Cellulose microfibrils are microcrystalline structures with an average diameter of 10 nm and a length much more pronounced than its width. Cellulose macromolecules are oriented parallel to the axis of the microfibril creating an elongated bundle. Microfibrils are characterized by an amorphous region and by a crystalline region which percentage depends on the bio-based material under study, 40-60 % in the case of balsa wood.

Contrary to cellulose, hemicellulose is composed by different groups of polysaccharides such as xylose, mannose and galactose which content depends on the plant under examination. This means that hemicellulose chemical composition is not univocally defined and depends highly on plant type. Another relevant difference of hemicellulose with respect to cellulose is the strong ramification of the polymer chains that tends to hinder the crystallization process.

Lignin is a cross-linked polymer composed by complex hydrocarbons of both aliphatic and aromatic nature. It has lower mechanical properties than cellulose but with hemicellulose constitute a matrix blend that keeps together cellulose microfibrils thus bringing life to a natural composite material [17,21].
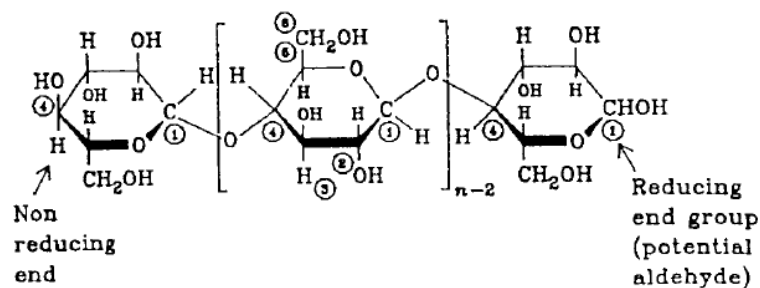
Figure 4: Cellulose chemical structure [21]

In light of the information introduced on balsa wood, it is not surprisingly that it is considered an appealing material to be used as core in sandwich structures. This awareness has led to the development of many research studies aimed to provide more information on balsa wood core sandwich structures and on their feasibility in industrial applications.

Some of these works focused on the quasi-static behavior and in particular the flexural behavior, which is the mechanical property of main interest, of these sandwich composites dealing with all experimental, analytical and finite modelling perspectives [22] and providing a comparison with other synthetic core materials such as polyethylene terephthalate (PET) to investigate their feasibility in wind turbine blades [23]. The results provided by Kaboglu et al. [23] demonstrated that the sandwich structures produced with balsa wood as core materials are characterized by a higher shear stiffness and strength than PET ones but these last have a better damage tolerance that allows to prevent catastrophic failure providing in some cases the time necessary to repair the component. Further studies addressed other quasi-static properties such as creep effect [24], compression properties after water immersion [25] and shear behavior [26]. In particular, Osei-Antwi et al.

[26] decided to investigate the shear properties of balsa wood because when applied as a core material shear loads are the main ones and are strongly interconnected with flexural ones. It was found out that shear strength and stiffness depend strongly on the shear plane because of the anisotropic microstructure of the wood. The shear properties also change as a function of wood density that in turn depends on cell wall thickness and therefore by the microstructure.

Considering the severe susceptibility of sandwich structures to impact events many works concentrated on the dynamic response of these bio-based composites addressing their fatigue behavior with both synthetic fibers [27] and natural fibers [28] skins, the low velocity impact behavior in comparison with the one of more traditional PVC foams [29,30], the high strain rate behavior in compression [31], the ballistic response [32] and the residual properties after impact both in compression [33] and bending [34].

The comparison of low velocity impact response of balsa wood and PVC foams sandwich composites proposed by Atas and Sevim [30] demonstrated that for low energy impacts balsa wood structures are characterized by a higher bending stiffness that determines a lower deflection and a higher contact force. This leads inevitably to a different damage mode in fact PVC foam sandwiches undergo a higher deformation with a resulting wide delamination area whereas balsa wood sandwiches suffer a local damaging. It is also worth noting that both types of structure are able to bear the same number of impacts before reaching perforation.

The work proposed by Vural and Ravichandran [31] addresses the dynamic compressive response and the energy dissipation capacity of balsa wood moving from quasi-static condition to Split Hopkinson Bar testing. The results obtained highlighted that balsa wood plateau stress is not affected by strain rate whereas the initial failure strength and the packing efficiency are markedly influenced by this parameter. In particular it was found out that initial failure strength tends to increase, and packing efficiency tends to degrade when the rate of deformation increases.

Jover et al. [32] studied the ballistic response of balsa wood sandwich structures made up with carbon fiber reinforced skins and with an overall thickness of 9.5 mm and observed a ballistic limit of 96 m/s that ensures their feasibility as shield against runaway debris originated by blasts, tornados, hurricane etc. The work also provides an analysis of the damage induced by multiple impacts proving that for this class of structures the influence of previous impacts has a limited influence.

Baran and Weijermars [34] provided information on the residual bending properties of glass/epoxy sandwich structures produced with balsa wood, PET foam and styrene-acrylonitrile (SAN) foam. They found out that balsa wood failure mode in bending is the same before and after impact and in particular a single shear crack determines a sudden failure of the composite. PET and SAN show the same failure mode before impact but are characterized by multiple shear cracks and by a progressive failure after impact. For what concerns bending stiffness and strength, all three core materials see a reduction of these parameters after impact and in particular a decrease of the stiffness equal to 30.5 % for balsa, to 35.2 % for SAN and to 55.6 % for PET and a decrease of the strength equal to 22.8 % for balsa, to 4.9 % for SAN and to 22.1 % for PET. Despite this unavoidable degradation of the flexural performances, balsa structures display always the highest bending properties.

1.2.2 Cork

Cork is a cellular material obtained from the bark of the oak species *Quercus Suberus L.* that is mainly cultivated in Western Mediterranean regions, such as Portugal, Italy, Spain and north Africa, but also in China [35–37]. The total amount of cork produced all over the word annually is 201 thousand tons and more than 80 % of the overall production is in Europe, in particular Portugal produces 49.6 % and Spain 30.5 % [35,36]. The bark of a tree represents its protective layer apt to shield the xylem from fire, animal and biological attacks, water loss, etc. therefore it is possible to say that cork is the protective tissue of *Quercus Suberus L.* made up of suberized

dead cells [35–37]. Cork harvesting is usually carried out manually by slicing large rectangular planks that are then pulled out. The first time that the oak is debarked the cork obtained is called virgin cork and is extremely irregular in all its characteristics: structure, density, thickness, etc. This operation takes place between 20-25 years from tree planting. After this first step cork is harvested every 9 years providing a reproduction cork that is more regular than the virgin one. Every year a layer of cork can grow on average 4.1 mm with variation between 1.7 mm and 6.0 mm. This means that the planks obtained can range in thickness from extra thin, <22 m, to extra thick, >54 mm [35,36]. Cork is characterized by remarkable properties such as lightness, resilience, stunning dimensional recovery capabilities, low permeability to liquids and gases, good thermal and acoustic insulation, wear resistance, chemical stability, durability, resistance to fire, etc. that are mainly ascribable to its microstructure and its chemical composition.

Concerning the microstructure, cork is characterized by three main directions as previously observed for balsa wood, in particular a longitudinal, radial and tangential directions can be recognized as shown by the micrographs and the schematization in Figure 5.
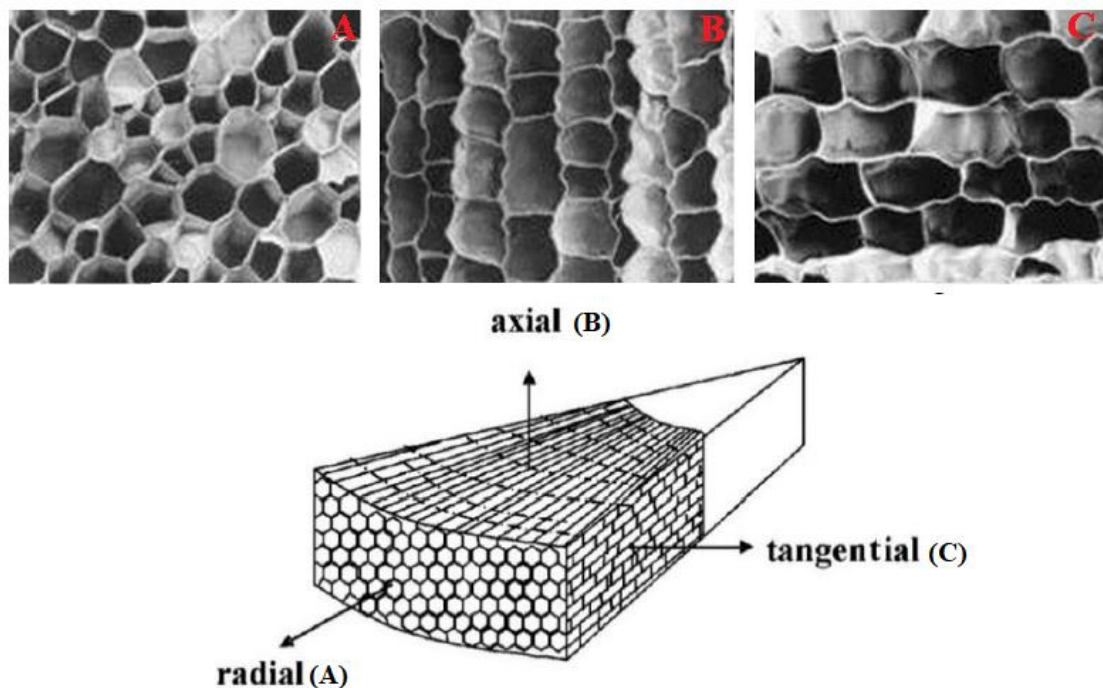
Figure 5: Schematization of cork microstructure along the three main directions [36] with some micrographs of the cross section of the radial (A), axial (B) and tangential direction (C) [35]

Cork is a cellular material characterized by an alveolar structure of closed cells that have the shape of prisms with a polygonal base. The cells are hollow and filled with air and the tissue that make up their thin walls is homogeneous and compact. They are base-to-base stacked along the radial direction giving life to parallel rows that are assembled together so that they produce an array similar to honeycomb arrangement. Considering the description given it is not surprisingly that cork microstructure appears different when observed in the three different sections. In particular, observing the cross section of the axial and the tangential direction a brick layered arrangement can be detected whereas the cross section of the radial direction allows to distinguish a honeycomb arrangement constituted by the various prism bases.

The polygons that made up the cell base can vary in side number from 4 to 9 but the most frequent shapes observed are the hexagonal, heptagonal and pentagonal ones [35–38]. The number of cells per unit volume varies between 4 and 7 x 10^7 cm^{-3}, taking into account that the solid mass of cork concentrates in the thin cell walls that have a thickness of 1-1.5 µm it appears evident that cork solid mass volume fraction is very small and close to 10 %. For sake of clarity, it is necessary to highlight that cork growth is not constant throughout the year, but it starts in April/May and stops in October/November. The cells formed during the first period of growth constitute the so called early cork characterized by the cell wall thickness previously introduced, whereas the cells produced in the last period of growth constitute the so called late cork characterized by thicker cell walls of 2 µm [35–37]. Cork cells are smaller than the ones of synthetic foams and are characterized by a height of 30-40 µm and a base edge of 13 to15 µm.

The main feature of cork cells is the undulation of the lateral walls that display two or three corrugations per face as it is possible to observe in Figure 5 B and C [35–38]. This number can increase if cork is submitted to a stress during its growth [35]. Even the period of cells formation can influence the number of corrugation in fact late cork cells are less corrugated because of the thicker cell walls [36]. The undulation of the cell walls is one of the points of strength of cork in fact the corrugations allows it to deform largely in compression without undergoing fracture and to recovery almost its initial dimension when the compressive load is relieved.

Lenticular channels are another feature of cork microstructure. They have the task to connect the inner tissues of the plant to the surrounding environment ensuring the exchange of gases. These channels run parallel to the radial direction and bring heterogeneity to the material even if their cylindrical symmetric shape permits to mitigate this drawback. As previously observed for balsa wood, cork microstructure is remarkably complex and this induces a certain anisotropy in its properties, in particular its mechanical properties can be considered orthotropic along the longitudinal, radial and tangential directions [35–37].

As mentioned earlier, cork properties depend not only on its microstructure but also on its chemical composition which in turn depends on other factors such as the geographic area were the plant grew, the conditions of the soil, the climate, the age of the plant, etc [36]. The main chemical component of cork is suberin a glyceridic polyester with a ribbon-like structure made up of glycerol and long linear chains of fatty acids and alcohols linked by ester bonds. It covers between 42 % and 50 % of cork chemical composition and it is responsible for some of the peculiar properties of this materials such as the capability of the cell walls to bend and collapse without fracture. Considering that suberin is a structural component its potential removal would compromise cell walls integrity. The second main structural component is lignin with an average value of 22 %. It provides structural rigidity to the cells ensuring them a good resistance to compression. For what concerns cellulose and hemicellulose, they play a less important role accounting for 10 % and 11 %, respectively [35–37].

Thanks to its peculiar structure, cork can be applied successfully in different industrial fields. Its good damping and energy absorbing capacities make it suitable for packaging and protective devices whereas the admirable acoustic and thermal insulating properties ensure its feasibility in buildings to optimize energy efficiency. The main application of natural cork is the production of wine stoppers in fact the low permeability to liquids and gases, the ease to be inserted and removed by the bottle and its amazing dimensional recovery capacity that ensures a perfect sealing preserving the quality of the wine in the bottle, make it the best choice [38].

The production of wine stoppers and natural cork disks causes the formation of huge amounts of wastes and by-products that can be exploited to produce other types of cork planks, such as

agglomerated cork, expanded cork and rubber-cork polymer composites, and to optimize cork employment. Cork granules are the unit base to manufacture all the types of cork planks mentioned and they are obtained sending to trituration the wastes and scraps of wine stoppers production. This process allows to obtain granules with different dimensions that once sifted and classified are sent to one of the three processing lines [35].

Agglomerated cork planks are manufactured mixing cork granules with a polymeric binder that can be thermosetting, such as urea-formaldehyde or phenol-formaldehyde resin, or thermoplastic, such as polyurethanes. The mixture is submitted to a moderate pressure and to heating in order to promote the curing of the polymeric binder [35,36,39]. Expanded cork planks are completely natural products in fact no-chemical binders are used and cork granules are bonded together taking advantage of the chemical compounds released from the thermal degradation of cork extractives. The agglomeration process is carried out in autoclave submitting cork particles to a pressure of 40 kPa and to heating at 300-350 °C by steam for 20 minutes. The degradation of hemicellulose and extractives provide the adhesive necessary to bond cork granules but leads to a mass loss of 30 %. Expanded cork is also called black cork because of the coloration assumed by the material as a result of the exposure to the high temperature of the production process [35,36]. Rubber-cork is obtained cross-binding cork particles with synthetic or natural rubber. The polymerization process is activated adding to the mixture catalysts and cross-linking agents after the mixture is molded through injection or compression. The product obtained allows to take advantage of the properties of both materials in fact cork provides a higher thermal and chemical stability as well as stunning recovery capabilities whereas rubber allows to increase the dimensional stability and the resistance [35,39].

The production of planks from cork granules allows to overcome the remarkable problem related to cork anisotropy in fact the random orientation of the particles enables to obtain an almost isotropic material. The panels obtained are mainly applied in construction for example in flooring, ceilings and walls but they cannot be used for structural purposes because of the low mechanical properties. Only agglomerated cork planks can be thought to play a structural role if applied as core materials in the production of sandwich structures.

This potential application raised an increasing interest in the academic world in hopes of finding a new core material that could meet the more restrictive European environmental regulations. This perspective leaded to the development of many research studies that considered worthwhile to provide a comparison of the quasi-static performances of traditional synthetic core sandwich structures with agglomerated cork core ones [40–42].

The works proposed by Reis et al. [40] and by Soares et al. [41] compared the shear and flexural behavior of three different types of agglomerated corks with the ones of ECA honeycomb and Roachell, a Polymethacrylimide (PMI) foam. For what concerns only agglomerated cork, the results obtained demonstrated a relationship between cork mechanical behavior and its density and grain size and in particular a higher density and a lower grain size leaded to better performances. Looking more in general at the overall outcomes of these works, it is possible to say that they endorse the suitability of agglomerated cork as core material in sandwich structures, but they also proved the superiority of Roachell foam and ECA honeycomb that are characterized by much higher mechanical performances. This is not surprising considering that they are specifically designed for aerospace and aeronautical applications that require an extensive degree of reliability. To make agglomerated cork more competitive appears evident the need of further improvements and optimization.

Considering that agglomerated cork undergoes an intergranular failure in shear, as demonstrated by Reis et al. [40] and by Soares et al. [41], a possible way to improve its mechanical performances is the development of new techniques of bonding and the optimization of granules shape and size. On this basis arose the work proposed by Castro et al. [42] who tried to develop a new agglomerated cork using an epoxy resin as granules binder. The results demonstrated a clear improvement of shear and flexural properties with respect to other agglomerated corks commercially available and a partial approach of Roachell and ECA honeycomb performances.

After this first step of investigation where the quasi-static properties of agglomerated cork core sandwiches were tested, the comparison of the mechanical response with more traditional cores went on addressing some aspects of the dynamic behavior [43–45].

Arteiro et al. [45] provided a comparison of the low velocity impact response of glass/epoxy sandwich composites produced with different core materials and in particular agglomerated cork, Roachell foam, a closed cell PVC foam and a rigid PUR foam. Thanks to an excellent compressibility and viscoplasticity agglomerated cork demonstrated to be a performing core material for all that structures which can suffer low velocity impacts during their service life. The authors discovered that for intermediate impact energies cork composites are characterized by a small damage area whereas PMI core sandwich structures undergo a severe damaging withstanding a considerable permanent indentation and core damage. The low velocity impact results permit to release cork from the lower quasi-static performances shown when compared to Roachell.

Bernard [44] and Wang et al. [43] addressed respectively the low and medium velocity impact response of aluminum face-sheet sandwich structures produced with five different types of core materials: cork, PS foam, PP honeycomb structure and high and low density balsa wood. Bernard provided also a comparison with glass/epoxy sandwich composites manufactured with the same core materials and Wang et al. completed the experimental work with a numerical finite element modelling that is a powerful tool to help designers choosing the best core material as a function of structure application. As general conclusions, it was found out that PP honeycomb and high-density balsa wood structures are stiffer and tend to undergo a higher local indentation and so a more likely penetration and perforation whereas PS and cork ones are more ductile and tend to buckle and to bend globally. This means that if energy absorption is the main goal of the composite PS foam and cork are suitable core materials whereas PP honeycomb and high-density balsa wood are recommended if the goal of the structure is minimal back face deformation.

Considering the promising results obtained with agglomerated cork as core material, some studies went further intended to produce almost a full natural sandwich structure employing natural fibers, such as basalt [46], flax [47]and jute [48], as skin reinforcement .

1.3 Natural Fibers

The substitution of the traditional synthetic components with more eco-friendly ones is a key point even in composite laminates design. Many studies intended to improve composite materials biocompatibility moving from no-biodegradable polymers of petrochemical origin to biodegradable plastics from renewable resources such as polylactic acid (PLA) [49] and polyhydroxyalkanoates (PHAs) [50,51]. This strategy proves to be successful in fields such as packaging where large amounts of wastes are produced every day and need to be disposed. Looking at other industrial fields, such as automotive and aeronautics, the problem was

approached from another point of view trying to replace the reinforcement rather than the matrix. In this perspective the main goal was to take advantage of the fibers available in nature to replace the synthetic ones. Since the beginning it appeared evident that natural fibers of every nature were not able to reach the mechanical properties achievable with carbon fibers, but the results obtained show promising perspectives for the replacement of glass fibers. This achievement was of paramount importance considering that glass fibers are the main reinforcement used in plastics accounting for more than 90 % according to the data provided by AVK in 2019 [52].

Natural fibers are usually classified as a function of their origin in vegetable, animal and mineral fibers [53–55]. Animal fibers, such as wool, are mainly constituted of proteins and are characterized by a lower strength and stiffness than vegetable ones. For this reason, plant fibers are preferred over animal ones to be applied as reinforcement in polymer composites to obtain satisfying mechanical performances. The only exception is made for silk that shows good strength but is rather expensive and less available [53]. In the class of vegetable fibers interesting results were achieved with flax fibers, hemp fibers, jute fibers, etc. whereas in the class of mineral fibers outstanding results were reached with basalt fibers. These last allow to take advantage of the noteworthy mechanical properties that were already known for asbestos avoiding all the health issues connected with the use of this material. Asbestos is banned in many countries because of its fibro genic and carcinogenic action whereas basalt can be used safely avoiding toxic effects. Even if the chemical composition of the two materials is similar, basalt fibers are characterized by a different morphology and different surface properties that permit their usage without harmful consequences for human health [56].

1.3.1 Vegetable fibers

Vegetable fibers display numerous advantages over glass fibers such as a lower density that permits to reach comparable tensile specific properties, a lower cost ascribable to a lower use of chemicals and energy consumption in the production phase, the exploitation of renewable resources, a lower abrasion of the processing equipment, less risks for human health and no irritation of the skin, good acoustic and thermal insulation capacities, but above all biodegradability [53,57].

Plants can be harvested with the aim of producing the fibers or can be harvested with other aims and fibers are obtained as a by-product. In the first case the plant is classified as primary plant whereas in the second case as secondary plant [58]. In turns the fibers extracted from these plants can be classified as stem fibers, leaf fibers and seed fibers [54,59]. Stem fibers, such as flax, hemp, jute, kenaf, etc., are the most performing ones from a mechanical point of view because their natural role is to support the plant fulfilling structural requirements [53]. Sisal fibers, agave fibers, banana fibers, etc. belong to the class of leaf fibers whereas cotton fibers belong to the class of seed fibers [54].

As previously mentioned, cellulose, hemicellulose and lignin are the main components that constitute the chemical composition of vegetable fibers as it is possible to observe from the data displayed in Table 1 [58]. The amount of each components varies as a function of plant type but also as a function of the part of the plant under study. Thanks to its linearity that allows crystallization and the formation of microfibrils, cellulose is the component responsible for fibers structural capacities and therefore it appears evident that its content is higher in stem fibers which fulfil structural purposes [53]. Other factors that can influence the chemical composition of the

fibers are the age of the plant, the climatic conditions in which it grew, the extraction method, etc. [21,53].

Table 1: Chemical composition of some natural fibers [58]

Fiber	Cellulose (wt.%)	Hemicellulose (wt.%)	Lignin (wt.%)	Waxes (wt.%)
Bagasse	55.2	16.8	25.3	-
Bamboo	26-43	30	21-31	-
Flax	71	18.6-20.6	2.2	1.5
Kenaf	72	20.3	9	-
Jute	61-71	14-20	12-13	0.5
Hemp	68	15	10	0.8
Ramie	68.6-76.2	13-16	0.6-0.7	0.3
Abaca	56-63	20-25	7-9	3
Sisal	65	12	9.9	2
Coir	32-43	0.15-0.25	40-45	-
Oil Palm	65	-	29	-
Pineapple	81	-	12.7	-
Curaua	73.9	9.9	7.5	-
Wheat Straw	38-45	15-31	12-20	-
Rice Husk	35-45	19-25	20	14-17
Rice Straw	41-57	33	8-19	8-38

Moving to the analysis of vegetable fibers microstructure, two possible schematizations are represented in Figure 6. An elementary fiber is a single cell with the shape of a tube characterized by a length that ranges from 1 to 50 mm and a diameter of around 10-50 μm [59]. Vegetable fibers microstructure is characterized by a primary cell wall (P) that encloses three secondary cell walls (S1, S2, S3) that in turn enclose a hollow region called lumen.
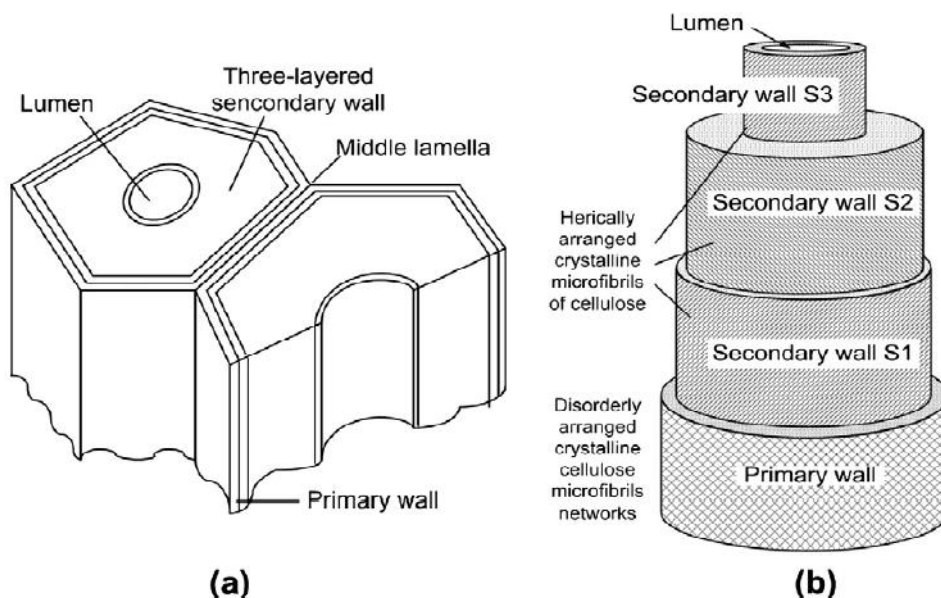
Figure 6: Two different schematizations of natural fibers microstructure [60]

All cell walls are composed by crystalline microfibrils of cellulose held together by an amorphous matrix of hemicellulose and lignin [21,55,59]. Cellulose microfibrils are responsible for the mechanical strength of the fibers and have a typical diameter of 10-30 nm [59]. The cell walls differ one another for their chemical composition, as a function of cellulose and hemicellulose/lignin ratio, and for the microfibrils spiral angle. This parameter is defined as the angle formed between the fiber axis and the helical spiral of microfibrils. The spiral angle, the content of cellulose and the degree of polymerization vary also as a function of the plant and that is the reason why the mechanical performance of vegetable fibers are so different from one another. Usually fibers with a higher degree of polymerization, a higher amount of cellulose and a lower spiral angle are characterized by higher tensile properties [21,55,59].

The lumen has the task to help plant water uptake and plays a major role in vegetable fibers properties. It provides good thermal and acoustic insulating capabilities to the lignocellulosic fiber but also a lower bulk density with respect to glass fibers allowing to obtain lightweight structures [54]. The lumen can be also used to produce self-healing composites namely composites materials able to regenerate themselves once damaged thanks to the release of the self-healing agent contained in the lumen.

Despite the use of lignocellulosic fibers as reinforcement in polymer matrix composites brings a conspicuous number of advantages, there are some criticisms to take into account in the design of these materials. First of all, lignocellulosic fibers mechanical properties vary not only as a function of plant types but also among plant of the same type. This happens because both fibers chemical composition and microstructure are influenced by factors such as the age of the plant, the climatic and soil conditions where the plant grows, the method of extraction of the fibers and so on [53]. This marked variability in the mechanical properties with respect to the more standardized glass fibers, which are also more homogeneous from a dimensional and geometrical point of view, causes an undesired uncertainty in the design stage of the composite material [61].

A second drawback connected with the use of lignocellulosic fibers, that delays their spread in some industrial fields, is the low thermal stability that permits their processability only at temperature lower than 200 °C to avoid a significant degradation of the fiber and consequently of the mechanical properties [54,61]. This leads inevitably to a strong limitation on the polymeric matrices that can be used, especially in the case of thermoplastic polymers that need to be processed at high temperatures. Polymers such as polyethylene (PE), PP, PS and PVC can be used without major problems whereas polymers such as poly(methyl methacrylate) (PMMA) and polycarbonate (PC) cannot be employed because their melting temperature is higher than 200 °C [53].

Another drawback connected with vegetable fibers is seasonality. Some plants grow only in some periods of the year and these ones may not coincide with the production peaks that can be observed in some industrial fields such as automotive. A further problem is connected with the fast degradation that vegetable fibers undergo when used to produce composites for outdoor applications. If biodegradability is desirable at the end of the life cycle of the composites, the degradation of the mechanical properties induced by chemical, biological or photochemical actions is strongly undesired during the service life of the component. To hinder the degradation process it is possible to modify partially the chemical composition of fiber cell walls inhibiting the hydroxylic groups (-OH) available on the surface [54]. An unmodified vegetable fiber can undergo degradation because of enzymes in 6-12 months whereas a fiber treated with suitable procedures can preserve its mechanical properties for 2 years [21].

In addition to all the points of weakness mentioned, it is necessary to introduce the main Achilles' heel of lignocellulosic fibers that is their hydrophilic nature. This characteristic makes them totally incompatible with the polymeric matrices characterized by a hydrophobic nature thus leading to a poor fiber-matrix interface and so to low mechanical performances of the composite [54,58]. The incompatibility of the two components also causes significant problems in fibers dispersion in fact they tend to form hydrogen bonds between them and this leads to the formation of agglomerates that worsen the mechanical properties of the composites [54]. It must also consider that the hydrophilic nature of vegetable fibers must be ascribed to the presence of hydroxylic groups (-OH) on their surface which tend to interact profoundly with water determining a conspicuous absorption of moisture or water when the application of the composite require its immersion. The uptake of moisture and water causes fibers swelling and consequently their detachment from the matrix with an unavoidable damaging of fiber-matrix interface that is already compromised by the strong incompatibility [54].

1.3.2 Surface treatments for interfacial improvement

As pointed out, hydrophilicity is the weakest point of lignocellulosic fibers and, as a consequence, the Achilles' heel of the natural composites produced with them. The incompatibility of the hydrophilic vegetable fibers with the hydrophobic polymeric matrix leads to a weak interface that is the means to transfer the load from the matrix to the fibers that are the load bearing components of the structure. The improvement of fiber-matrix interface is a challenge of paramount importance to achieve natural fiber composites with satisfying mechanical properties. To reach this aim many physical and chemical surface treatments were developed in order to modify the surface structure and the surface energy of the fibers to increase their wettability by the matrix.

The improvement of interfacial bonding can take place through different mechanisms, such as mechanical interlocking, chemical bond and interdiffusion bond, depending on the surface treatment selected. Mechanical interlocking takes place when the roughness of fiber surface increases thus leading to an increment in interfacial shear strength and so to a better load transferring. This type of bond is less effective for the transverse loads. Much more performing is the chemical bond that forms following a reaction between chemical groups in the matrix and on the surface of the fiber. Lastly interdiffusion bond takes place when the atoms and the molecules of both matrix and fibers interact at the interface [53].

Physical treatments modify the properties and the structure of fiber surface and the most used ones are corona treatment and plasma treatment [21,53,58]. Chemical treatments intervene on the chemistry of the fibers in order to create compatibility with the matrix and this class of treatments includes alkali treatment [21,53,58], acetylation [53,58], enzymatic treatment [58], silane coupling agents [21,53,58,62] and maleated coupling agents [21,53,58,63].

Corona treatment allows the activation of surface oxidation thus leading to a change in the surface energy of the lignocellulosic fiber. This treatment takes advantage of the corona effect that is a mechanism that permits the formation of plasma through the ionization of an oxygen-containing fluid, i.e. air. To reach this aim an electric current has to flow from a sharp electrode with an elevated electric potential through air in order to reach the gradient of potential necessary to activate ionization. The plasma produced is used to treat the fiber at low temperature and atmospheric pressure determining an increase of surface polarity and roughness.

Plasma treatment has almost the same operating mechanism of corona treatment, the only difference is in the gas submitted to ionization. The gases are chosen as a function of the desired

results: introduction of crosslinking, production of reactive groups and free radicals, etc., that aim to increase surface roughness and hydrophobicity. Seghini et al. [64] investigated the effect of oxygen plasma on the surface morphology and chemical composition of flax yarns and found out an increase in surface roughness and the introduction of functional groups that enhance fiber/matrix wetting.

Another way to take advantage of the plasma technique is the employment of the plasma polymerization treatment also known as PECVD (Plasma Enhanced Chemical Vapor Deposition). Thanks to this process is possible to create a thin plasma polymer film on the fiber that acts as a compatible interlayer which improves fiber wettability and, as a consequence, the adhesion with the matrix. Plasma allows to fragment and ionize monomers and gas molecules that turn into ions and free radicals. These excited species recombine onto fiber surface creating the polymeric film. This coating process is characterized by the main advantage of providing a very thin film on the fiber reducing the amount of chemical needed with respect to other processes such as grafting and salinization. This technique was deeply studied by Seghini et al. who investigated its effectiveness on flax yarns [64] and basalt fibers [65]. It was found out that PECVD improves significantly flax yarns adhesion with both vinyl ester and epoxy matrices and provides an adhesion quality superior to the one of the commercial fibers that are supplied with a commercial sizing.

Alkali treatment is also called mercerization and allows to remove components such as hemicellulose, lignin, pectin and waxes from fiber surface through the employment of an alkaline solution thus leading to a higher exposure of cellulose. Through this action it is possible to increase fiber roughness and to induce changes in cellulose microstructure. The increase of surface roughness ensures a better mechanical interlocking and the exposure of cellulose acts as a nucleation site allowing to increase the degree of crystallinity of all that matrix that are crystallizable. Light treatments tend to increase cellulose crystallinity thanks to the removal of other components that hinder the crystallization process whereas harsher treatments tend to transform crystalline cellulose in an amorphous one. This parameter strongly affects fibers performances in fact a higher degree of crystallinity means greater rigidity and strength whereas a decrease in crystallinity leads to a higher elongation [66]. Even if a lack of NaOH concentration and immersion time monitoring can cause a degradation of natural fibers mechanical performances, a correct application of the alkali treatment induces a remarkable enhancement of water absorption resistance, mechanical and thermal properties and fatigue and wear resistance [67].

Acetylation is another chemical treatment that allows to modify natural fiber surface making it more hydrophobic. The idea behind this process is to cover the hydrophilic hydroxylic groups (-OH) located on fiber surface with acetyl groups (CH3CO-), which are more hydrophobic, inducing an esterification reaction. An example of acetylation process is given in Figure 7 where acetic anhydride is applied as reactant.
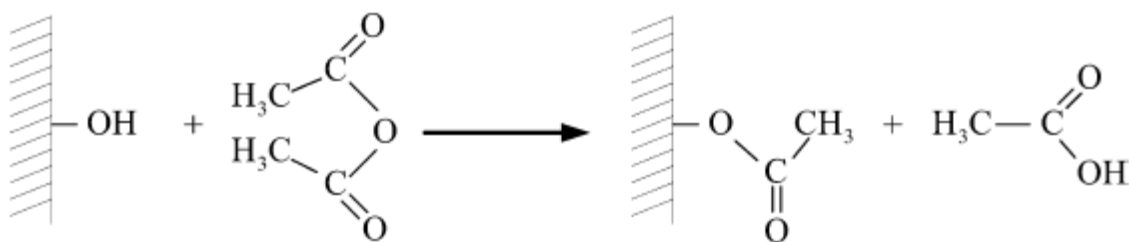
Figure 7: Main chemical reaction of the acetylation treatment [53]

46

Acetylation turns out to be a valid technique to improve fibers dimensional stability, biological attack resistance and degradation resistance to UV (ultraviolet) radiations [68] but also to improve their mechanical performances and the ones of the polymeric composites reinforced with them, i.e. flax [69], sisal [70], bagasse [71], banana [72] and palm [73] fibers.

The use of coupling agents, such as silane and maleic anhydride grafted polymers, is another chemical way to improve fiber-matrix interface inserting a third component that is compatible with both of them. Silanes are silicon chemical compounds where silicon is bonded to bifunctional groups that are able to interact with both polymer matrix and lignocellulosic fiber creating a bridge between them. In particular, silicon (Si) is bonded to hydroxylic groups (-OH), essential to guarantee an interaction with the hydrophilic vegetable fiber, and to organic groups that can interact successfully with the polymeric matrix. The silane hydroxylic group can create with the ones of the fiber covalent bonds, as a result of the elimination of a water molecule, and hydrogen bonds, as shown in Figure 8. For what concerns the organic groups, vinyl, methacryloxy, amino groups are the organo-functionalities most largely used in the production of silanes.
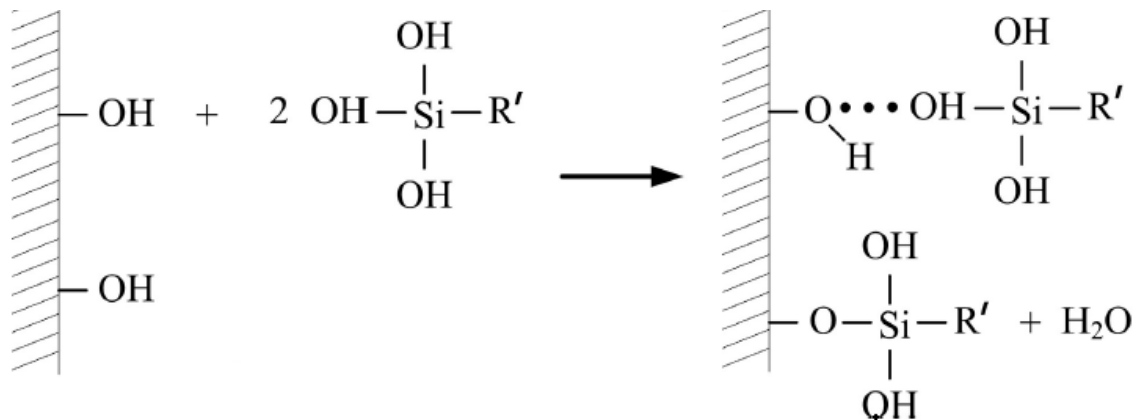
Figure 8: Schematization of the possible reactions of an organo-silane with a natural fiber

Silanes can be applied on fiber surface employing three different techniques: spraying, grafting and impregnation that affect fiber properties in different ways. Spraying technique requires to dissolve the silane in an organic solvent in order to obtain a solution that can be nebulized on fiber surface. Considering that organic solvents evaporate quickly, the silanes do not have enough time to diffuse towards the inner parts of the fiber and will be able to cover only its surface. The second technique entails to graft the silane on a thermoplastic polymer in order to obtain a prepolymer that can be added directly to the compound of fibers and thermoplastic matrix pellets. Impregnation is the most effective technique because lignocellulosic fibers are treated with a solution of pre-hydrolyzed silanes guaranteeing them the time necessary to diffuse throughout fiber cell walls and to reach the lumen. A more superficial technique such as spraying can ensure a reduction of water absorption velocity but will not have effect on the total amount of water uptake whereas a more bulky treatment such as impregnation provide the covering of some hydroxylic groups even in the inner parts of the fiber reducing the amount of water absorbed. This is confirmed by the study of Hossen et al. [74], Chandekar et al. [75] and Kusmono et al. [76] who found out a significant reduction in water uptake after lignocellulosic fiber impregnation with silanes for jute-coir hybrid PLA and PCL (Poly-caprolactone), jute PP and fan palm polyester composites, respectively. The mentioned studies also pointed out a meaningful improvement of

fiber-matrix interface confirmed by tensile and flexural properties better than the ones of the composites produced with the raw fibers.

Maleic anhydride grafted polymers are largely used as coupling agents especially for the production of thermoplastic composites. The polymer on which maleic anhydride is grafted coincides most of the times with the matrix selected to produce the composite and this ensures a perfect compatibility of the coupling agent with the matrix. Furthermore, the anhydride groups are able to interact with the hydroxylic groups located on the natural fiber surface creating covalent and hydrogen bonds as shown in Figure 9. Even in this case the coupling agent acts as a bridge between the matrix and the fiber leading to a strong improvement of the interface and, as a consequence, of the mechanical properties of the composite. Another advantage of this technique is the low cost connected with the production of the coupling agent. Indeed, the grafting process can be easily obtained placing the polymer pellets and the maleic anhydride in an extruder and adding a suitable peroxide. Modifying the type of peroxide used and the operating temperature, it is possible to tailor the amount of anhydride grafted on the polymer. This is the key point of the production process in fact an increase of maleic anhydride content leads to a decrease of coupling agent viscosity and molecular weight because of a reduction of polymer chains length. A molecular weight too low is not advisable because the interaction of the coupling agent with the matrix would be inadequate and unsatisfying, but also a molecular weight too high is undesired because the scarce amount of anhydride groups would prevent their interaction with the hydroxylic groups of the natural fiber and so the creation of the chemical bonds that are responsible for the interface improvement.
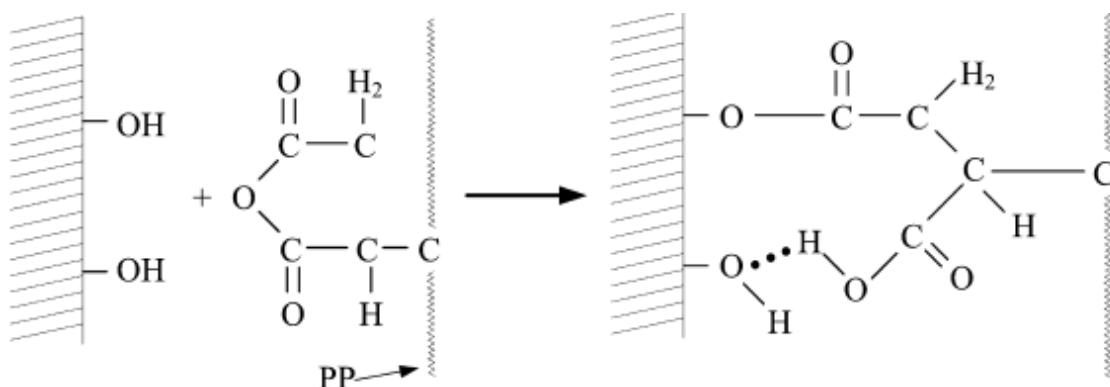
Figure 9: Reaction between a maleic anhydride grafted PP and a natural fiber

1.3.3   Hybridization technique

In the last decades natural fiber composites (NFCs) gained an ever-increasing interest in many industrial fields such as automotive, building and constructions, sports, aircraft, aerospace, etc, in order to meet the guideline imposed by the IPPC regulations issued to face the environmental challenge. Automotive is the main industrial sector that employs NFCs in the production of interior items, such as seat backs, door and instruments panels, dashboards, sun visors, hat racks, parcel shelves, package trays, etc., and exterior components such as the middle section placed between the headlights of a bus [53,77,78]. Even the aircraft industry takes advantage of the lightweight structures achievable with NFCs to produce interior paneling. Natural fiber composites are largely used even in civil engineering mainly in non-structural applications such as window and door frames, insulating panels, modular exterior constructions, facades, pipes

48

strengthening, fencing, decking, etc. Other goods that can be produced with this type of composites are toys, packaging, laptop and mobile phone cases, surfboards, tennis rackets, fishing rods, etc. [53,77,78].

An automotive component produced with a natural fiber composite allows to reduce the cost of 20 % and the weight of 30 % and this leads to a reduction of fuel consumption, of greenhouse gases emission and of waste disposal [77]. This happens because lignocellulosic fibers are characterized by a density of 1,2-1,5 g/cm^3 and a cost of 200-1000 US$/tones that are definitely lower than the 2,5 g/cm^3 and 1200-1800 US$/tones of glass fibers [54]. Despite the remarkable advantages brought by the use of natural fibers, it is necessary to point out that NFCs are not able to ensure the same mechanical properties that can be reached with glass fibers ones. In light of, this they can be applied only for non-structural and, in some cases, for semi-structural applications.

A possible solution to face this problem is the use of hybrid composites namely composite materials where the matrix is reinforced with two different types of fiber. The basic idea is to fill the polymer matrix with both glass and natural fibers in order to take advantage of the properties of both reinforcements and to compensate lack of one with the qualities of the other. The hybridization technique would allow to obtain composites with satisfying mechanical performances thanks to the presence of glass fibers but also composites characterized by a lower weight and costs and a higher eco-compatibility thanks to a partial replacement of the latter with lignocellulosic fibers.

Focusing on the environmental advantages brought by the employment of natural fibers, in Table 2 are summarized some of the main environmental parameters connected with the production of glass fibers and two different types of natural fibers, hemp and china reed. From the data reported it appears evident that the use of vegetable fibers ensures a reduction of both energy consumption and greenhouse gases emission.

Table 2: Environmental parameters related to the production of glass fibers [79], hemp [79]S fibers and china reed fibers [80]

Parameters	Glass Fibers	Hemp fibers	China Reed Fibers
Power Consumption (MJ/kg)	48.3	3.4	3.64
CO_2 Emission (kg/kg)	20.4	0.64	0.66
SO_x Emission (g/kg)	8.8	1.2	1.23
NO_x Emission (g/kg)	2.9	0.95	1.07
BOD (mg)	1.75	0.265	0.36

1.3.4 Basalt Fibers

Basalt is a natural inert material that can be extracted from effusive volcanic rocks formed as a result of lava cooling. It has a melting temperature of 1450-1500 °C and its degree of crystallization depends on the cooling rate. A rapid quench is responsible for an almost complete amorphous glassy-like structure whereas a slower cooling process allows a more or less complete crystallization [81–83] . Basalt chemical composition is similar to glass fibers one in fact both materials are characterized by SiO_2 and Al_2O_3 as main constituents, as shown by the oxides weight percentage summarized in Table 3. The major discrepancy in chemical composition can be attributed to iron oxide amount that is largely abundant in basalt and present in traces or totally

absent in glass fibers. Iron oxide is responsible for the typical color of basalt that can varies from brown to grey depending on the weight percentage. Soviet Union was the first country which thought to exploit the abundant basalt deposits present in the country to produce high-tech fibers considering its similarity with glass. After 30 years of deep researches and studies, the first industrial furnace was started in 1985 in Ukraine [81].

Table 3: Glass [84] and basalt [83] fibers chemical composition

Constituents	E-Glass Fibers (wt.%)	S-Glass Fibers (wt.%)	Basalt Fibers (wt.%)
SiO_2	55.0	65.0	42.43-55.69
Al_2O_3	14.0	25.0	14.21-17.97
Fe_2O_3	-	-	10.8-11.68
CaO	22.0	-	7.43-8.88
MgO	1.0	10.0	4.06-9.45
Na_2O	0.5	-	2.38-3.79
TiO_2	0.2	-	1.1-2.55
K_2O	0.3	-	1.06-2.33

Basalt fibers production is similar to glass fibers one and a schematic processing line for the manufacture of continuous basalt fibers is represented in Figure 10. In the spinneret method, basalt crushed stones are stored in a silo (1) from which are fed to a furnace passing through a loading station (2), a transport system (3) and a quantitative feeder (4). The furnace, fed with basalt stones and natural gases (6), consists of two zones: a primary melting zone (5) and a secondary heating (7) zone where the temperature is strictly controlled. The molten basalt is then pushed through a platinum/rhodium bushing (8) in order to obtain continuous filaments taking advantage of the continuous spinning process. The spun filaments pass through an applicator (9) in order to cover their surface with a sizing to improve the wettability and compatibility with the polymeric matrix and to avoid agglomeration phenomena. After this step all the filaments are joint together through a strand formation station (10) that allows to obtain the final fiber that is then tensioned (11) and wind up automatically (12) [81,83,85].
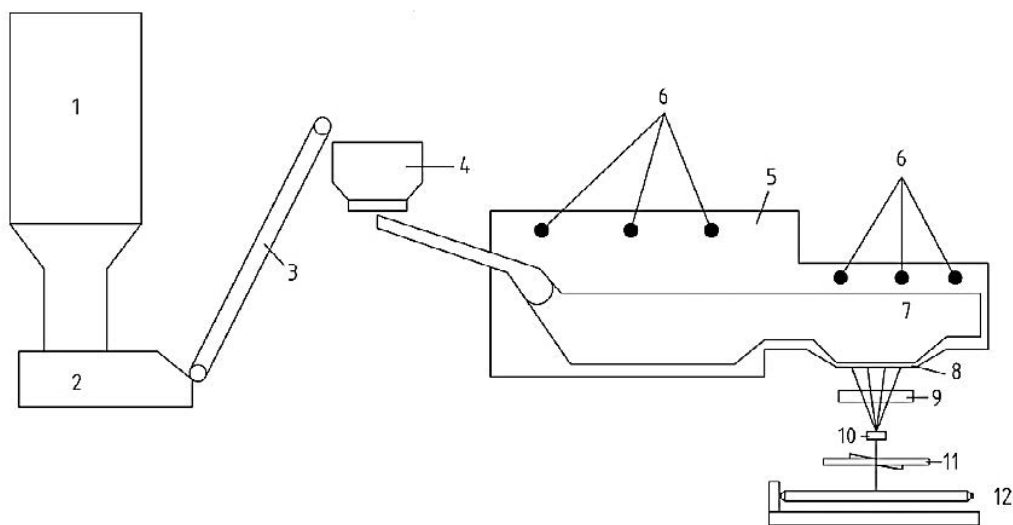
Figure 10: Basalt fibers processing line schematization [85]

The chemical and mechanical properties of the produced fibers depend on the quality of the raw materials used in fact little differences in the initial chemical composition can induce significant changes in the chemical and thermal stability and, as a consequence, in the physical and mechanical properties. Despite this flaw, basalt fibers have the remarkable advantage that can be produced using the conventional processes employed for glass fibers which is highly standardized and optimized thus reducing the amount of investments that a company should make to convert the manufacturing process. Moreover, basalt fibers production does not require the use of additional chemicals providing bio-based high-tech fibers with a higher eco-compatibility [81].

From an economic point of view, basalt fibers are cheaper than S-glass fibers but are more expensive than E-glass ones and this can be ascribed to their lower current widespread in the industrial market universally governed by the demand-supply principle. From the mechanical properties point of view, basalt fibers are totally comparable with glass ones and in some cases show higher performances, as demonstrated by the data summarized in Table 4. It is worth noting that even if basalt fibers are characterized by a higher density than glass ones, their specific tensile properties are anyway higher. In light of these observations, it is possible to legitimize the application of basalt fibers as a valid environmentally- friendly alternative to glass ones in many industrial fields, such as automotive, marine and sports.

The use of basalt fibers ensures interesting advantages over glass fibers one even from a thermal and chemical point of view. They are characterized by a higher thermal stability that enables their application in a broader range of temperatures and in particular from -200 °C to 600-800 °C [81–83]. Even basalt chemical stability proved to be higher than glass fibers one especially in an acid environment, such as a HCl solution, where basalt fibers undergo a mass loss three times lower than glass fibers one as demonstrated by Li et al. [85] and by Wei et al. [86]. As a consequence of the mass loss, both fibers types suffer a reduction of the tensile properties that is however higher for glass than basalt. As a matter of fact, basalt fibers are able to partially recover their mechanical performances after an initial steep drop. This can be explained considering that in the first step of the acid etching basalt fibers suffer a severe damage that appears with the formation of axial cracks. These cracks are partially healed in the second step of the etching thanks to the deposition of Ca^{2+}, Fe^{3+}, Fe^{2+}, Al^{3+} ions that were previously dissolved in the solution [86]. For what concerns the chemical stability in alkali both glass and basalt fibers undergo a strong reduction of their mechanical performances in this type of environment due to the breakage of the -Si-O- bonds induced by the OH$^-$ ions of the solution. The -Si-O- bonds make up the main structure of the fibers and their breakage leads to the formation of a porous surface and so to a faster degradation of fibers mechanical properties with respect to the acid environment [85,86].

Table 4: Values of some mechanical properties of E glass and basalt fibers available in literature [87]

Property	E-Glass fibers	Basalt Fibers
Density [g/cm^3]	2.56	2.8
E modulus [GPa]	76	89
Tensile strength [GPa]	1.4-2.5	2.8
Elongation to fracture [%]	1.8-3.2	3.15
Specific E modulus [GPa/g/cm^3]	30	31.78
Specific tensile strength [GPa/g/cm^3]	0.5-1	1

For a long time, composite materials were disposed in landfills, but the increasing environmental concerns and the more severe regulations encouraged reuse, biodegradation and recycling. The common procedures employed to recycle composites materials are oxidation in fluidized beds, chemical recycling and pyrolysis which is the preferred one. This technique requires to expose fiber to approximately 600 °C in an air atmosphere in order to obtain the complete removal of the thermoset char from fiber surface [88]. Considering the recycling conditions and the higher thermal stability of basalt, the employment of this type of fibers instead of glass ones as reinforcement in composites provides interesting advantages at the end of the component life cycle. Glass fibers undergo an excessive degradation of their mechanical properties after the prolonged exposure to pyrolysis conditions and cannot be further employed as reinforcement. Even basalt fibers suffer a partial reduction of their mechanical performances at the end of the incineration process but the residual powder obtained can be successfully used as filler in new polymer composites [88,89]. In light of this, some studies focused on how to partially restore basalt mechanical strength after the lost caused by the high temperature exposure of the recycling process. Lilli et al. [90] found out that a chemical treatment with a NaOH 3 molar solution for 10 minutes is able to promote a strength recovery of 94 % and 45 % on basalt fibers thermally treated at 400 °C and 600 °C, respectively, for 25 minutes.

Even the recyclability of chopped strand thermoplastic composite proved to be better when basalt fibers are used rather than glass ones. In fact the work proposed by Ralph et al. [91] demonstrated that basalt fibers are characterized by an increased resistance to processing that ensures a higher final length of the fiber with respect to glass ones. This means that, as a result of reprocessing, basalt undergoes a length reduction that is much lower than glass ensuring superior mechanical properties to the recycled component.

In the last years, thanks to the excellent mechanical properties and the good thermal and chemical stability, basalt fibers were largely used as reinforcement in polymer matrix composites with both thermosetting and thermoplastic matrices. For what concerns thermosetting polymer composites, epoxy resin was the most investigated matrix because, even if it is more expensive than vinyl ester one, it is characterized by better mechanical properties, by a higher resistance to moisture absorption and by lower toxic emissions. Colombo et al. [92] investigated quasi-static and fatigue behavior of basalt epoxy and basalt vinyl ester composites demonstrating the superior mechanical properties achievable with epoxy both in tension and compression. Many studies provided valuable comparisons of quasi-static and dynamic behavior of epoxy-basalt and epoxy-glass composites allowing to evaluate the point of strength and weakness of one against the other. Quasi-static properties at tension, compression and bending were investigated by Liu et al. [93] and by Chelliah et al. [94] who also provided information on the abrasive response. Sfarra et al. [95] addressed the dynamic behavior, and in particular the low impact response, whereas Lopresto et al. [96] presented an overview on the mechanical behavior of these two types of composites addressing tensile, compressive, flexural, and low impact properties. The fatigue behavior of these composites was also investigated together with carbon-epoxy composites one [97]. Other studies were interested in the comparison of the chemical durability [98] and sea water degradation [99] of glass and basalt epoxy composites.

From a quasi-static point of view, all the studies demonstrate that basalt fiber epoxy composites are characterized by mechanical performances comparable or better than glass fibers ones. In particular Liu et al. [93] found out similar properties for basalt and glass composites in tension, compression and bending whereas Chelliah et al. [94] observed a better mechanical behavior of basalt composites over glass ones. In particular a tensile strength 23 % higher, a compression strength 43.8 % higher and an interlaminar shear strength 48% higher were detected. These

superior mechanical properties ensure also a higher wear resistance of the laminate thanks to a better fiber-matrix interface. Looking at the dynamic response to low velocity impacts, both Sfarra et al. [95] and Lopresto et al. [96] observed comparable values of maximum force for the two types of composite but a higher energy absorbing capacity of basalt ones. This can be ascribed to the different damage mode in fact delamination is the main dissipation mechanism of glass fiber composites whereas fiber breakage is the main mechanism of basalt fiber ones. The results provided by Dorigato et al. [97] with regard to the fatigue behavior of these epoxy composites demonstrated the superiority of basalt fibers characterized by enhanced capability to sustain progressive damage and by higher damping properties. Of paramount importance is the study proposed by Wei et al. [99] which demonstrates that basalt-epoxy composites behavior in sea water is perfectly comparable with glass fiber ones thus ensuring their feasibility in all those marine applications where glass fibers are largely employed.

Moving to thermoplastic composites many studies were carried out on basalt composites produced with commercial matrices extensively used such as PP [100,101] and low density Polyethylene (LDPE) [102–104], but also with more performing matrices such as nylon 6 [105], poly(butylene succinate) [106], polytetrafluoroethylene (PTFE) [107] and polyimide [108]. The results obtained exhibit an improvement of matrix mechanical performances when basalt fibers are added and, in particular, an increase in Young's modulus, ultimate strength and impact resistance. The improvement of the mechanical performances is even greater when coupling agents are added to the compound thanks to an enhancement of fiber-matrix interface as explained in the previous paragraphs for lignocellulosic fiber composites. Even if basalt is not biodegradable, it is a material from renewable resources with a higher eco-compatibility than glass fibers and can be successfully employed to reinforce biodegradable matrices such as PLA. For this reason some studies focused on the mechanical performances achievable with PLA-basalt long fibers composites [109] and PLA-basalt chopped strands composites [110]. Liu et al. [111] proposed a comparative study of the tensile, flexural and impact properties of PLA composites produced with glass and basalt fibers and demonstrated that basalt fibers are able to provide a better toughening and reinforcing effect on PLA with respect to glass fibers.

1.3.5 Hybridization with basalt fibers

As previously demonstrated, hybridization is an effective technique to combine satisfying mechanical properties provided by glass fibers with a partial biodegradability and a greener nature of the composite ensured by the presence of lignocellulosic fibers. Considering that basalt fibers are characterized by mechanical properties comparable or superior to glass fibers ones and that are undoubtably more environmental-friendly, the idea to employ these fibers instead of glass ones in the production of hybrid composites appears as a direct consequence to obtain a greener laminate. The development of performing hybrid composites requires to know the effects induced on the structure by the substitution of traditional fibers, such as carbon and glass, with basalt ones. For this reason, many studies focused on the mechanical performances achievable with glass/basalt [87,112,113], carbon/basalt [114–116] and aramid/basalt [117,118] hybrid composites.

The comparative studies proposed by Fiore et al. [87], by De rosa et al. [112] and by Sarasini et al. [113] on glass/basalt hybrid composites demonstrated the slight superiority of basalt fibers over E-glass ones in flexural, tensile and post-impact properties. Applying the ply substitution technique, all the studies demonstrated that the symmetric configuration, where glass fibers are

applied as core and basalt fibers are applied in the external layers, provides the best results. In light of this, basalt fibers can be considered as a compelling alternative to glass ones for the production of naval components characterized by satisfying mechanical performances and by a lower environmental impact. The research work proposed by Chikhradze et al. [114] on carbon/basalt epoxy hybrid composites investigates the feasibility of these materials in the manufacture of wind turbine blades. The study demonstrates that the substitution of 20 % - 40 % of carbon fibers with basalt ones causes an acceptable reduction of tensile and compressive properties allowing their application in wind power generation and providing an eco-friendly and cost-effective solution. Similar conclusion was drawn by Subagia et al. [116] who also investigated the influence of the stacking sequence and found out better flexural performances when carbon fibers are placed at the compressive side.

Considering the promising results of the mentioned studies which promote more environmental-friendly and cheaper composites, the interest in basalt fibers appears even greater when lignocellulosic fiber hybrid composites are taken into account. The substitution of glass fibers with basalt ones in the manufacture of these hybrid composites would lead to more eco-friendly materials. In light of this, many researchers started to investigate the effect of the hybridization of basalt fibers with different lignocellulosic fibers such as jute [119–121], hemp [101,122–125] and flax [126–129].

The studies proposed by Prasath et al. [119] and by Amuthakkannan et al. [120] on jute/basalt polyester composites show that the addition of basalt fibers in jute composites allows to overcome the dearth of jute mechanical properties. Amuthakkannan et al. also investigated the influence of fibers plies stacking sequences and found out that the alternation of basalt and jute plies with basalt located in the outer layers allows to obtain the better results. Further investigations were performed by Fiore et al. [121] who addressed the influence of basalt fibers hybridization on the aging resistance of jute bio epoxy composites to legitimate their feasibility in outdoor applications. The presence of basalt fibers turns out to increase the aging resistance of the composites and to slow down the degradative effect especially when placed in the external layers providing a shield protection effect.

There is a huge amount of works on hemp/basalt hybrid composites carried out employing many different polymeric matrices of both thermosetting and thermoplastic nature. Dhakal et al. [123] studied the residual flexural properties of hemp/basalt hybrid unsaturated polyester composites after low velocity impact whereas Suresh Kumar et al. [122] carried out the same type of work on hemp/basalt hybrid epoxy composites taking into account also the effect of temperature. The results provided by Dhakal et al. remark the low resistance of lignocellulosic fibers laminates to impact events that produce a significant damage of the structures and compromise their residual mechanical properties. The study also proves that the hybridization of hemp fibers with basalt ones allows to improve considerably the post-impact residual properties and the damage tolerance of the composite. As a matter of fact, hemp composites are characterized by lower flexural properties than hybrid ones and after an impact of 9 J undergo a reduction of strength and stiffness of 46 % and 34 % respectively, whereas hybrid composites see a reduction of only 23 % of both these parameters ensuring a higher reliability of the component. Kumar et al. found similar results in fact basalt fibers composites turn out to be much tougher than hemp ones demonstrating that the production of a hybrid composite allows to improve hemp composites resistance to impact. These findings proved to be true for all the temperatures investigated in fact the hybridization technique allows to obtain a performance index close to basalt composites one.

Moving to thermoplastic matrix composites Czigany [101] investigated the tensile, flexural and fracture mechanical properties of PP mono composites made up with basalt, glass, hemp and

carbon fibers and the resulting basalt hybrid composites. Sarasini et al. [124] studied the thermal and mechanical properties of HDPE hemp/basalt hybrid composites whereas Sergi et al. [125] addressed the durability of the same type of hybrid composites investigating the effect of accelerated ageing and water absorption. The results establish that the hybridization of hemp fibers with basalt ones allows to increase strongly the tensile properties of the composites and their Vicat softening temperature especially in presence of a maleated coupling agent. Indeed, it was found out that both basalt and hemp fibers take advantage of the addition of the compatibilizer undergoing a strong improvement of fiber-matrix interface and, as a consequence, of the mechanical properties. Sarasini et al. also demonstrated that both basalt and hemp fibers undergo a strong reduction of their length when mono composites are produced through injection molding and that hybridization allows to reduce the damage with respect to the one that would be obtained with basalt/basalt and hemp/hemp pure interactions. Sergi et al. demonstrated that the hybridization of hemp fibers with basalt one is an effective way to decrease composite water uptake and to preserve the tensile properties after an accelerated ageing thus ensuring the feasibility of these hybrid composites for outdoor applications that require a prolonged exposure.

Many studies were also carried out on vinyl ester flax/basalt hybrid composites in fact Almansour et al. [127] investigated the interlaminar fracture toughness of these composites taking also into account the effect of water absorption [126]. The influence of moisture was also considered by Zivkovi et al. [128] who addressed its effect on the impact properties of vinyl ester flax/basalt hybrid laminates. Due to the great interest of the dynamic response of these composites Boria et al. [129] provided a numerical model of the falling weight impact behavior through the program LS-DYNA. The favorable results provided by all these studies led to more complex scenarios like the one proposed by Petrucci et al. [130] who addressed the impact behavior and the post impact flexural properties of ternary basalt hybrid epoxy composites produced alternating flax, hemp and glass textiles. The higher perforation energy was reached with flax/hemp/basalt composites in fact the absence of glass allows a higher bent of the laminate and so a higher resistance to penetration. This result is notable if it is considered that basalt hybrid laminates are also characterized by higher flexural performances, before and after impact, than glass/hemp/basalt ones thus ensuring a composite with better mechanical performances but also with a greener nature.

1.4 Aims of the work

Mankind took advantage of synthetic materials for decades neglecting the huge consequences that this attitude could have on the planet. The exploitation of crude oil for the production of plastics led to a massive contamination of air, water and soil not only because of the considerable emissions of pollutants and chemicals in the production process but also because of the difficulties connected with the disposal of these no-biodegradable materials. An appropriate way to face these problematics and to meet the more environmental-friendly regulations promulgated in many countries, is the use of bio-based materials from renewable resources that allows to reduce the carbon footprint in the production phase and that most of the times are also biodegradable and allow to overcome the disposal problems. For all these reasons, one of the main aims of this research work is to propose a high eco-friendly sandwich structure made up with an agglomerated cork core and with PP skins reinforced with a flax/basalt hybrid fabric.

Agglomerated cork is a good alternative to the traditional synthetic foams used as core materials, in fact it is from renewable resources, is biodegradable and is produced taking advantage of the wastes of wine cork stoppers production ensuring a full exploitation of the harvested material. Furthermore, it is a good thermal and acoustic insulator proving to be an added value for buildings and construction energy efficiency and is characterized by a great dimensional recovery capacity that ensures a good dimensional stability of the overall sandwich structure guaranteeing almost a constant distancing of the face-sheets. Three agglomerated corks with different densities were considered in this work in order to investigate the influence of this parameter not only on the physical, thermal and mechanical properties of the sole core but also on the mechanical response of the overall sandwich structures produced with them. The knowledge of density influence is of main importance to optimize sandwich composite properties and weight in order to obtain the most performing structure with the lower possible weight. Well established PVC foams, with the same densities of the agglomerated corks selected, were subjected to the same experimental campaigns in order to provide a good benchmark and to help highlighting cork advantages and drawbacks. The comparison of the results obtained would also help to legitimate agglomerated cork feasibility as core materials in several industrial applications.

In order to increase as much as possible sandwich structure eco-friendliness, a flax/basalt hybrid fabric was selected as skin reinforcement. The application of the hybridization technique allows to obtain a composite with satisfying mechanical properties, thanks to the high-tech basalt fibers, together with a partial biodegradability and a reduction of laminate weight, thanks to the presence of flax. In this way it is possible to overcome the weaknesses of the single types of fibers and to enhance the quality of the laminates taking advantage of the points of strength of both fibers. Even the application of basalt fibers rather than glass ones in the hybrid fabric is a strong contribution to the achievement of a more environmental-friendly structure.

As largely discussed previously, sandwich composites are heavily susceptible to impact events that can compromise their structural integrity and stability, induce a significant reduction of their residual mechanical properties and jeopardize the reliability of the component. For this reason, the knowledge of damage resistance and damage tolerance is a key point when designing a sandwich structure in order to be aware of the numerous failure mechanisms that can intervene and to be able to estimate the residual bearing capabilities of the component. In sight of this, the second main aim of this work is to provide an extensive characterization of the impact behavior of the novel bio-based sandwich structures proposed in order to grant their feasibility in all those industrial fields where impact resistance needs to be included in the design criteria.

To reach this goal different impact conditions were considered and, in particular, puncture impact tests, impact tests with compression after impact (CAI) support and ballistic tests were carried out on the sandwich composites. The execution of puncture and CAI impact tests allows to evaluate the influence of different boundary conditions on composites behavior. CAI constraints are less restrictive than puncture ones and this means that further mechanisms of deformation and damage could intervene to face the impact loads. Moreover, the execution of ballistic impact tests permits to assess the effect of impact mass and velocity moving from low velocity impacts performed with a heavy mass to more localized high velocity impacts performed with a little mass. In order to provide a thorough understanding of the damage scenario that takes place in the sandwich composites, not only the overall structures but also the sole core and the sole skins were subjected to the same type of testing. This strategy permits to split up the impact behavior of the single components analyzing the effect of different parameters, such as density, and to evaluate at a later time how it evolves as a consequence of composite ensemble. Another parameter that can significantly affect sandwich, skins and cores impact response is temperature. A variation in the

operating temperature can totally modify structure reaction to impact determining an unpredictable structural failure. In light of this, CAI impact tests were performed not only at room temperature but also at extremely low and high temperatures (-40 °C and 60 °C) in order to obtain an overview on behavior evolution of all components. To fully complete the impact characterization of the sandwich composites under study, the resulting damage scenario and the morphology of the overall structures and of the single components were investigated through the help of non-destructive techniques such as profilometry and scanning electron microscopy (SEM) that are valuable tools to support the dynamic analysis of structures.

Since agglomerated cork main feature is the peerless dimensional recovery after an imposed deformation and, in particular, after a compressive deformation, further impact investigations were carried out on the sole core materials to examine more in depth the compressive behavior. Drop weight tower dynamic compression tests and split Hopkinson pressure bar (SHPB) tests were performed in order to study the effect of different strain rates on cores compressive response. SHPB tests were also carried out on samples cut with different orientations from the provided planks in order to investigate a potential material anisotropy induced by the production process whereas drop weight tower dynamic compression tests were also carried out at extremely low and high temperatures. Moreover, multiple-impact tests were performed in drop weight tower dynamic compression conditions and puncture impact conditions in order to evaluate the effect of an accumulation of damage over time induced by minor impact events rather than the detrimental effect caused by a single impact.

Considering the two main goals of the work, it is now possible to justify the choice to employ skins manufactured with a PP matrix. Polypropylene is a thermoplastic polymer, and this means that at the end of its life cycle it can be easily reprocessed and recycled unlike thermosetting polymers that can only be disposed and used to waste-to-energy to exploit their heating value. In light of this, the employment of a thermoplastic matrix allows to increase the environmental friendliness of the sandwich structure. The application of a PP matrix is also useful to face the second problems connected to sandwich structures namely their predisposition to impact damage. Because of their 3D network macromolecular structure, thermosetting matrices are characterized by a brittle behavior and can dissipate the energy of an impact only through delamination, fibers breakage and matrix fracture. Thermoplastic matrices are intrinsically more ductile in fact macromolecules are free to flow allowing to reach huge plastic deformations providing an additional mechanism for energy dissipation.

As previously mentioned, the major point of weakness of natural fibers laminates is fiber-matrix interface and a possible way to enhance the adhesion and, consequently, the mechanical properties of the composite is the addition of a coupling agent that acts as a bridge between the hydrophilic fiber and the hydrophobic matrix. For this reason, the skins studied in this research work were produced with and without a maleic anhydride grafted PP as coupling agent in order to evaluate its effect on both quasi-static and dynamic properties of skins and sandwich structures. If the enhancement of fiber-matrix interface plays a positive role on the quasi-static performances of the composite providing an increase of Young's Modulus and maximum strength, it causes embrittlement when the laminate is submitted to impact determining a decrease of its capability to dissipate energy. That said, the use of coupling agent needs to be carefully evaluated as a function of composite application.

To legitimate the extensive work carried out with the experimental campaign also provided of a quasi-static, morphological and thermal characterization of the single components, a finite element modelling analysis was carried out on agglomerated cork and the PVC foams. This allows to standardize the modelling of an innovative and relatively new material as agglomerated cork,

encouraging its spread at an industrial level where the use of well-established materials is normally preferred to reduce the possibility of setbacks. The possibility to predict the response of a material through the fulfilment of a numerical simulation is a valuable tool for the industrial companies to reduce the manufacturing costs.

1.5 Novelty and implications

The results reported in the present PhD thesis allowed to enrich the already well-established baseline that encourages the employment of natural material from renewable resources in the production of composites material with an improved biodegradability and a reduced environmental impact. In particular, additional results on agglomerated cork and its sandwich structures were provided in the hope to foster the use of these materials at an industrial scale.

The first merit of the work is to provide a comprehensive overview of agglomerated cork properties assessing at the same time physical, morphological, thermal and mechanical perspectives to disclose the relationships that exist between them. Many works addressed these aspects individually preventing the investigation of all cause-and-effect interconnections that is essential to provide a thorough understanding of material response and to validate its feasibility for a certain application. Morphological characterization permitted to identify the peculiar microstructure of cork that is responsible for its good thermal insulation capacity, which makes it a compelling solution in wall-paneling, as much as its outstanding dimensional recovery capabilities, which makes it a primary choice in safety devices. Thermal characterization provided a valuable support to understand the evolution of quasi-static and dynamic properties of cork at low and high operating temperatures disclosing potential variation in material response as a function of work environment.

Concerning work environment, some studies wondered about the harsher conditions that agglomerated cork sandwich structures may face when employed in marine environment thus assessing the effect of water absorption [46,131] and salt fog exposure [132,133] on their quasi-static and dynamic response. It must be considered that cork enclosure between skin laminates tends to reduce water uptake and the exposure to salt fog, but impact events can cause skin damage and perforation phenomena which can imply a direct exposure of the core to the work environment. In this perspective the knowledge of sole core response is fundamental and for this reason the effect of both water absorption and salt fog exposure on neat agglomerated cork compressive behavior was investigated in the present PhD work.

The way a sandwich structure reacts to an external load is strictly correlated to the out-of-plane, i.e. compressive, properties of the core material. Considering that both quasi-static and dynamic load can affect an in-service component the investigation of core compressive properties evolution as a function of strain rate is of main importance. Many works already addressed the strain rate sensitivity of both PVC foam and agglomerated cork considering low and high strain rate ranges, but completely neglecting medium strain rates [134–140]. The intermediate strain rates are fundamental as demonstrated by Wouts et al. [141] who investigated the strain rate sensitivity of the compressive properties of two types of woods, i.e. beech and spruce, highlighting a stronger sensitivity of the material in the medium-high velocity range thus disclosing a change in its compressive response. The importance of the medium-velocity conditions was acknowledged also by Zhai et al. [142] who investigating the Poisson's ratio of an auxetic polyurethane foam as a function of strain rate found out an auxetic behavior in the low

medium working range and a positive Poisson's ratio in the higher working range. In consideration of this, the present thesis addressed the whole strain rate range joining together quasi-static, drop weight tower and Split Hopkinson pressure bar compression data overcoming the lacks of previous works which focused on limited working conditions preventing an overview of the overall compressive behavior.

A further field of concern for sandwich structures is the accumulation of damage over time due to multiple-impacts which can reduce the long-term structural efficiency of the panel. In this perspective, some research studies assessed the issue like the one proposed by Lu et al. [143] who investigated the multiple-impact behavior of a polyethylene foam or the one proposed by Fernandes et al. [144] who focused on expanded polystyrene (EPS) and expanded polypropylene (EPP) foams. Concerning agglomerated cork, the topic was addressed always by Fernandes et al. [144] who employed a hemispherical impactor in dynamic compressive conditions and by Sanche-Saez et al. [145] who studied the dynamic compressive response of only one type of agglomerated cork using a flat impactor. The results presented in this study provide a significant improvement to the theme evaluating not only two types of impact conditions, i.e. drop weight tower dynamic compression with a flat impactor and puncture impact conditions, but also the effect of density. Therefore, the steps forward of this work are the assessment of impact conditions not considered in previous studies and in particular puncture impact conditions which were never addressed before and the evaluation of density effect. Moreover, the evaluation of agglomerated corks and PVC foams behavior and damage up to 10 impacts, number that was not achieved in previous studies, allows to detect impact properties trend as a function of impacts number.

Focusing on the impact behavior of agglomerated cork and the resulting sandwich panels many steps forward were taken in this PhD thesis with respect to state of the art. Concerning the low-velocity impact response, a lot of studies assessed the impact resistance of this natural core and of its sandwich structures, as already reported in section 1.2.2, but none of them addressed the effect of temperature. In view of this dearth, the present work investigated the effect of both low (-40 °C) and high (60 °C) temperatures on the impact performance of agglomerated cork sandwich structures. Moreover, the employment of two different specimen supports allowed to disclose the effect of boundary conditions highlighting a different impact susceptibility not only of the complete sandwich structures, but also of the sole cores and skins as a function of sample constraints. Concerning the ballistic behavior, Sarasini et al. [146] and Sanchez-Saez et al. [147] already addressed the topic investigating flax/epoxy and aluminum face sheets sandwich panels response, respectively. To further increase the data base in this field, some parameters neglected in the previous works were evaluated, i.e. core density and coupling agent integration in skins.

Finally, valuable results were also provided in the field of numerical modelling. Mancuso et al. [148] and Potes et al. [149] presented a Finite Element Analysis (FEA) on agglomerated cork sandwich components employed in sailing boats and in the aeronautical field, respectively. Both research studies were mainly focused on structure layout optimization rather than in cork behavior modelling in fact they modelled the natural core as an isotropic material described only by its elastic modulus and its Poisson's ratio neglecting peculiar features such as its pronounced visco-elastic nature. A thorough modelling of cork behavior was provided by Fernandes et al. [150] who described cork elastic behavior through an hyper-elastic model coupled with Mullins effect to describe material damage at high deformations. Despite the excellent results achieved, the model allows to describe only the dynamic compressive behavior of the material, but not the perforation phenomena resulting from an impact. In view of this, the present study proposes a compelling model to simulate the puncture impact behavior of agglomerated cork and to reproduce the perforation phenomena that may be involved.

Chapter 2: Materials and Methods

2.1 Material Selection

2.1.1 Core materials

Three agglomerated corks, produced from the same type of cork but characterized by different densities of the planks because of a different degree of compactness, were used in this research work in order to evaluate the effect of this parameter on the physical, thermal and mechanical properties. Agglomerated cork planks with a thickness of 15 mm and an average density of 140 kg/m^3 (NL10), 200 kg/m^3 (NL20) and 250 kg/m^3 (NL25) were supplied by Amorim Cork Composites$^®$. The three types of agglomerated corks differ also in grain size in fact NL10 is characterized by a grain size of 2-4 mm whereas NL20 and NL25 by a grain size of 0.5-2 mm. A polyurethane binder formulated specifically for cork was employed to bond together cork granules and to ensure their compatibility with all the polymeric resins industrially used to produce composites such as epoxy, polyester, vinyl ester and phenolic. Agglomerated cork properties were compared with the ones of well-established rigid PVC foams characterized by the same densities that can act as benchmarks validating the feasibility of agglomerated cork as a suitable core material in sandwich composites. The comparison of the results is also useful to highlight the drawbacks and the advantages of agglomerated corks over the closed cells PVC foams. The synthetic foam plates were provided by Diab$^®$ always with a thickness of 15 mm and an average density of 130 kg/m^3 (Divinycell-HP130), 200 kg/m^3 (Divinycell-HP200) and 250 kg/m^3 (Divinycell-HP250).

2.1.2 Skins production

Sandwich skins were produced by hot compression molding using a PP matrix and a natural hybrid woven fabric as reinforcement. LINCORE® HF T2 360 is a balanced twill 2/2 fabric made up with 50 wt.% of basalt and 50 wt.% of flax as represented in Figure 11. It is provided by Depestele Group and is characterized by an areal density of 360 g/m^2. The employment of a twill rather than a plain-woven fabric allows to reduce fiber crimp leading to better mechanical properties and to a higher fiber packing density. Bormod^{TM} HF955MO is the polypropylene used as skin matrix, it is supplied by Borealis AG and is characterized by a melt flow index (MFI) at 230 °C of 20 g/10 min. Skin composites were produced with and without coupling agent in order to investigate the influence of an improved fiber-matrix interface on both quasi-static and impact performances. Polybond® 3000 is the coupling agent used and is a maleic anhydride grafted polypropylene (MA-g-PP) with a maleic anhydride content of 1.2 wt.%. It is supplied by Chemtura Corporation and has a MFI at 190 °C of 405 g/10min. The neat PP was modified with a 2 wt.% of coupling agent mixing them by means of a corotating twin screw extruder Collin Teach-Line® ZK25T working with a screw speed of 60 rpm and a temperature profile of 180 °C - 190 °C - 205 °C - 195 °C -185 °C. To be able to produce skin composites by hot compression molding the polymeric matrix, neat polypropylene (PP) or compatibilized one (PPC), has to be available in the form of a thin film. To reach this aim PP and PPC films with a thickness of 35-40 μm were produced through a film blowing extrusion line Teach-Line® E 20 T supplied by

Collin GmbH operating with a screw speed of 55 rpm and a temperature profile of 180 °C - 190 °C - 200 °C - 190 °C -185 °C. The extrusion line was equipped with a calender CR72T provided by the same production company.

Figure 11: LINCORE® HF T2 360 flax/basalt hybrid twill woven fabric employed as skin reinforcement

Thermoplastic skins were manufactured by hot compression molding applying the film-stacking technique alternating films of matrix with a ply of hybrid fabrics for a total number of four twill layers. The molding machine is a P400E supplied by Collin GmbH and the manufacturing process was carried out according to the optimized operating cycle reported in Figure 12. Table 5 reports the final characteristics of the manufactured skins.
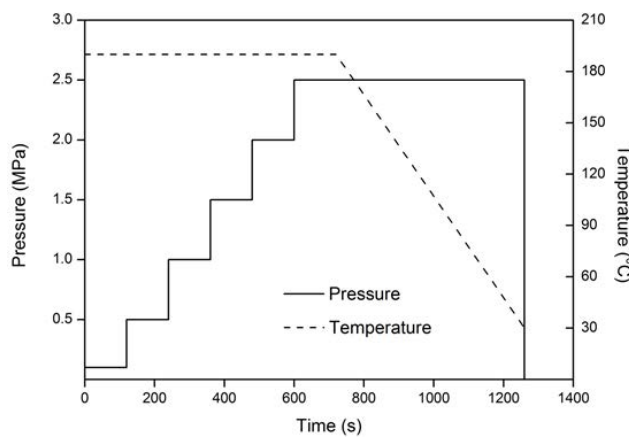
Figure 12: Temperature and pressure conditions used in skin manufacture process

Table 5: Final characteristics of the manufactured skins

Skin Type	Fiber Volume Fraction	Thickness (mm)
PP	0.36 ± 0.02	2.2 ± 0.1
PPC	0.35 ± 0.03	2.1 ± 0.1

2.1.3 Sandwich structures production

Sandwich composites structures were produced bonding together the skin laminates and the core material with the bicomponent epoxy resin Elan-tech® ADH 46.46 provided by Elantas. The adhesive is characterized by a setting time of 420 minutes and a curing profile of 14 hours at 25

°C. The structures were produced through a two steps process gluing the first skin to the core and waiting 24 hours to be sure of the complete curing of the resin before gluing the second skin. During the curing process the overall structure was placed under a constant weight in order to promote skin-core adhesion and the glued skin was placed below the core in order to facilitate the removal of the resin in excess. Elan-tech® ADH 46.46 is a high-performing structural adhesive that bonds perfectly with PVC foam, cork and fiber fabrics, but struggles to adhere with polyolefins that are characterized by low surface energy. In light of this, the only way to ensure a good interfacial adhesion between core and skins, and as a consequence satisfying mechanical performances of the sandwich structure, was to partially remove the last polymeric layer through a scratching process with a coarse-grained sandpaper. This operation allows to expose part of the neat fibers that are able to join perfectly with the resin. This solution was the best one considering that neither bicomponent acrylic resins, such as the 3M™ Scotch-Weld™ DP8005, specifically designed for polyolefins were able to ensure the required core-skin interface adhesion. Based on cores characterization only three core materials were selected to produce the sandwich structures subjected to the dynamic characterization and in particular: NL10, NL25 and HP130. The employment of NL10 and HP130, as core materials, provides a direct comparison of the response of structures characterized by the same weight, whereas the employment of NL25 and HP130 allows to compare the performances of two structures produced with the agglomerated cork and the PVC foam which displayed the closest behavior during core characterization. The six sandwich structures configurations used for the impact characterization in this work are summarized in Table 6.

Table 6: Sandwich structures configurations employed in this work

	NL10	**NL25**	**HP130**
Neat Polypropylene	PP_NL10	PP_NL25	PP_HP130
Compatibilized Polypropylene	PPC_NL10	PPC_NL25	PPC_HP130

2.2 Core Morphological Characterization

2.2.1 Scanning Electron Microscopy

The analysis of cores microstructure is a valuable tool to justify the physical, thermal and mechanical properties of these materials. For this reason, both PVC foams and agglomerated corks were subjected to a morphological characterization by means of a field-emission scanning electron microscope (FE-SEM) MIRA 3 by Tescan. This type of analysis allows to detect the differences that arise because of material nature but also the ones that can be ascribed to changes in density which can strongly influence core material response. Considering that out of plane properties are key parameters to take into account when selecting a core material, a direct consequence is that material compressive behavior is one of the main aspects to take into account. In light of this, the classic morphological characterization carried out on as-received core materials was supported by an analysis of pre-stressed samples in order to investigate how material morphology evolves as a function of the compressive load applied. In particular, every core material was assembled on a screw stub and was subjected to a constant compressive stress applied through a thin metal sheet that allows to distribute uniformly the clamping force exerted by the tightening of the screw. The higher the screw displacement the greater the load applied to

the sample. Considering that both cork and PVC are characterized by a low electrical conductivity, all specimens were sputter coated with a thin layer of gold to prevent charging and to improve micrograph quality. The coating process was carried out in vacuum conditions (0.4 mbar) for 2 minutes by a sputter coater Edwards S150B applying a voltage of 1 kV and an electrical current of 40 mA to the gold electrode.

2.2.2 Wettability

Agglomerated corks and PVC foams surface wettability was evaluated measuring the contact angle of water droplets. Tests were carried out at room temperature with an optical analyzer OCA 15Pro of the DataPhysics Instruments selecting a static sessile method and a droplet volume of 3 μl. An ultrapure water, Milli-Q, characterized by 18 MΩcm was used as testing liquid. The values of contact angle were estimated analyzing the shape of the droplet through the software module DataPhysics SCA 20. In order to obtain statistically significant results a minimum number of ten contact angles was recorded for each core material in different zones of the specimen.

2.3 Core Thermal Characterization

2.3.1 Thermal conductivity

Agglomerated corks and PVC foams thermal conductivity, thermal diffusivity, specific heat and resistance value (R-value) were estimated through a modified transient plane source, TCi Thermal Conductivity Analyzer provided by C-Therm. The main components that constitute the thermal analyzer are shown in Figure 13. A known electric current is applied to the spiral heating element of the sensor in order to heat it and to induce a temperature increase at the interface between the sample and the sensor. This increase in temperature causes in turn a change in the voltage drop of the sensor and considering that the rate of increase in sensor voltage is inversely proportional to the thermal conductivity of the material tested this thermal property can be directly measured by the instrumentation. Once obtained this measurement and providing the value of sample actual density to the software, it is able to calculate thermal diffusivity, specific heat and R-value of the core materials. Tests were performed in five different points of a square sample characterized by 15 mm of thickness and 100 mm of side, as depicted in the schematic picture in Figure 14.
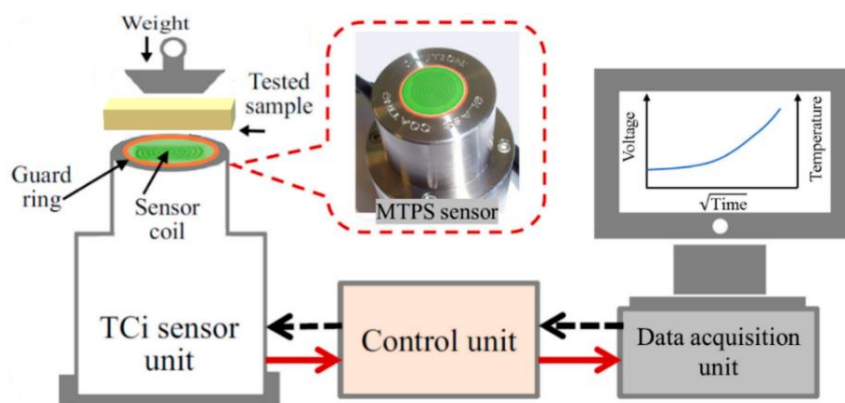
Figure 13: Schematic operating mechanism of C-Therm TCi thermal conductivity analyzer [151]
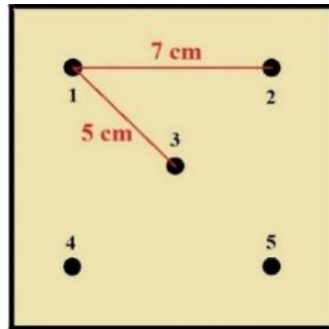
Figure 14: Schematic representation of specimen sampling points for thermal conductivity analysis

Ten measurements were carried out in each point. Tests were performed on as-received samples but also on pre-conditioned samples in order to investigate the effect of moisture on core material thermal conductivity. Pre-conditioned samples were oven-dried at 60 °C for 24 hours in order to obtain almost a complete removal of the moisture.

2.3.2 Thermogravimetric Analysis (TGA)

Core materials thermal stability was addressed performing a thermogravimetric analysis with a Setsys Evolution supplied by Setaram. The machine consists of a vertical balance connected to the alumina crucible where the sample to analyze is placed. Through this balance is possible to record mass sample changes as a function of temperature while the material is heated with a constant rate of 10 °C/min. Tests were performed under a nitrogen gas purge in order to ensure an inert atmosphere and to avoid any oxidative reaction that could take place working in oxygen or air and could induce undesired alterations in sample mass.

2.3.3 Dynamic Mechanical Analysis (DMA)

Dynamic mechanical analysis was employed to study the variation of core materials mechanical properties with temperature. In particular, the evolution of storage and loss moduli with temperature was recorded and the glass transition temperature was extrapolated from the resulting graphs. Tests were carried out with a rheometer Anton Paar MCR 501 subjecting the specimens to a torsion stress with a frequency of 1 Hz and to a heating rate of 2 °C/min. A gaseous nitrogen flow of 160 ml/min was used during the cooling and heating steps to keep a controlled atmosphere.

2.4 Core Quasi-Static Characterization

2.4.1 Shear tests

Shear tests were carried out in tension loading at room temperature with a speed of 2 mm/min on rectangular samples with a length of 300 mm, a width of 50 mm and a thickness of 15 mm. All test conditions were selected in order to fulfil ASTM C273. To transfer the shear load from the

loading plates to the sample, the latter was glued to the plates through the structural bicomponent epoxy resin Elan-tech ADH 46.46 by Elantas. Unfortunately, only agglomerated corks could be tested in shear because the higher mechanical properties of the PVC foams leaded to a premature detachment of the sample from the loading plates hindering test execution. NL10 and NL20 were shear tested with the universal testing machine Zwick/Roell Z010 equipped with a 10 kN loading cell whereas NL25 needed to be tested in an Instron 5584 equipped with a 150 kN loading cell because of its higher mechanical properties. Five specimens were tested for each type of agglomerated cork. Both testing machines provide the force-displacement record and it was necessary to apply the equation reported in ASTM C273 to obtain the stress-strain curves of each material. In particular:

$$\tau = \frac{P}{(Lb)} \qquad (2.1)$$

$$\gamma = \frac{u}{t} \qquad (2.2)$$

where τ is core shear stress in MPa, P the instantaneous force on the specimen in N, L and b the length and the width of the specimens in mm, γ core engineering shear strain, u the instantaneous displacement between the loading plates in mm and t the thickness of the specimen in mm.

2.4.2 Bending tests

Three-point bending tests were performed to evaluate core materials flexural properties. Tests were carried out in agreement with ASTM C393 and ASTM D7250 on parallelepiped samples with a length of 250 mm, a width of 50 mm and a thickness of 15 mm. The support employed has a span of 150 mm and was equipped with 10 mm tips radius. Tests were performed on a Zwick/Roell Z010 universal testing machine equipped with a climatic chamber employing a test speed of 6 mm/min and applying a preload of 1 N. Samples mid-span deflection was measured following machine crosshead displacement whereas the reaction force was measured through a 10 kN load cell. The resulting force-displacement curves were converted by the Zwick/Roell software in stress-strain curves employing Equations (2.3) and (2.4):

$$\sigma_f = \frac{3\,F\,L}{2\,b\,t^2} \qquad (2.3)$$

$$\varepsilon_f = \frac{6\,D\,t}{L^2} \qquad (2.4)$$

where σ_f and ε_f are the stress (MPa) and strain, respectively, L the support span (mm), b specimen width (mm), t specimen thickness (mm), F material reaction force (N) and D sample mid-span deflection (mm). In order to investigate the influence of operating temperature on the flexural properties of agglomerated corks and PVC foams, flexural tests were performed at room temperature, 40 °C, 60 °C and 80 °C. The selection of the mentioned temperatures allows to analyze agglomerated cork behavior evolution up to an upper limit at which the polyurethane binder employed generally experiences a significant reduction of the mechanical properties. Before testing, samples were conditioned for two hours to achieve a homogeneous temperature across the whole specimen. Five specimens were tested for each core family at every operating temperature.

Flexural test results were supported by statistical analysis and inferential statistics were employed to determine if the parameter selected as independent variables, namely core density and operating temperature, met the criteria for statistical significance proving to have an effect on the dependent variable, namely flexural modulus and flexural strength. The t-test was used to carry out the statistical analysis and a p-value < 0.05 was adopted as statistically significant limit meaning that a p-value lower than 0.05 confirms that the parameter under consideration had an actual effect on the dependent variable. In order to pinpoint the correlation that exist between the dependent and independent variables, regression coefficients were also estimated. Statistical analysis was performed through R-studio, an integrated development environment designed for the statistical computing programming language R, applying the linear model (lm).

2.4.3 Compression tests

Compression tests were carried out on cubic samples with an edge of 15 mm assessing the effect of temperature, anisotropy and test speed on the compressive response of PVC foams and agglomerated corks cores. Temperature effect was evaluated performing tests at room temperature, 40 °C, 60 °C and 80 °C with a speed of 5 mm/min. Even in this case samples were pre-conditioned for two hours to reach temperature equilibrium. Anisotropy effect was studied testing the cubic samples with a speed of 5 mm/min along the out of plane and in plane directions of the original planks. Cores strain rate sensitivity was addressed performing tests at room temperature with increasing test speeds: 5 mm/min, 25 mm/min, 50 mm/min, 100 mm/min, 150 mm/min and 200 mm/min. All tests were performed in the Zwick/Roell Z010 universal testing machine already mentioned for the bending tests and five specimens were tested for each core family in every test condition described. Even compression test results were supported by statistical analysis. In this case the independent variables employed for the inferential statistics were core density and test speed and the dependent variables considered compressive modulus and plateau stress. The t-test was employed to evaluate the p-values and the regression coefficients always through the integrated development environment R-studio and the application of a linear model (lm). Materials dimensional recovery capability was evaluated as a function of strain rate by submitting all the samples tested at room temperature to a periodic measurement.

2.4.4 Water absorption

The effect of water absorption on the compressive properties of two types of agglomerated corks, NL10 and NL25, and one type of PVC foam, HP130, was investigated. Six cubic samples with 15 mm of edge were fully submerged until they reached saturation for each core type. In order to remove the moisture absorbed by the as received planks, all samples were pre-conditioned in oven at 60 °C for 24 hours. The evolution of samples weight was strictly controlled performing a periodic measurement through the digital analytical balance AE160 by Mettler Toledo. Even samples swelling was monitored trough a periodic measurement of sample dimensions thanks to a digital caliper. Samples were submerged in pure distilled water and simulated sea water in order to investigate the effect of the two different fluids. The distilled water was provided by Tito Menichelli s.r.l whereas the simulated sea water was obtained adding 35 g of 98+% pure sodium chloride (NaCl) provided by Sigma-Aldrich to 1 kg of distilled water. This choice was made considering that ocean waters are characterized by a salinity of 35 ‰ namely 35 g of salts for kilogram of water and that NaCl accounts for 27.123 g of the total amount.

Once achieved saturation, all cubic samples were tested in compression in the Zwick/Roell Z010 universal testing machine with a test speed of 5 mm/min. Half of the samples for each core type were tested in wet condition whereas the other half were submitted to oven drying at 60 °C until all water was removed. In this way it was possible to investigate the direct and residual effect of water on the compressive response of the core materials.

2.4.5 Salt fog ageing

In addition to direct water absorption, the effect of salt fog accelerated ageing on the compressive behavior of the two types of agglomerated corks (NL10 and NL25) and of the PVC foam, (HP130) was investigated. The ageing process was carried out on cubic samples with 15 mm of edge in an Angelantoni DCTC 600 climatic chamber according to ASTM B117. The salt fog employed is a 5 % NaCl solution with a pH between 6.5 and 7.2 and the operating temperature was set to 35 °C. Twelve samples for each core type were picked up from the climatic chamber after 30, 60 and 90 days. Six of the twelve samples for each core family were tested in wet condition whereas the other six were oven dried at 60 °C in order to promote water removal. Of the six samples, in each testing condition, three samples were tested along the original plank thickness in order to investigate their out of plane properties and the other three samples were tested along the direction perpendicular to original plank thickness in order to investigate the in-plane properties.

2.5 Core Dynamic Characterization

2.5.1 Drop weight tower dynamic compression tests

Drop weight tower dynamic compression tests were performed on cubic samples with a 15 mm edge in a drop weight tower Ceast Fractovis® employing a circular flat impactor with a diameter of 58 mm and an overall mass of 4.134 kg and a 19 kN load cell. All tests performed in drop weight tower allows to record material reaction force evolution through the load cell and impactor initial velocity through an optical sensor located above the impact zone. Starting from these two parameters, it is possible to evaluate the evolution of impact velocity, displacement and energy as a function of impact time. The force applied on the sample can be described as:

$$F(t) = mg - ma(t) \qquad (2.5)$$

where m is the impactor mass, g the gravity acceleration and a(t) the deceleration imposed to the impactor as a consequence of the interaction with the sample. This means that being m, g and F(t) known, it is possible to evaluate the deceleration suffered by the impactor:

$$a(t) = g - \frac{F(t)}{m} \qquad (2.6)$$

Considering that impact initial velocity, v_0, was accurately measured with the optical sensor, it is possible to calculate the impact velocity evolution through the integration process shown in Equation (2.6):

$$v(t) = v_0 + \int_0^{t_i} \left(g - \frac{F(t)}{m} \right) dt, \text{ with v(t)=v}_0 \text{ at t=0} \tag{2.7}$$

Considering that x(t) = 0 when t = 0, it is possible to further integrate the previous equation to obtain displacement evolution with time according to Equation (2.7):

$$x(t) = 0 + \int_0^{t_i} v(t) dt \tag{2.8}$$

Finally impact energy evolution with time can be calculated applying the kinetic energy equation to v(t) data set.

All core materials were tested at different impact energies, summarized in Table 7, in order to obtain information on the evolution of material compressive behavior as a function of this parameter but also to acquire medium strain rate data useful to study material strain rate sensitivity.

Table 7: Impact energies used to test each core material

Sample	2J	5J	7J	13J	30J
NL10	X	X	X		
NL20		X	X		
NL25		X	X	X	
HP130		X	X	X	
HP200		X	X	X	X
HP250		X	X	X	X

It is appropriate to underline that, in contrast to quasi-static compression, drop weight tower dynamic compression does not work with a constant strain rate leading to the need of defining a univocal criterion for strain rate identification. In these tests, impact velocity is recorded throughout all test time allowing to evaluate automatically strain rate evolution with time. In light of this, every strain rate value was estimated computing the mean of all strain rate values included between the starting point of the impact and the point where the compressive property of interest occurs. For example, the strain rate at 30 % of deformation is obtained calculating the average value of all strain rates from t = 0 s up to the time corresponding to 30 % of deformation.

In order to study the evolution of core materials dynamic compressive properties in a wide range of operating temperatures, tests were performed not only at room temperature but also at -40 °C and 60 °C. The achievement of these temperatures was possible thanks to a climatic chamber incorporated in the tower and equipped with nitrogen cooling connectors and heaters. To ensure a homogeneous temperature profile across the specimen, all samples were pre-conditioned for

two hours at the desired temperature. In temperature tests were performed at diverse impact energies, i.e. 5 J, 7 J and 13 J, in order to study the combined effect of impact energy and temperature. A minimum number of five samples was tested in every testing condition presented.

Room temperature tests were recorded with Fastcam SA-Z, a high- speed camera by Photron®, to visually inspect the progressive effect of the impact on the core material. The resulting videos were analyzed through the program Photron FASTCAM Viewer 3. This procedure could not be applied for -40 °C and 60 °C tests because of the need to keep the climatic chamber closed in order maintain constant the temperature inside.

2.5.2 Drop weight tower dynamic compression Multiple-Impacts tests

Drop weight tower dynamic compression multiple-impacts tests were carried out at room temperature employing the same tower and the same set up previously introduced for the single drop weight tower dynamic compression tests. Even in this case, tests were recorded with the Fastcam SA-Z high speed camera and the resulting videos were processed with the program Photron FASTCAM Viewer 3. This tool is even more important in this context because allows to control the evolution and to quantify the deformation of all core materials with progressive impacts.

Each core material was tested at two different impact energies that were accurately selected to fulfil two different conditions: maintain the maximum deformation in the plateau region after the first impact and reach the densification stage of the stress-strain curve after the first impact. The impact energies were picked out on the basis of the single tests results and were chosen in order to accomplish another condition, namely to induce a maximum deformation of the core material included between 55 % and 65 % for the lower impact energy and between 75 % and 85 % for the higher one. The impact energies for each core material were selected on the basis of the single impact results and are summarized in Table 8.

Table 8: Lower and Higher Impact energy values selected for each core material

Samples	Lower Impact Energy	Higher Impact Energy
NL10	2J	5J
NL20	2J	5J
NL25	7J	10J
HP130	7J	10J
HP200	13J	18J
HP250	18J	25J

A total number of three samples were tested for each type of core and each impact energy. Five minutes were allowed between subsequent impacts to leave the material a reasonable time to partially recover its initial dimension after the imposed deformation. This choice was made in order to point out the remarkable difference in behavior between PVC foam and agglomerated cork.

2.5.3 Split Hopkinson Pressure Bar tests

Dynamic compression Split Hopkinson Pressure Bar tests were carried out with the apparatus shown in Figure 15 that consists of three aligned bars named pre-stressed, input and output bar. All of them are characterized by a diameter of 18 mm and a length of 3.0 m, 7.5 m and 4.0 m, respectively. The pre-stressed bar is the section of the apparatus where is generated the pressure wave necessary to plastically deform the sample. The bar is statically pre-loaded through an electro-mechanical actuator and when the elastic energy stored is suddenly released the pressure wave is generated. The release of energy occurs thanks to the failure in shear of the sacrificial element placed between the pre-stressed bar and the actuator. The input wave produced is a compressive wave that moves through the input bar in order to be transmitted to the sample placed between the latter and the output bar. The pressure wave travels in the input bar at the sound speed of the bar material. Once the compressive wave deformed the sample with a high strain rate, it is partially transmitted to the output bar and partially reflected back into the output bar. All bars are designed to remain within their elastic limit even when the sample undergoes a large deformation. The strain induced in the sample, by the incident $\varepsilon_i(t)$, reflected $\varepsilon_r(t)$ and transmitted $\varepsilon_t(t)$ waves, is measured by foil strain gage rosettes placed on the input and output bars.
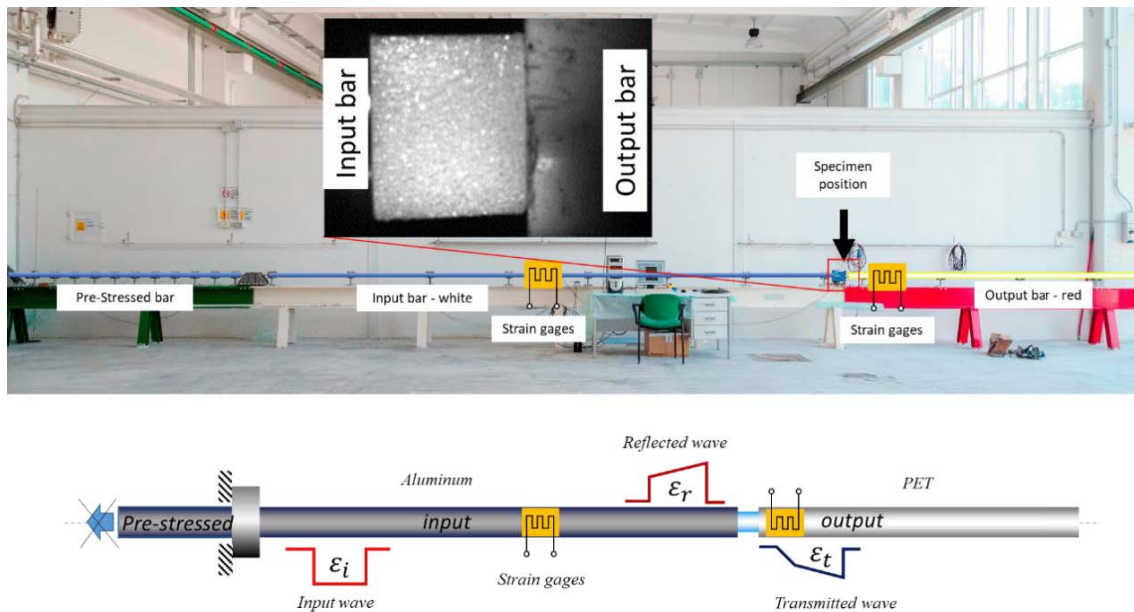
Figure 15: Apparatus employed to perform SHPB tests

The registered signals are used to compute the input (I) and output (O) load of the specimen according to the equations:

$$P_I(t) = E_I \cdot A_I[\varepsilon_I(t) + \varepsilon_R(t)] \tag{2.9}$$

$$P_O(t) = E_O \cdot A_o[\varepsilon_T(t)] \tag{2.10}$$

where E is the elastic modulus and A the cross-section area of the bars. Once calculated the loads, each stress value can be easily determined dividing the load for sample cross section area.

Even the input (I) and output (O) velocities can be computed according to the equations:

$$\dot{u}_I(t) = C_I[\varepsilon_I(t) - \varepsilon_R(t)] \qquad (2.11)$$

$$\dot{u}_O(t) = C_O[\varepsilon_T(t)] \qquad (2.12)$$

where C is the sound speed of the bar material.

Through the integration of equations (2.11) and (2.12), according to equation (2.13), is possible to calculate the engineering strain experienced by the core material:

$$\varepsilon(t) = \frac{1}{L_s} \int_0^t [\dot{u}_I(t) - \dot{u}_O(t)]dt \qquad (2.13)$$

where L_s is specimen length.

As previously mentioned, bars are designed to remain in their elastic limit even when the sample is subjected to large deformation and that is the reason why they are usually made up of a high strength metal. When a soft material, like cork or a polymeric foam, is tested it is necessary to improve system sensitivity, especially for the measurement of loads, and for this reason a polyethylene terephthalate output bar was employed to test both PVC foams and agglomerated corks. Thanks to the reduced stiffness, it is able to achieve measurable strains even when the pressure waves transmitted in the test is weak. For what concerns the pre-stressed and the input bars, the ones employed for agglomerated cork are always made up of PET, whereas the ones employed for the PVC foams are made up of aluminum (AA7075T6). This choice is the best compromise to have a reasonable impedance mismatch between bars and sample that ensures sample deformation and a reasonable amplitude of the signals in both input and output bars. Moreover, this configuration allows to reach high strain rates guaranteeing simultaneously the dynamic equilibrium in the sample. This statement is confirmed for both PVC foams (A) and agglomerated cork (B) by the input and output signals of force, computed according to equations (2.9) and (2.10), shown in Figure 16.
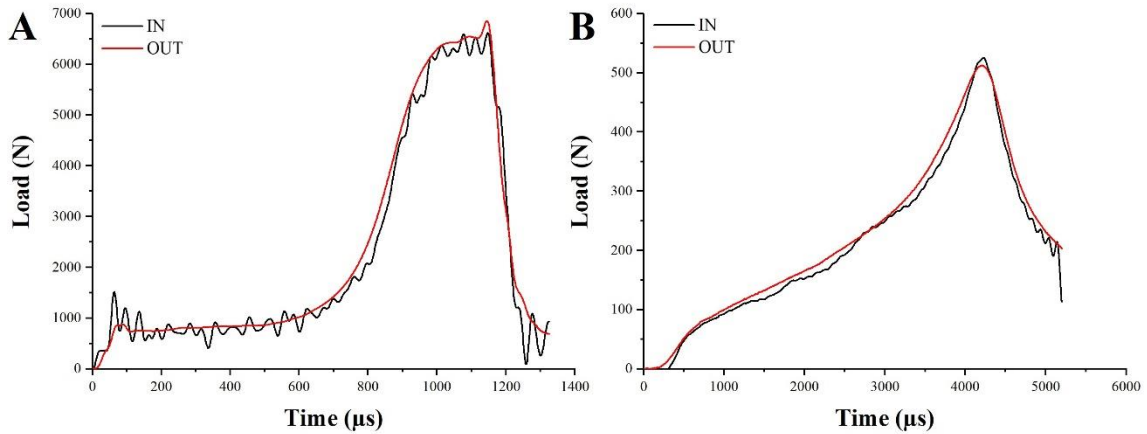
Figure 16: Input and output force signals of the tests carried out at the highest strain rates on PVC foam (A) and agglomerated cork (B).

Average strain rates between 500-1000 1/s were reached in PVC foams testing whereas average strain rates of 150-200 1/s were reached in agglomerated corks testing. In Figure 17 the engineering strain rate as a function of strain is depicted for both PVC foam (A) and agglomerated cork (B) and, as it is possible to observe, it appears reasonably uniform and constant during the deformation after experiencing an initial ramp and a final decrease due to material densification.
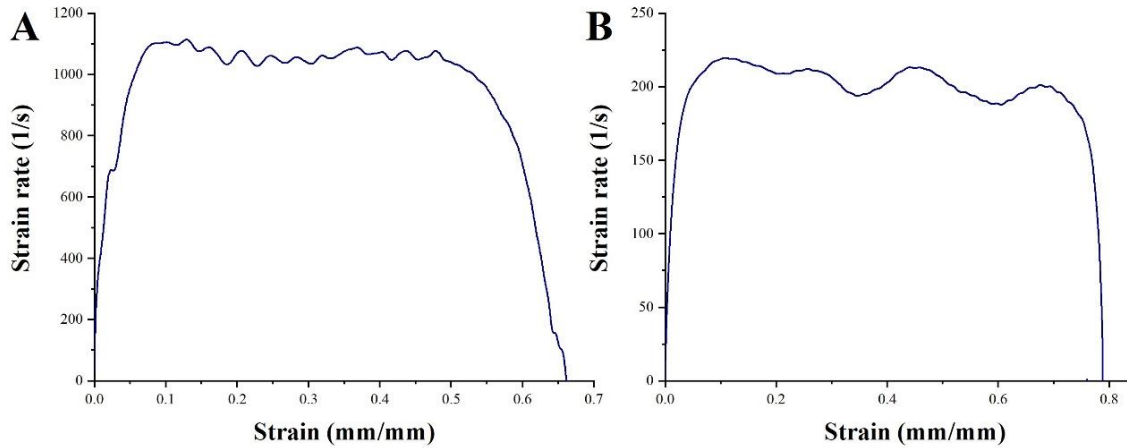
Figure 17: Evidence of strain rate regularity for the tests carried out at the highest strain rates on PVC foam (A) and agglomerated cork (B).

Due to PET viscoelastic nature the elastic modulus E_O, and as a consequence the sound speed C_O, of the output bar are not perfectly constant thus determining an attenuation and dispersion of the travelling wave. In light of this, the dedicated sensor calibration proposed by Martarelli et al. [152] and the post processing procedure proposed by Sasso et al. [153] were employed to overcome the problem. The analytical procedure based on the wave propagation theory was implemented in Matlab® thus permitting to numerically shift backward of forward the waves measured by the rosettes and allowing to compute how the waves appear when they interact with the sample.

SHPB tests were performed on parallelepiped samples, characterized by a height of 15 mm and by a square base with 12 mm of side, addressing the strain rate and the anisotropy effect. For what concerns the strain rate effect, the performed tests allowed to investigate the effect of this parameter on the compressive properties of the core materials in a strain rate range higher than the one achievable with quasi-static compression and drop weight tower dynamic compression. Therefore, the realization of these tests allowed to evaluate cores compressive behavior evolution along a wide range of strain rates thus providing an overview from the low strain rate range to the high strain rate range passing through the medium one. The anisotropy effect was investigated testing the samples along the out of plane and the in-plane directions of the original planks as shown in Figure 18. [A] samples allow to investigate the z-axis compressive properties of the core materials, [B] samples the y-axis properties and [C] samples the x-axis properties. Considering that the preliminary quasi-static compression tests performed to investigate cores anisotropy were performed on cubic samples (15 mm side) and neglecting a potential difference in behaviour between direction [B] and [C], further quasi-static tests were carried out on samples with the same dimensions employed in the SHPB tests (15mm height and square base with 12 mm side) and considering both orientations. Tests were carried out with a pneumatic testing machine Si-plan® equipped with a 3 kN load cell and employing three nominal strain rates, i.e. $10^{-3}, 10^{-1}$ and 10 s^{-1}. A minimum number of three samples was tested in every operating condition.
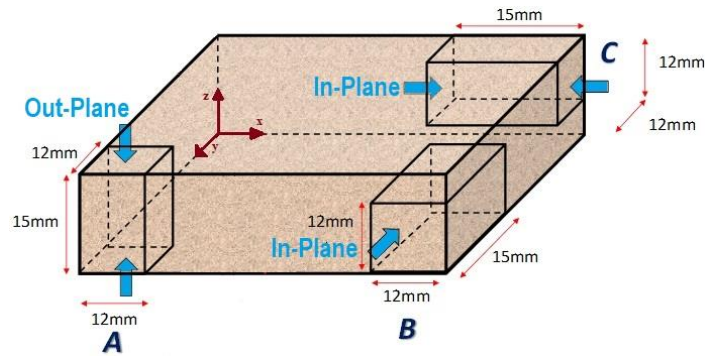
Figure 18: Specimens orientations employed to examine a potential anisotropy of cores compressive behavior. The arrows indicate test direction and the specific property under consideration (in-plane/out-of-plane)

2.5.4 Puncture impact tests

Puncture impact tests were carried out at room temperature in an instrumented drop weight tower Instron Ceast 9340 equipped with the CEAST Data Acquisition Systems DAS 64K that allows to record all the data acquired by the load cell during the impact and the actual initial velocity of the impactor thanks to an optical sensor placed just above the impacted area. From the force record acquired, velocity, displacement and energy records can be extrapolated thanks to an integration process performed directly by the data system. Square samples with 100 mm of side and 15 mm of thickness were tested with a hemispherical impactor characterized by a 12.7 mm diameter and an overall mass of 3.055 kg, as shown in Figure 19.A. The sample is placed on a circular hollow base support with an inner diameter of 40 mm, as shown in Figure 19.B, and is fixed to it through a pneumatic clamping system. The tower is also equipped with an anti-rebound system that blocks the impactor after the first rebound preventing a second impact that could compromise the results of the post-impact analysis.
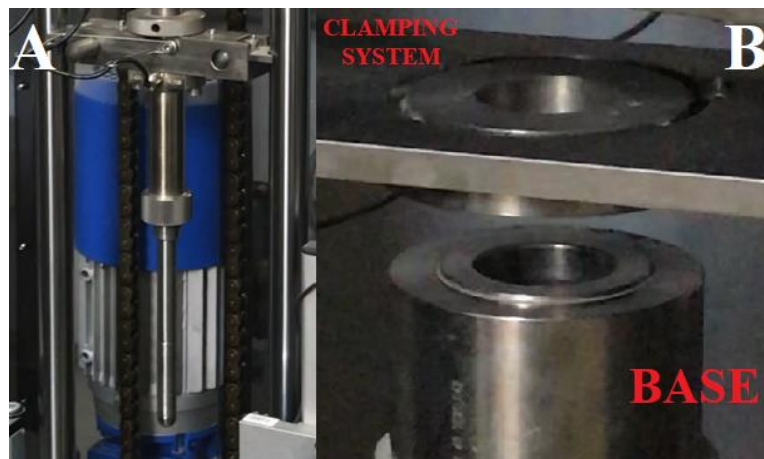
Figure 19: Impactor (A) and circular base support (B) employed to perform puncture tests

After some preliminary impacts which allowed to identify energy perforation threshold, agglomerated cork cores were tested at three different energies: perforation energy (5 J), 50 % (2.5 J) and 25 % (1 J) of perforation energy. For what concerns the PVC foams, they were

impacted at the same energies used for agglomerated cork, in order to provide a direct comparison of the results obtained, but also at increasing energies until their perforation energy was detected. A summary of the impact energies employed for each core material is given in Table 9. Three samples were tested for each core type and each impact energy.

Table 9: Impact energies selected to test the core materials

Samples	1 J	2.5 J	5 J	10 J	15 J	17.5 J
NL10	X	X	X			
NL20	X	X	X			
NL25	X	X	X			
HP130	X	X	X	X		
HP200	X	X	X	X	X	
HP250	X	X	X	X	X	X

In order to evaluate the damage extent produced by the impact, samples were subjected to a post-impact analysis and, in particular a, profilometric analysis that allowed to quantify the residual indentation depth. This analysis was executed with the laser profilometer Talyscan 150 by Taylor Hobson and the scanned image was processed and analyzed through the software TalyMap 3D. Profilometric analysis could be performed only on PVC foams samples, but not on agglomerated corks ones because of the remarkable recovery capability of the green core material that tends to cancel the indentation already after a short lapse of time from the impact. A typical PVC foam profile obtained by scanned image processing is shown in Figure 20.
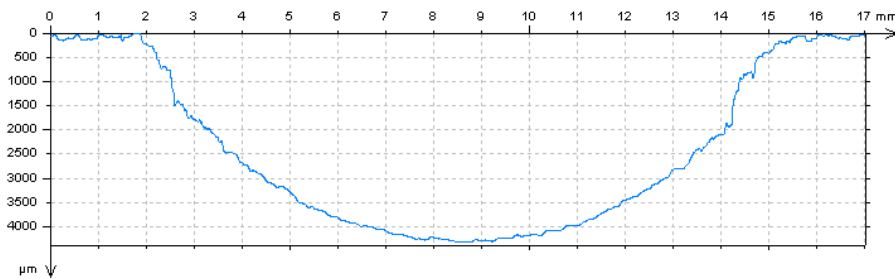
Figure 20: Profile of the indentation depth of a HP250 sample impacted at 5 J.

2.5.5 Puncture Multiple-Impacts tests

Puncture multiple-impacts tests were carried out at room temperature employing the same tower and the same set up previously introduced for the single puncture impact tests. The most suitable impact energies to carry out the experimental campaign were selected on the basis of the single impact test results. Considering that all three agglomerated corks are characterized by a perforation threshold of 5 J, all core materials were tested at 25 % and 50 % of agglomerated corks perforation energy, namely 1.25 J and 2.5 J, in order to provide a direct comparison between PVC foams and agglomerated cork response. Moreover, in view of the higher perforation threshold of the polymeric foams, namely 10 J for HP130, 15 J for HP200 and 17.5 for J HP250, each of them was also tested at 25 % and 50 % of its perforation threshold. An overview of all impact energies employed is given in Table 10. Three samples were tested for each core type and each impact energy.

In order to study the evolution of the residual indentation depth, and as a consequence of the damage extent, as a function of the number of impacts, all PVC foams underwent a profilometric post-impact analysis after every impact with the same equipment previously introduced for the single impact configuration. One hour was allowed between subsequent impacts in order to leave enough time to carry out the post-impact analysis.

Table 10: Overview of the impact energies selected to carry out multiple puncture impacts

Samples	1.25 J	2.5 J	25 % of Perforation Threshold (P.T.)	50 % of Perforation Threshold (P.T.)
NL10	25 % P.T.	50 % P.T.	-	-
NL20	25 % P.T.	50 % P.T.	-	-
NL25	25 % P.T.	50 % P.T.	-	-
HP130	X	25 % P.T.	-	5 J
HP200	X	X	3.75 J	7.5 J
HP250	X	X	4.35 J	8.75 J

2.5.6 Impact tests with CAI support

CAI support impact tests were carried in a drop weight tower Ceast Fractovis® on parallelepiped samples with a length of 150 mm, a width of 100 mm and a thickness of 15 mm. Samples were placed on a rectangular hollow support with inner dimensions of 75 mm by 125 mm and were clamped to it through four manual handles placed at the corners of the samples as shown in Figure 21. Considering the soft nature of cork, an aluminum frame, characterized by outer dimensions coinciding with sample ones, inner dimensions coinciding with rectangular hole ones and a thickness of 0.4 mm, was inserted between the sample and the handles in order to prevent local indentation of the sample that could have altered the impact response. A hemispherical impactor with a diameter of 12.7 mm and an overall mass of 6.763 kg was employed to perform the test.
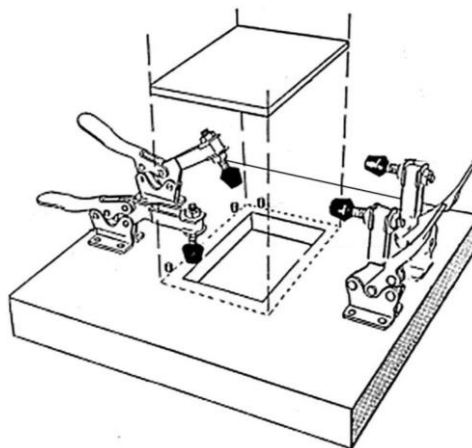
Figure 21: Schematization of the CAI support employed to impact the core materials [154]

The energy profile diagram technique was employed to pinpoint the perforation energy of each core material. An energy profile diagram is a graph that allows to monitor the evolution of the energy absorbed by the material against the impact energy and that permits to identify the perforation threshold thanks to its peculiar shape shown in Figure 22. The diagram can be divided

in three regions: no penetration region (I), penetration region (II) and perforation region (III) [155]. In the first region the curve is characterized by a parabolic shape and is located below the equal energy line meaning that the energy dissipated by the sample is lower than impact one. The residual impact energy returns to the impactor to make it rebound. In the second region the curve coincides with the equal energy line meaning that all impact energy is dissipated by the sample and that the impactor sticks into the sample. This region ends when sample perforation takes place. In the third region sample perforation always occurs and the energy dissipated is constant and coincides to the perforation threshold energy, located at the beginning of this region, that is the maximum energy that the material is able to absorb. Therefore, perforation energy can be identified as the point resulting from the intersection of the horizontal line in the third region and the curve from the first two regions [155]. It is necessary to make one point on both region II and III. For what concerns region II, its extension can vary significantly as a function of the material under study degenerating in a point in the most critic cases like some of those presented by Sayer et al. [156]. For what concerns region III, it is necessary to highlight that a certain dispersion in the absorbed energy data could be detected due to the randomness of the damage caused by the impactor. Two examples of the implementation of this technique to identify core materials perforation threshold is given in Figure 23. Once pinpointed the perforation threshold, each core material was tested at 75 %, 50 % and 25 % of its perforation energy in order to investigate impact response and damage evolution as a function of the impact energy.
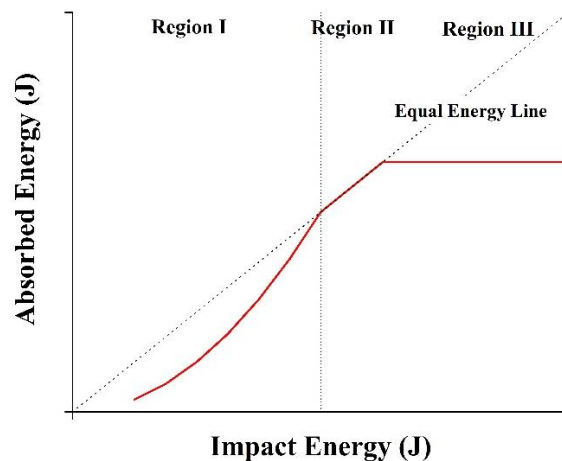
Figure 22: General schematization of an energy profile diagram
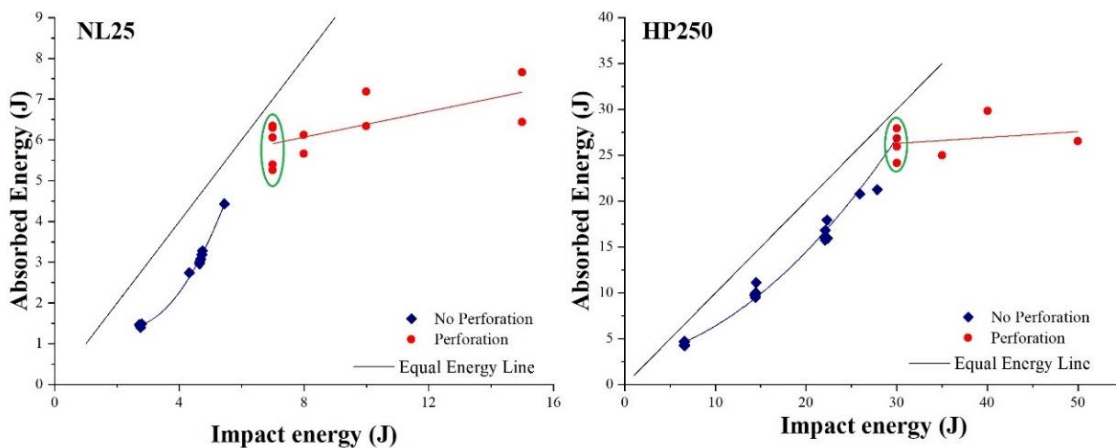
Figure 23: Two examples of energy profile diagram at room temperature employed to identify NL25 agglomerated cork and HP250 PVC foam perforation threshold

76

The employment of the energy profile diagram and the fulfilment of the experimental campaign illustrated for the CAI impact tests was carried out not only at room temperature, but also at extremely low (-40 °C) and high (60 °C) temperatures in order to investigate the influence of this further operating parameter. The climatic chamber incorporated in the tower and equipped with both nitrogen cooling connectors and heaters permitted to reach the desired temperatures. Every sample plate was pre-conditioned for two hours at the operating temperature to ensure a homogeneous temperature profile across the specimen. A minimum number of five samples was tested in each testing condition.

Once terminated the impact campaign, a post impact analysis was carried out on the samples in order to determine the damage extent on both front and back side. Front side analysis provides for a profilometric analysis apt to quantify the residual indentation depth left by the impactor. As previously said for puncture impact tests, this analysis was carried out with the laser profilometer Talyscan 150 by Taylor Hobson and could be performed only on PVC foam samples because agglomerated cork indentation tends to fade after a short time from the impact because of its remarkable recovery capability. Back side analysis aimed to detect and quantify the extent of the fracture produced on the back side of the sample pursuant to the bending induced by the impact. The analysis was carried out with a two steps process. The first step aims to highlight the crack in order to make it easily detectable. Unfortunately, the traditional Dye Penetrant Inspection method could not be employed because of the porous nature of the PVC foam that would have led to an uncontrolled infiltration of the penetrating liquid along the whole surface of the sample. For this reason, the crack was locally infiltrated with a red paint, that was manually applied through the help of a syringe, making it easily detectable. Once highlighted the fracture, every sample was photographed and the resulting image was processed with the program Image J that allows to measure the length of the crack as shown in Figure 24.
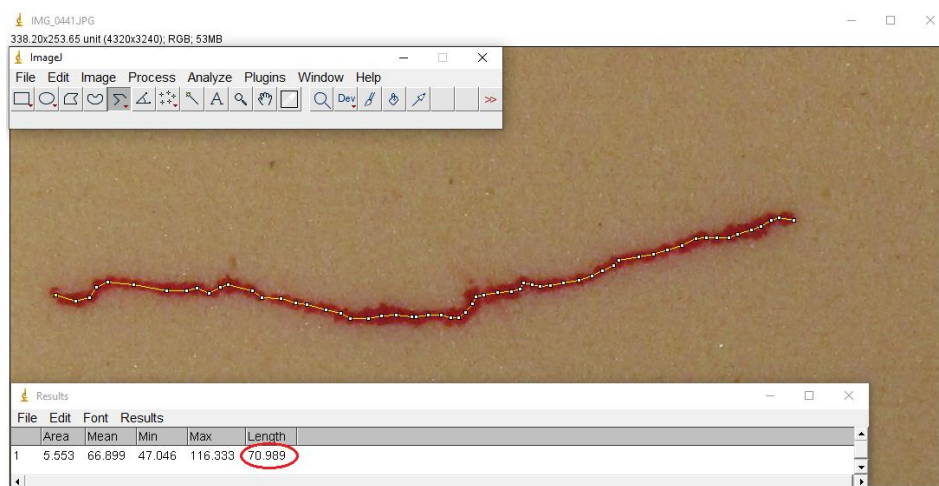
Figure 24: Example of the procedure employed to measure samples back fracture extension through the program Image J

2.5.7 Ballistic impact test

Ballistic impact tests were performed on square samples with 100 mm of side and 15 mm of thickness with a gas gun, shown in Figure 25, fed with a gas blend of Ar and CO_2 and with a spherical projectile made of steel and characterized by a weight of 1.7 g and a diameter of 7.5 mm.

Figure 25: Gus gun and projectile used to perform ballistic impact tests

All impacts were recorded with a high-speed camera by Photron®, Fastcam SA-Z, and the resulting video was processed with the program Photron FASTCAM Viewer 3 to compute the impact velocity of the projectile, V_{imp}, and its residual velocity after the impact, V_{res}. A minimum number of 15 samples was impacted for each core type and the resulting set of data was plotted and used to estimate the ballistic limit applying the Lambert-Jonas correlation [157]:

$$V_{res} = a(V_{imp}^2 - V_{bl}^2)^{\frac{1}{2}} \qquad (2.14)$$

In this correlation V_{imp} and V_{res} are the known velocity values obtained by test video processing whereas a and V_{bl}, ballistic limit, are two unknown parameters that can be calculated through an error minimization process. The Lambert-Jonas correlation and error minimization process were applied to the impact and residual velocity data set taking advantage of the program Kaleida Graphs and the ballistic limit of each core material was calculated.

Even for ballistic impact tests a post impact analysis was performed on the specimens in order to evaluate core material damage extension as a function of impact velocity. The damage area extension was quantified through the image processing program Image J applying the procedure shown in Figure 26.
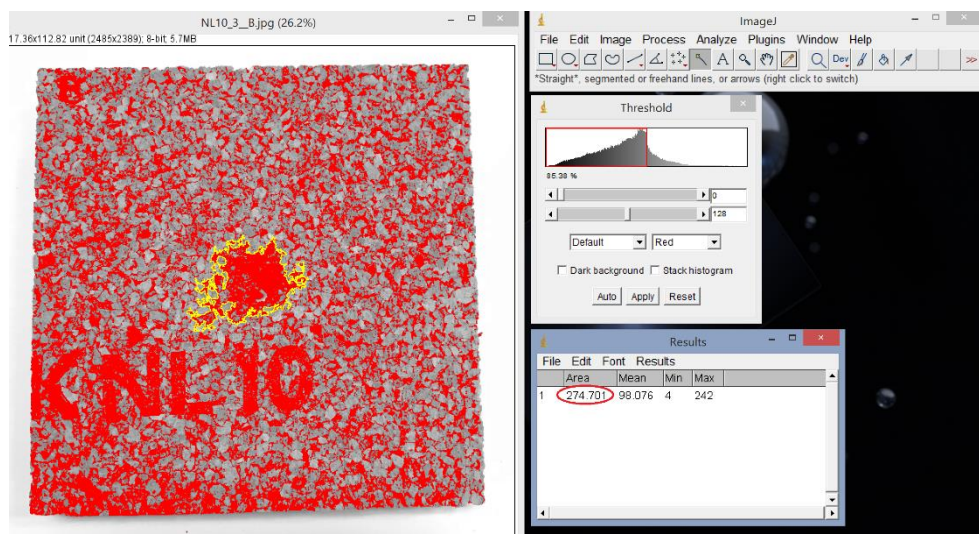
Figure 26: Example of the procedure employed to measure the damage area through the program Image J

Once modified the impacted sample image in a black and white image, it is possible to perform a thresholding process that is an image segmentation that converts an image from color or grayscale in a binary image. This process is largely employed to highlight and select areas of interest of an image thus turning out to be perfect to identify the damage area that, once pinpointed, can be measured automatically by the program.

2.5.8 Finite Element Analysis (FEA)

On the basis of the results obtained, agglomerated cork NL25 and PVC foam HP130 were selected to reproduce numerically the puncture impact tests. The setup used to carry out the finite element analysis is shown in Figure 27 and consists of a square plate characterized by the same dimensions of the experimental specimen and of a half sphere that models the steel impactor. Once arranged the impact conditions, the non-linear explicit dynamic solver LS-DYNA was used to carry out the simulation.
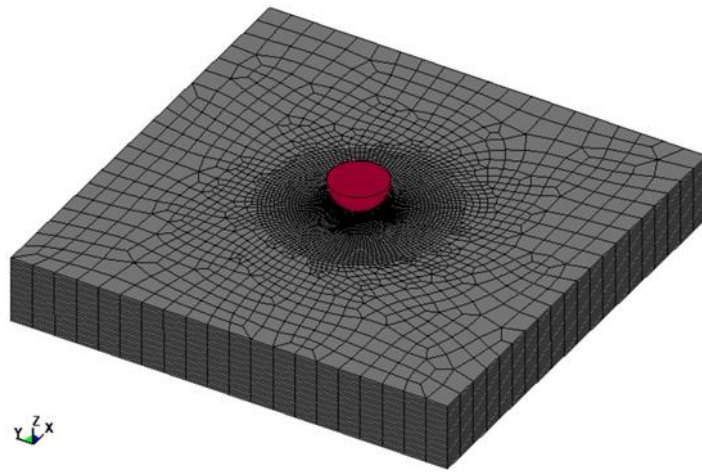
Figure 27: Numerical setup used to simulate puncture impact tests

Concerning the finite element model, both PVC foam and agglomerated cork were discretized with eight-node brick elements. Warped and distorted elements were accurately avoided when creating the meshes and particular attention was paid to element size in order to achieve reliable results not influenced by mesh size, but at the same time keeping reasonable the computational time. The hemispherical impactor was modelled with rigid tetrahedral elements and is characterized only by one degree of freedom, the direction of impact, as happens in the experiments. More complex was the mesh of the sample in fact several simulations had to be performed increasing elements number to reach results convergence and to define the optimal number of elements. In order to improve results accuracy, a finer mesh of 0.3 mm per side was employed in the impact region, as it is possible to observe from Figure 27.

Sample boundary conditions were also included in the simulation to reproduce the same clamping conditions used in the experiments. A node-to-surface contact was used to model the interaction between the rigid body and the sample. To model such interaction, a friction coefficient of 0.2 was selected in agreement with the work of Fernandes et al. [150] that used this value to model cork/steel interaction. The same friction coefficient was adopted for the foam, but an AUTOMATIC_SINGLE_SURFACE was included in this case to avoid inner penetrations during crushing.

The different impact energies were modelled keeping constant impactor mass and changing its initial velocity. Several built-in material models are available in LS-DYNA to model a huge variety of foams, but MAT63-CRUSHABLE_FOAM seemed to provide the best results for both PVC foam and agglomerated cork after trying various solutions. MAT63 material type permits to model cork cellular structure allowing core material compression when impacted, as expected for the air cells that characterize cork structure. MAT63 was designed to model crushable foam and is commonly employed to model polystyrene in dynamic impact simulations [158]. The unloading of this material type was treated as fully elastic and tension is defined as elastic-perfectly plastic at the tension cut-off value. Element deletion during crushing was reproduced by adding MAT_ADD_EROSION card to the finite element model.

2.6 Skin and Sandwich Composites Thermal and Quasi-Static Characterization

2.6.1 Thermal analysis

Skins thermal stability was investigated by thermogravimetric analysis (TGA) employing a SDT Q600 thermogravimetric analyzer by TA Instruments. Samples were heated from room temperature up to 1000 °C in a nitrogen atmosphere with a flow of 100 ml/min and with a heating rate of 10 °C/min.

Skins were also analyzed through differential scanning calorimetry (DSC) using a TA DSC 2920 calorimeter by TA Instruments. Samples were heated from −40 °C up to 200 °C and were then cooled following the same path with a heating rate of 10 °C/min. Before starting the measurement, samples were hold at -40 °C for five minutes. Such low temperatures were reached with a nitrogen cooled cell and a flow rate of 70 mL min^{-1}.

2.6.2 Tensile tests

Skins were tensile tested in agreement with ASTM D3039 in an Instron 5584 machine equipped with a 150 kN loading cell and with extensometers that allows to obtain a direct and more accurate extension measurement. Extensometers are characterized by sensor arms that are in direct mechanical contact with the specimen through knife-edges. Tested samples were obtained by cutting rectangular samples with a length of 150 mm and a width of 20 mm from the hot compression molded laminates. A test speed of 2.5 mm/min, a gauge length of 40 mm, a grip-to-grip separation of 70 mm and a preload of 1 MPa were used in the tests. PP and PPC samples were tested along both basalt and flax directions in order to point out differences due to fiber nature and fiber volume fraction. Five samples for each configuration were tested.

Once tensile tested, skin samples were subjected to a fracture surface analysis in order to assess the effect of the coupling agent on fiber-matrix interface and, as a consequence, on the mechanical response of the skin. Fracture surface was observed by means of a field-emission scanning electron microscope (FE-SEM) MIRA 3 by Tescan. In light of the low electrical conductivity of both PP matrix and basalt and flax fibers, all samples were sputter coated with a thin layer of gold to prevent charging and to improve micrograph quality. As previously seen for core materials, the coating process was carried out in vacuum conditions (0.4 mbar) for 2 minutes by a sputter coater

Edwards S150B applying a voltage of 1 kV and an electrical current of 40 mA to the gold electrode.

2.6.3 Bending tests

Both skins and sandwich composites were subjected to three-point bending tests in order to evaluate their flexural properties. Flexural tests were carried out on a Zwick/Roell Z010 universal testing machine equipped with a 10 kN load cell. For what concerns the skins, the tests were performed in agreement with ASTM D790 on rectangular samples with a length of 125 mm and a width of 20 mm. In order to improve flexural strain accuracy, the testing machine was equipped with a sensor arm connected with an automatic extensometer. A span length of 80 mm, tips with 5 mm of radius, a preload of 2 MPa and a test speed of 5 mm/min were employed in the tests. As previously seen for tensile tests, skin samples were tested with two different orientations, namely once with flax fibers along the longitudinal direction and once with basalt ones. Five samples for each configuration were tested. Even in this case, the effect of coupling agent on fiber-matrix interface was studied observing the gold sputter coated fracture surface of the samples with the field-emission scanning electron microscope (FE-SEM) MIRA 3 by Tescan.

For what concerns sandwich composites, tests were performed in agreement with ASTM D7250 on parallelepiped samples with a length of 250 mm, a width of 50 mm and an average thickness of 19.5 mm. A span length of 150 mm, tips with 10 mm of radius, a preload of 0.5 MPa and a test speed of 6 mm/min were employed in the tests. Considering that flexural properties are the point of strength of sandwich structures and in order to have an overview of the performance achievable, this part of the experimental campaign was carried out on all possible sandwich structure configurations achievable with the skins and core materials under study. A summary of the tested configurations is given in Table 11. Three samples for each configuration were tested.

Table 11: Sandwich composites configurations tested in three-point bending conditions

	PP	PPC
NL10	PP_NL10	PPC_NL10
NL20	PP_NL20	PPC_NL20
NL25	PP_NL25	PPC_NL25
HP130	PP_HP130	PPC_HP130
HP200	PP_HP200	PPC_HP200
HP250	PP_HP250	PPC_HP250

2.7 Skin and Sandwich Composites Dynamic Characterization

2.7.1 Puncture impact tests

Puncture impact tests were carried out for both skins and sandwich structures at room temperature in the instrumented drop weight tower Instron Ceast 9340 equipped with the CEAST Data Acquisition Systems DAS 64K already introduced for core testing. Tests were performed using

the same setup previously illustrated for core materials, the only difference is in impactor mass that was increased to 8.055 kg. The increase in impactor mass has to be ascribed to the need of reaching higher impact energies that otherwise would not be achievable because of tower height upper limit. Tests were carried out on square samples with 100 mm of side. For what concerns the skins, they were tested in a range of impact energies between 5 J and 30 J, as summarized in Table 12. Three samples were tested for each impact energy.

Table 12: Impact energies used to test skin samples in puncture impact conditions

Samples	5 J	10 J	15 J	20 J	30 J
PP	X	X	X	X	X
PPC	X	X	X	X	

With regard to sandwich composites, four different configurations were considered employing both PP and PPC skins and NL25 agglomerated cork and HP130 PVC foam. Tests were performed in a range of impact energies between 20 J and 80 J, as summarized in Table 13. Three samples were tested for each impact energy.

Table 13: Impact energies used to test sandwich composites in puncture impact conditions

Samples	20J	30J	40J	60J	80J
PP_NL25	X	X	X	X	X
PPC_NL25	X	X	X	X	
PP_HP130	X	X	X	X	X
PPC_HP130	X	X	X	X	

After the impact campaign skin and sandwich samples underwent a post impact analysis to evaluate impact damage extent. The permanent indentation depth left by the impactor on both skins and sandwich composites was measured through the laser profilometer Talyscan 150 by Taylor Hobson. Sandwich structures were further analyzed by cutting in half the sample in order to have a direct observation of the damage left by the impactor in the inner parts of the composite.

2.7.2 Impact tests with CAI support

CAI support impact tests on skins were carried out in the drop weight tower Ceast Fractovis® previously introduced for core samples employing the same support, shown in Figure 21, and the same impactor with the same mass. Skin samples are always characterized by a length of 150 mm, a width of 100 mm. For core testing, an aluminum frame was inserted between the sample and the clamping system in order to avoid local indentation of the sample spreading the clamping force across its whole surface. The use of this frame appears inevitable for core materials testing, in particular for agglomerated cork, but it is necessary to highlight that its employment modifies sample boundary conditions making them more severe and restrictive. In light of this, the aluminum frame was employed even for skin testing in order to keep the same boundary conditions of core testing. As already done for cores, energy profile diagrams were employed to detect the perforation energy and as a consequence the 75 %, 50 % and 25 % perforation energies necessary to investigate impact response and damage evolution as a function of impact energy. Energy profile diagrams of PP and PPC tested at room temperature are shown in Figure 28.
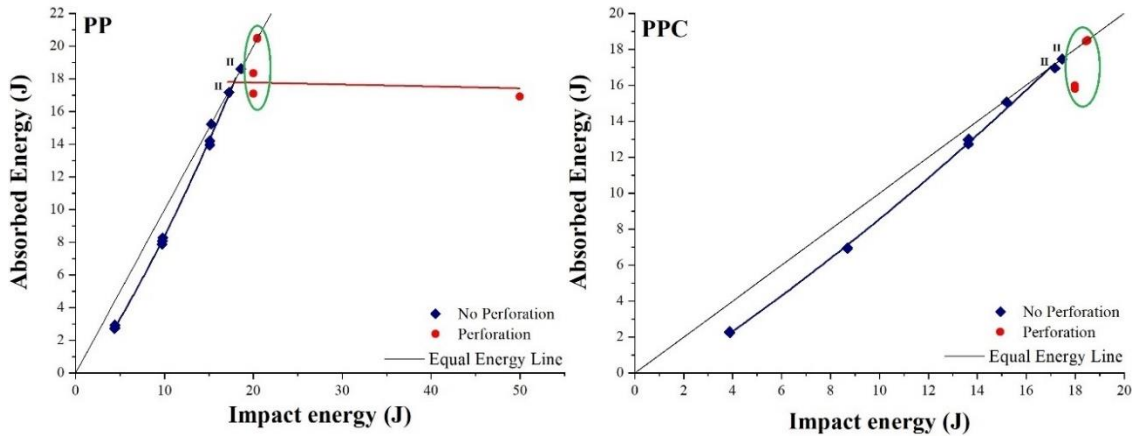
Figure 28: Energy profile diagram at room temperature employed to identify PP and PPC perforation threshold

Skins impact tests with CAI support were performed at room temperature and at extremely low (-40 °C) and high (60 °C) temperatures taking advantage of the climatic chamber incorporated in the tower and pre-conditioning samples for two hours at the desired temperature to ensure a homogeneous temperature profile across the specimen. A minimum number of three samples was tested in each testing condition.

CAI support impact tests on sandwich structures were carried out in the drop weight tower Instron Ceast 9340 equipped with the CEAST Data Acquisition Systems DAS 64K. The same support employed for cores and skins testing was applied and the same hemispherical impactor with a mass of 12.055 kg was used. The same sample dimensions (150 mm length and 100 mm width) were considered. Six different sandwich configurations were considered, as previously described in Table 6, employing three different core materials NL10 and NL25 agglomerated corks and HP130 PVC foams and the two types of skins PP and PPC. Even in this case energy profile diagrams were employed to detect the perforation energy and the 75 %, 50 % and 25 % perforation energies and the results obtained at room temperature for all sandwich structures are summarized in Figure 29.

The tests at low and high temperatures, i.e. -40 °C and 60 °C, were performed pre-conditioning the samples for two hours at the desired temperature in the climatic chamber by Instron equipped in the tower.

After the impact campaign sandwich samples were subjected to a post impact analysis to evaluate impact damage extent by cutting in half the sample in order to have a direct observation of the damage left by the impactor in the inner parts of the composite.

2.7.3 Ballistic impact test

The same equipment, the same sample geometry and the same setup previously introduced for core materials were employed to perform skins and sandwich structures ballistic impacts. The only difference is in the gas employed to test sandwich structures in fact helium at high-pressure was needed as propellant gas to reach the higher impact velocities. Even in this case six different sandwich configurations were considered, as previously described in Table 6, employing the three core materials NL10 and NL25 agglomerated corks and HP130 PVC foams and the two types of skins PP and PPC.
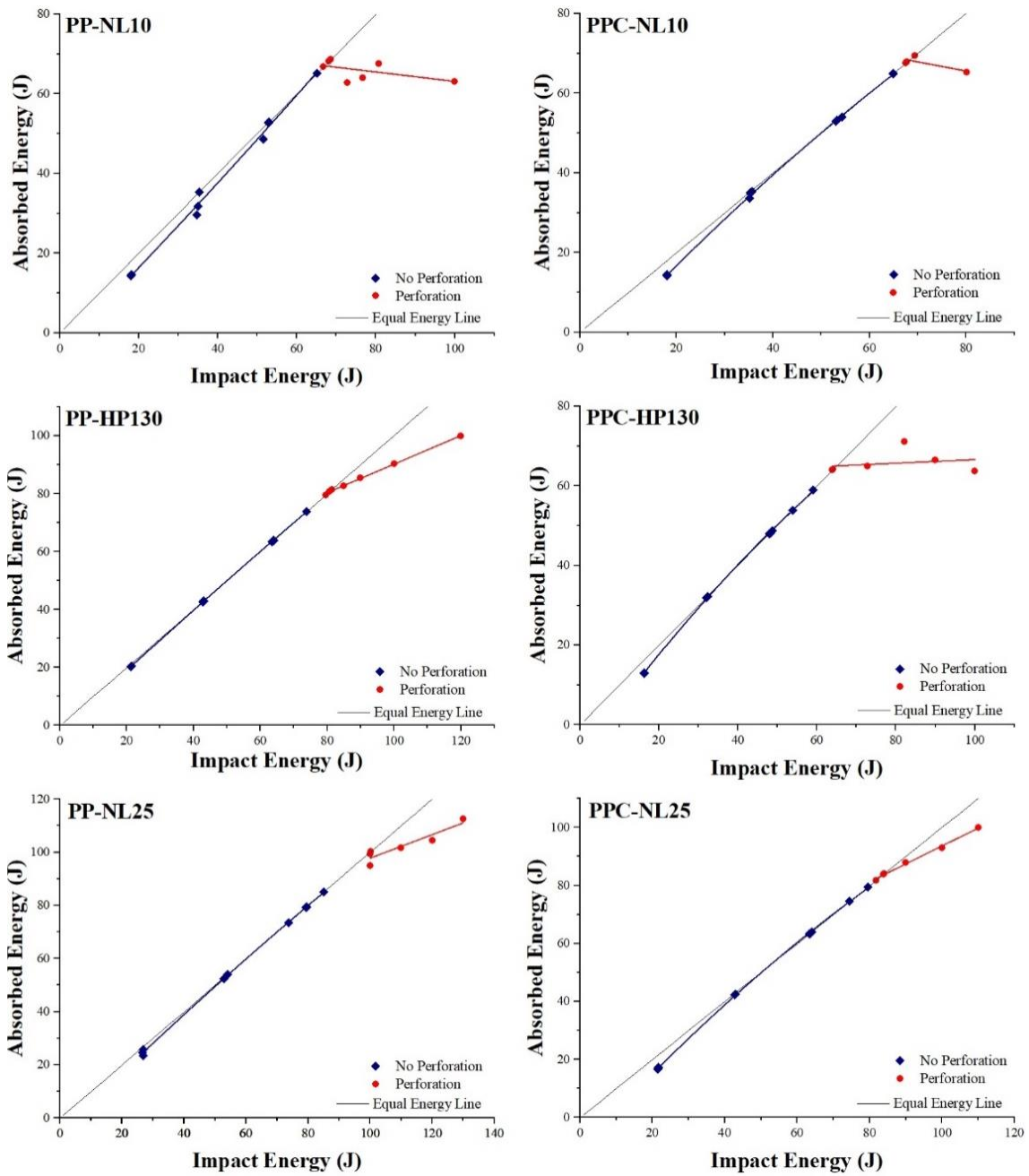
Figure 29: Energy profile diagram at room temperature for all six sandwich structures configurations

Chapter 3: Core Characterization

3.1 Morphological Characterization

3.1.1 Scanning Electron Microscopy

Cork is a natural cellular material and its closed cells are characterized by thin walls. It is characterized by an alveolar structure that is extremely regular and symmetric, like the one of honeycomb, and does not present intercellular voids. Three main directions, i.e. radial, tangential and axial directions, can be identified in cork microstructure and they can be easily distinguished one from the other thanks to cell shape. Cork closed cells are characterized by a prismatic geometry and by a polygonal base whose number of edges can vary from four to nine. The prismatic cells are stacked base-to-base along the radial direction meaning that the observation of cork in this direction leads to the identification of a polygonal shape. Instead, a brick-layered structure, caused by cells parallel arrangement, characterizes the observation of tangential and axial directions [35–38].

The microstructure of cork, described and observed in previous studies, was identified and recognized even in this study through the morphological analysis carried out on agglomerated cork. Figure 30.A shows the typical polygonal shape that characterizes prism base and reveals the radial orientation of the cells. Instead, Figure 30.B displays the common brick-layered structure that characterizes the tangential and axial directions. Figure 30 also allows to observe another key feature that is responsible for cork remarkable recovery capability, i.e. cell walls undulation. When cork is subjected to a compression load, its cell walls undergo buckling and their corrugation starts to increase progressively. This leads to cells densification or collapse but does not imply a significant damage or a severe permanent deformation in fact cell walls are free to unfold once removed the compression load thus leading to an exceptional dimensional recovery.
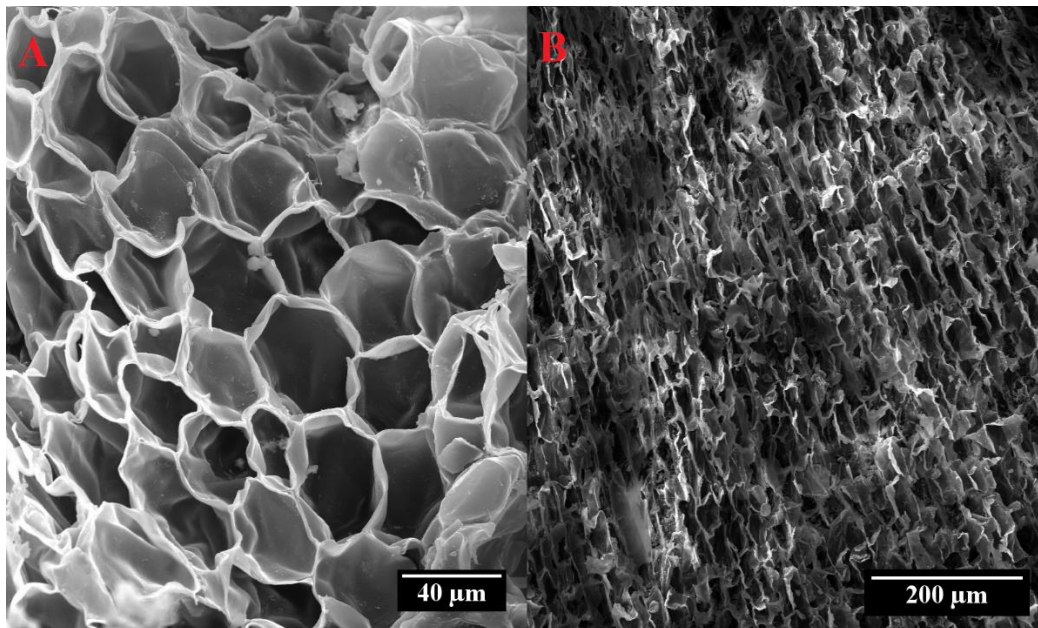
Figure 30: Identification of the radial direction (A) and of the axial/tangential directions (B) from a NL20 and NL25 micrographs, respectively

As previously mentioned, prism polygonal base is characterized by a number of edges ranging from four to nine, but pentagonal, hexagonal and heptagonal shapes are the most frequent from a statistical point of view [36,38] as also confirmed by the micrograph shown in Figure 31.
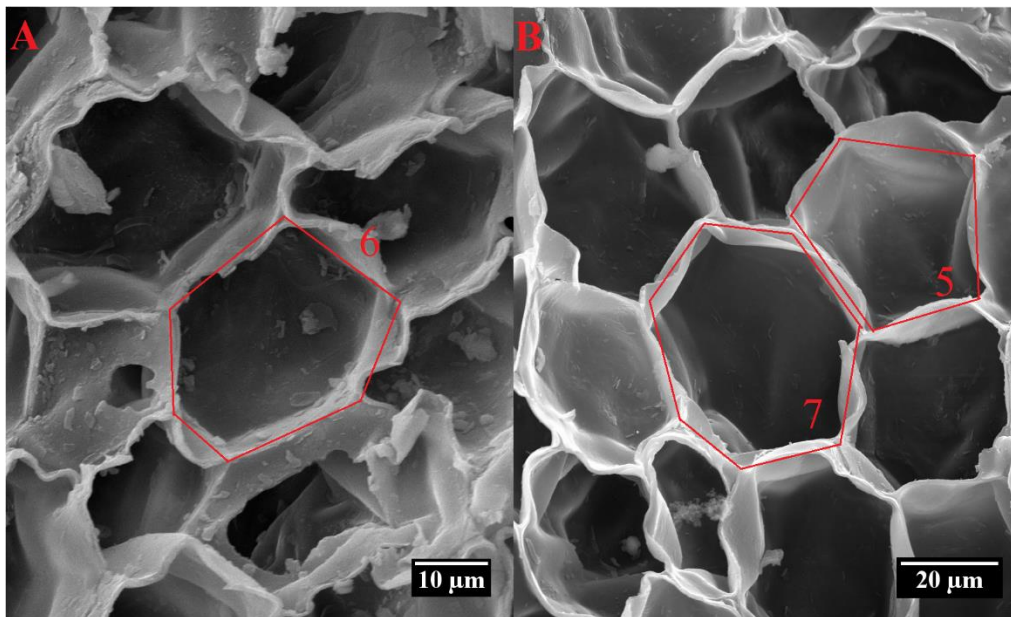
Figure 31: Hexagonal (A), heptagonal and pentagonal (B) prism bases from a NL10 and a NL20 micrographs, respectively

The average cell-wall thickness values available in literature range between 1-1.5 mm for early cork [35,37] and up to 2 mm for late cork [36]. In this work cork cell wall thickness was evaluated through the program Image J as shown in Figure 32 for all NL10, NL20 and NL25. The data obtained are in perfect agreement with those reported in literature.
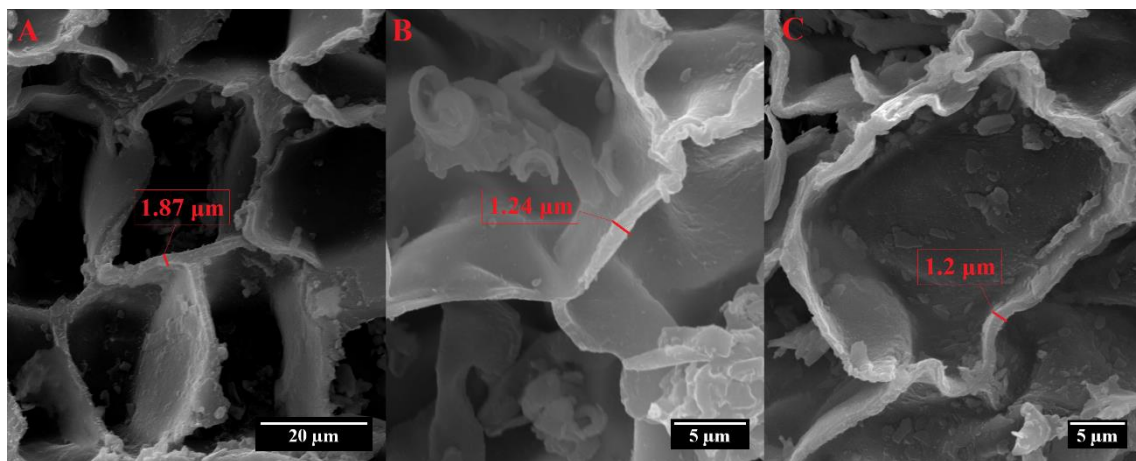
Figure 32: Cell-wall thickness evaluation for NL10 (A), NL20 (B), and NL25 (C)

All the observations made up to now concerns generically natural cork and its derivatives, but in this research work agglomerated cork and not natural cork was selected as core material meaning that cork granules are bonded together through a polymeric binder, and in particular a polyurethane binder. The morphological analysis allowed to point out even this feature

86

identifying the boundary region between two adjacent granules as shown in Figure 33. The transition region from one cork granule to another can be recognized not only by the presence of the polymeric binder but also by a different shape of the cells, hence by a different orientation of the granules.
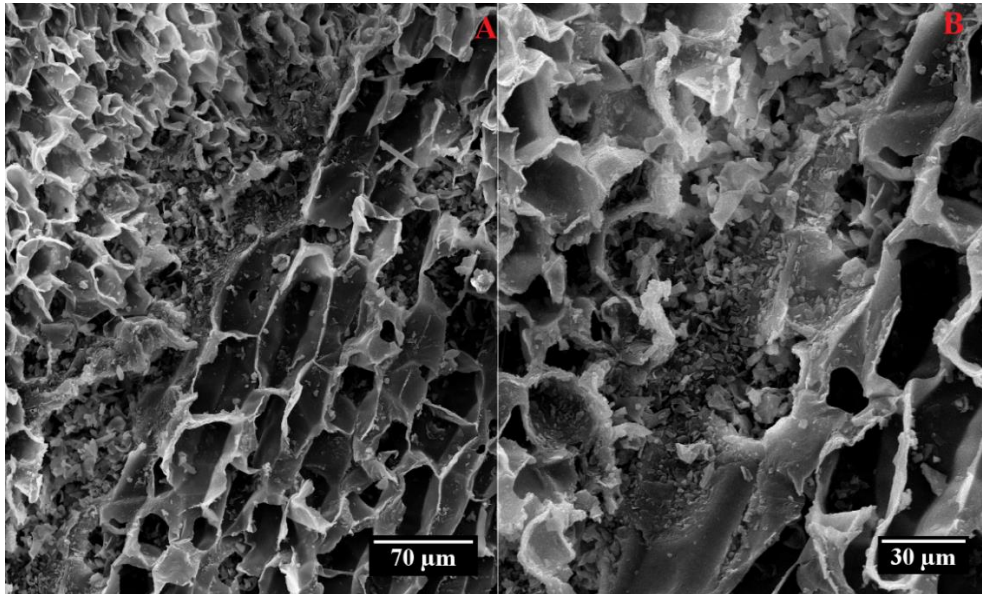
Figure 33: Boundary region between two adjacent cork granules (A) and blow-up on the polyurethane binder (B) in a NL10 sample

Moving on to the polymeric foams, in Figure 34 is shown the typical closed-cell microstructure of the PVC foams under study. This connotative architecture was already acknowledged by Lim and Altstädt [159] and by Colloca et al. [160], who found out that an increase in foam density leads to an increment in cell walls thickness and to a reduction of cells size. If the denser foams, i.e. HP200 and HP250, are characterized by bulky cell walls that clearly outline the confines between two cells, the lighter foam HP130 is characterized very thin walls surrounded by highly porous areas that separates different cells, as shown in Figure 35.
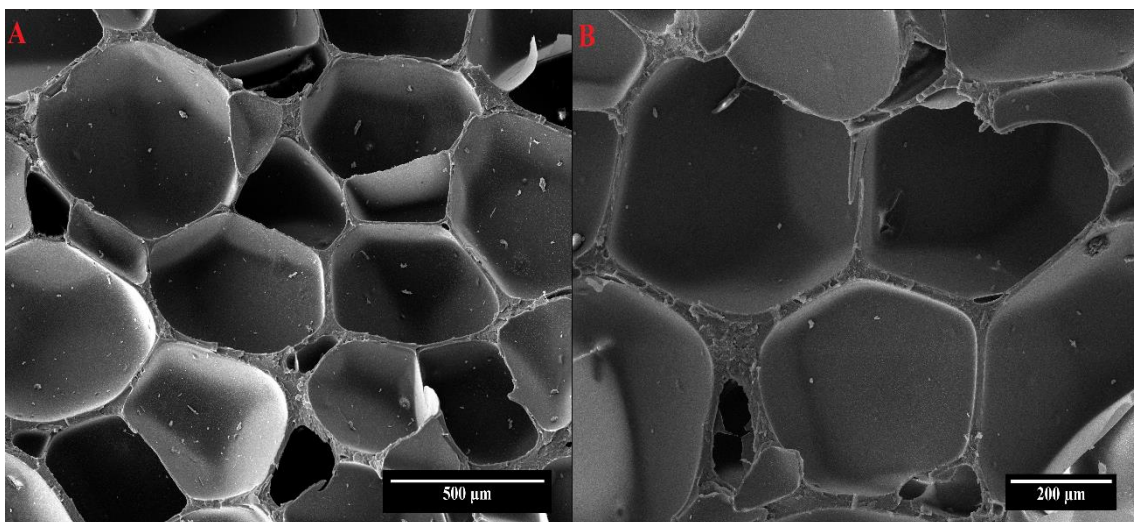
Figure 34: Typical closed-cell microstructure of HP250 (A) and HP200 (B)

The presence of smaller closed cells that surround the main ones, is due to the production process in fact to reach the low density values required for foams like HP130, a higher amount of gas needs to be inflated in the polymer mass.
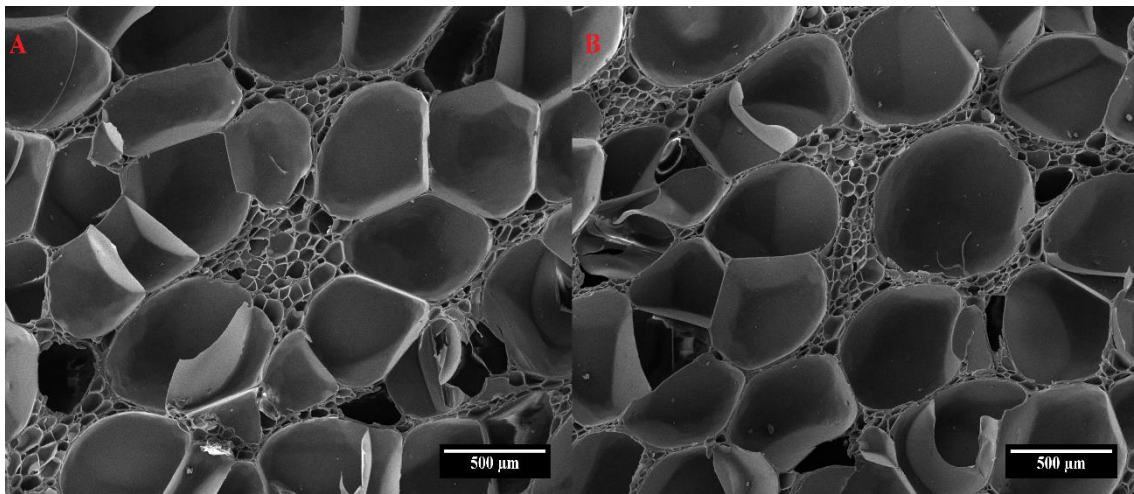
Figure 35: Porous cell walls in HP130 foam in two different parts of the specimen (A) and (B)

3.1.2 Wettability

Core materials wettability was investigated and the average values of the contact angles obtained are summarized in Figure 36. The contact angle for the three agglomerated corks varies between 115° and 125°, whereas it varies between 105° and 117° for the three PVC foams. In light of these results, it is possible to conclude that both core types are characterized by a hydrophobic nature, but agglomerated cork hydrophobicity is higher than PVC foam one. This conclusion is also corroborated by the visual observation of the water droplets in Figure 37, set down on agglomerated cork NL20 and PVC foam HP130 during wettability tests. Cork hydrophobic nature was already pinpointed by Abenojar et al. [161] who found out a contact angle between 90° and 100° for natural cork, and by Gomes et al. [162] who obtained similar results and in particular an average contact angle of 84° ± 2°.
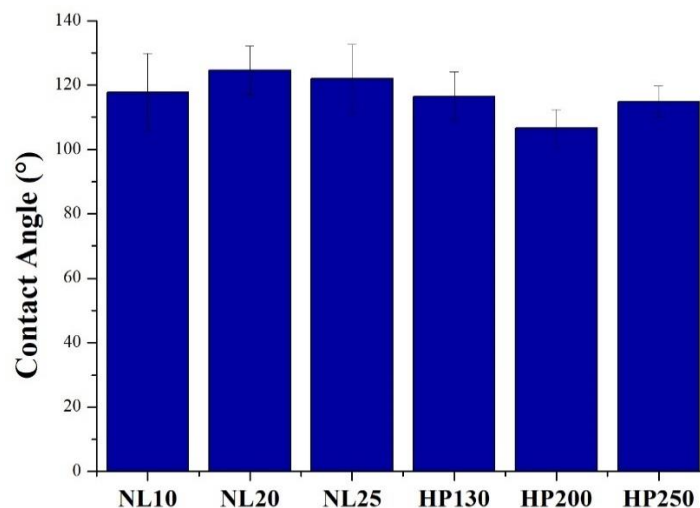
Figure 36: Average contact angles of the three agglomerated corks and the three PVC foams
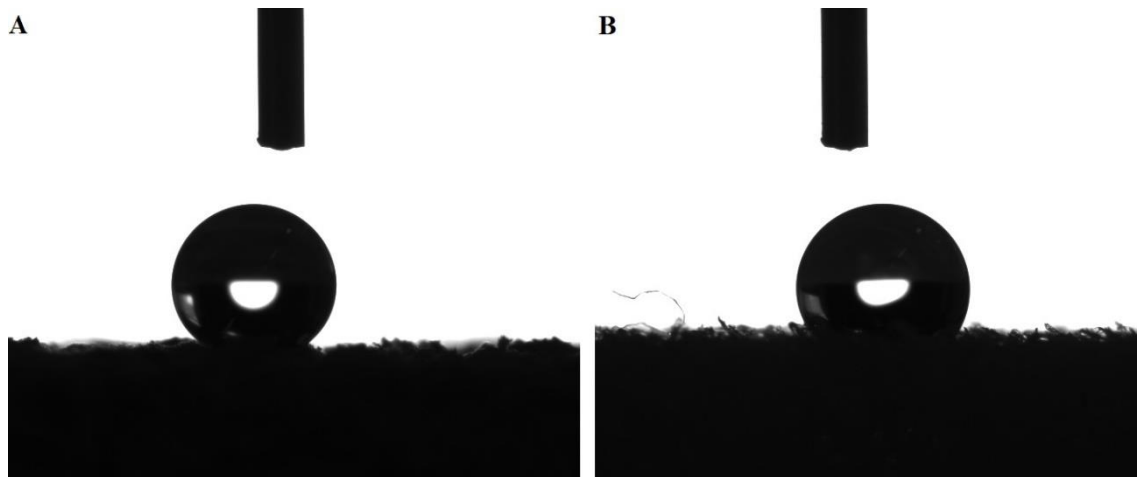
Figure 37: Water droplets on NL20 (A) and HP130 (B) samples surface while performing wettability tests

The contact angle values reported in literature are lower than those reported in this study and this discrepancy can be explained considering the difference in surface roughness that arises between agglomerated and natural cork. It is universally acknowledged that an increase in surface roughness induces a reduction in hydrophobic material wettability, hence an increase in contact angle. Considering that agglomerated cork is endowed with the typical roughness that characterizes natural cork and with a macro roughness induced by granules discontinuity, this explains the variance with respect to literature values. This conclusion is corroborated when PVC foams contact angles are considered. In their study on PVC films, Mcginty et al. [163] found out a static contact angle at around 82° for a traditional PVC film and this value is definitely lower than the ones reported in this study. Even in this case, the differences in contact angle values have to be ascribed to a different surface morphology and in particular to a higher surface roughness of the foam.

3.2 Thermal Characterization

3.2.1 Thermal conductivity

Natural and synthetic cores thermal conductivity values were measured, and the resulting values are summarized in Figure 38. The comparison of agglomerated cork with the corresponding PVC foam with the same density, discloses a higher thermal conductivity of cork in both as received and dried conditions. Moreover, both core materials exhibit a pronounced dependence of thermal conductivity on density and, in particular, a higher density entails an increase in thermal conductivity. Indeed, a lower core density implies a higher dry air content that acts as good thermal insulator leading to the above-mentioned results. This dependence is also confirmed by the data reported in Figure 39 which represent NL10 thermal conductivity average values in the five different sampling points of the specimen. The standard deviation connected to the measurements in each point is very limited and this means that the deviation of the five thermal conductivity values from the total average one must be ascribed to local density variations that can be observed across the specimen. The thermal conductivity values summarized in Figure 38 also reveal a strong dependence of this parameter on moisture content and in particular a lower

moisture content leads to lower thermal conductivity values as observable for the dried samples of each core type. The huge influence of moisture can be explained considering that water is characterized by a thermal conductivity of 0.6 w/mK which is of one order of magnitude higher than cork and PVC foam ones. Similar findings were presented by Matias et al [164] and by Limam et al. [165], who carried out their tests on black agglomerated cork considering the water content of the sample.
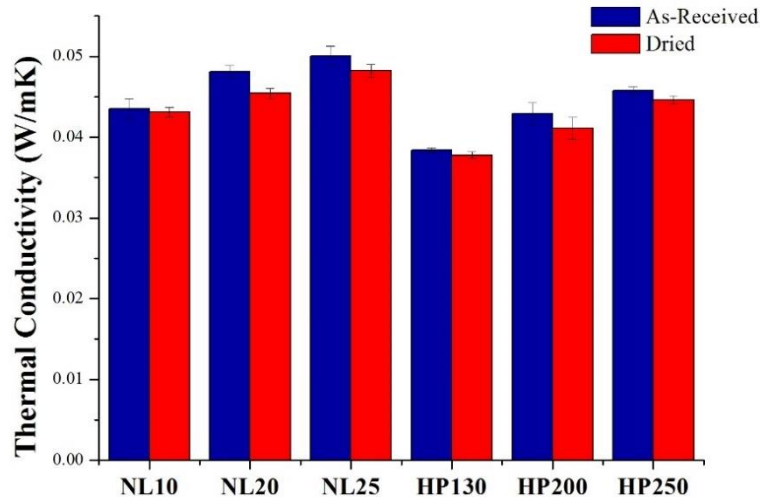
Figure 38: Thermal conductivity values of agglomerated corks, NL10, NL20 and NL25, and PVC foams, HP130, HP200 and HP250, in as-received and dried conditions
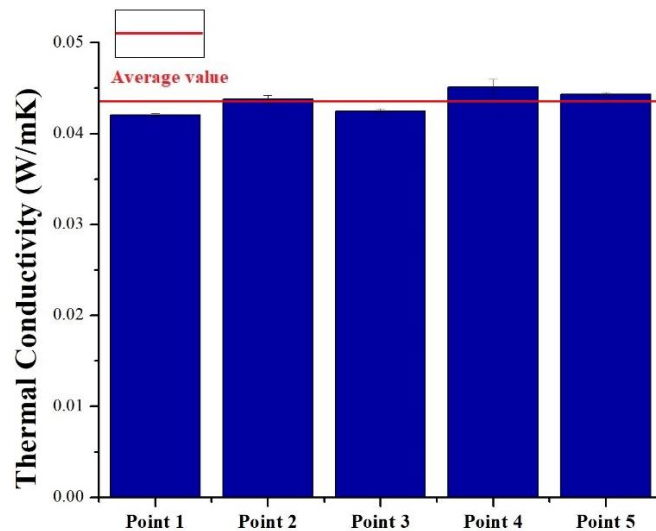
Figure 39: Variation of thermal conductivity in a NL10 samples considering five different sampling points in the same specimen

The resistance value of insulation, R-value, is a parameter strictly interconnected to thermal conductivity and permits to define how well an insulating material can resist heat flow. It is defined as the ratio between the thickness and the thermal conductivity of a material. In light of this and considering the R-values reported in Figure 40, PVC foams turn out to be better thermal insulators than agglomerated corks and the lower the density the better the insulation capability. Even if the R-value is a useful parameter when addressing the thermal behavior of a material, it

is not sufficient to define the insulation performances of a material because it takes into account only conduction phenomena neglecting other important heat transfer mechanisms such as radiation and convection which however depend on the cells size of the core materials. For what concerns convection, its contribution to heat transfer is not significant when cell size is lower than 1 mm that is the case of both agglomerated corks and PVC foams [38]. Regarding radiation mechanism, a smaller cell size is responsible for a lower flow rate increasing the time necessary to absorb and reradiate heat. In light of this, cork turns out to be a better thermal insulator, from the radiation point of view, thanks to a much smaller dimension of the cells with respect to all synthetic foams [38].
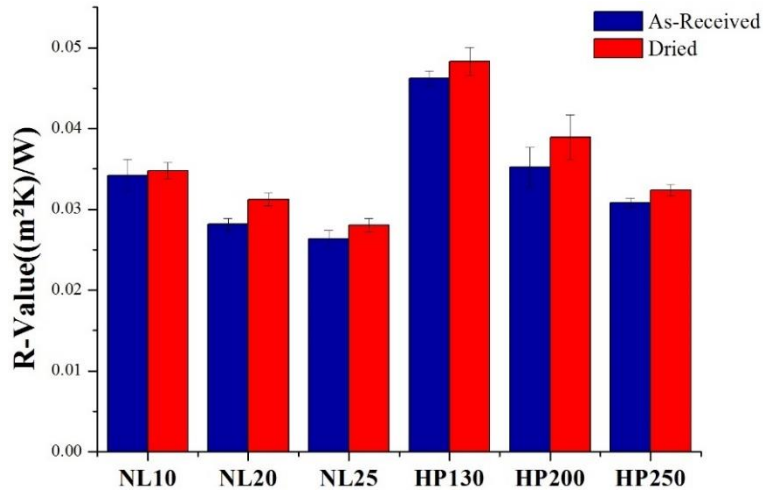
Figure 40: R-values of agglomerated corks, NL10, NL20 and NL25, and PVC foams, HP130, HP200 and HP250, in as-received and dried conditions

In Figure 41 the heat capacity values of each core material are reported. Heat capacity is defined as the ability of a material to store heat and, thanks to the peculiar honeycomb structure, agglomerated cork turns out to be a good heat absorber [165] with storage capabilities higher than PVC foams ones.
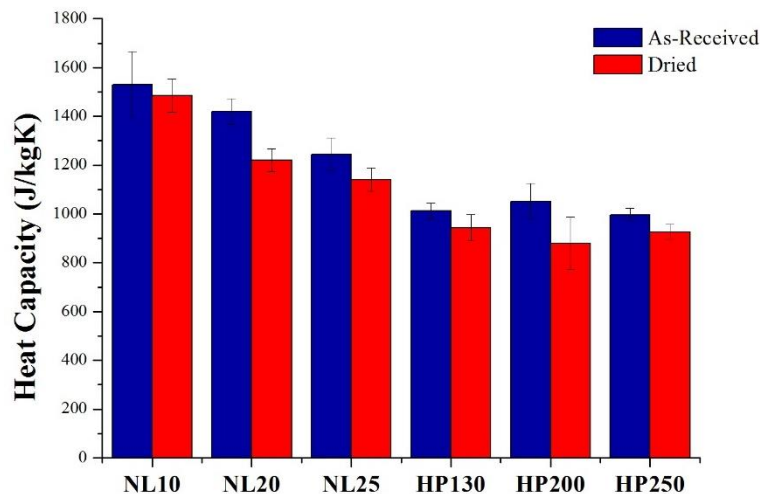
Figure 41: Heat capacity values of agglomerated corks, NL10, NL20 and NL25, and PVC foams, HP130, HP200 and HP250, in as-received and dried conditions

91

Dried samples are characterized by a specific heat always lower than the corresponding as received sample one because, as previously seen for thermal conductivity, water is characterized by a specific heat of 4180 J/kgK in the liquid state and 1996 J/kgK in the vapor state which are significantly higher than cork and PVC foam ones.

Another important parameter, to take into account when studying material thermal insulation behavior, is thermal diffusivity that is a specific property to describe unsteady heat conduction. It can be calculated as the ratio of thermal conductivity and specific heat per unit volume and allows to measure the heat transfer rate through a material. More specifically, it enables to describe how quickly a material reacts to temperature changes and the higher the thermal diffusivity the faster the heat propagation into the material. Thermal diffusivity values of the six core materials under study are shown in Figure 42. It is possible to notice that, even if agglomerated cork displayed a higher thermal conductivity than the PVC foam with the corresponding density, it is characterized by a lower thermal diffusivity thanks to its major ability to store heat [165].
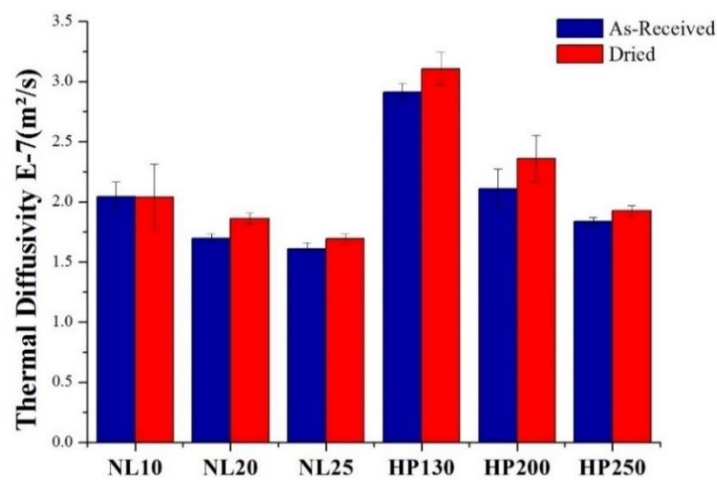
Figure 42: Thermal diffusivity values of agglomerated corks, NL10, NL20 and NL25, and PVC foams, HP130, HP200 and HP250, in as-received and dried conditions

In conclusion, if PVC foam seems to be a better thermal insulator than agglomerated cork thanks to a lower thermal conductivity and hence a higher R-value, the inclusion of further heat transfer contributions, i.e. radiation and convection, permits to reveal a higher resistance of agglomerated cork to radiation phenomena and hence a lower thermal diffusivity responsible for a slower heat propagation throughout the material.

3.2.2 Thermogravimetric Analysis (TGA)

The results of thermogravimetric analysis, including TGA and DTG (Differential Thermogravimetry) curves, are reported in Figure 43 for agglomerated corks NL10, NL20 and NL25 and in Figure 44 for PVC foams HP130, HP200 and HP250. For what concerns agglomerated cork, NL10 displays a first mass loss of 2.6 wt. % at around 100 °C due to moisture removal. The temperature related to this first drop shifts to 106 °C for NL20 and to 108 °C for NL25 and this increase is mainly due to the increase in agglomerated cork density that implies a porosity reduction delaying moisture removal from the sample. A second mass loss ranging from 11.5 wt. % to 13.5 wt. % was detected for all three types of agglomerated cork between 200 °C and 300 °C. In this second step of decomposition three concurring phenomena take place, i.e. polyurethane binder decomposition, extractives volatilization and hemicellulose degradation.
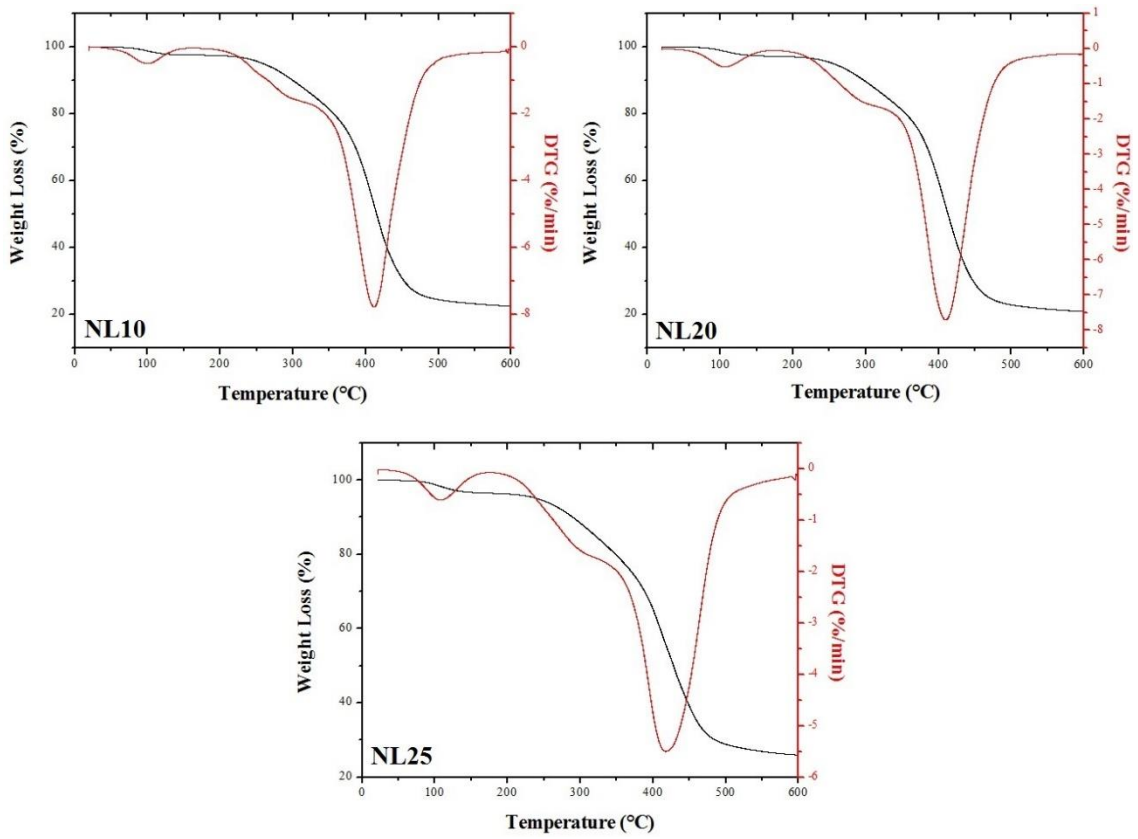
Figure 43: NL10, NL20, and NL25 TGA and DTG curves
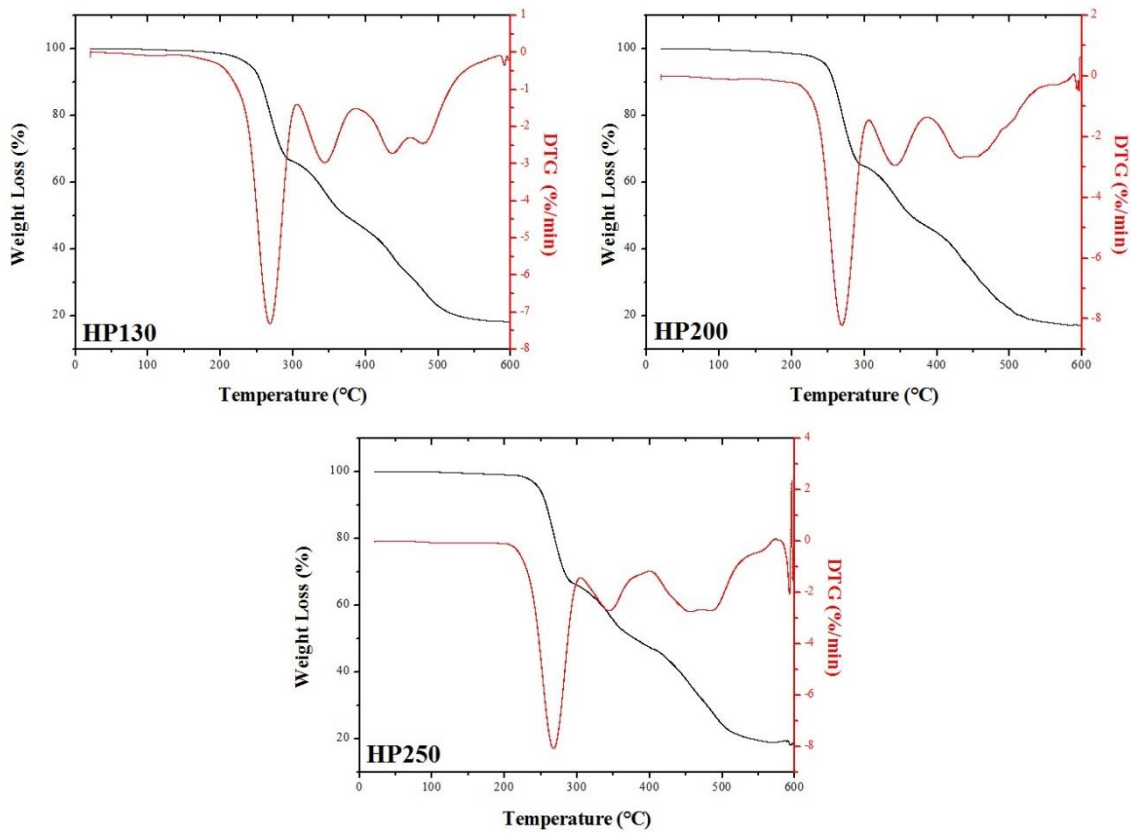
Figure 44: HP130, HP200, and HP250 TGA and DTG curves

Extractive volatilization was already detected for natural cork at around 315 °C by Sen et al. [166] whereas hemicellulose degradation in a temperature range of 220 °C and 315 °C was identified by Shangguan et al. [167]. A third decomposition step can be observed between 410 °C and 418 °C and it refers to suberin and lignin degradation, which are the most stable components [167]. The final mass loss for each agglomerated cork at 600 °C is 77.5 wt. % for NL10, 79 wt. % for NL20 and 74 wt. % for NL25.

Moving to the TGA and DTG curves of the PVC foams in Figure 44, an initial mass loss due to moisture elimination can be detected between 110 °C and 120 °C, as previously observed for agglomerated cork. After moisture removal, two important degradation steps responsible for a mass loss of 33-36 wt. % and 18-19 wt. % can be recognized at around 268 °C and 343 °C. These two mass drops can be ascribed to the plasticizer loss and to polymer dehydrochlorination that promotes the formation of a linear polyene structure and the emission of vinyl chloride, HCl and benzene [168]. A fourth degradation step responsible for a mass loss between 24.5 wt. % and 27.5 wt.% can be detected in the temperature range between 430 °C and 490 °C. This step promotes the breakage of the double bonds of the polyene structure leading to the formation of volatile hydrocarbons. The residual mass at the end of the analysis at a temperature of 600 °C ranges from 17 wt. % to 18 wt. %

3.2.3 Dynamic Mechanical Analysis (DMA)

The DMA curves of the three agglomerated corks and the three PVC foams are shown in Figures 45 and 46, respectively. A decrease in the storage modulus can be observed for both natural and petroleum-based cores when temperature analysis increases. With regard to agglomerated cork tanδ curves, a double peak can be recognized. The first one is at around -45 °C and is due to the glass transition of the polyurethane binder, whereas the second one concerns directly cork behavior being caused by suberin melting as already studied by Paiva and Magalhães [169]. In the case of the PVC foams, the transition from the glassy state to the viscoelastic one can be easily recognized by the sharp change in the curve slope of the storage modulus that highlights a significant reduction of the latter and by the huge increase in loss modulus and tanδ. The same trend in both storage and loss moduli was already observed by Khoshnoud and Abu-Zahra [170]. From the DMA curves, the glass transition temperatures of both agglomerated corks and PVC foams were extrapolated and the resulting values are summarized in Table 14. They are in perfect agreement with those reported in literature [169–171]. From the reported data, it appears clear that at room temperature agglomerated cork works in a viscoelastic regime whereas all PVC foams work in a glassy state. A further point to make is that the glass transition temperatures of all agglomerated corks are very close to room temperature and this is an important item to take into account when selecting a material for design purposes, because changes in the mechanical behavior are likely to occur.

Table 14: Cores glass transition temperature evaluated by DMA

Sample	Glass Transition Temperature (°C)
NL10	11.75 ± 0.78
NL20	10.90 ± 2.12
NL25	15.80 ± 1.27
HP130	85.40 ± 0.56
HP200	79.80 ± 1.98
HP250	76.80 ± 0.99
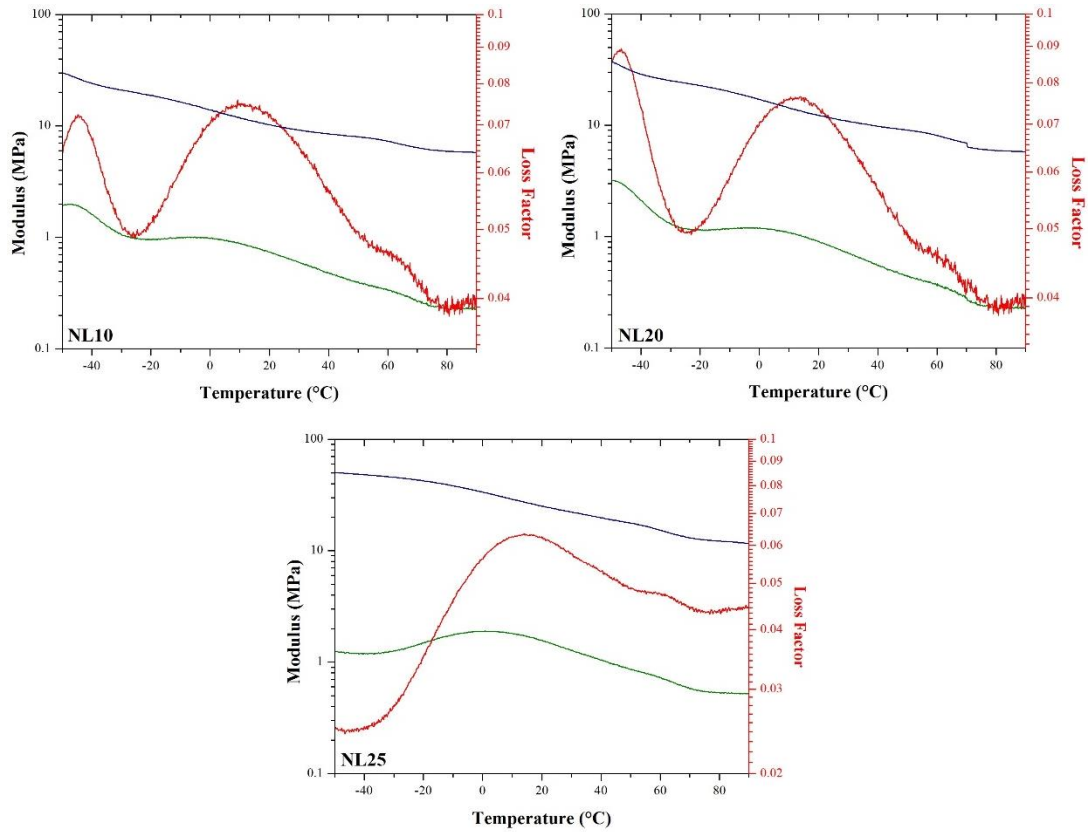
Figure 45: NL10, NL20, and NL25 storage modulus (blue line), loss modulus (green line) and loss factor (red line)
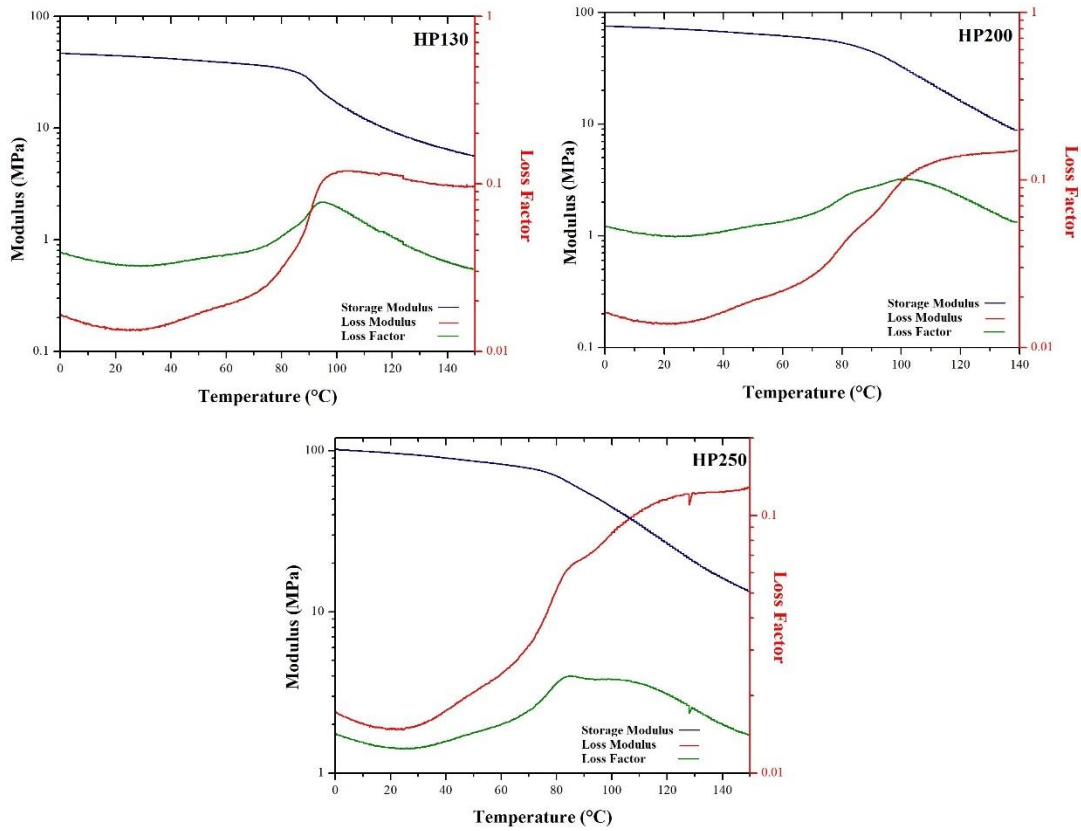
Figure 46: HP130, HP200, and HP250 storage modulus (blue line), loss modulus (green line) and loss factor (red line)

3.3 Quasi-Static Characterization

3.3.1 Shear tests

The shear modulus and shear strength values of the three agglomerated corks are summarized in Table 15. Both shear parameters are characterized by a clear dependency on cork density and in particular an increase of this physical property leads to an improvement of the shear response of the sample.

Table 15: Shear modulus and shear strength of NL10, NL20 and NL25 agglomerated cork

Sample	Shear Modulus (MPa)	Shear Strength (MPa)
NL10	1.00 ± 0.05	0.26 ± 0.04
NL20	1.26 ± 0.04	0.57 ± 0.03
NL25	1.92 ± 0.27	0.75 ± 0.04

In Figure 47 the evolution of cork shear behavior throughout the test can be observed. After an initial elastic regime, sample permanent damage starts to appear along specimen diagonal in the form of small and isolated cracks. The gradual increase of the deformation applied to the sample induces a progressive enlargement of the little cracks until they coalesce in few main cracks.

Figure 47: Crack propagation in a NL25 specimen while performing a shear test

Once reached this damage state, the load bearing capacities of the material are seriously reduced and compromised leading to the final failure. This characteristic shear behavior of agglomerated cork was already acknowledged by Reis and Silva [40]. Looking at agglomerated cork fracture in shear shown in Figure 48, it is possible to notice that it is an intergranular fracture due to binder or to cork/binder interface fracture and not to cork granule failure. This damage mode is in common to all agglomerated corks independently on sample density and this underline clearly that the point of weakness of this material is granules interface. This point will turn out to be very useful in the impact response analysis of this type of material.

Figure 48: Intergranular fracture occurred in a NL10 specimen tested in shear

3.3.2 Bending tests

The bending curves of the six core materials obtained by the tests at room temperature are shown in Figure 49 and the corresponding parameters are summarized in Table 16. Thanks to a higher flexural modulus and strength, all PVC foams display much higher flexural performances than agglomerated corks and this is true not only being equal the density in fact all PVC foams turned out to be more performing than all agglomerated corks. Because of the higher flexural modulus, PVC foams are also characterized by a more brittle behavior that causes foam fracture at lower deformations. In light of the flexural results, it is possible to conclude that the foam with the closest behavior to agglomerated cork is HP130, i.e., the foam characterized by the lowest density. The flexural modulus and strength as a function of operating temperature are reported in Figures 50 and 51 for agglomerated corks and PVC foams, respectively. An increase in operating temperature leads to a progressive decrease of the flexural modulus and strength of both type of core materials.
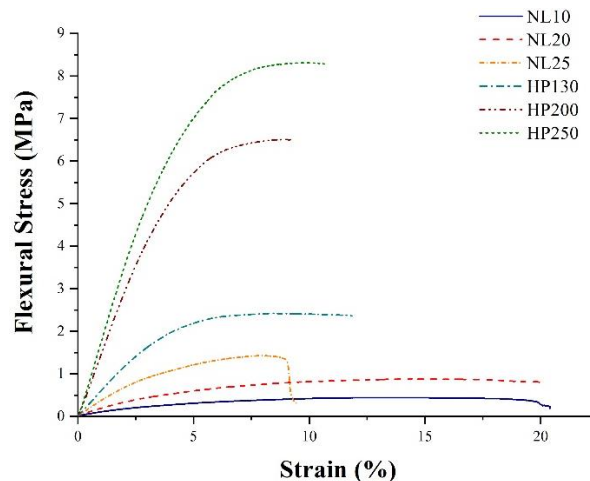
Figure 49: Typical stress-strain bending curves at room temperature for all cellular cores

Table 16: Room temperature flexural modulus and strength of all core materials

Sample	Flexural Modulus (MPa)	Flexural Strength (MPa)
NL10	9.24 ± 0.32	0.46 ± 0.01
NL20	17.20 ± 0.52	0.86 ± 0.02
NL25	37.28 ± 2.20	1.42 ± 0.04
HP130	62.00 ±3.49	2.42 ± 0.08
HP200	147.80 ± 2.68	6.54 ± 0.19
HP250	182.80 ± 4.71	8.31 ± 0.27

Concerning the continuous reduction of agglomerated cork flexural strength with temperature, it can be ascribed to a progressive thermal degradation of the mechanical performances of the polymeric binder. Moving to PVC foams results, the flexural modulus trend with temperature is perfectly consistent with the DMA results. The storage modulus, studied with DMA, is defined as the capability of a material to store energy in an elastic way and its continuous decrease with temperature permits to explain flexural modulus decrease. The main drop in flexural modulus is detected at 80 °C and this can be explained taking advantage of the glass transition temperature values obtained by DMA that ranges between 77 °C and 85 °C. The transition from the glassy state to the viscoelastic state is responsible for the drop in flexural modulus. This statement is also corroborated by the analysis of the PVC foam damage mode as a function of temperature shown in Figure 52.
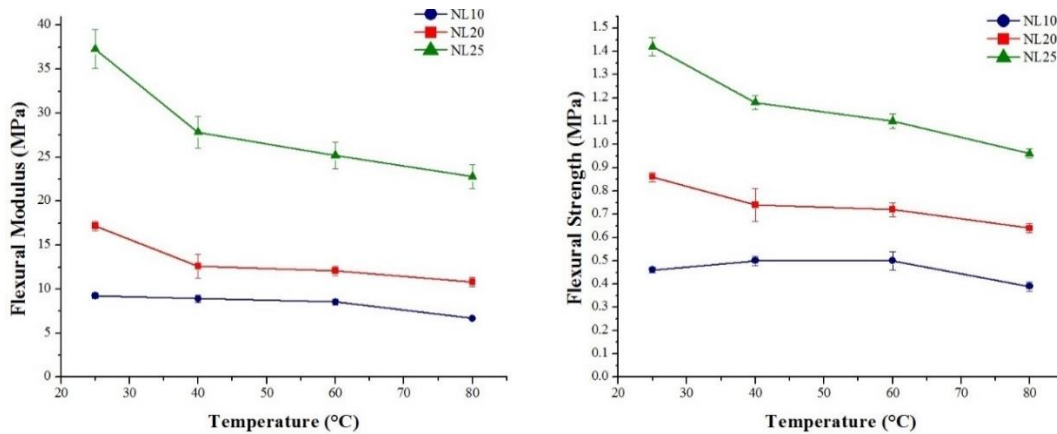
Figure 50: Agglomerated cork flexural modulus and strength as a function of temperature
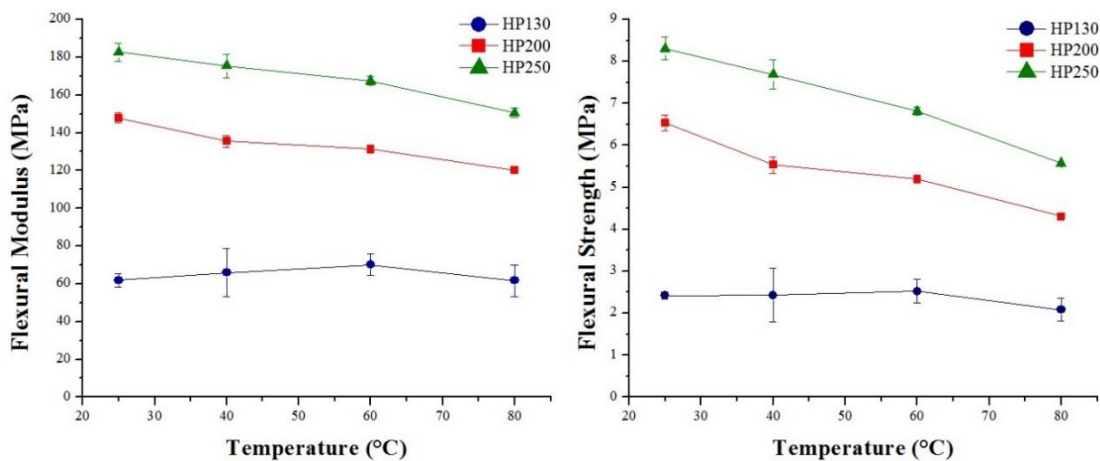
Figure 51: PVC foam flexural modulus and strength as a function of temperature

All PVC foams are characterized by a brittle fracture, which origins on the tensile side of the sample, until 60 °C but do not show any type of damage when tested at 80 °C.
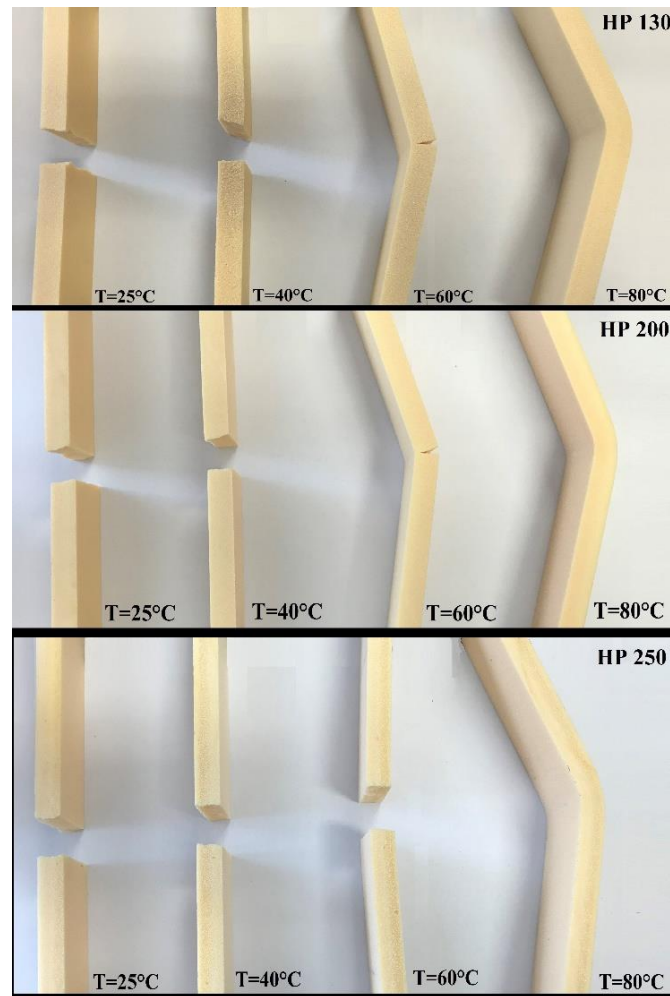
Figure 52: PVC foams failure mode evolution in bending as a function of testing temperature

All the data obtained were statistically analyzed in order to support the conclusions drawn and, looking at the p values gathered in Tables 17 and 18 for flexural modulus and strength respectively, it is possible to conclude that density (ρ), temperature (T) and their interaction are statistically significant and that they actually have an effect on the flexural property under consideration. In almost all cases, the statistical significance turned out to be so high that the chances of the results of being due to error alone were less than 1 %, which is a significance limit somewhat lower than the usually selected 5 % ($p < 0.05$).

Table 17: Statistical significance of the effect of different testing parameters, i.e. density, temperature and their interaction, on the flexural modulus of PVC foams and agglomerated corks

Flexural Modulus parameter	Agglomerated Cork Pr(>|t|)	PVC foam Pr(>|t|)
Density (ρ)	4.67×10^{-14}	$<2.00 \times 10^{-16}$
Temperature (T)	3.05×10^{-2}	4.17×10^{-3}
Density x Temperature (ρxT)	6.08×10^{-4}	2.10×10^{-5}

Table 18: Statistical significance of the effect of different testing parameters, i.e. density, temperature and their interaction, on the flexural strength of PVC foams and agglomerated corks

Flexural Strength parameter	Agglomerated Cork Pr(>|t|)	PVC foam Pr(>|t|)
Density (ρ)	$<2.00 \times 10^{-16}$	$<2.00 \times 10^{-16}$
Temperature (T)	4.42×10^{-4}	7.09×10^{-5}
Density x Temperature (ρxT)	1.71×10^{-7}	5.22×10^{-10}

The estimation of the regression coefficients of each parameter led to the relationships reported in Equations (3.1) - (3.4):

$$E_{PVC} = -78.57 + 1.13\, \rho_{PVC} + 0.61\, T_{PVC} - 0.005\, \rho_{PVC}\, T_{PVC} \tag{3.1}$$

$$\sigma_{max\_PVC} = -4.75 + 0.058\, \rho_{PVC} + 0.04\, T_{PVC} - 3.64 \times 10^{-4} \rho_{PVC}\, T_{PVC} \tag{3.2}$$

$$E_{CORK} = -29.56 + 0.27\, \rho_{CORK} + 0.22\, T_{CORK} - 0.0017\, \rho_{CORK} T_{CORK} \tag{3.3}$$

$$\sigma_{max\_CORK} = -0.84 + 9.35 \times 10^{-3} \rho_{CORK} + 7.44 \times 10^{-3}\, T_{CORK} - 5.89 \times 10^{-5} \rho_{CORK}\, T_{CORK} \tag{3.4}$$

where Equation (3.1) permits to evaluate PVC foam flexural modulus (E), Equation (3.2) PVC foam flexural strength (σ_{max}), Equation (3.3) agglomerated cork flexural modulus and Equation (3.4) agglomerated cork flexural strength. The correlation between the linear model and the experimental datasets is very accurate as confirmed by the multiple R^2 values gathered in Table 19 and by the good fitting shown in Figure 53.

Table 19: Multiple R^2 values for all flexural interpolation models

Dependent Variable	Multiple R^2
PVC foam flexural modulus	0.976
PVC foam flexural strength	0.978
Agglomerated Cork flexural modulus	0.865
Agglomerated Cork flexural strength	0.951
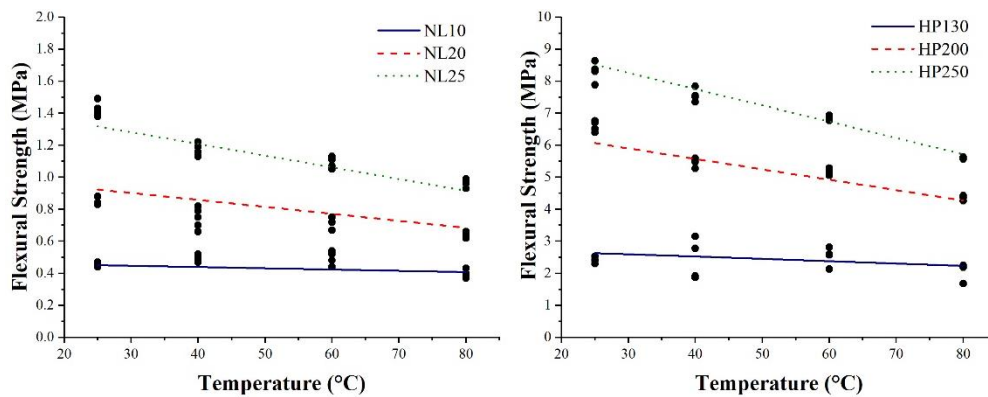
Figure 53: Experimental flexural strength data of natural agglomerated corks and synthetic PVC foams and corresponding fitting curves evaluated at constant density

3.3.3 Compression tests

The typical compression curves of agglomerated corks and PVC foams are depicted in Figure 54. The curves disclose a certain difference in PVC foams and agglomerated corks behavior. Synthetic foams compressive behavior is characterized by three main steps [159,160]. The first part of the curve is characterized by a straight line and describes the elastic response of the cell walls to the applied deformation. The elastic region ends at the yielding point where foam plastic deformation begins due to cells collapse. The second part of the curve is the plateau region characterized by an almost constant stress where foam cells undergo a progressive buckling and collapse. The plateau region continues until foam densification occurs due to cell walls interaction. When opposite cell walls start to touch each other, the stress required to go on deforming the polymeric foam increase steeply.

Moving to the more eco-sustainable agglomerated cork, a different compressive behavior can be observed due to the marked differences in cell walls chemical composition and morphology. Three main steps were identified in cork compressive curve and they were extensively studied by Pereira [37], by Anjos et al. [172,173] and by Rosa and Fortes [174]. The first region, as previously seen for the polymeric foam, is the elastic region that extends up to approximately 5 % and is due to the elastic bending of the cell-walls. After this first part, a wide plateau region from 5 % to 60 % - 70 % strain can be detected. In this region cork cells experience buckling without undergoing fracture. If PVC foam cell walls are straight and rigid and tend to fracture and collapse once reached the critical stress, the undulations of cork cell walls allow them to adapt to the deformation without cracking. This ability of cork to increase wall corrugation, when the applied compressive deformation increases, is due to suberin macromolecules, i.e. its main chemical component, a glyceridic polyester with a ribbon like structure characterized by an extreme flexibility. The final strain of the plateau region strictly depends on cork density in fact the third part of the compressive curve is the densification region where cell walls experience mutual contact and it appears clearly earlier when cork density is higher [175]. Suberin is able to prevent cells fracture and failure even when they reach complete folding and for this reason when the compressive load is removed cork is able to recover almost its initial height thanks to cell walls unfolding [37]. The limited residual permanent deformation is mainly due to pores and lenticular channel deformation.
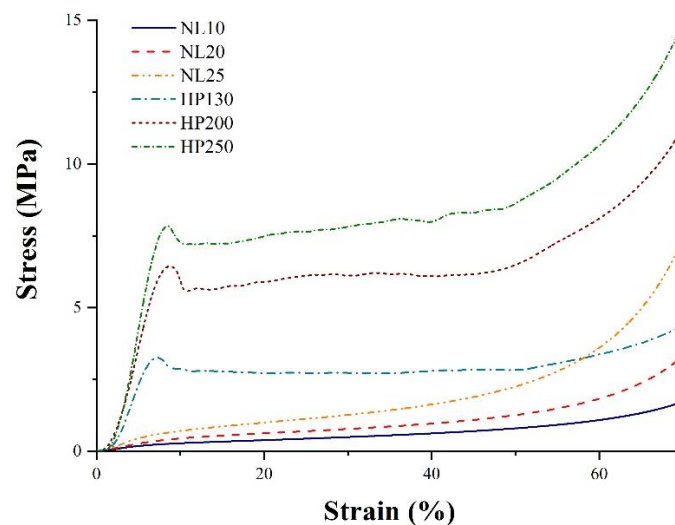
Figure 54: Agglomerated corks and PVC foams typical compressive curves

A deeper understanding of the compressive behavior of both natural and synthetic core materials can be achieved through the microstructural analysis carried out on pre-stressed samples that allow to investigate how material morphology evolves as a function of the compressive load applied. Figures 55 and 56 show the changes in microstructure underwent by NL25 and HP130, respectively, during a compression test. The observation of NL25 micrographs reveal an initial elastic reaction of the material (Figure 55.A) before entering the plateau region. Once approached this part of the curve, cell walls undulations become more pronounced (Figure 55.B) and this condition preempts the progressive approach of opposite cell walls as exhibited in Figure 55.C and D. Once reached the complete cell collapse (Figure 55.E), the material approaches the densification region where opposite cell walls experience mutual contact (Figure 55.F) thus determining the steep increase in the compressive stress. These micrographs definitely prove the main feature of cork, i.e. the capability of the cell walls to fold completely without undergoing cracks or fracture and to unfold once removed the compressive load ensuring the material impressive dimensional recovery capabilities.
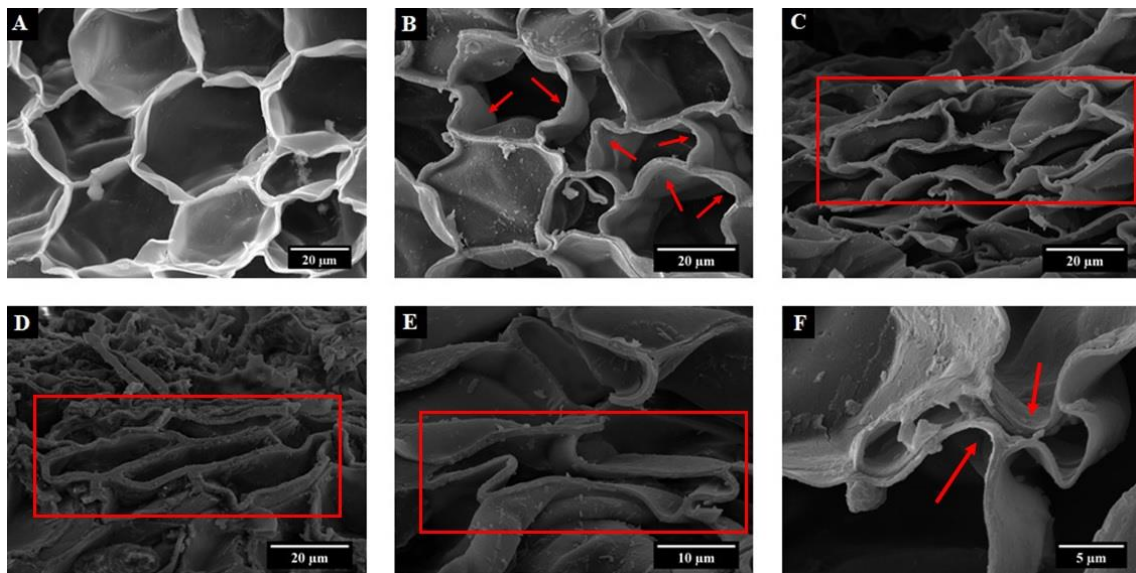
Figure 55: Cells microstructure evolution under increasing compressive loads of NL25
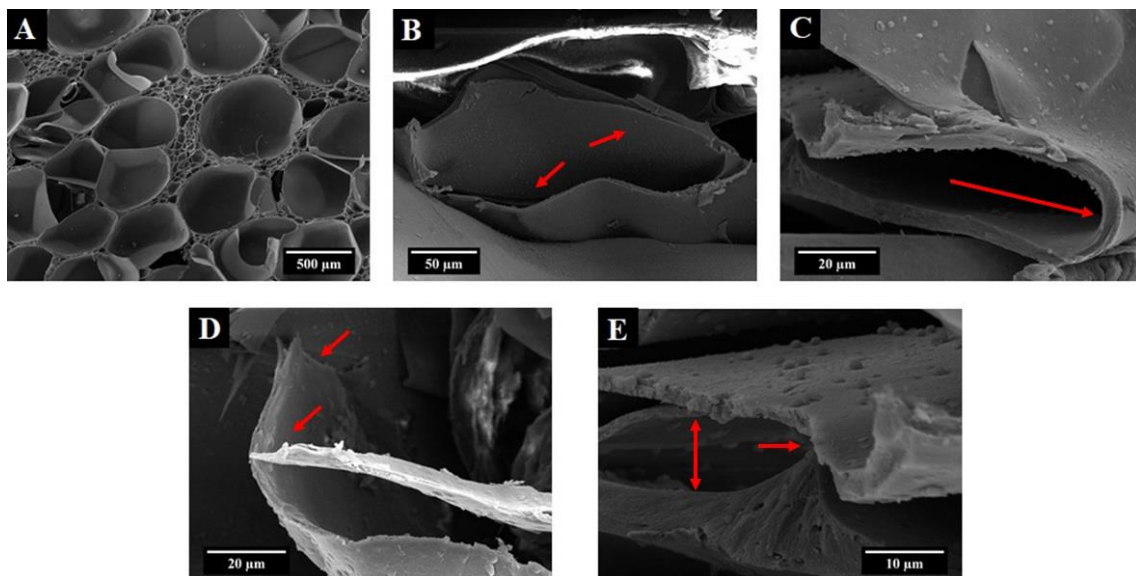
Figure 56: Cells microstructure evolution under increasing compressive loads of HP130

102

Looking at the micrographs in Figure 56, the differences in PVC foam damage progression can be recognized and appreciated. After the first elastic response (Figure 56.A), even PVC foam enters the plateau region where a progressive approach of opposite cell walls through bending can be recognized (Figure 56.B). Once reached walls bending limit (Figure 56.C), the polymeric wall undergoes fracture (Figure 56.D) causing a complete collapse of the cell (Figure 56.E) and the beginning of the densification step. The brittle nature of HP130 leads to the formation of cracks and to cells collapse making the material lose every chance to recover its initial shape.

In light of the information provided on cores compressive response, it is now possible to introduce the tools employed to compute the main compressive properties. Thanks to the steep increase in curve slope, the densification region can be easily recognized in the stress-strain curves, but if the identification of this step is straightforward the evaluation of the densification stress, i.e. the stress value at which densification starts, is more complex and less unequivocally. Avalle et al. [176] developed a compelling method to overcome this problem and to calculate precisely the densification stress. A good energy absorbing material must dissipate the energy of an impact keeping low the exerted reaction force and this is the case of both PVC foams and agglomerated corks characterized by a wide plateau region were the reaction force is kept small. Efficiency is a good parameter to quantify the energy absorbing capacities of a material and is defined as the ratio between the energy absorbed by the material up to a certain strain ε and the stress σ itself:

$$Efficiency = \frac{\int_0^{\varepsilon} \sigma(\varepsilon) d\varepsilon}{\sigma} \tag{3.5}$$

Plotting the efficiency as a function of stress, the resulting curve is characterized by a maximum peak like the exemplificative one reported in Figure 57. This peak is due to the fact that, beyond the densification stress, the increase in absorbed energy becomes much lower than the corresponding stress growth thus causing a drop in the absorbing efficiency. It appears clear that the stress at which the efficiency reaches its maximum is exactly the densification stress that therefore can be identified unequivocally.
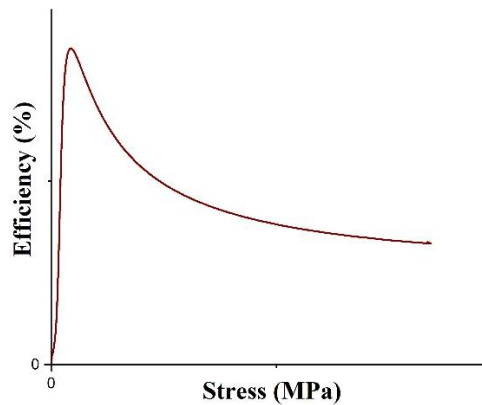
Figure 57: Typical efficiency-stress curve

The evaluation of the densification stress and, as a consequence, of the densification strain is of main importance to calculate accurately another essential compressive property of the PVC foams, i.e. the plateau stress. Indeed, it can be calculated according to Equation (3.6):

$$\sigma_{pl} = \frac{\int_{\varepsilon_{cr}}^{\varepsilon_{dens}} \sigma(\varepsilon) d\varepsilon}{\varepsilon_{dens} - \varepsilon_{cr}} \tag{3.6}$$

where ε_{dens} is the densification strain and ε_{cr} is the strain corresponding to the base of the collapse stress peak. The situation is different for agglomerated cork because its plateau region is characterized by a slight slope that provokes a progressive increment of the plateau stress with increasing strain. To consider this feature of the bio-based core material, its plateau stress was not computed according to Equation (3.6) and rather three different values were considered, i.e. plateau initial value and plateau value at 20 % and 30 % of strain. Plateau initial value was calculated according to the procedure shown in Figure 58. The elastic and the plateau regions of the compressive curve were isolated and the corresponding interpolation lines was computed. The plateau initial value is obtained by the intersection of the elastic region and plateau region interpolation lines.
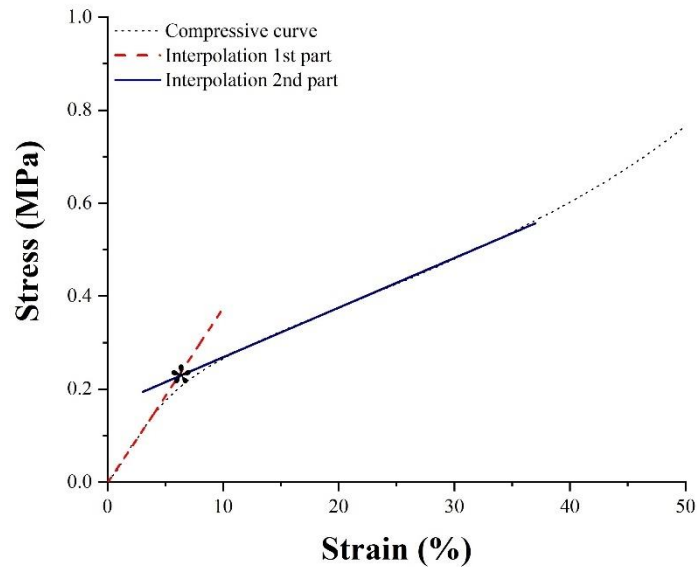
Figure 58: Exemplificative procedure for intersection plateau value calculation

Going back to the analysis of the compressive results, the curves in Figure 54 reveal, as previously observed also in the bending tests, higher mechanical properties, i.e. higher compressive modulus and plateau stress, for all PVC foams with respect to all agglomerated corks. The results show also a sharp dependency of foam compressive properties on density and, in particular, an increase in yielding strength and plateau stress when sample density increases. An increase in foam density entails thicker cell walls, as confirmed by the previous morphological analysis, characterized by an improved resistance against buckling. Even agglomerated cork compressive response strongly depends on sample density and, as in PVC foams case, the higher the density the higher plateau stress and compressive modulus. These results are in perfect agreement with those presented by Anjos et al. [172,173] who addressed the compressive behavior of cork as a function of density and test direction.

A preliminary investigation of the strain rate sensitivity of both agglomerated corks and PVC foams was carried out through quasi-static compression tests increasing the test speed from 5 mm/min to 200 mm/min, i.e. from 0.0055 1/s to 0.222 1/s. For what concerns agglomerated cork, the trend of compressive properties, i.e. compressive modulus, initial plateau stress, plateau stress at 20 % and 30 % of deformation and densification stress, as a function of test speed is shown in Figure 59 and the corresponding data are gathered in Table 20 and 21. All compressive modulus, plateau stresses and densification stress are characterized by an increase with increasing test speeds and these results are in perfect agreement with those reported by Rosa and Fortes [174],
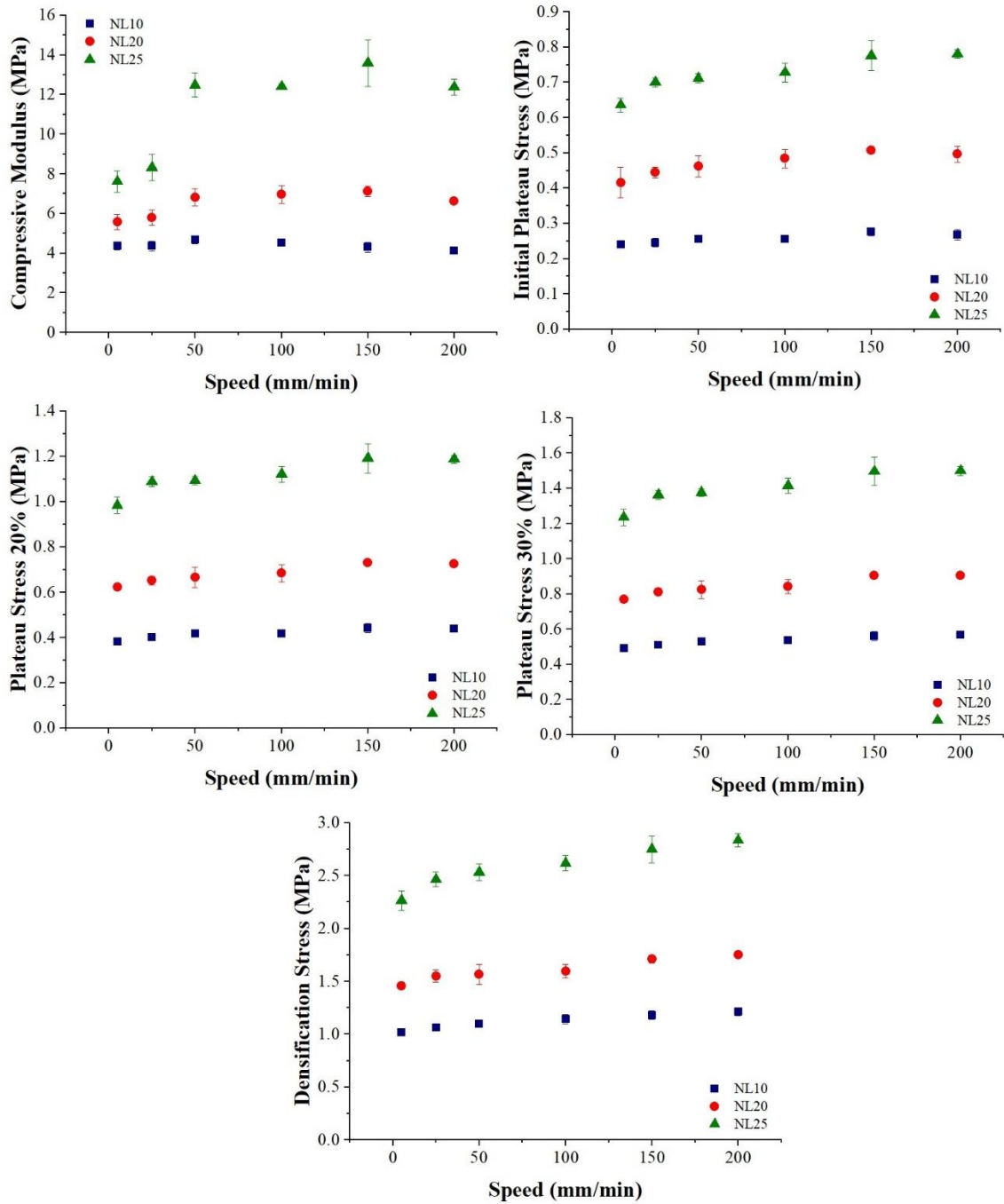
Figure 59: Agglomerated corks compressive modulus and initial plateau stress, plateau stress at 20 % and 30 % of deformation and densification stress as a function of test speed

Table 20: Agglomerated corks compressive modulus and densification stress as a function of test speed

Test speed (mm/min)	Compressive Modulus (MPa)			Densification Stress (MPa)		
	NL10	NL20	NL25	NL10	NL20	NL25
5	4.36 ± 0.18	5.58 ± 0.38	7.62 ± 0.54	1.02 ± 003	1.46 ± 0.03	2.26 ± 0.09
25	4.36 ± 0.25	5.80 ± 0.38	8.32 ± 0.66	1.07 ± 0.01	1.55 ± 0.06	2.47 ± 0.07
50	4.68 ± 0.19	6.82 ± 0.43	12.48 ± 0.61	1.10 ± 0.04	1.57 ± 0.09	2.53 ± 0.08
100	4.54 ± 0.15	6.96 ± 0.44	12.40 ± 0.12	1.15 ± 0.04	1.60 ± 0.06	2.62 ± 0.07
150	4.30 ± 0.25	7.12 ± 0.25	13.60 ± 1.17	1.18 ± 0.04	1.71 ± 0.04	2.75 ± 0.13
200	4.12 ± 0.13	6.62 ± 0.11	12.38 ± 0.40	1.21 ± 0.03	1.75 ± 0.02	2.83 ± 0.06

Table 21: Agglomerated corks initial plateau stress and at 20% and 30% strain

Test speed (mm/min)	Initial Plateau Stress (MPa)			Plateau Stress at 20 % (MPa)			Plateau Stress at 30 % (MPa)		
	NL10	NL20	NL25	NL10	NL20	NL25	NL10	NL20	NL25
5	0.24±0.01	0.42±0.04	0.64±0.02	0.38±0.01	0.62±0.01	0.98±0.04	0.49±0.01	0.77±0.01	1.24±0.05
25	0.25±0.01	0.44±0.02	0.70±0.01	0.40±0.01	0.65±0.02	1.09±0.02	0.51±0.02	0.81±0.02	1.36±0.03
50	0.26±0.01	0.46±0.03	0.71±0.01	0.42±0.01	0.67±0.04	1.09±0.02	0.53±0.01	0.83±0.05	1.38±0.02
100	0.26±0.01	0.48±0.03	0.73±0.03	0.42±0.01	0.68±0.04	1.12±0.04	0.54±0.01	0.84±0.04	1.41±0.04
150	0.28±0.01	0.51±0.01	0.78±0.04	0.44±0.02	0.73±0.01	1.19±0.06	0.56±0.03	0.91±0.02	1.50±0.08
200	0.27±0.01	0.50±0.02	0.78±0.01	0.44±0.01	0.73±0.01	1.19±0.02	0.57±0.02	0.91±0.01	1.50±0.03

who investigated the strain rate sensitivity of natural cork along its three main directions, and with those of Le Barbenchon et al. [177], who addressed the strain rate sensitivity of a particular type of agglomerated cork in which a thermoset resin reinforced with short fibers is used as binder. When test speed increases, agglomerated cork struggles to adapt to the applied deformation thus leading to a higher reaction force and, as a consequence, to an increase in plateau and densification stress. The agglomerated cork that underwent the highest variation in compressive properties, was NL25 which displayed an increase of 43 % in compressive modulus, of 18 % in plateau stresses and of 20 % in densification stress. This outcome is due to the higher density which implies a higher amount of material that has to adapt to the applied deformation.

Moving to the synthetic PVC foams, the trend of compressive properties, i.e. compressive modulus, yield strength, plateau stress and densification stress, as a function of test speed is shown in Figure 60 and the corresponding data are gathered in Table 22 and 23.
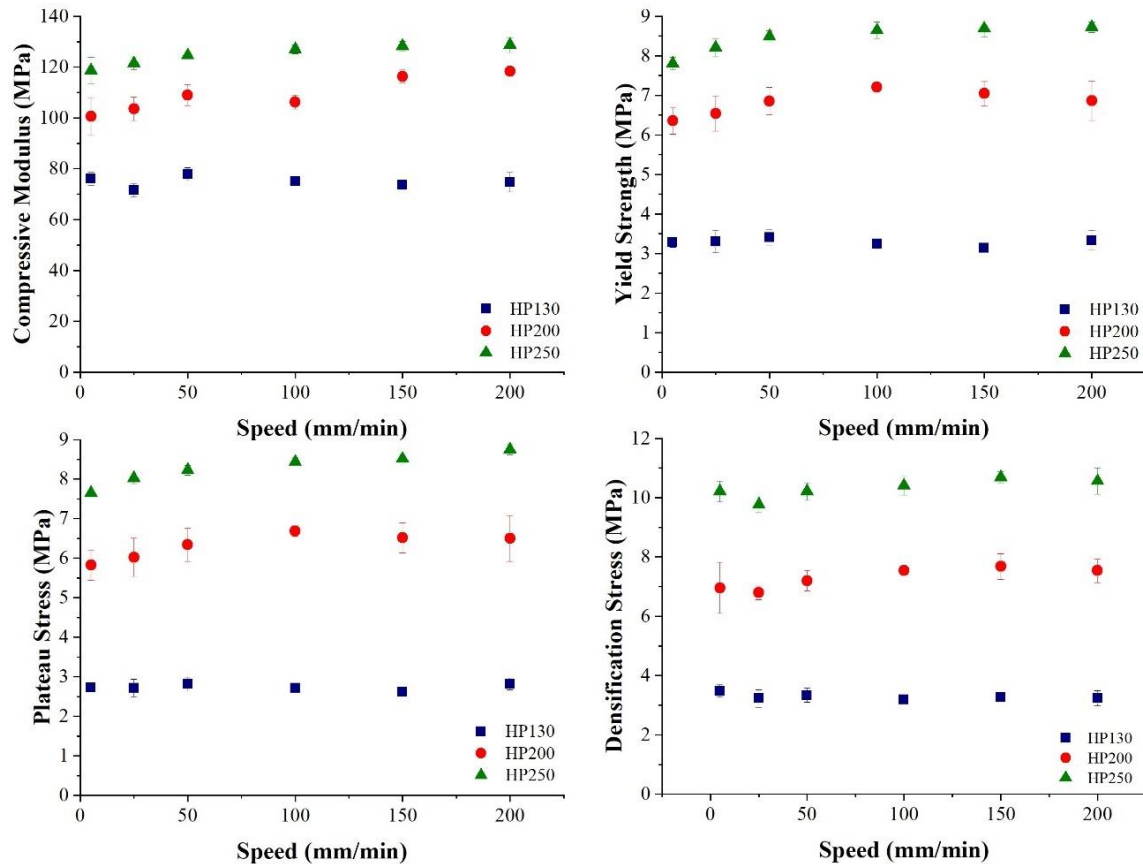
Figure 60: PVC foams compressive modulus, yield strength, plateau stress and densification stress as a function of test speed

Table 22: PVC foams compressive modulus and plateau stress as a function of test speed

Test speed (mm/min)	Compressive Modulus (MPa)			Plateau Stress (MPa)		
	HP130	HP200	HP250	HP130	HP200	HP250
5	75.08 ± 2.13	100.58 ± 7.43	118.68 ± 5.15	2.73 ± 0.10	5.82 ± 0.38	7.65 ± 0.08
25	71.52 ± 2.54	103.57 ± 4.61	121.40 ± 2.35	2.71 ± 0.23	6.02 ± 0.49	8.02 ± 0.14
50	67.92 ± 2.24	109.00 ± 4.10	124.62 ± 1.14	2.82 ± 0.18	6.34 ± 0.42	8.20 ± 0.13
100	65.78 ± 0.63	106.20 ± 2.77	127.00 ± 1.69	2.71 ± 0.10	6.68 ± 0.13	8.44 ± 0.10
150	66.56 ± 2.87	116.36 ± 2.47	128.20 ± 1.83	2.61 ± 0.04	6.52 ± 0.38	8.51 ± 0.14
200	70.68 ± 4.74	118.30 ± 1.46	128.68 ± 2.89	2.82 ± 0.15	6.50 ± 0.58	8.75 ± 0.13

Table 23: PVC foams yielding strength and densification stress as a function of test speed

Test speed (mm/min)	Yielding Strength (MPa)			Densification Stress (MPa)		
	HP130	HP200	HP250	HP130	HP200	HP250
5	3.27 ± 0.12	6.09 ± 7.43	7.80 ± 0.16	3.48 ± 0.20	6.95 ± 0.86	10.21 ± 0.35
25	3.30 ± 0.28	6.25 ± 4.61	8.20 ± 0.23	3.23 ± 0.29	6.79 ± 0.23	9.76 ± 0.26
50	3.40 ± 0.20	6.36 ± 4.10	8.49 ± 0.14	3.34 ± 0.24	7.20 ± 0.34	10.21 ± 0.29
100	3.25 ± 0.12	6.31 ± 2.77	8.64 ± 0.21	3.19 ± 0.11	7.54 ± 0.11	10.40 ± 0.31
150	3.14 ± 0.03	5.93 ± 2.47	8.69 ± 0.20	3.26 ± 0.09	7.67 ± 0.42	10.68 ± 0.19
200	3.34 ± 0.25	5.82 ± 1.46	8.73 ± 0.13	3.23 ± 0.26	7.54 ± 0.40	10.56 ± 0.45

The strain rate sensitivity analysis of the polymeric foams displays a more complex scenario in fact, in agreement with the results proposed by Daniel et al. [134], the compressive modulus does not display any dependence on test speed, whereas a certain increase in plateau stress and yield strength can be observed, especially for the two foams with the higher density. The dependence of these compressive properties on test speed appears less evident than in the work presented by Daniel et al. because of the limited speed working range achievable in quasi-static conditions.

As previously done for flexural tests, a statistical analysis was performed on the data obtained in order to support the conclusions drawn and the p values obtained for compressive modulus and plateau stress are gathered in Tables 24 and 25, respectively. Test speed proved to have actually an effect on both agglomerated cork compressive modulus and initial plateau stress showing a $p < 0.03$ that is lower than the selected limit value, i.e. $p = 0.05$. For what concerns PVC foams, no statistical significance was observed for test speed effect on compressive modulus, but it was detected for test speed effect on plateau stress, in perfect agreement with the experimental data providing a solid support. It is necessary to highlight that, even if the statistical significance of test speed effect on plateau stress is lower than the selected limit of $p < 0.05$, it proved to be higher than the value corresponding to density effect which is lower than $p < 0.01$. This lower reliability connected with speed test effect can be explained considering what has been said previously about the restricted speed working range connected with the use of sole quasi-static tests, that do not allow to identify enough markedly material strain rate sensitivity.

Table 24: Statistical significance of the effect of different testing parameters, i.e. density, test speed and their interaction, on the compressive modulus of PVC foams and agglomerated corks

Compressive Modulus parameter	Agglomerated Cork Pr(>|t|)	PVC foam Pr(>|t|)
Density (ρ)	3.33×10^{-12}	$<2.00 \times 10^{-16}$
Speed (T)	6.09×10^{-5}	9.15×10^{-2}
Density x Speed (ρxT)	4.18×10^{-7}	-

Table 25: Statistical significance of the effect of different testing parameters, i.e. density, test speed and their interaction, on the plateau stress of PVC foams and agglomerated corks

Plateau Stress parameter	Agglomerated Cork Pr(>|t|)	PVC foam Pr(>|t|)
Density (ρ)	<2.00 x 10^{-16}	<2.20 x 10^{-16}
Speed (T)	2.91 x 10^{-2}	1.27 x 10^{-2}
Density x Speed (ρxT)	6.01 x 10^{-5}	1.27 x 10^{-4}

Once confirmed the statistical significance, the regression coefficients related to each parameter, i.e. density (ρ), test speed (V) and their interaction (ρV), were estimated leading to Equations (3.7) – (3.9):

$$E_{CORK} = -1.285 + 0.039\,\rho_{CORK} - 0.037\,V_{CORK} + 2.37\text{x }10^{-4}\,\rho_{CORK}V_{CORK} \tag{3.7}$$

$$\sigma_{plateau_{CORK}} = -0.3023 + 3.81 \times 10^{-3}\rho_{CORK} - 4.76 \times 10^{-4}\,V_{CORK} + 4.49 \times 10^{-6}\rho_{CORK}\,V_{CORK} \tag{3.8}$$

$$\sigma_{Plateau_{PVC}} = -2.75 + 0.043\,\rho\,PVC - 5.17\text{x }10^{-3}\,V_{PVC} - 4.08 \times 10^{-5}\rho_{PVC}\,V_{PVC} \tag{3.9}$$

where Equation (3.7) permits to evaluate agglomerated cork compressive modulus, Equation (3.8) agglomerated cork initial plateau stress and Equation (3.9) PVC foam plateau stress. The linear model allows to fit accurately the data set providing a good correlation as proved by the coefficients of determination reported in Table 26.

Table 26: Multiple R^2 values for all compressive interpolation models

Dependent Variable	Multiple R^2
Agglomerated Compressive modulus	0.842
Agglomerated Initial plateau stress	0.975
PVC foam Compressive modulus	0.981

This preliminary investigation on cores strain rate sensitivity through sole quasi-static compression tests disclosed an effective dependency of materials mechanical response on strain rate because of their viscoelastic nature. In light of the promising results obtained, the strain rate sensitivity analysis was expanded involving higher strain rate ranges through the help of drop weight tower dynamic compression tests and Split Hopkinson Pressure bar tests in order to evaluate the evolution of material behavior in a more consistent working range. The mentioned results are presented in Section 3.4.

The notable dimensional recovery capabilities of agglomerated cork, especially when compared with rigid foams ones, are universally acknowledged and the results shown in Figure 61 for agglomerated corks and Figure 62 for PVC foams, which display the instantaneous recovery and the residual deformation as a function of test speed, are an additional proof supporting this statement. Indeed, the instantaneous recovery, which is mainly an elastic recovery, varies between 65 % and 70 % for agglomerated corks and only between 25 % and 35 % for PVC foams, whereas

the residual deformation ranges between 10 % and 15 % for agglomerated corks and between 55 % and 65 % for PVC foams. This sharp difference in behavior is due to the different morphology that characterizes the two types of core as previously shown in the micrographs in Figure 55 and 56. PVC foams rigid cell walls are prone to fracture and collapse when subjected to a compressive load and this permanent damage prevent any recovery of the initial dimension. Instead, cork corrugated cell walls are able to fold completely without undergoing fracture and, when the compressive load is removed, they are free to unfold ensuring the extensive dimensional recovery. Focusing on cork dimensional recovery behavior in Figure 61, it is possible to notice a decrease in the instantaneous recovery and an increase in the residual deformation for increasing cork densities. This can be explained considering that a higher cork density entails a lower number of cells per unit area [173] and, considering that recovery phenomena are due to cell walls unfolding, this implies lower recovery capabilities. Furthermore, an increase in the instantaneous recovery and in the residual deformation for all agglomerated corks can be observed for increasing tests speed. The instantaneous recovery increase is due to the faster application of the compressive load that causes a decrease in the reaction time of the material which struggles to deform. This leads to a higher disorder in cell walls folding and this suggest that they recover faster their deformation when the compressive load is removed.
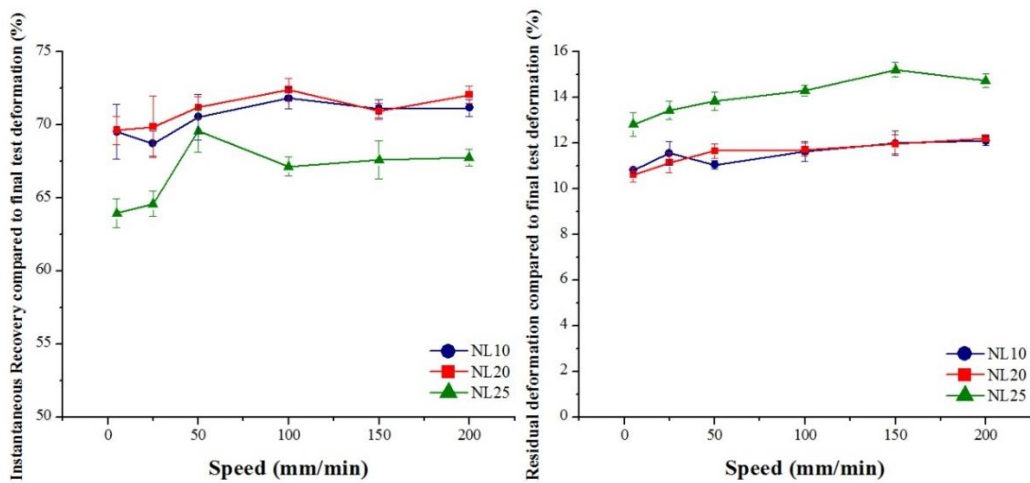
Figure 61: Evolution as a function of test speed of agglomerated corks instantaneous recovery and residual deformation normalized with respect to final test deformation
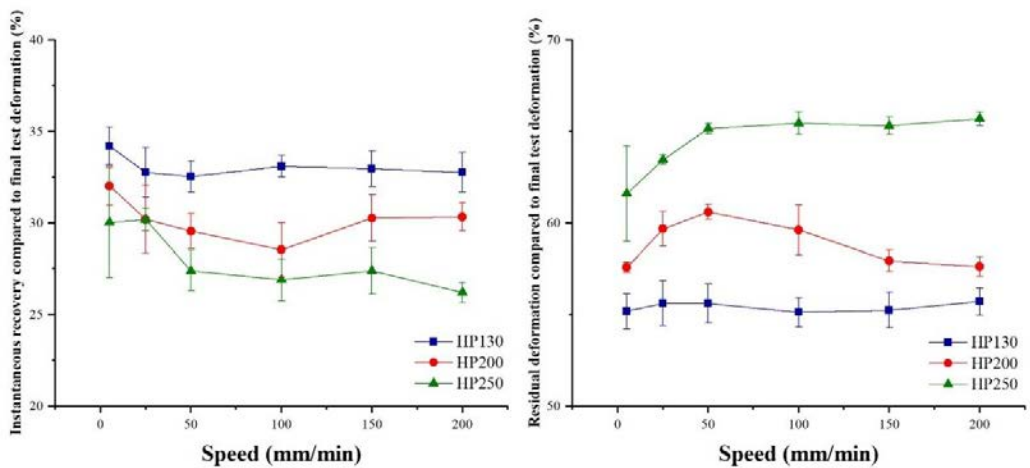
Figure 62: Evolution as a function of test speed of PVC foams instantaneous recovery and residual deformation normalized with respect to final test deformation

The higher disorder in cells folding is also responsible for the increase in residual deformation because it augments the risk of lenticular channels and pores deformation and collapse, which are the main phenomena responsible for cork permanent deformation.

A preliminary investigation of the potential anisotropy of cores compressive properties was carried out considering only two main directions: out plane and in plane directions, i.e. the direction along plank thickness and the two directions perpendicular to plank thickness. The results obtained are shown in Figure 63 for agglomerated corks and Figure 64 for PVC foams. Agglomerated corks compressive properties are supposed to be almost isotropic thanks to granules random orientation that allows to counteract the intrinsic anisotropy of natural cork whose performances varies in the radial, tangential and axial directions [37]. Even if the employment of agglomerated cork allows to reduce the problems connected to the intrinsic anisotropy of the material, it is not able to ensure a perfect isotropic material as confirmed by the data shown in Figure 63. The in-plane compressive modulus and plateau stress for all agglomerated corks proved to be higher than out-plane ones and, in particular, an increase between 45 % and 61 % was observed for compressive modulus and between 10 % and 35 % for plateau stresses values. The cause of this anisotropy can be researched and ascribed to the production process in fact agglomerated cork planks are manufactured by mixing cork granules with a polymeric binder and exposing the mixture to a moderate pressure and to heating. The employment of pressure causes a certain compression of cork particles thus inducing residual stresses and promoting a partial densification of the natural core [35]. In light of these observations, it is not surprising that the greatest differences between in-plane and out-plane compressive performances were observed for the denser cork NL25 in fact, being equal the operating pressure, the higher the density the earlier agglomerated cork enters the densification region [175] thus experiencing more residual stresses along z-axis.
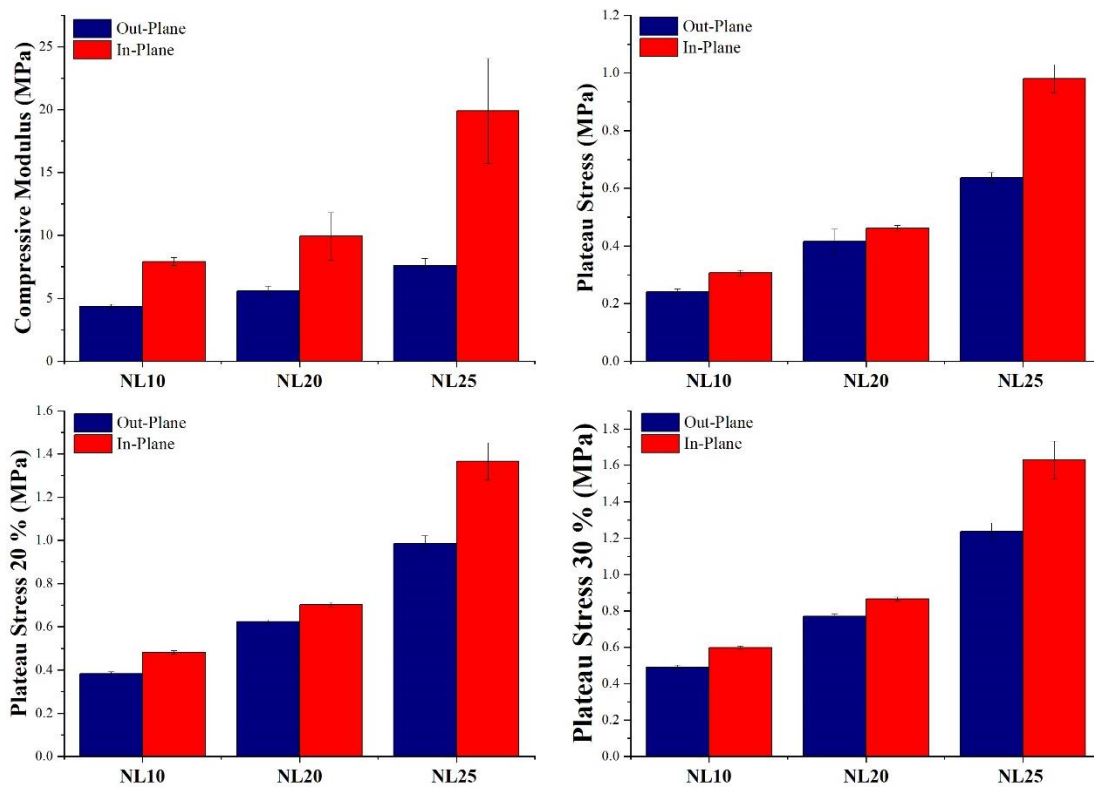
Figure 63: Out-of-plane and in-plane compressive properties of NL10, NL20 and NL25 agglomerated corks

Moving to the synthetic PVC foams, even in this case a certain anisotropy between the in-plane and out-plane properties can be detected as it is possible to infer from the data gathered in Figure 64 in perfect agreement with the results reported in literature by Kanakkanatt [178]. In contrast to agglomerated corks, PVC foams are characterized by out-plane compressive properties higher than in-plane ones. Even in this case the production process is responsible for cores anisotropy in fact all foam cells are elongated along the z axis due to the insufflation of gas in the polymeric mass. When observed perpendicularly to the x-y plane, cells look almost circular and this arrangement makes the planes parallel to the z axis denser because of the presence of numerous and thicker cell walls that makes the material stiffer and stronger along the out of plane direction [179]. This hypothesis is corroborated by the analysis of the difference between the in-plane and out-plane properties as a function of foam density in fact the lower the foam density the higher the discrepancy in the compressive performances. In particular, HP130 is characterized by an increase of 69 %, 66 % and 51 % of the out of plane compressive modulus, yielding stress and plateau stress respectively whereas HP200 and HP250 by an increase of 10.97 %- 12.9%, 35.8 % - 50.7 % and 42.3 %- 49.9 % of the same compressive properties. A lower density implies a higher amount of air trapped in the polymeric mass that causes a more pronounced discrepancy in cell walls arrangement.
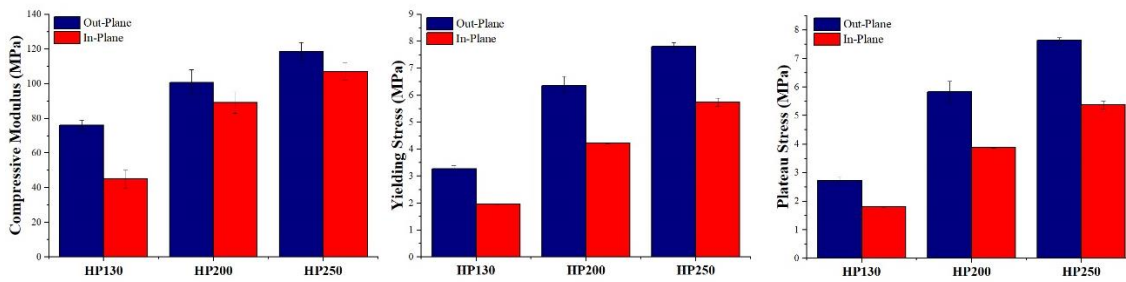
Figure 64: Out of plane and in-plane compressive properties of HP130, HP200 and HP250 PVC foams

The effect of temperature on both agglomerated corks and PVC foams compressive properties was also investigated and the trend of the results obtained shows a perfect agreement with the one obtained with flexural tests proving that the same mechanisms of deformation and damage are involved. The evolution of agglomerated corks compressive modulus and plateau stress with temperature is shown in Figure 65 and displays a progressive reduction of both compressive modulus and plateau stress with temperature. This decreasing trend can be ascribed to two different effects. The first one is the thermal degradation of the polymeric binder that jeopardizes its mechanical performances and leads to the formation of an increasing number of intergranular fractures of the sample as shown in Figure 66. The second effect is the progressive softening of cork that is much more pronounced when cork density and hence its solid mass increases thus leading to a reduction of 34.5 % of the compressive modulus of 16.5-20 % of the plateau stress for NL10, of 59.4 % of the compressive modulus of 31.3-33 % of the plateau stress for NL20 and of 67.1 % of the compressive modulus of 41.9-43.6 % of the plateau stress for NL25. The trend of PVC foams compressive modulus and plateau stress with temperature is shown in Figure 67. As already detected for the flexural performances, a progressive reduction of the mechanical properties of the synthetic material can be detected when temperature increases due to the progressive approach of the glass transition temperature. In particular, it was observed a reduction

of 35.5 % of the compressive modulus and 27 % of the plateau stress for HP130, of 25.22 % of the compressive modulus and 31.8 % of the plateau stress for HP200 and of 10.7 % of the compressive modulus and 37 % of the plateau stress for HP250.
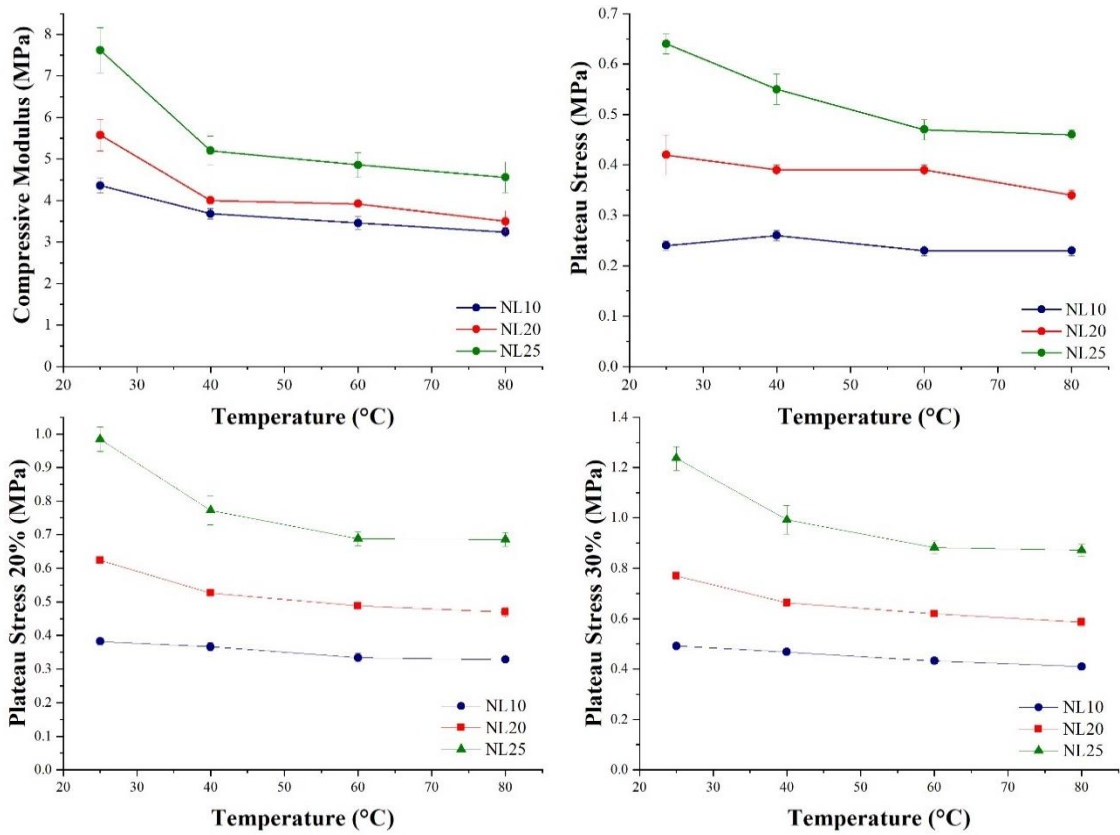
Figure 65: Agglomerated cork compressive modulus, initial plateau stress and plateau stress at 20 % and 30 % of deformation as a function of operating temperature
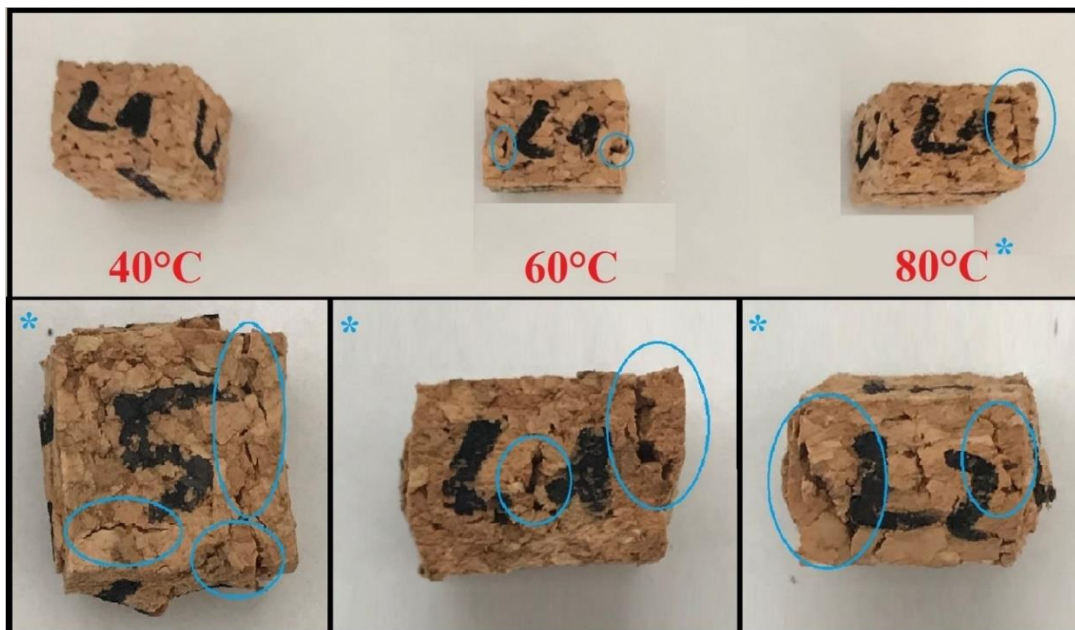
Figure 66: Damage progression of agglomerated cork compressed samples as a function of operating temperature
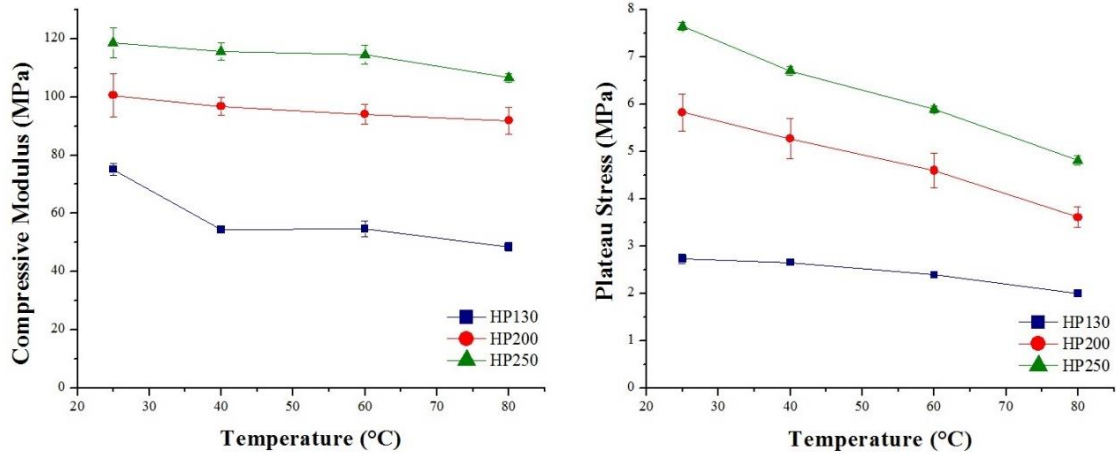
Figure 67: PVC foams compressive modulus and plateau stress as a function of operating temperature

3.3.4 Water absorption and its effect on compressive properties

The water absorption behavior of NL10, NL25 and HP130 core materials was investigated by immersing the samples in distilled and sea water until they reached saturation. Samples mass and swelling were accurately controlled over time, and all variations were calculated according to Equations (3.10) [180,181] and (3.11), respectively:

$$M = \left[\frac{M_t - M_0}{M_0}\right] x \ 100 \tag{3.10}$$

$$\varepsilon_i = \left[\frac{\varepsilon_{i,t} - \varepsilon_{i,0}}{\varepsilon_{i,0}}\right] x \ 100 \tag{3.11}$$

In Equation (3.10), M_t is sample mass at a general weighting time t and M_0 is the initial sample mass whereas in Equation (3.11) $\varepsilon_{i,t}$ is the length of sample side i at a general weighting time t with i = x, y, z, i.e. one of the three main directions that characterize the sample, and $\varepsilon_{i,0}$ is the initial length of that side. Indeed, at every measuring time t, swelling was calculated as the average value along the three main directions. Thanks to the water absorption curves obtained, it was possible to calculate the diffusion coefficient for each water type according to Equation (3.12) [180–182]:

$$D = \pi \left[\frac{h}{4 \ M_\infty}\right]^2 \left[\frac{M_2 - M_1}{\sqrt{T_2} - T_1}\right]^2 \tag{3.12}$$

The water absorption and swelling curves as a function of immersion time are shown in Figure 68, while the final water uptake and swelling values are reported in Figure 69 and the diffusion coefficient values are gathered in Table 27. From the reported results, the first conclusion that can be drawn is that despite its hydrophobic nature cork displays a water uptake much higher with respect to PVC which is characterized by a water uptake of only 16.77 % in distilled water and 15.44 % in sea water which are almost comparable. This could be explained considering that even

113

if suberin and lignin, which are the two main chemical components in cork (53 % and 26 %, respectively [37]), are hydrophobic and spread this characteristic to cork, the immersion in water is a long-term process in which cellulose and hemicellulose, the other two main chemical components in cork (10 % and 12 %, respectively [37]), must be taken into account. Their hydrophilic nature may convert cork into a sponge after a prolonged exposure time in water. For what concerns the effect of density on agglomerated cork water uptake, it is possible to conclude that the lower the density the higher the mass change underwent by the material: in fact NL10 is characterized by a mass change between 36.7 % and 46.5 % higher than NL25. This is coherent with the fact that the solid mass of agglomerated cork is concentrated in the polymeric binder and in the cell walls and hence a lower density implies a higher air content and a higher number of voids and channels that can hold a higher amount of water, once it has diffused through the cell walls, and promote capillarity phenomena. Moreover, NL10 diffusion coefficient is of one order of magnitude higher than NL25 and this is in perfect agreement with the work proposed by Earl and Shenoi [180] who studied the mechanisms of water uptake in closed cell polymeric foams and found out that the diffusant has a greater mobility when foam density is lower.
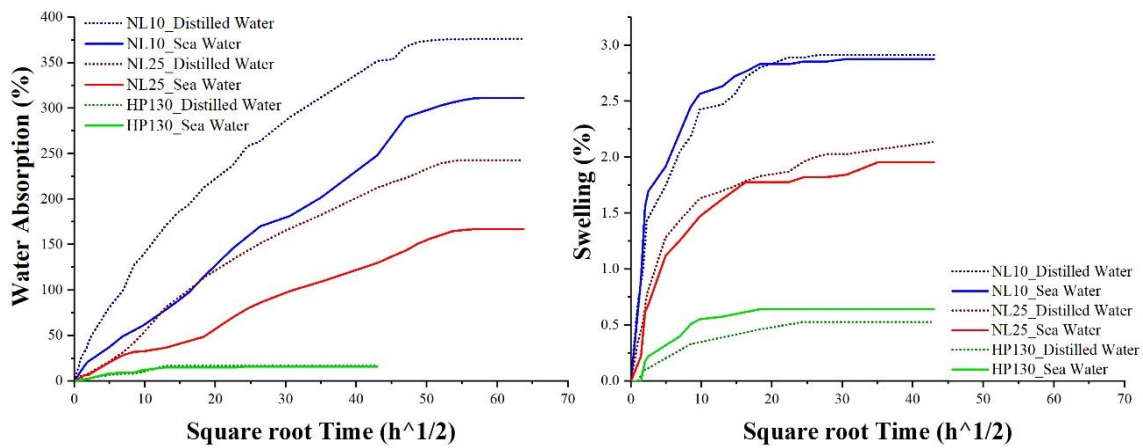
Figure 68: Water absorption and swelling curves as a function of immersion time for agglomerated corks NL10 and NL25 and PVC foam HP130
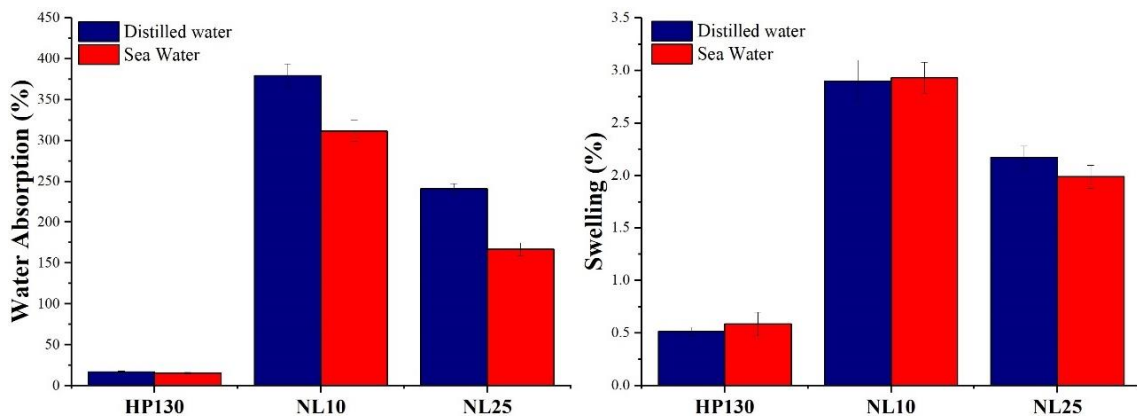
Figure 69: Water absorption and swelling final values for agglomerated corks NL10 and NL25 and PVC foam HP130

Table 27: Distilled and sea water diffusion coefficient in the three core materials

Core material	Distilled Water Diffusivity (m²/s)	Sea Water Diffusivity (m²/s)
NL10	5.92×10^{-8}	1.59×10^{-8}
NL25	6.66×10^{-9}	6.21×10^{-9}
HP130	2.87×10^{-7}	1.90×10^{-7}

Moving to the comparison between distilled water and sea water, it is possible to notice that all three core materials are characterized by a lower water uptake when immersed in sea water rather than distilled water and by a lower diffusion coefficient. In particular, HP130 shows a mass change 8.5 % lower in sea water, NL10 21.8 % lower and NL25 44.4 % lower. These results are in perfect agreement with the ones presented by May-Pat and Avilés [183] who investigated the effect of water uptake on the microstructure and mechanical properties of a 48 kg/m³ PVC foam and found out a lower water absorption in sea water. These outcomes can be ascribed to the presence of salt ions in sea water that are characterized by a bigger size (0.386 nm Na+ hydrated and 0.291 nm Cl- hydrated [184]) than water molecules (0.27 nm) thus decreasing the diffusion rate with respect to distilled water. Moreover, the addition of salt to pure water leads to a slight increase in water viscosity thus slowing down the diffusion process. In light of the work carried out by Rosa and Fortes [182] who studied the water absorption of natural cork as a function of operating temperature taking also into account the volumetric changes of the material, the swelling suffered by the samples was also evaluated. HP 130 displays a very limited increase in cube edge length that ranges between 0.52 and 0.59 % whereas agglomerated cork shows a significant change of cube dimensions between 2.9 and 2.93 % for NL10 and 1.99 and 2.17 % for NL25 in perfect agreement with the results by Rosa and Fortes [182], who found out a linear dimensional change of around 2 % for natural cork in both axial and tangential directions.

Once samples reached saturation, they were tested in compression in order to evaluate the effect of water absorption on the mechanical response of the core materials. In Figure 70 the compressive modulus values of the three cores are reported. All of them experienced a reduction of the compressive modulus after a prolonged immersion in water due to its plasticizing effect that causes a decrease between 35.1 % and 37.9 % in NL10, between 17.7 % and 21 % in NL25 and between 29.2 % and 31.4 % in HP130. This hypothesis seems to be corroborated by the fact that each core material experiences a partial recovery of this property after drying and, in particular, a recovery between 22.2 % and 27.8 % in NL10, between 9.5 % and 12.7 % in NL25 and between 8.5 % and 11.4 % in HP130.
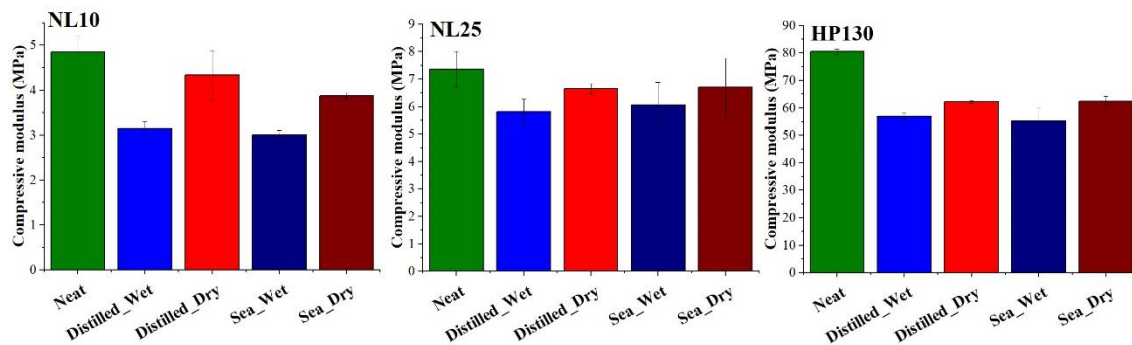
Figure 70: NL10, NL25 and HP130 compressive modulus before and after distilled and sea water immersion

These results are in perfect agreement with the ones presented by May-Pat and Avilès [183] for the 48 kg/m^3 PVC foam and by Rosa et al. [185] who studied the effect of hot water treatment on cork compressive properties. Moving to the analysis of agglomerated cork plateau stress, the values of the initial plateau and of the plateau stresses at 20 % and 30 % of deformation are gathered in Figure 71 for NL10 and Figure 72 for NL25. NL10 and NL25 samples display a comparable trend of plateau stress values in both wet conditions. Wet samples initial plateau is always lower than neat samples one and this is mainly due to the plasticizing effect of water already mentioned for the compressive modulus. In particular a decrease of 45 % was observed for NL10 and between 55 % and 58 % for NL25. Once reached the plateau region, cork cell walls start to move close reducing cell volume and hence the space available for water which will start exerting a counter pressure that will counteract the plasticizing effect allowing wet samples plateau value at 20 % and 30 % of deformation to progressively approach neat samples one. This hypothesis is corroborated by two evidences. The first evidence is connected to the fact that samples immersed in distilled water are characterized by a higher plateau stress at 20 % and 30 % of deformation because of the higher water uptake that determines a higher filling of cork cells and hence a higher counter pressure. The second evidence is given by samples damage mode shown in Figure 73 where it is possible to observe how lateral facets deform and fracture outwards. This behavior can be ascribed to the excessive internal pressure reached in the sample due to water compression that leads to agglomerated cork fracture in order to allow water flow out. Moving to dry samples plateau stress values, it is possible to notice that NL10 samples treated in distilled water display a plateau stress comparable to neat samples one and that dry samples treated in sea water are always characterized by the highest plateau stress value with an increase between 20 % and 30 % with respect to neat samples.
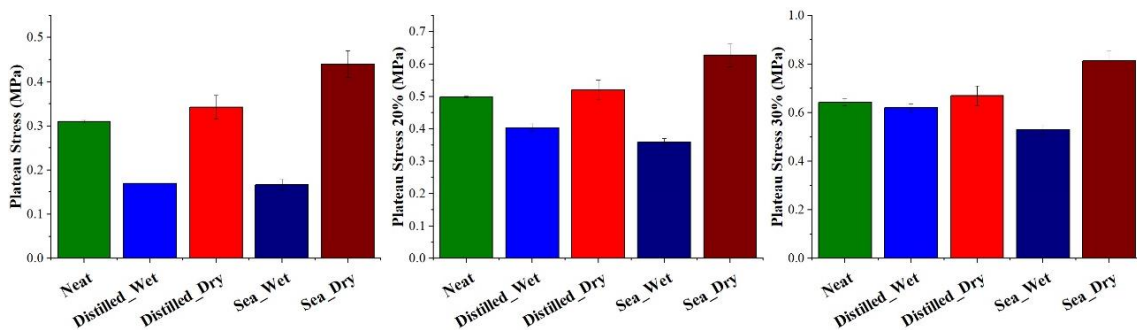
Figure 71: NL10 initial plateau and plateau at 20 % and 30 % of deformation before and after distilled and sea water immersion
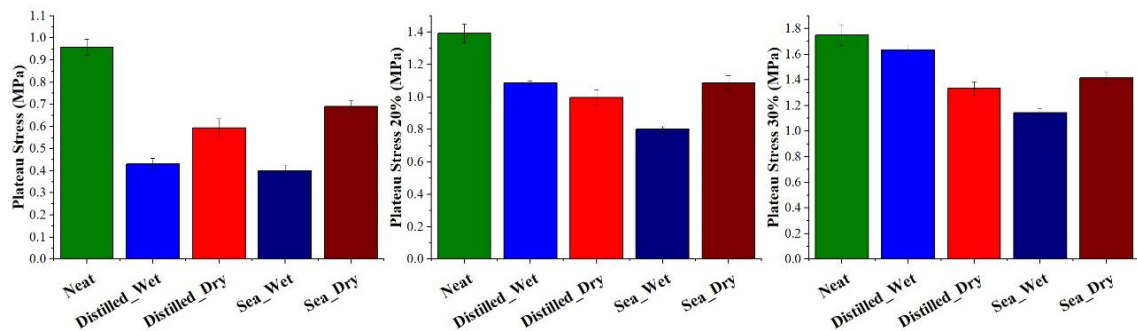
Figure 72: NL25 initial plateau and plateau at 20 % and 30 % of deformation before and after distilled and sea water immersion
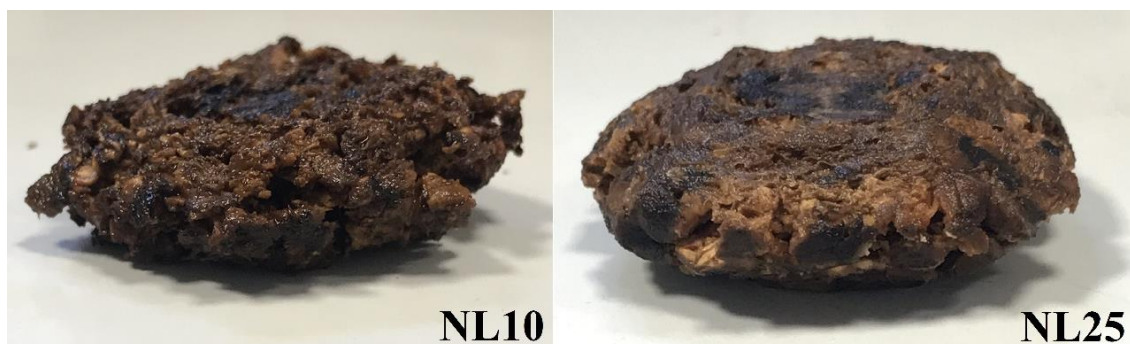
Figure 73: Damage mode of NL10 and NL25 wet samples

The situation is different for NL25 samples where plateau stress values are significantly lower than neat samples ones especially in the case of samples submerged in distilled water that experience the highest degradation. In particular, a decrease of plateau stress values between 31 % and 61.5 % was detected for samples treated in distilled water and between 23.5 % and 39 % for samples treated in sea water. The different trend in plateau stress values observed for NL10 and NL25 can be ascribed to their different density and hence their compactness. The dimensional changes underwent by NL10 and NL25 following water absorption were previously introduced and a variation between 2.9 % and 2.93 % was detected for NL10 and between 1.99 % and 2.17 % for NL25. Considering that water absorption does not affect only the external cells of the samples but also inner ones, it is reasonable to think that even the inner parts of the samples undergo swelling. In the case of NL10 the higher porosity provides granules with enough empty space to swell thus having the possibility to adapt to the dimensional changes. On the contrary, the higher compactness of NL25 hinders the swelling phenomena leading to the formation of internal stresses that can undermine the integrity of the polymeric binder and hence the compressive performances even of the dried samples. It was previously mentioned that sea water dried samples are characterized by the highest plateau stress value in the case of NL10 samples and by a lower degradation of the mechanical performances in the case of NL25. These results are due to the penetration of NaCl in cork cell walls and to the deposition of salt crystals in cork voids, such as lenticular channel and cells, resulting from water removal which act like a reinforcement. This explanation is supported by the morphological analysis carried out through SEM and Energy Dispersive Spectroscopy (EDS) which allowed to detected salt sediments in cork cells and NaCl traces in cork cell walls. Salt crystals deposited in NL10 agglomerated cork cells can be detected in the micrograph shown in Figure 74. The EDS analysis corroborates these findings allowing to identify a considerable amount of sodium (Na) and chloride (Cl). Further elements detected are carbon (C) which is the main macromolecular backbone of cork and gold (Au) whose presence is due to the sputter coating process employed to make the sample conductive.

Moving to HP130 PVC foam, the evolution of its yielding and densification stresses are shown in Figure 75 and 76, respectively. As previously observed for the compressive modulus, both yielding and densification stresses undergo a decrease when tested in wet condition and recover partially their strength when dried. The decrement in wet condition must be ascribed to the plasticizing effect of water and the only partial recover of the compressive strength must be ascribed to the permanent changes and damage induced in foam microstructure as pointed out by May-Pat and Avilès [183]. In their study they highlighted a permanent damage of the outer cells after 28 days water exposure which appears in the form of small pits and walls breakage. It must point out that in the case of HP130 the densification stress in wet condition is lower than in neat

conditions because the water uptake is slow and the water contained in the cells is not enough to induce a significant counterpressure as happens for agglomerated cork. Considering the densification stress values of agglomerated cork NL10 and NL25 shown in Figure 75, it is possible to conclude that this parameter is characterized by the same tendency already acknowledged in plateau stress analysis. Even for the HP130 foam the combined SEM and EDS analysis allowed to identify NaCl crystals deposits in the cells as shown in Figure 77.
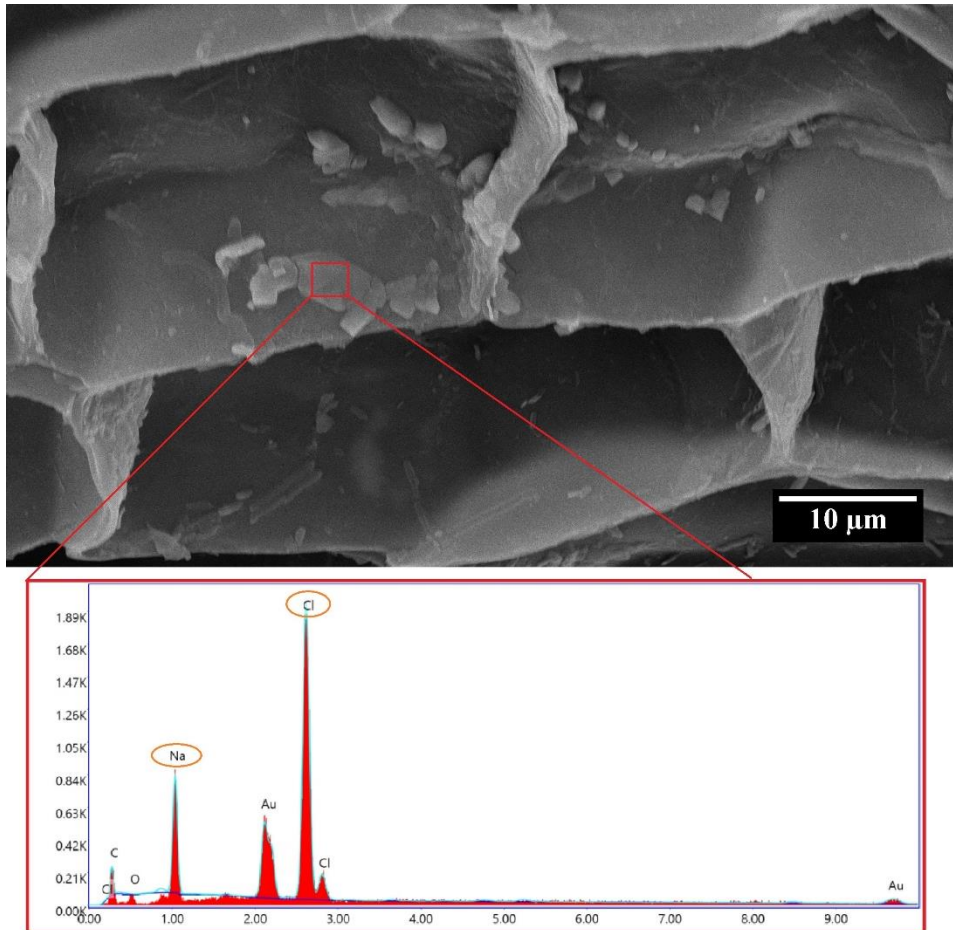
Figure 74: Salt crystal deposit in a NL10 cell and the corresponding EDS analysis
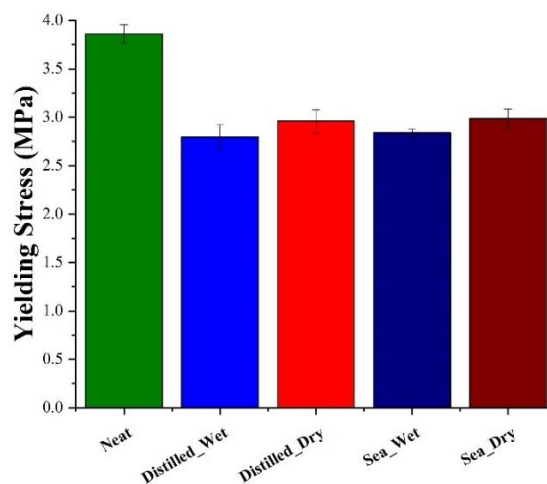
Figure 75: HP130 yielding stress before and after distilled and sea water immersion
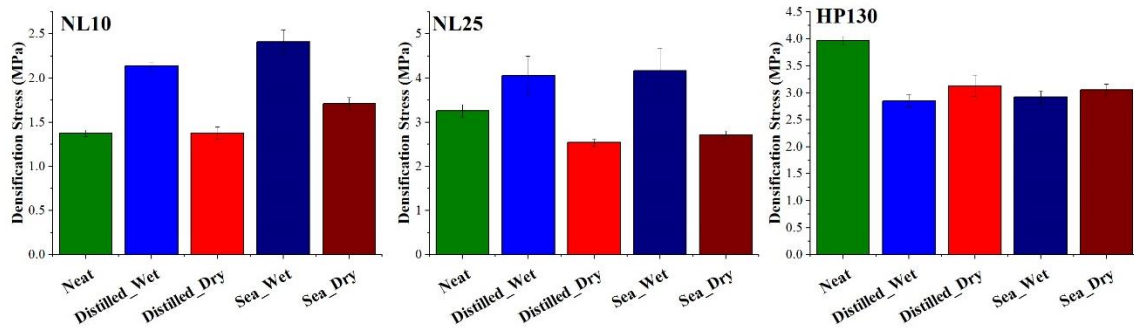
Figure 76: NL10, NL25 and HP130 densification stress before and after distilled and sea water immersion
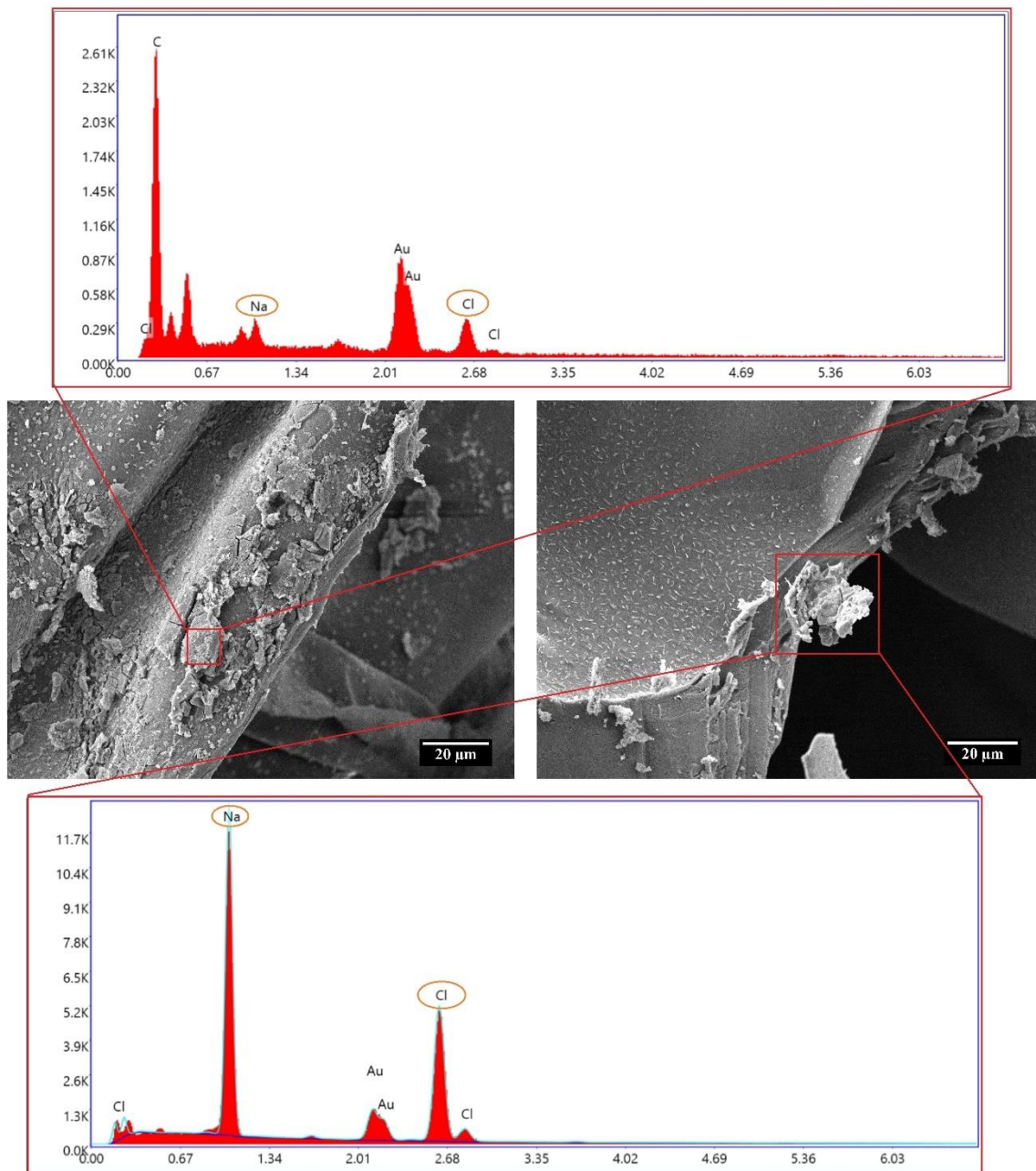
Figure 77: Salt crystal deposits in a HP130 foam and the corresponding EDS analysis

3.3.5 Salt fog ageing effect on compressive properties

The same type of cores, i.e. NL10, NL25 and HP130, subjected to water absorption were also selected to investigate the effect of salt fog prolonged exposure on compressive properties in both out of plane and in plane directions. Compressive modulus, plateau stress and densification stress values are shown in Figures 78, 79 and 80, respectively, and for out of plane results a compelling comparison with prolonged sea water immersion was provided. Concerning the compressive modulus, a reduction of this parameter in wet conditions can be recognized as already acknowledged after a prolonged immersion in water due to the plasticizing effect played by the moisture. A decrease between 52 % and 67 % was observed for NL10 along the out of plane direction and between 65 % and 74 % along the in-plane direction, between 24 % and 45.2 % for NL25 along the out of plane direction and between 71.6 % and 76.1 % along the in-plane direction and between 21.2 % and 25.9 % for HP130 along the out of plane direction and between 19.6 % and 37.9 % along the in plane direction. Similar results were observed by Fiore et al. [133] and by Scalici et al. [132] who investigated the salt fog spray ageing effect on the flexural behavior of agglomerated cork sandwich structures with flax and basalt fibers reinforced skins, respectively, and found out a reduction in both flexural modulus and strength of the composite. Each core material experienced a partial recovery of this property when tested in dry condition as already observed in the case of prolonged water immersion. For the HP130 foam, the higher the exposure time to salt fog the higher the detrimental effect on the dry compressive modulus that becomes maximum in the case of sea water prolonged immersion. Moving to plateau stress analysis, it is possible to observe a strong decrease in this parameter for all core materials when tested in wet conditions always due to the plasticizing effect played by moisture. More complex is the analysis of the results in dry conditions. Concerning NL10 samples along the out of plane direction, it is possible to notice that the samples immersed in sea water display the highest plateau stress and that the higher the exposure time to salt fog, the higher the plateau stress value in both out of plane and in-plane directions. These outcomes can be explained remembering the results presented in section 3.3.4 and considering that the higher the exposure time, the higher the penetration of NaCl in cork cell walls and the deposition of salt crystals in cork voids as a consequence of water removal. Even in this case the previous statement is corroborated by a morphological analysis carried out by SEM and EDS. Figure 81 displays a huge NaCl deposit on NL10 cell walls and the corresponding elemental analysis.
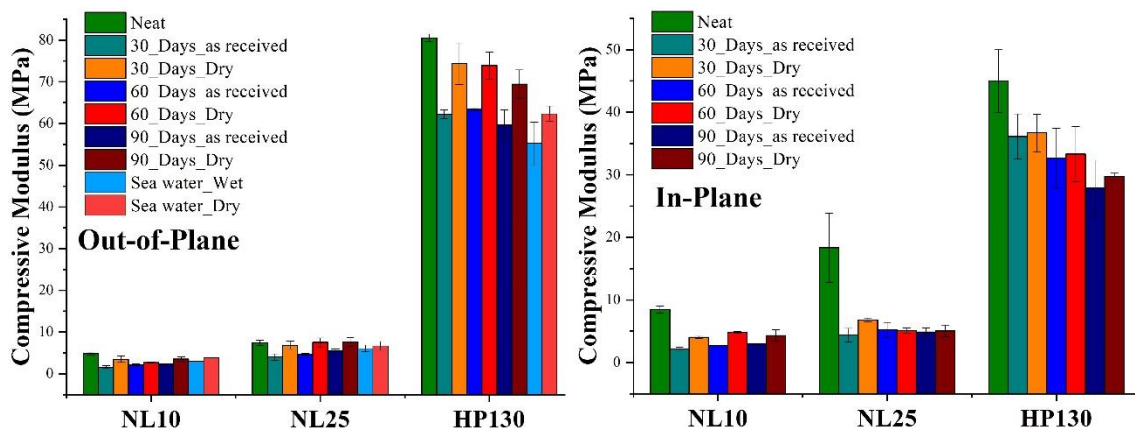
Figure 78: Wet and dry compressive modulus of NL10, NL25 and HP130 as a function of salt fog exposure time along out of plane and in-plane directions

Moving to NL25, in section 3.3.4 it was observed that the prolonged exposure to water immersion led to a conspicuous inner swelling of the samples with the consequent formation of internal stresses which undermine the integrity of the polymeric binder and hence the compressive performances of the dried samples. In these conditions the healing effect played by NaCl absorption and deposition did not allow to obtain a full recovery of the initial plateau stress value. The situation is different in the case of samples subjected to salt fog ageing as proved by the deformation mode of NL25 wet samples as a function of exposure time in Figure 82. Samples exposed to salt fog and tested in wet conditions remain compact and do not display outwards fractures as in the case of samples exposed to prolonged water immersion. This means that the sample is not saturated and that likely the internal swelling is not so severe to compromise polymeric binder integrity. This hypothesis would allow to explain why NL25 acts like NL10 displaying a higher plateau stress for an increasing exposure time. Considering that the polymeric binder is not significantly undermined, NL25 is able to take advantage of the reinforcing effect played by NaCl. Salt crystal deposits were identified by SEM and EDS analysis also in NL25 structure as proved by the micrograph and the elemental spectrum shown in Figure 83.
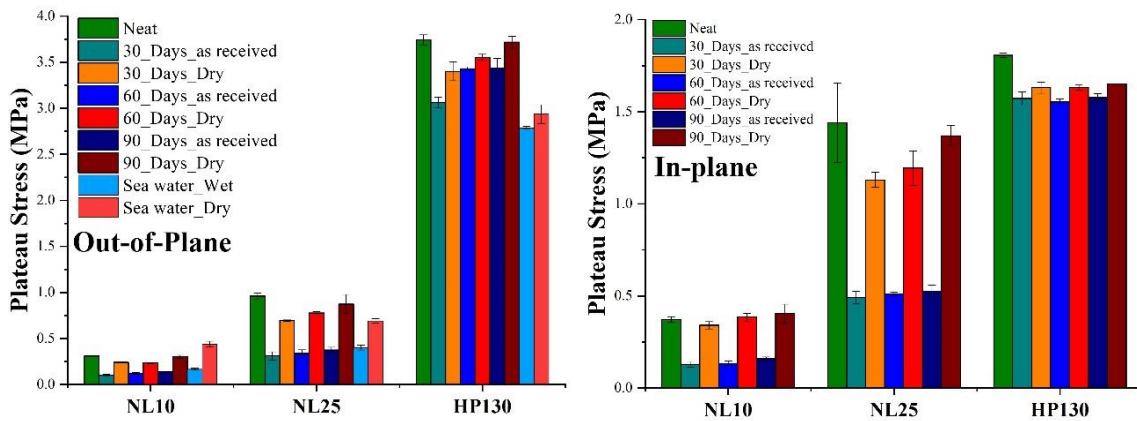
Figure 79: Wet and dry plateau stress of NL10, NL25 and HP130 as a function of salt fog exposure time along out of plane and in-plane directions
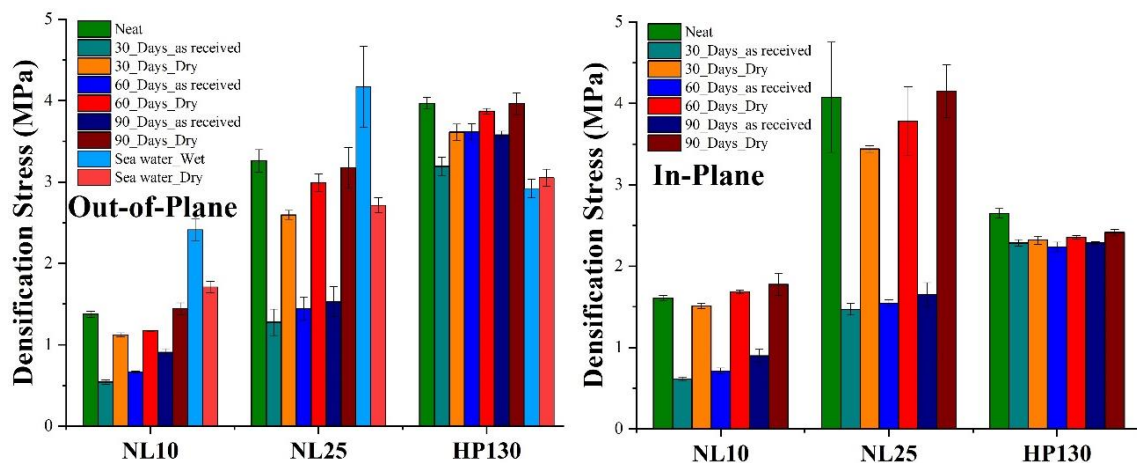
Figure 80: Wet and dry compressive modulus of NL10, NL25 and HP130 as a function of salt fog exposure time along out of plane and in-plane directions

Moving to HP130 polymeric foam, it is possible to observe that along the in-plane directions the decrease in plateau stress due to the detrimental effect played by salt fog is almost constant and does not depend on the exposure time, whereas in the out of plane direction the higher the exposure time, the lower the decrease suffered in the plateau stress. This could be

explained considering that PVC foam cells are elongated along the z-axis thus making the planes parallel to this axis denser and hence the higher NaCl deposition the better it could contribute to material strengthening counteracting the detrimental effect of moisture on foam microstructure. This effect cannot be detected along x and y axes because the planes parallel to them are characterized by wide hollow areas left by the elongated cell and little deposition of NaCl crystals is not able to provide the reinforcing effect to such an extent. Concerning the densification stress, all core materials are characterized by results perfectly comparable with plateau ones when tested in dry conditions, but few clarifications have to be made for agglomerated corks wet results. If the plateau stress in wet conditions is almost constant regardless of the exposure time, this is not true for the densification stress that becomes higher for increasing exposure time until reaching the highest value after reaching saturation in sea water immersion. This can be explained considering that a higher exposure time implies a higher water and moisture content that makes the densification process shifting to lower strain values and induces an increase in material reaction force due to the compression of the water trapped in cork cells and walls.
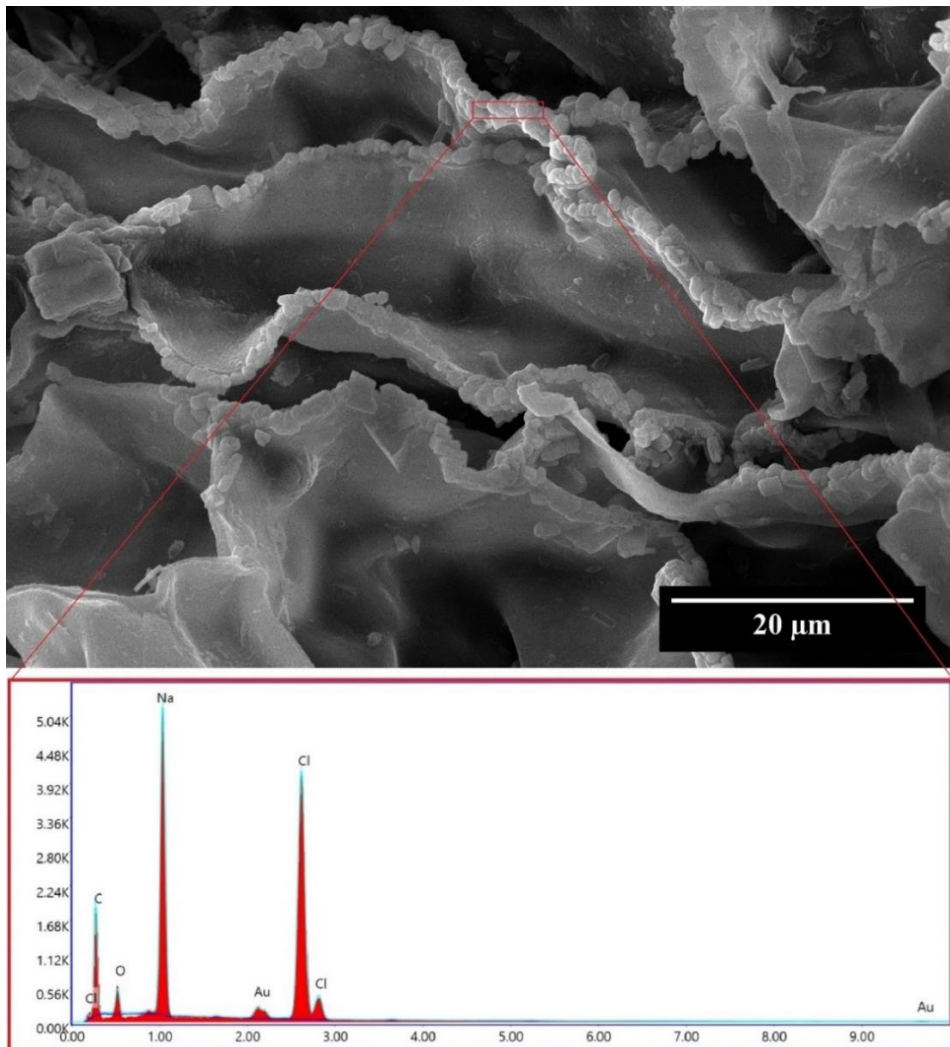
Figure 81: Salt crystal deposit on NL10 cell walls and the corresponding EDS analysis

Figure 82: NL25 samples deformation mode as a function of salt fog and sea water exposure time
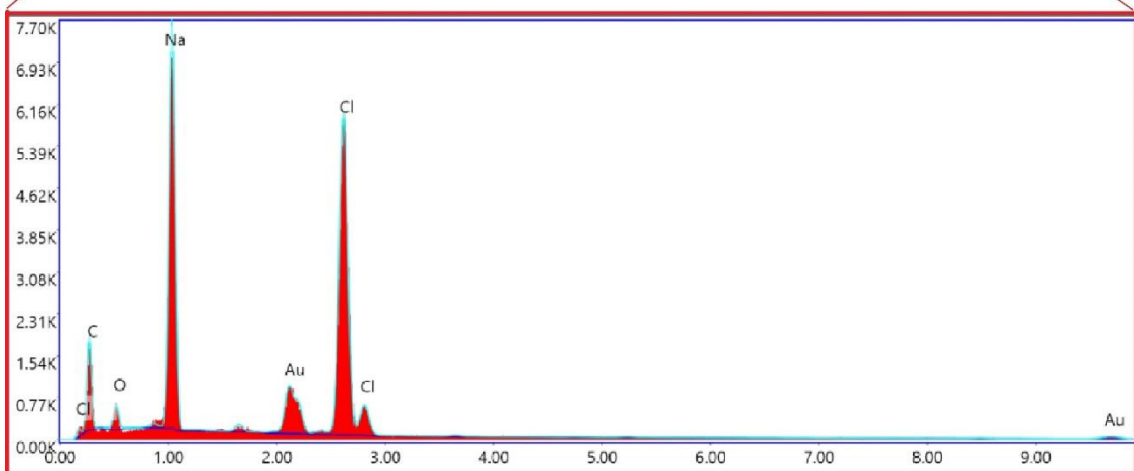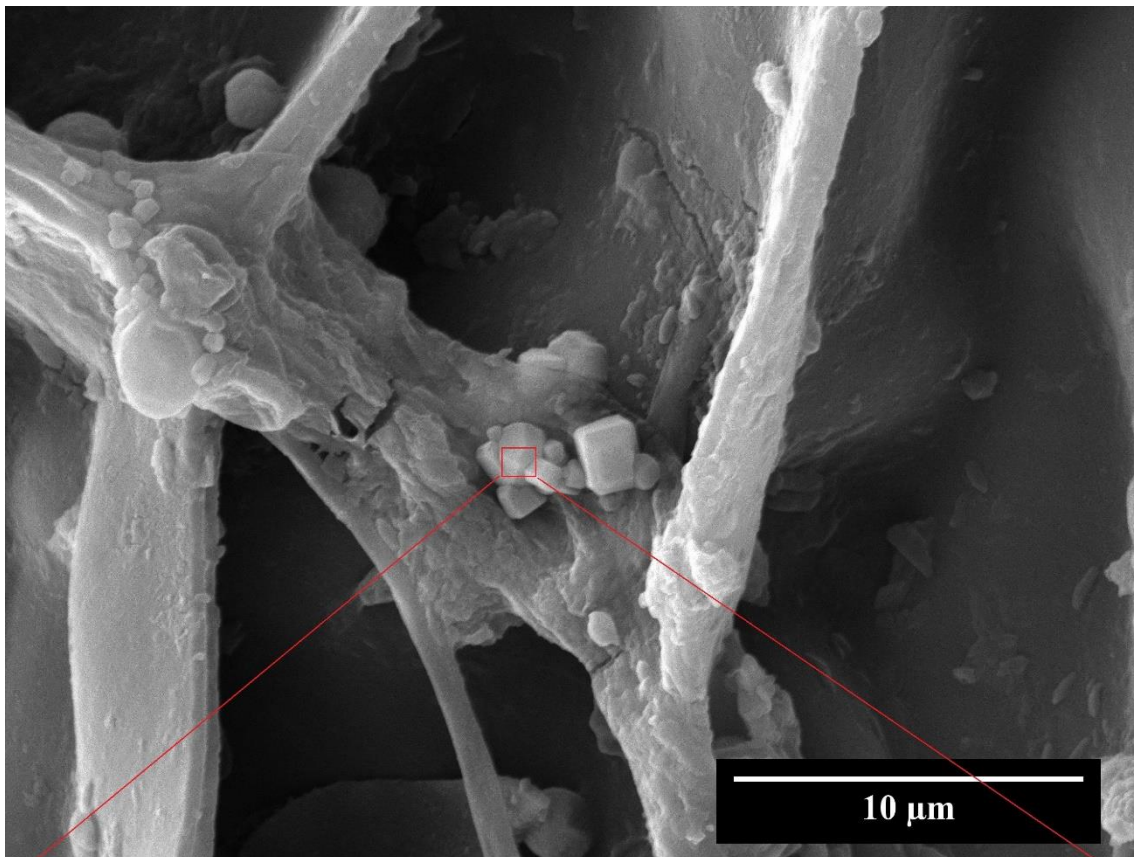
Figure 83: Salt crystal deposit on NL25 cell walls and the corresponding EDS analysis

3.4 Dynamic Characterization

3.4.1 Drop weight tower dynamic compression tests

The evolution of natural and synthetic cores dynamic compressive properties in a wide temperatures range, i.e. room temperature, 60 °C and -40 °C, was investigated through drop weight tower tests. Some works already addressed this topic studying the effect of low and high temperatures on expanded and agglomerated cork dynamic compressive response, but taking into account a single impact energy [186,187]. In this study it steps forward considering the combined effect of impact energy and operating temperature performing tests at 5 J and 7 J on all core types and at 13 J for NL25 and all PVC foams. Ptak et al. [188] carried out a similar experimental campaign investigating the effect of both impact velocity and high temperature, i.e. 50 °C, on expanded and agglomerated cork samples, but employing a hemispherical impactor. The mentioned work considered only a temperature higher than room temperature neglecting the low temperatures addressed in the present work. Moreover, the employment of a hemispherical impactor prevents the achievement of a perfect uniaxial compression in contrast to the flat impactor used in the present work that ensures a more uniform and homogeneous distribution of the compressive load throughout the sample. At first, the sole energy effect was investigated analyzing the results at room temperature shown in Figure 84 and 85 which gather the maximum force, maximum displacement and percentage absorbed energy values of all cores impacted at room temperature at 7 J and 13 J, respectively.
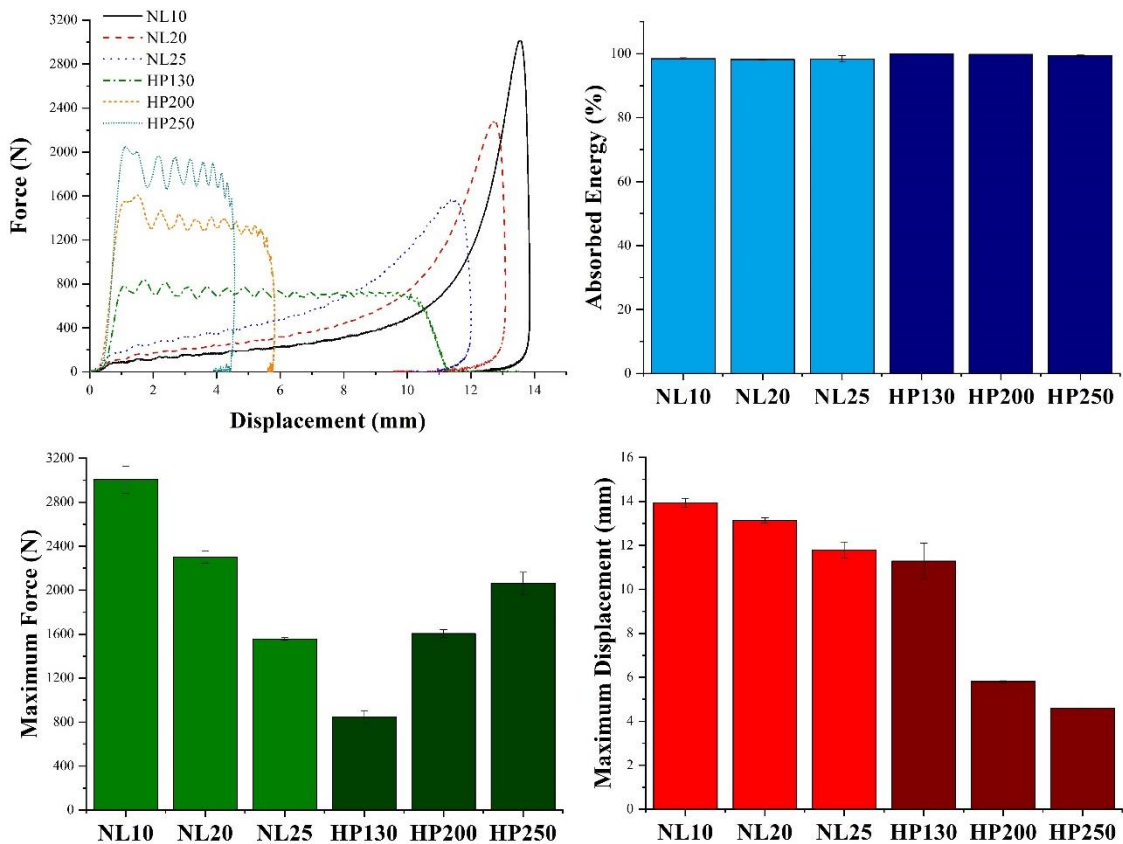
Figure 84: Compressive response curves, percentage absorbed energy, maximum force and displacement of the six cores subjected to a 7 J impact at room temperature
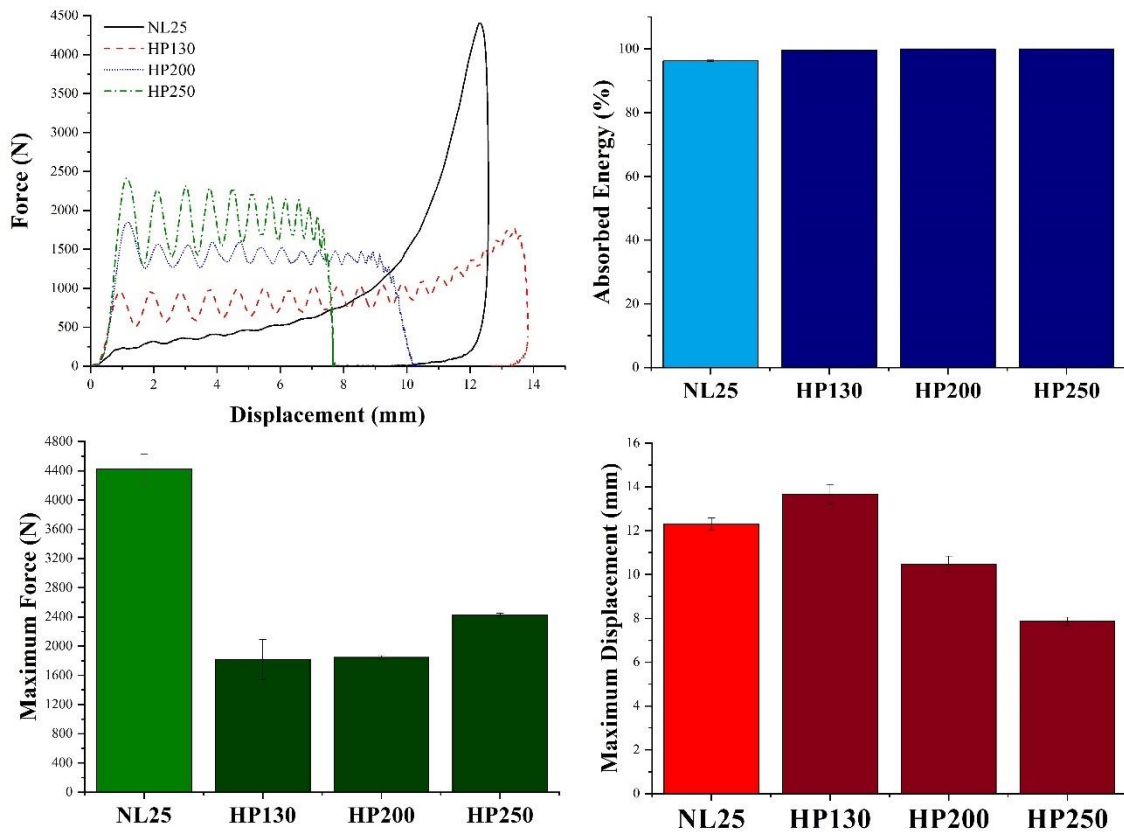
Figure 85: Compressive response curves, percentage absorbed energy, maximum force and displacement of the six cores subjected to a 13 J impact at room temperature

5 J impact results are not reported considering that are characterized by the same tendency detected for the 7 J impact. The 7 J impact results in Figure 84 underline the notable absorbing capabilities of both agglomerated corks and PVC foams that display a percentage absorbed energy around 98 % and 100 %, respectively. For what concerns the maximum displacement, both core types are characterized by a decrease of this parameter when core density increases and this is due to the fact that it is more difficult to deform a material with thicker cell walls being equal the impact energy. In particular, NL10 maximum displacement is 24.2 % higher than NL25 for a 5 J impact and 11.6 % for a 7 J impact whereas HP130 maximum displacement is 52 % higher than HP250 for a 5 J impact and 59.3 % for a 7 J impact. The analysis of maximum force data discloses the first disagreement in the compressive behavior of the two types of core in fact for a 7 J impact agglomerated cork undergoes an increase of maximum force for decreasing plank density whereas PVC foams are characterized by the opposite trend. This discrepancy can be explained considering that the two core materials are working in two different compressive regions. All agglomerated corks have already entered the densification region where small increases in the displacement are responsible for a strong increase of the stress and considering that NL10 reaches a higher maximum displacement than NL25 it will be also characterized by a higher maximum force. Opposite situation can be observed for the PVC foams that are still working in the plateau region where the maximum force is reached at the yielding point which increases with foam density. Moving to the results of the 13 J impact in Figure 85, the first thing to underline is that NL10 and NL20 agglomerated corks could not be tested at this energy because of the high maximum deformation that would have been reached and that would have implied an excessive maximum force too close to the operating limit of the load cell that could have experienced a

deterioration of its integrity and functionality. Despite these limitations, the tests performed on NL25 prove that its absorbing capability is still comparable with PVC foams one. PVC foams maximum displacement is characterized by the same tendency already acknowledged for the 7 J impact, but some differences arise in maximum force trend. Indeed, HP130 maximum force almost equals HP200 one because the lowest density foam approached the densification region. If drop weight tower dynamic compression results seem to confirm the results obtained in the quasi-static characterization and hence the better mechanical properties of PVC foams able to withstand higher impact energies, the employment of the high-speed camera permitted to confirm and corroborate the major advantage of agglomerated cork over PVC foams that is its outstanding dimensional recovery capability. Some frameworks of NL25 (upper) and HP130 (lower) samples, before and after 10 ms a 13 J impact, were selected from the impact record and are shown in Figure 86. The two cores experienced almost the same maximum deformation, i.e. 12 mm NL25 and 13 mm HP130, but after almost 10 ms from the impact NL25 has almost recovered its initial dimension whereas HP130 displays a halving of its initial height. These findings are in perfect agreement with the dimensional recovery analysis carried out in section 3.3.3, where a higher instantaneous dimensional recovery was detected for agglomerated cork with increasing test speed and will turn out to be even more relevant in the following section 3.4.2.
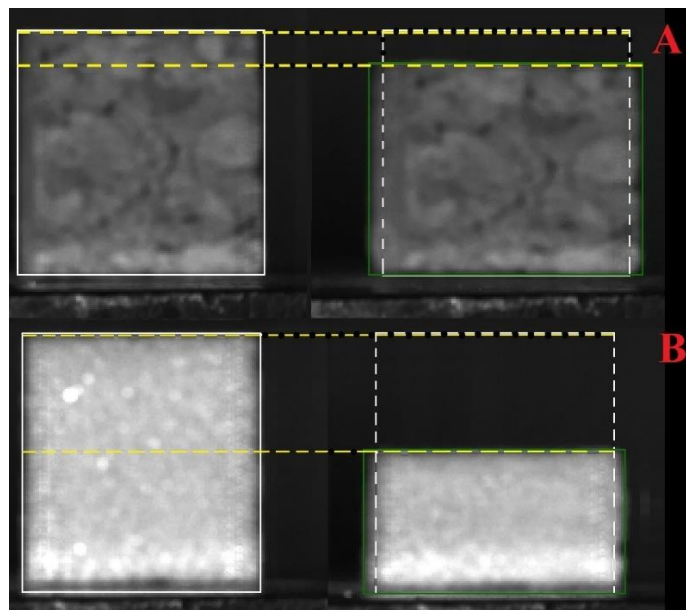
Figure 86: NL25 (A) and HP130 (B) specimens before and after almost 10 ms a 13 J impact

After this preliminary analysis of the effect of impact energy at room temperature, it is possible to go further with the analysis of the combined effect of impact energy and temperature. Figure 87 gathers the maximum force and displacement values of all cores after a 5 J impact at the three operating temperatures. Due to their viscoelastic nature both types of cellular core are characterized by an increase in maximum displacement for rising operating temperature, in fact the lower the temperature the more brittle the compressive response. Even in this case the compressive behavior of the bio and petroleum-based core materials diverges when maximum force data are investigated. As previously seen, for a 5 J impact PVC foams maximum force is reached at the yielding point and hence in the plateau region, as also proved by HP130 compressive curves shown in Figure 88. This means that synthetic foams maximum force depends on material strength that definitely increases for decreasing operating temperature.
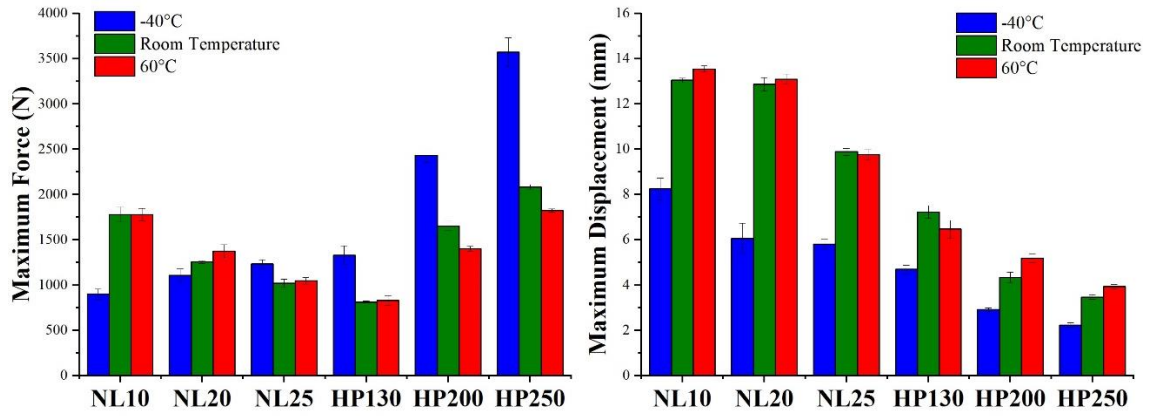
Figure 87: Maximum force and displacement of all cores at -40 °C, room temperature and 60 °C after a 5 J impact
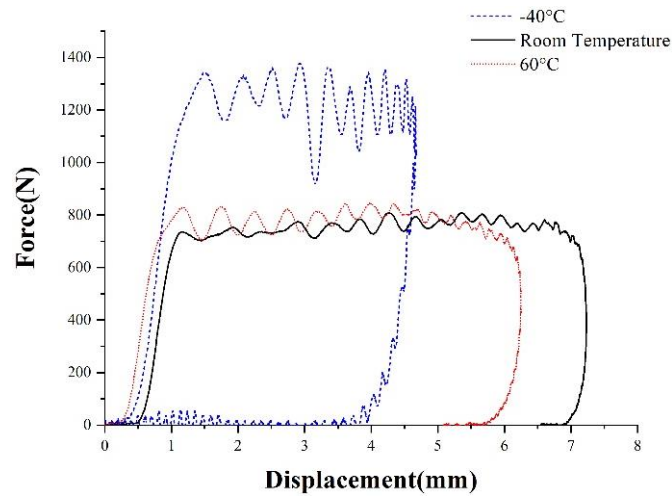
Figure 88: Dynamic compressive response curves of HP130 PVC foam subjected to a 5 J impact at the three testing temperatures

Agglomerated cork results are more scattered in fact NL10 and NL20 display an increase in maximum force for increasing temperature because at the higher operating temperatures they have already reached the densification region as confirmed by NL10 compressive curves in Figure 89.
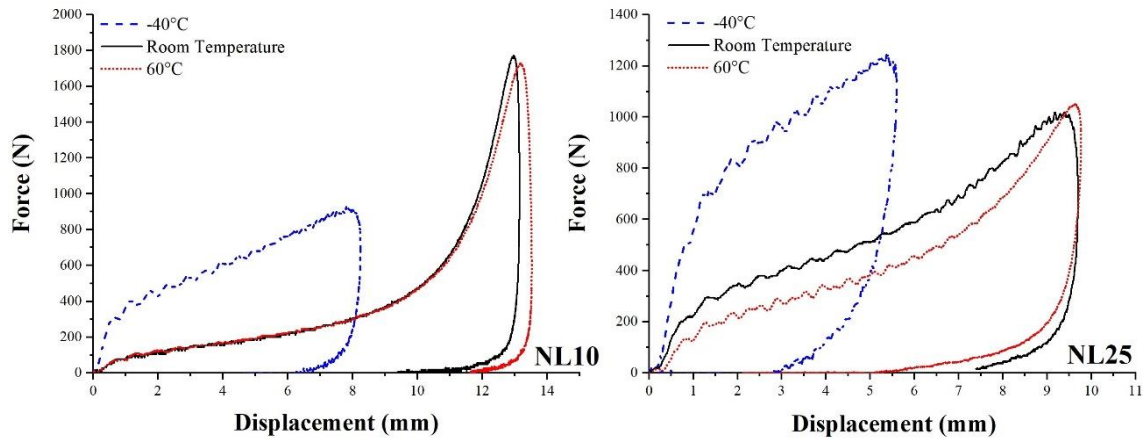
Figure 89: Dynamic compressive response curves of NL10 and NL25 agglomerated corks subjected to a 5 J impact at the three testing temperatures

The situation is different for NL25 that, at this impact energy, did not approached the densification region yet and behaves like a PVC foam displaying its maximum force in correspondence of the plateau region characterized by a higher stress when temperature is lower as demonstrated in Figure 89. Moving to the 7 J impact data shown in Figure 90, it is possible to observe that the results are almost equal to 5 J impact ones with the exception of NL25 maximum force trend. The denser cork as finally entered the densification region, as also confirmed by the dynamic compressive curves in Figure 91, meaning that the maximum force is not dictated anymore by the plateau stress thus leading to a compressive response perfectly coherent with NL10 and NL20 one. At last, 13 J impact results summarized in Figure 92 disclose a variation in HP130 maximum force trend. The foam with the lowest density reaches densification in all three operating temperature and considering that in this region small increases in the displacement causes a steep increase of the stress and that the maximum displacement at 60 °C is much higher than the one at -40 °C, as also confirmed by the compressive curves in Figure 93, it is possible to explain the change in HP130 maximum force trend that increases for increasing temperatures at this impact energy. An essential parameter that was not considered until this moment in temperature effect analysis is the percentage absorbed energy whose values are gathered in Figure 94 for all core materials, all operating temperatures and all impact energies. The results show that this parameter keeps almost constant regardless of the impact energy for all core materials, but it is strongly affected by temperature pointing out a significant reduction when operating temperature decreases.
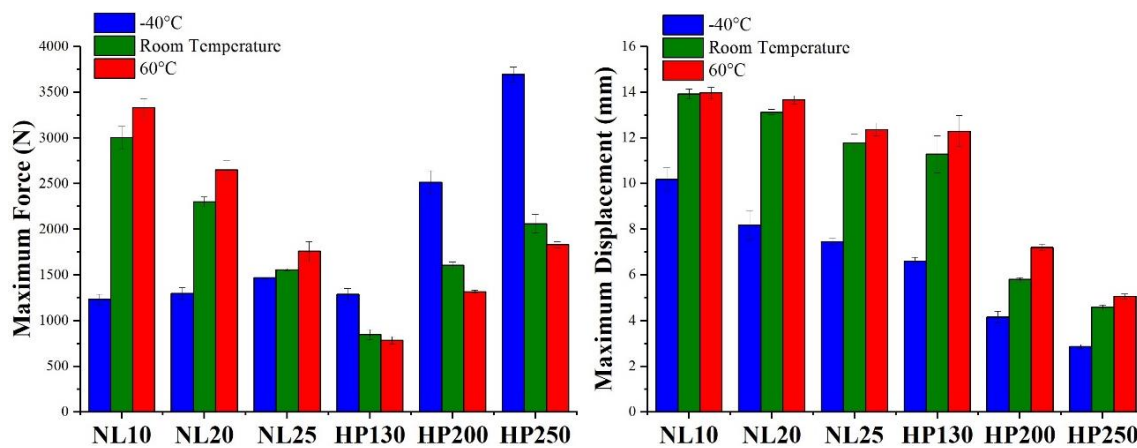
Figure 90: Maximum force and displacement of all cores at -40 °C, room temperature and 60 °C after a 7 J impact
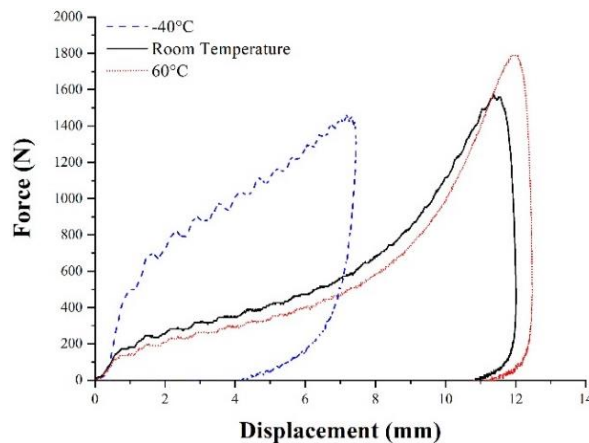
Figure 91: Dynamic compressive curves of the NL25 cork subjected to a 7 J impact at the three testing temperatures
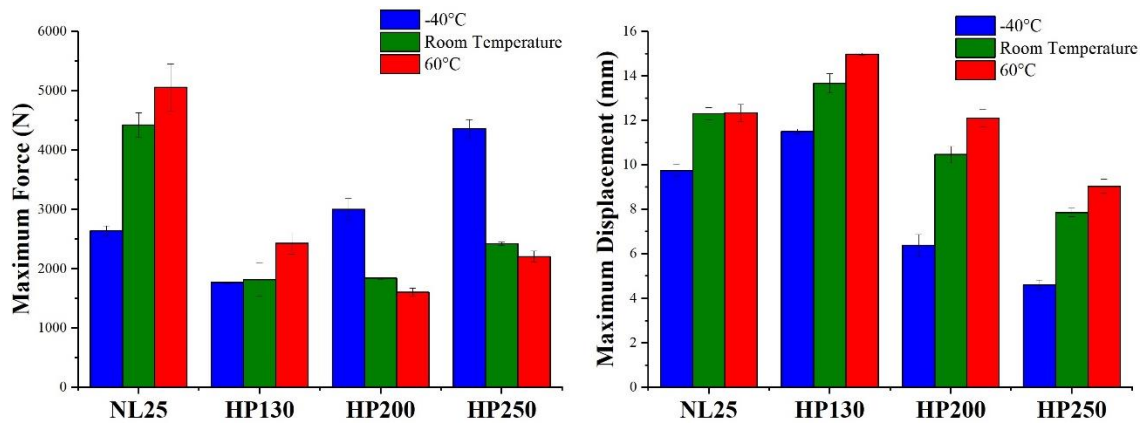
Figure 92: Maximum force and displacement of all PVC foams and NL25 at -40 °C, room temperature and 60 °C after a 13 J impact
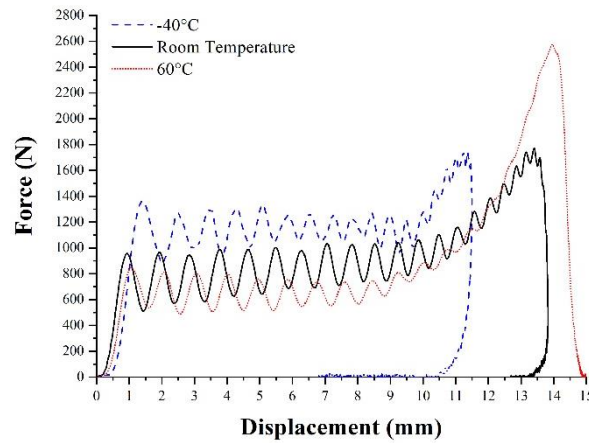
Figure 93: Dynamic compressive curves of the NL25 cork subjected to a 7 J impact at the three testing temperatures
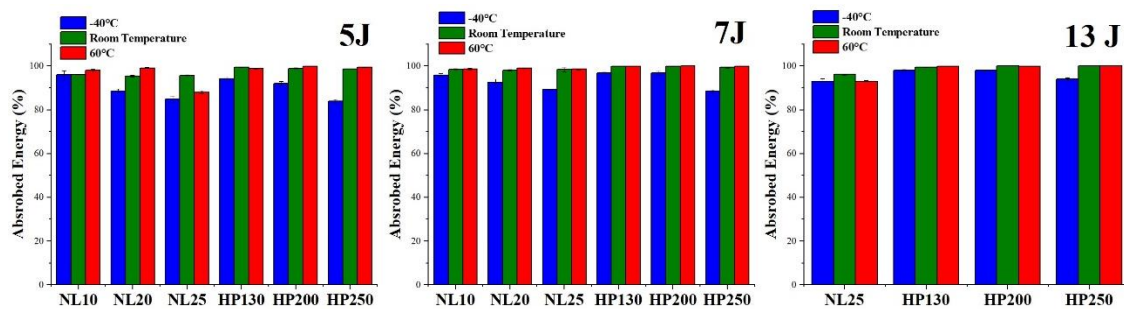
Figure 94: Percentage absorbed energy of all cellular materials at the three testing temperatures for 5 J, 7 J and 13 J impact energies

An embrittlement effect caused by a reduction of materials mobility at a molecular scale undermines their capability to adapt to the applied deformation and so to dissipate energy in a viscoelastic way increasing the elastic absorption component. The embrittlement effect played by temperature on agglomerated cork is confirmed by the damage mode reported in Figure 95 for NL10 and NL20 samples. A conspicuous detachment of a portion of the sample can be observed and it can be mainly ascribed to the occurrence of an intergranular fracture due to the transition

from the viscoelastic state to the glassy state of the polymeric binder as confirmed by the DMA data previously introduced in section 3.2.3. The embrittlement proved to be less marked on the synthetic foams, whose kept the same damage mode over the whole temperature range, because they are characterized by a glass transition temperature around 85 °C and 90 °C and works always in the glassy state.

Figure 95: Damage mode of NL10 (A) and NL20 (B) specimens tested at 7 J and -40 °C

3.4.2 Drop weight tower dynamic compression multiple-impacts tests

The execution of dynamic compressive multiple-impact tests allowed to take into account various aspects of natural and synthetic cellular cores dynamic behavior enabling to further highlight the deep differences that arises in the compressive response of these two materials due to their microstructure and chemical composition. Interpreting the dynamic compressive curves at 7 J and 10 J of NL25 and HP130 in Figure 96 and examining their maximum force, permanent deformation and percentage absorbed energy trends for an increasing impacts number in Figure 97, a marked divergence in the multiple-impacts response of PVC foams and agglomerated cork can be detected. NL25 and more generally agglomerated cork keep almost unchanged the shape of their dynamic compressive curves thus ensuring an almost constant response to the impact. The situation is completely different for HP130 and the other rigid PVC foams that experience a drastic change in the shape of their compressive curves. The classic plateau region, which characterizes most polymeric foams and guarantees great energy absorption capacity together with a small increase in the reaction force, disappears after two impacts at 7 J (Figure 96.B) and after just one impact at 10 J (Figure 96.D) and is replaced by a steep increase in the maximum reaction force. Both HP 130 and NL25 proved to be exceptional energy absorbing materials distinguished by a high percentage absorbed energy which displays a decreasing trend almost comparable in the two cases. To be more precise, NL25 undergoes an overall energy absorption reduction of 3.5 % at 7J, from 96.7 % to 93.2 %, and of 3.7 % at 10 J, from 97.7 % to 94 %, whereas HP130 suffers an overall reduction of 3.8 % at 7 J, from 99.8 % to 96 %, and of almost 2 % at 10 J, from 99.99 % to 98 %. If a certain similarity can be identified in the energy absorption capabilities of NL25 and HP130, clear and marked differences arises in the maximum force trend. NL25 maximum force increases with the number of impacts following a logarithmic path ($R^2 =$ 0.999 at 7 J and $R^2 = 0.995$ at 10 J) whereas HP130 maximum force increases linearly with the number of impacts ($R^2 = 0.991$ at 7 J and $R^2 = 0.997$ at 10 J). Maximum force increase is even more severe when the two denser foams are considered as can be inferred from the data shown in Figure 98, in fact HP200 and HP250 suffer an exponential increase of this parameter when impacts number increases. This is mainly due to their initial lower air content that speeds up the densification process facilitating the achievement of the bulky state.

130
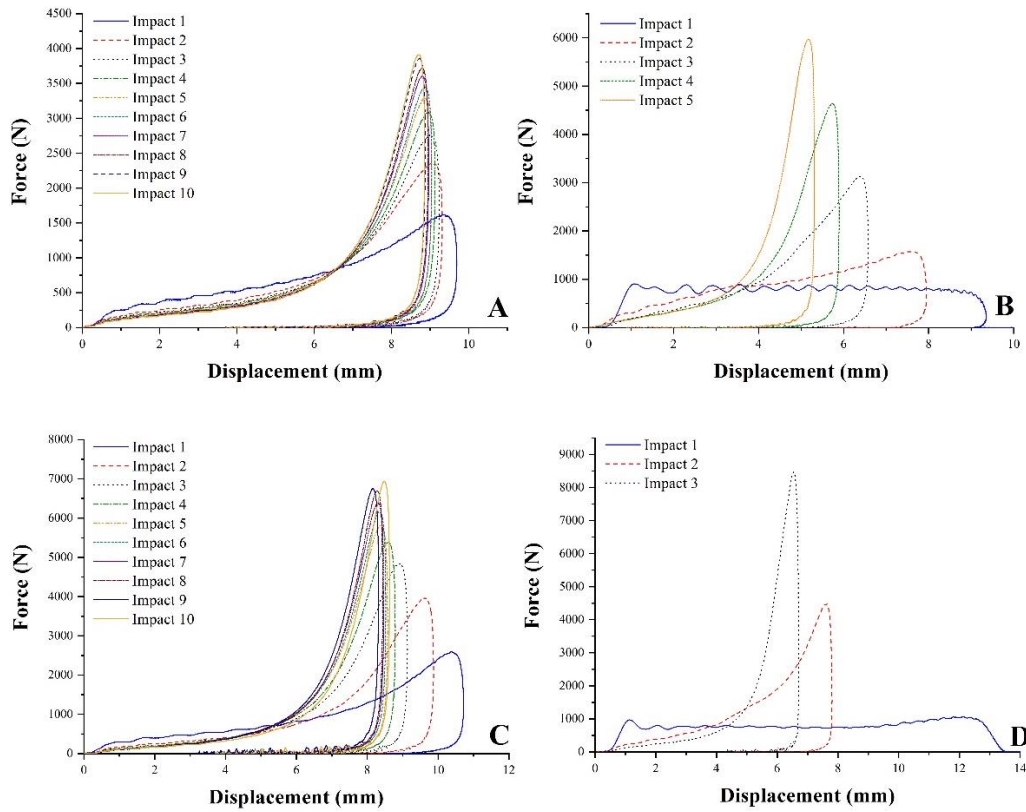
Figure 96: Multiple impacts dynamic compressive curves of NL25 and HP130 at 7 J (A and B, respectively) and at 10 J (C and D, respectively)
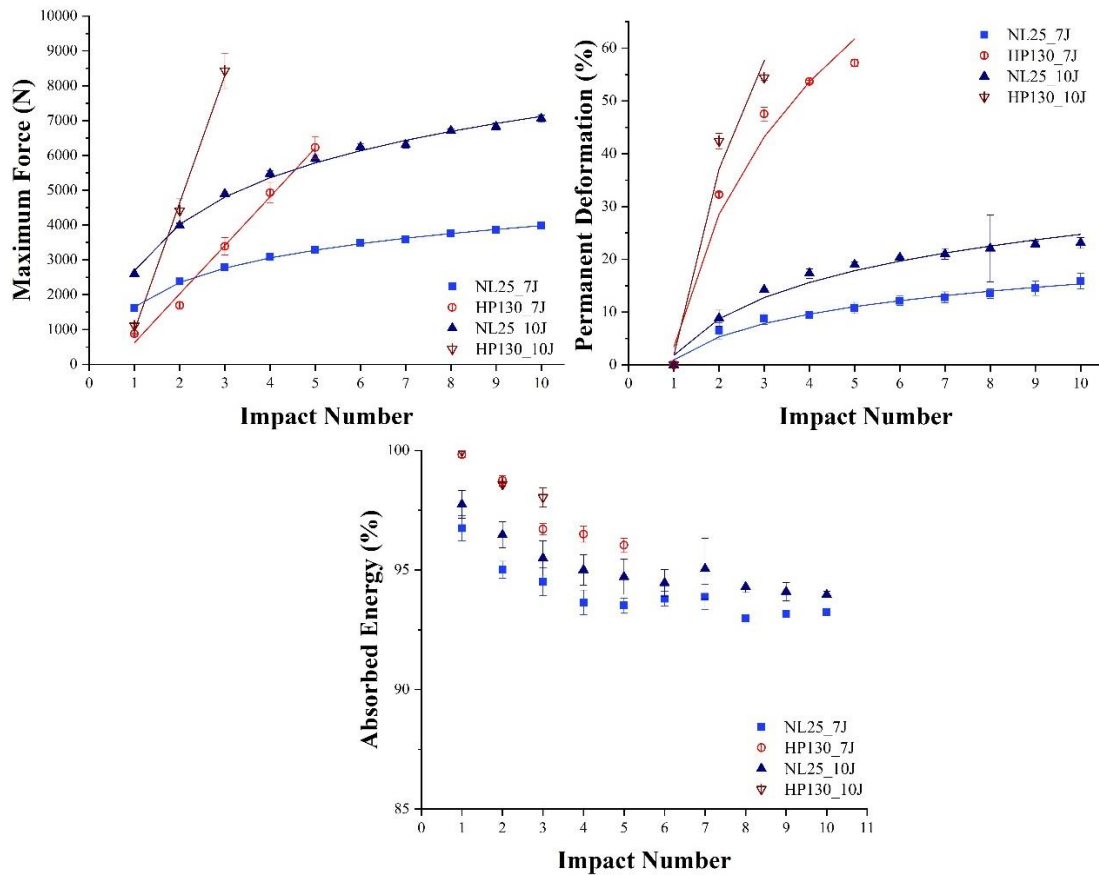
Figure 97: NL25 and HP130 maximum force, permanent deformation and percentage absorbed energy evolution with increasing impacts number at 7 J and 10 J

131
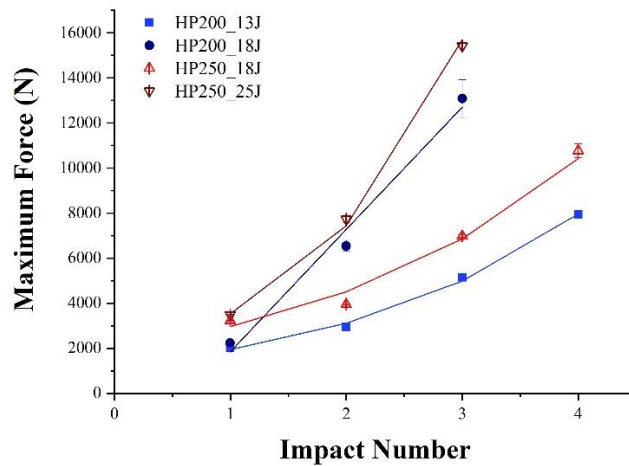
Figure 98: HP200 and HP250 maximum force trend with increasing impacts number at 13 J, 18J and 25 J

Moving back to NL25 and HP130 and considering the upper limit of 19 kN of the load cell, it is possible to conclude that NL25 ensures a safe maximum reaction force for more than 10 impacts at both 7 J and 10 J whereas tests on HP130 must be suspended at the fifth impact at 7J and at the third impact at 10 J to prevent load cell damage. Another substantial difference in the behavior of these two core materials can be recognized in the permanent deformation as shown in Figure 99 and in its trend in Figure 97.
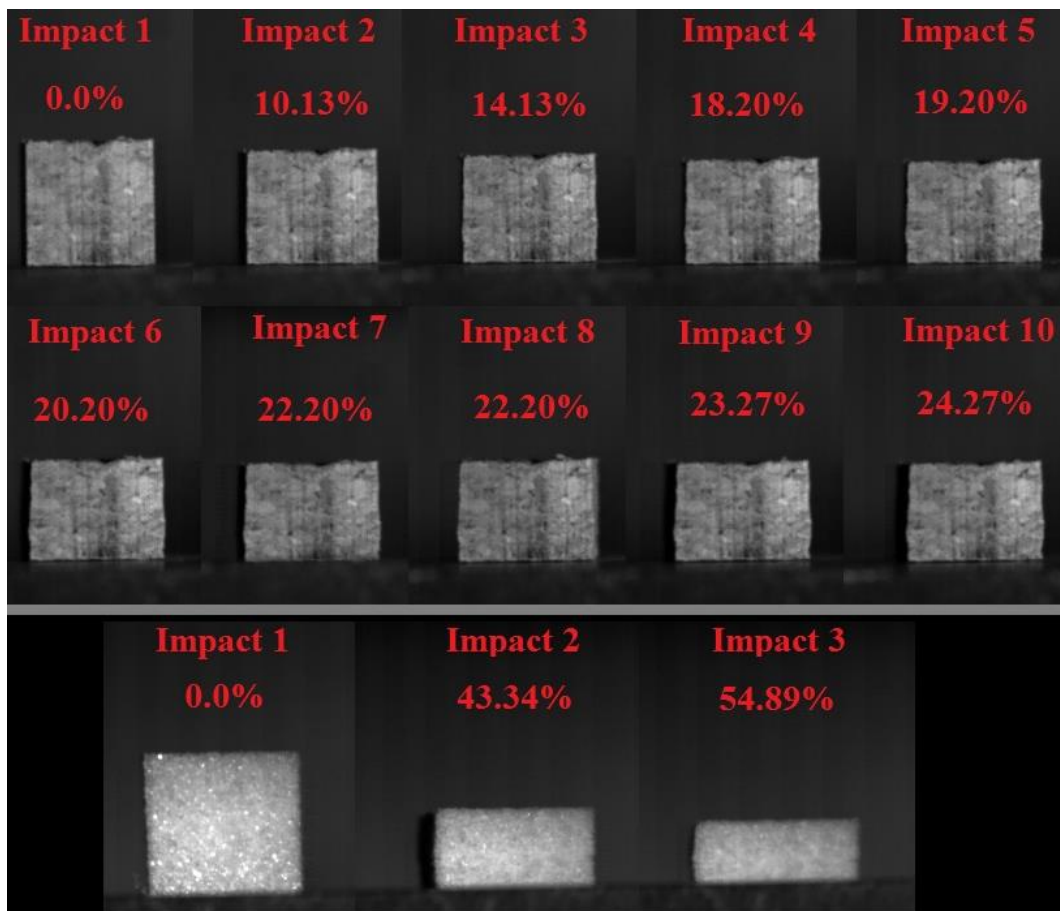
Figure 99: NL25 and HP130 permanent deformation after each impact at 10 J

The outstanding dimensional recovery of agglomerated cork allows NL25 to withstand 10 impacts at 10 J suffering a permanent deformation of only 24 % whereas the rigid nature of PVC foams cell walls dooms HP130 to undergo a 55 % reduction of its initial height after three only impacts at 10 J. Similar outcomes were obtained at 7 J where NL25 experiences a 16 % height reduction after 10 impacts and HP130 displays a permanent deformation of 57 % after half of NL25 impacts number. In light of the results presented, an important conclusion can be drawn namely that NL25 guarantees a greater dimensional stability to the sandwich structure produced with it ensuring, in case of impact, a more constant spacing of the skins preventing dramatic reduction in the flexural strength and stiffness of the sandwich composite that depends heavily on skin distance.

Multiple-impact tests energies were also selected in order to investigate the effect of density on agglomerated cork response performing tests at 2 J and 5 J on NL10 and NL20 samples. The trends of maximum force, permanent deformation and percentage absorbed energy of both agglomerated corks are reported in Figure 100. The first feature to point out is that, irrespective of density, both agglomerated corks can bear more than 10 impacts in both energy configurations without approaching load cell upper limit. NL10 and NL20 display excellent energy absorbing capacities, as previously seen for NL25, and the percentage absorbed energy trends are almost equal in both energy conditions. This remark raises a great interest considering that NL10 proves to be as efficient as NL20 in absorbing energy but with a density two times lower. In particular, at 2 J NL10 shows an initial percentage absorbed energy of 92.6 % and an overall decrease of 9.6 % whereas NL20 shows an initial percentage absorbed energy of 91.4 % and an overall decrease of 8.5 %.
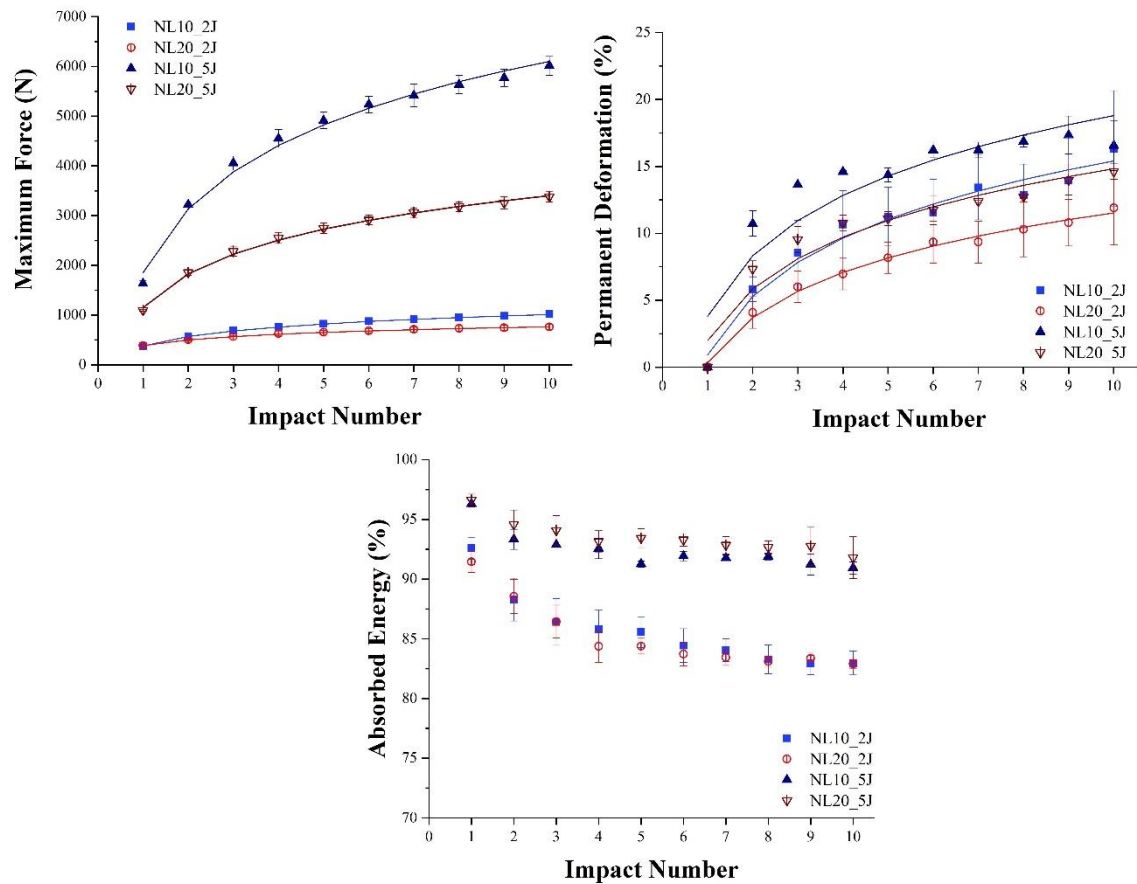
Figure 100: NL10 and NL20 maximum force, permanent deformation and percentage absorbed energy evolution with increasing impacts number at 2 J and 5 J

Similar conclusions were achieved at 5 J where J NL10 shows an initial percentage absorbed energy of 96.3 % and an overall decrease of 5.4 % and NL20 shows an initial percentage absorbed energy of 96.6 % and an overall decrease of 4.8 %. The effect played by density on agglomerated cork multiple-impact response becomes more noticeable when permanent deformation and maximum force trends are analyzed. Both natural cores are characterized by low values of permanent deformation, in particular lower than 17 %, but an increase in agglomerated cork density seems to guarantee a higher dimensional stability thanks to the lower air content which delays the densification phenomena being equal the impact energy. These considerations are strictly related to maximum force trend analysis, in fact NL10 shows a maximum force higher than NL20 especially for the impacts performed at higher energy. In the lower impact energy condition NL10 is characterized by a maximum force between 14 % and 33.7 % higher than NL20 and in the higher impact energy condition by a more pronounced difference that ranges between 73.9 % and 79.8 %. This discrepancy can be explained remembering that in the densification region little increase in the deformation induces steep increases in the maximum force. As already acknowledged for NL25, NL10 and NL20 maximum force evolution follows a logarithmic trend in both energy conditions ($R^2 = 0.9997$ and $R^2 = 0.9974$ at 2 J and $R^2 = 0.9908$ and $R^2 = 0.9982$ at 5 J, respectively) thus confirming the main advantage of agglomerated cork over PVC foams hence the progressive decrease of force increment for increasing number of impacts.

3.4.3 Split Hopkinson Pressure Bar tests

The execution of Split Hopkinson pressure bar tests in conjunction with the results obtained with quasi-static compression tests and drop weight tower dynamic compression tests allowed to examine more in depth two features of the core materials under study, i.e. strain rate sensitivity and anisotropy. The combination of the three classes of compressive tests mentioned permits to follow the evolution of cellular cores compressive properties in a wide range of strain rates enclosing low, medium and high velocity conditions to provide a thorough characterization. Concerning PVC foams, many works already proved the strain rate sensitivity of these polymeric foams [134–136,139,189], but considering only quasi-static and high velocity conditions and neglecting the medium velocity range fundamental to describe properly the whole strain rate range. The outcomes resulting from these studies highlight an increase in yielding and plateau stress when test speed increases thus agreeing perfectly with the results of this work that underline an upward shifting of the curves when strain rate increases, as confirmed by the PVC compressive curves evolution as a function of strain rate shown in Figure 101. It is worth noting that the medium velocity compressive curves obtained through drop weight tower tests fit perfectly the blank space between quasi-static and Split Hopkinson pressure bar curves. It is appropriate to make two brief comments on the different shape that characterizes drop weight tower dynamic compressive curves. First of all, the latter are distinguished by a closed loop in contrast to quasi-static and Split Hopkinson pressure bar curves characterized by an open line. This is due to the capability of the load cell to record sample reaction force even in the impactor rebound stage thus allowing to gather information on the unloading phase. The second feature of the curves under examination is the large oscillation in force register due to the inevitable reflection of the mechanical waves in drop weight apparatus. This noisy signal proved to be detrimental in the evaluation of some compressive parameters such as the densification stress thus requiring a signal processing to increase the reliability of the results obtained. Locally estimated scatterplot smoothing (LOESS) is the smoothing tool selected to carry out the signal processing of the efficiency curves. It allowed to obtain well-defined curves able to trace accurately the original
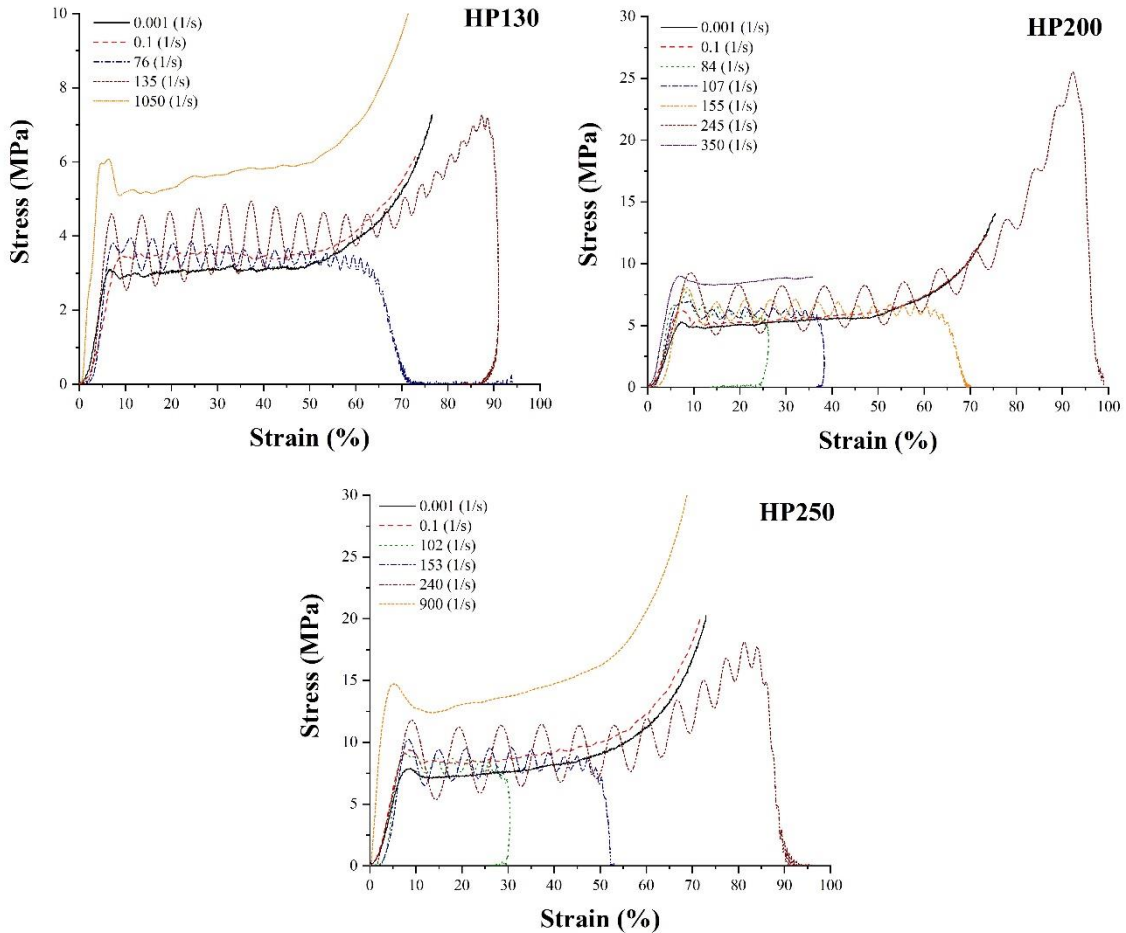
Figure 101: Strain rate effect on HP130, HP200 and HP250 compressive behavior

ones, especially in correspondence of the peak value, increasing enormously the precision of the densification stress value calculated. Going back to PVC foams strain rate sensitivity, a deeper understanding of their behavior can be achieved through the analysis of the plateau and densification stress data plotted in Figure 102 as a function of strain rate in logarithmic scale. Both plateau and densification stresses are characterized by slight increases in the low-medium strain rate range and by much more pronounced increases in the medium-high one.
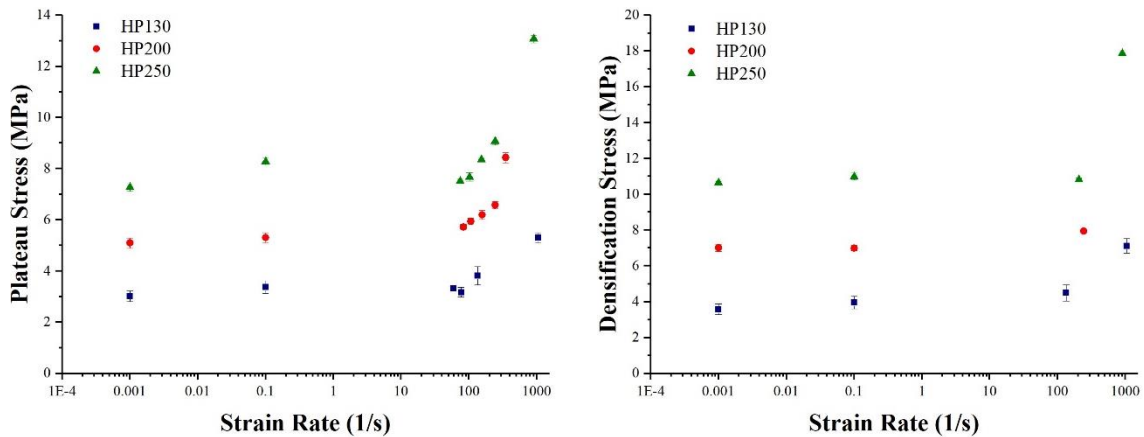
Figure 102: Average plateau stress and densification stress of all synthetic foams as a function of strain rate

In particular, in this working range a steep increase in plateau stress was detected with greater improvements corresponding to increasing density. PVC foams compressive properties dependency on strain rate must be ascribed to the viscoelastic nature of the foams that plays an ever more important role when foam density and hence polymer content increases. Even for cork it is possible to find some studies which addressed its dynamic compressive response, but none of them provides an exhaustive overview in the whole range of strain rates, as already pointed out for PVC. Sasso et al. [137] provided an extensive description of agglomerated cork strain rate sensitivity including local accelerations and inertia stresses evaluation trough Digital Image Correlation (DIC) analysis, but focusing only on quasi-static and high velocity conditions. Gameiro et al. [138] considered the same range of strain rate in their investigation on the dynamic compressive response of agglomerated and micro agglomerated cork. Due to its viscoelastic nature, agglomerated cork displays a marked strain rate sensitivity as already acknowledged for PVC foams and in perfect agreement with the results obtained in the previous mentioned studies. Figure 103 show all agglomerated corks compressive curves whereas Figures 104 and 105 report plateau stress and densification stress as a function of the logarithmic scale of strain rate. As previously observed for the PVC foams, agglomerated corks dynamic compressive curves obtained through drop weight tower tests fit flawlessly the blank space between the quasi-static and the Split Hopkinson bar curves thus ensuring a thorough description of the material behavior even in the intermediate strain rate range. Going more in detail in the analysis of the data plotted in Figures 104 and 105, it is possible to notice that in the medium-high strain rate range agglomerated cork displays a trend of the various compressive parameters totally comparable with PVC foam ones and characterized by a sharp increase of the compressive property under consideration, i.e. plateau and densification stresses.
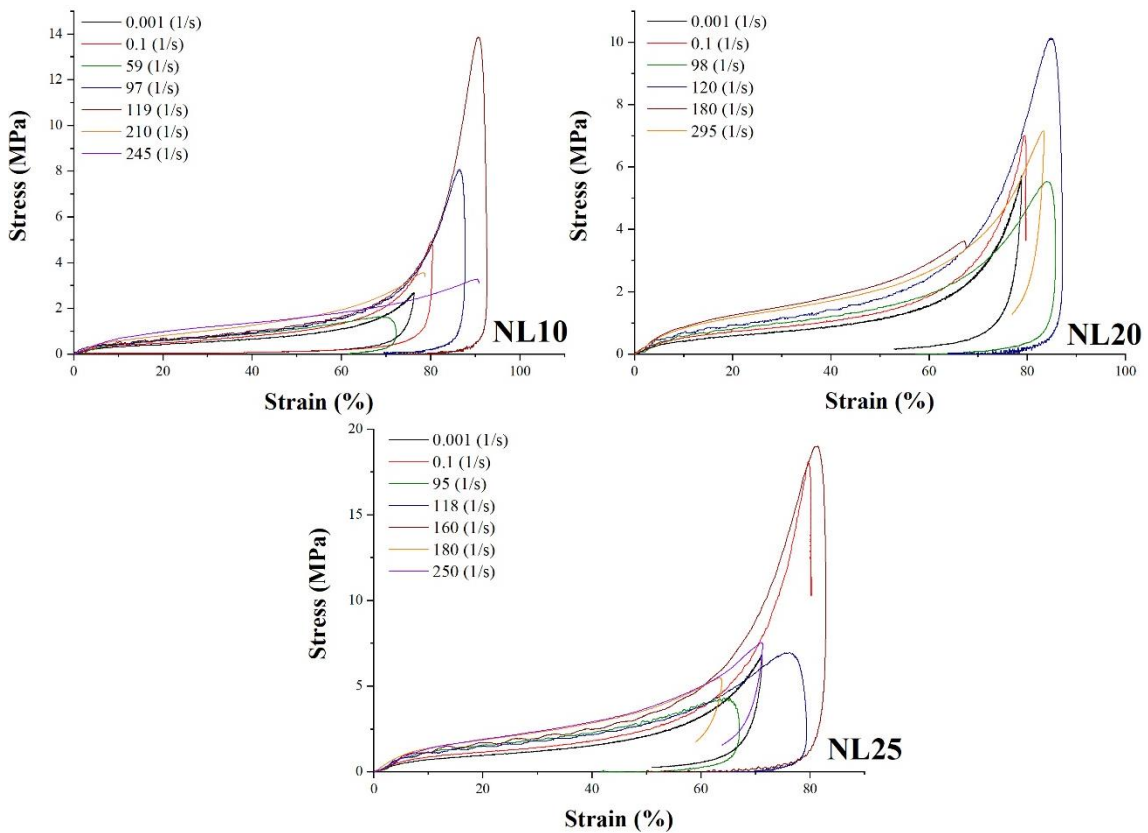
Figure 103: Strain rate effect on NL10, NL20 and NL25 compressive behavior
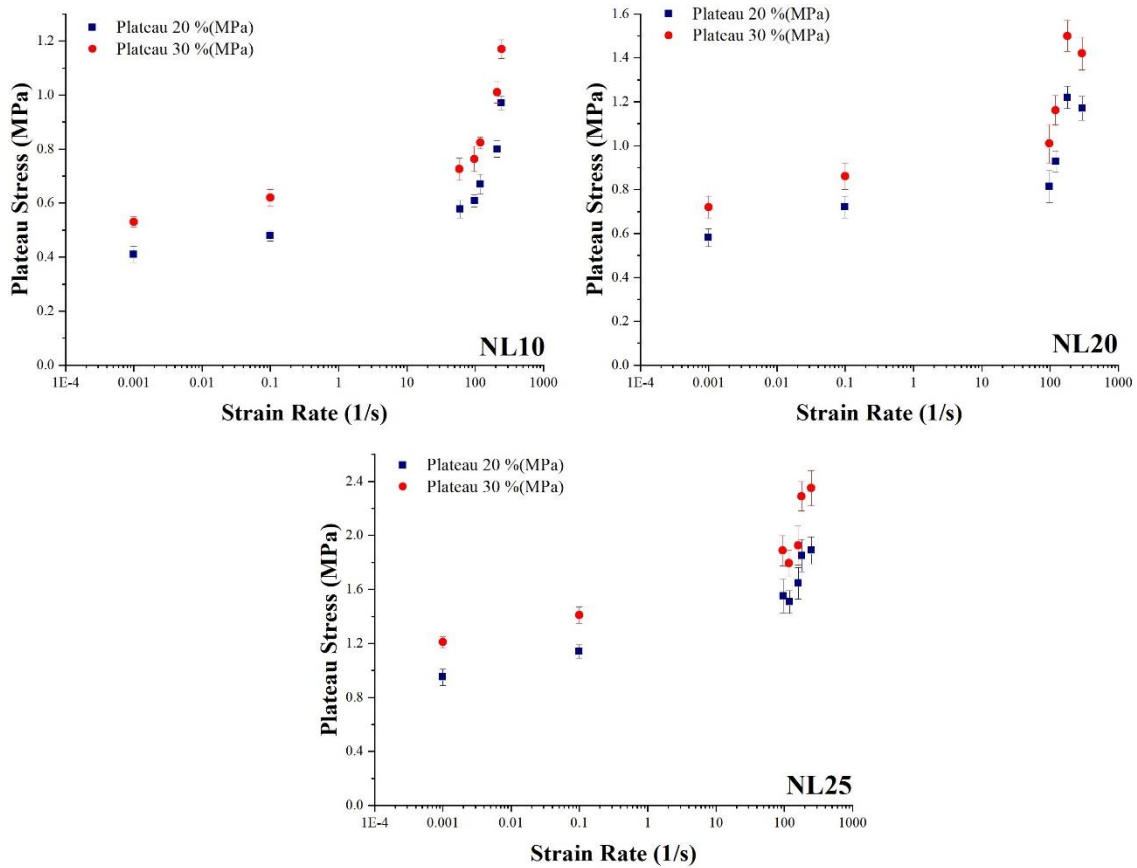
Figure 104: Average plateau stress at 20 % and 30 % deformation of the three agglomerated corks
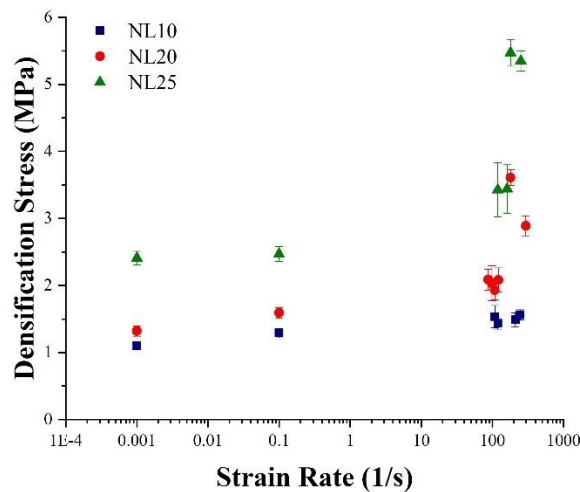
Figure 105: Average densification stress of the three agglomerated corks as a function of strain rate

The situation changes when the low-medium strain rate range is considered in fact PVC foams and agglomerated cork compressive parameters trends tend to diverge. In particular the percentage increase underwent by PVC foams plateau and densification stresses is much lower when compared to agglomerated cork. Agglomerated cork experiences an increase between 40 % and 60 % of both plateau stress and densification stress whereas PVC foams only a 13 % increase. This discrepancy in the evolution of the compressive properties in the lower strain rate range can

be ascribed to the intrinsic higher mechanical properties of PVC foams with respect to agglomerated cork. The results obtained for both PVC foams and agglomerated corks were corroborated by a strain rate sensitivity analysis. Strain rate sensitivity can be calculated according to Equation (3.13):

$$m = \frac{ln\left(\frac{\sigma_2}{\sigma_1}\right)}{ln\left(\frac{\dot{\varepsilon}_2}{\dot{\varepsilon}_1}\right)} \qquad (3.13)$$

where σ_2 and σ_1 are the stress values calculated at the same fixed strain during two tests carried out at different strain rates $\dot{\varepsilon}_2$ and $\dot{\varepsilon}_1$. This means that strain rate sensitivity can be computed as the slope of the interpolation line obtained plotting the logarithm of the compressive property under study, i.e. yielding, plateau and densification stresses, against the logarithm of the corresponding strain rates. Due to the sudden change in cellular cores response moving from the low-medium to the medium-high strain rate range, two different interpolation line can be identified thus leading to the extrapolation of two different strain rate sensitivity values as shown in the exemplifying graphs in Figure 106. Agglomerated cork strain rate sensitivity ranges between 0.029 and 0.041 in the first segment and between 0.26 and 0.34 in the second one whereas PVC foams one ranges between 0.009 and 0.026 in the first segment and between 0.16 and 0.27 in the second one. The strain rate sensitivity of both core types experiences an increase of one order of magnitude moving from the lower to the higher strain rate range. Moreover, strain rate sensitivity values confirm the differences observed between agglomerated cork and PVC foam in the low-medium velocity range. This change in material strain rate sensitivity according to the working range was already observed in other studies carried out on beech woods [141] and on metals such as ultrafine-grained alloy Ti-6Al-4V [190]. The introduction of the medium strain rate data proved to be fundamental to unveil the change in material compressive response that otherwise would have been lost. It is important to highlight that the statistical analysis carried out on cores strain rate sensitivity in quasi-static conditions in section 3.3.3, which revealed a linear correlation between the compressive property under study and test speed and density, is further corroborated by the data presented in this section considering that a linear correlation between the compressive parameter and the strain rate was observed in the first segment.
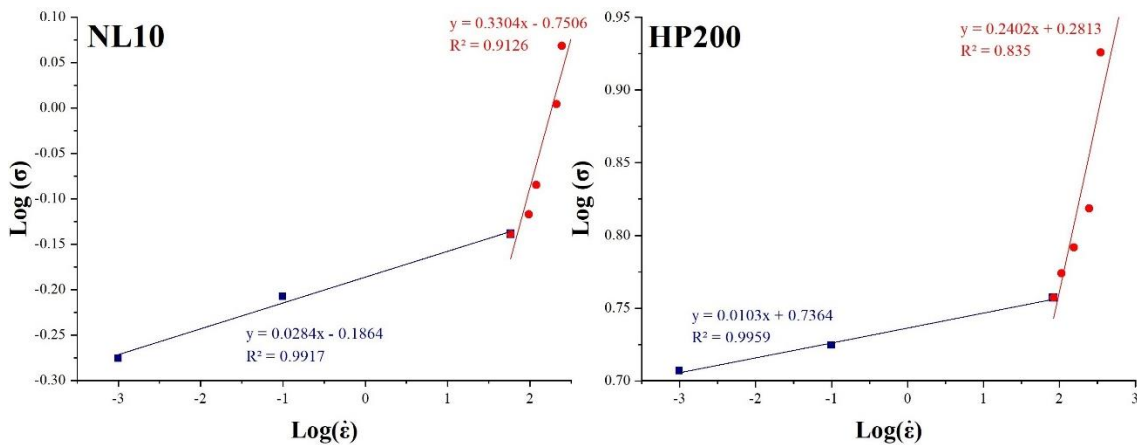
Figure 106: Plots employed to compute the strain rate sensitivity of NL10 30 % deformation plateau stress and HP 200 plateau stress

The execution of Split Hopkinson pressure bar tests in conjunction with the results obtained with quasi-static compression tests performed along the three main axis of core planks allowed to amplify the analysis on materials anisotropy. The out-of-plane properties (z axis [A]) and the in-plane properties along the x axis [C] and the y axis [B] were split and their evolution as a function of strain rate was addressed. Concerning PVC foams, Figures 107 and 108 represent their plateau and densification stresses, respectively, along the three axis and as a function of strain rate. The results obtained confirm the superior compressive out of plane performances of the foams and do not reveal significant differences along the two in-plane directions corroborating the conclusions drawn in section 3.3.3 that ascribe material anisotropy to cells elongation along the z-axis because of the production process. These conclusions are further confirmed by the fact that the higher differences between out-of-plane and in-plane properties were observed for the foam with the lowest density. In particular, HP130 plateau stress varies between 95 % and 100 %, HP200 plateau stress between 65 % and 80% and HP250 plateau stress between 55 % and 60 %. It is reasonable that the higher the air content in the foam the higher the discrepancy in cell walls arrangement. As previously discussed for the out-of-plane compressive properties, even in-plane results are characterized by a strong strain rate sensitivity and display a trend equal to out of plane one.
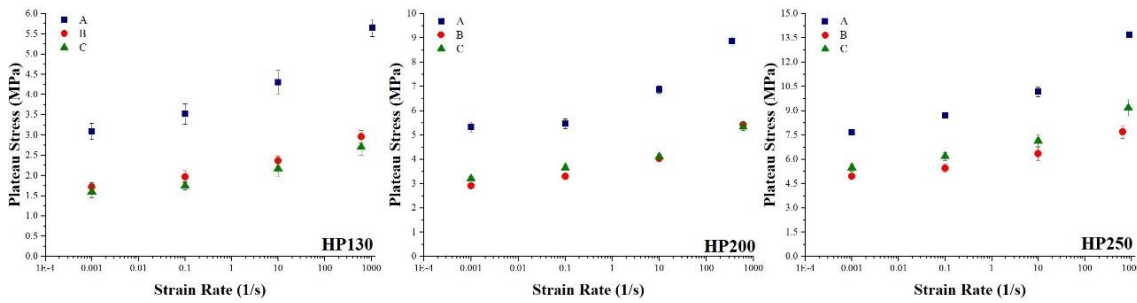
Figure 107: HP130, HP200 and HP250 average plateau stress along the three axis directions as a function of strain rate
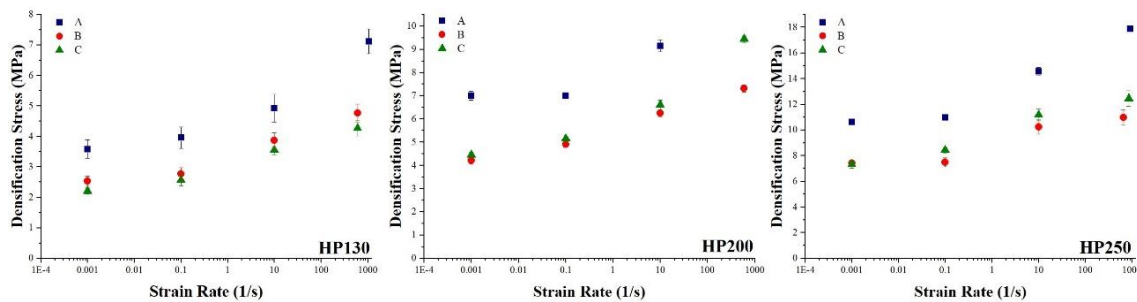
Figure 108: HP130, HP200 and HP250 average densification stress along the three axis directions as a function of strain rate

Alike characterization was performed on agglomerated corks and the data of plateau stress and densification stress for NL10, NL20 and NL25 are gathered in Figures 109, 110 and 111, respectively. As already discussed in section 3.3.3, agglomerated corks compressive properties are supposed to be almost isotropic thanks to granules random orientation that allows to counteract the intrinsic anisotropy of natural cork, but despite all efforts is not possible to obtain a perfectly isotropic material because of the pressure employed in the agglomeration process that can compress cork granules and induces residual stresses. This hypothesis was supported by the fact that the greatest discrepancies between in-plane and out-plane compressive performances

were observed for the denser cork NL25 which, being equal the operating pressure, enters earlier the densification region and withstands more residual stress along the z-axis. This conclusion is corroborated by the data in Figures 109, 110 and 111. NL10, i.e. the less dense cork, displays almost an isotropic behavior being negligible the differences along the three different axes thus confirming that the random orientation of granules is a valid choice to overcome natural cork anisotropy. Different is the situation for NL20 and NL25 where arose variations between in-plane and out of plane, being the latter lower. Considering that the random orientation of the granules would lead to an isotropic material if the effect of the production process could be neglected, the strain rate sensitivity detected for the in-plane compressive properties and their trend similar to out of plane one is not surprising.
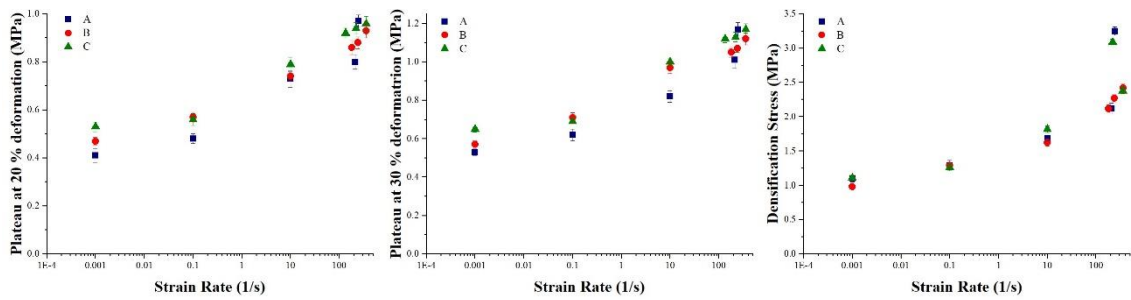
Figure 109: NL10 plateau stress at 20 % and 30 % of deformation and densification stress along the three axes direction
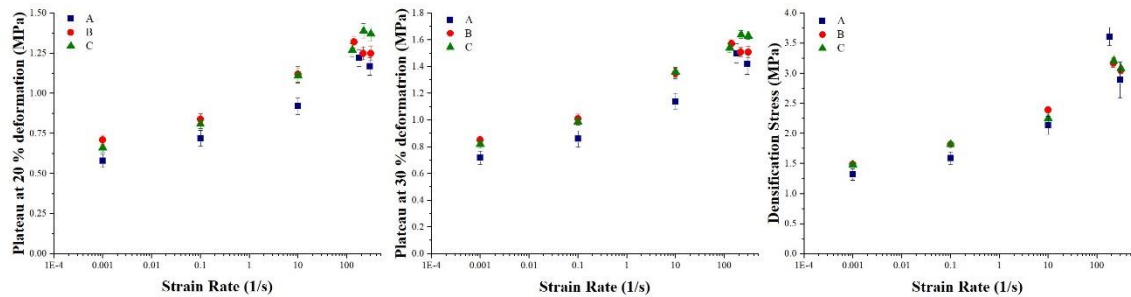
Figure 110: NL20 plateau stress at 20 % and 30 % of deformation and densification stress of along the three axes direction
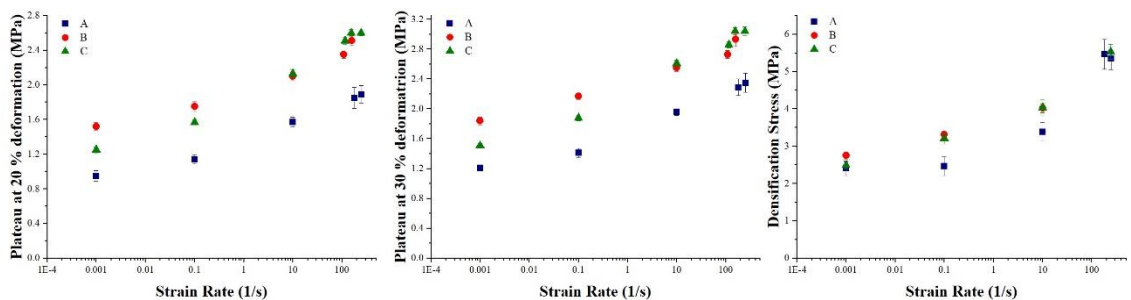
Figure 111: NL25 plateau stress at 20 % and 30 % of deformation and densification stress of NL25 agglomerated cork along the three axes direction

140

3.4.4 Puncture impact tests

Puncture impact test results of the six core materials are shown in Figure 112, which summarizes maximum force and maximum displacement values, and in Figures 113 and 114 that show agglomerated corks and PVC foams impact response curves, respectively. An increase in maximum force and maximum displacement for increasing impact energies can be observed for all core materials considering that the higher the impact energy the higher the deformation underwent by the material and hence the reaction force exerted. Another common trend can be pointed out in core materials dependency on density, in fact, being equal the impact energy, both agglomerated corks and PVC foams experience an increase in maximum force and a decrease in maximum displacement when core density increases due to an increase in material stiffness.
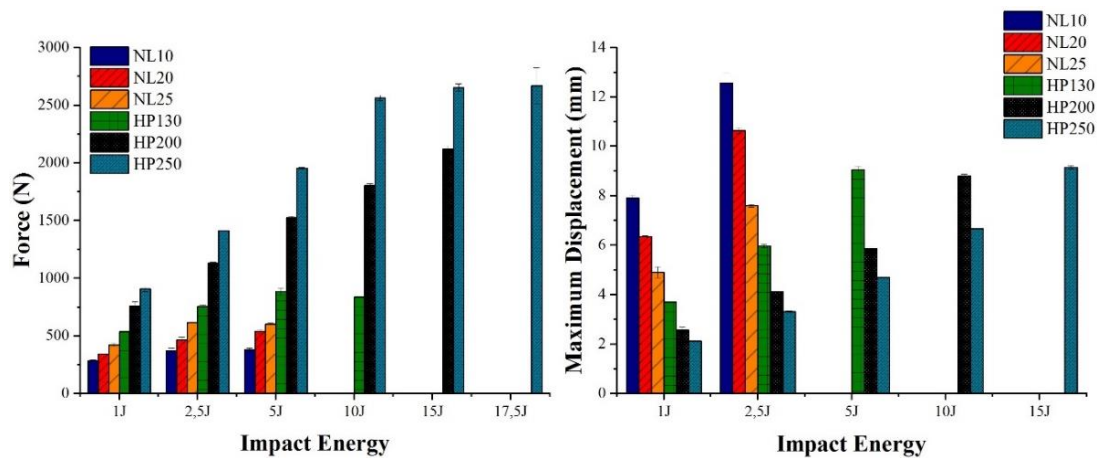
Figure 112: Maximum force and displacement of the six core materials as a function of impact energy
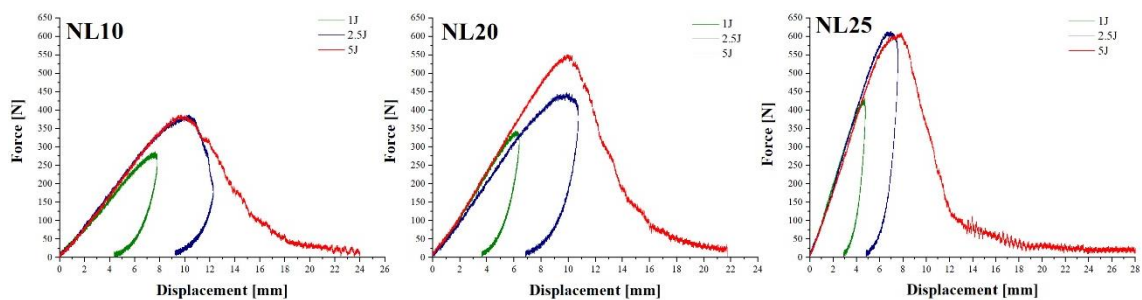
Figure 113: NL10, NL20 and NL25 impact curves
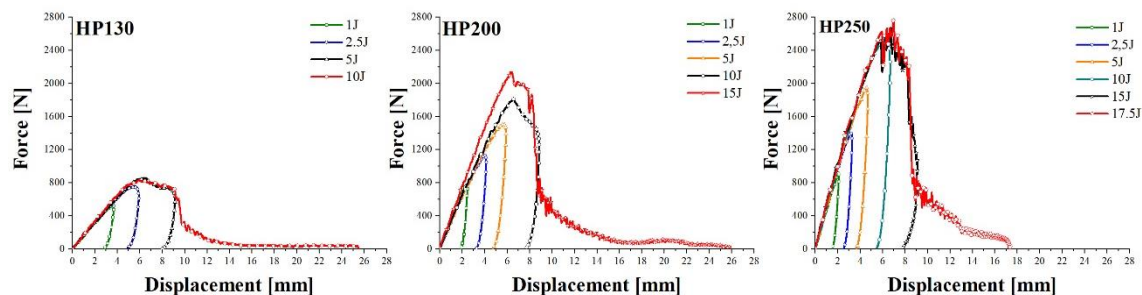
Figure 114: HP130, HP200 and HP250 impact curves

Despite the same tendency of impact parameters with density, it is mandatory to highlight that the impact response of the two types of cellular cores is completely different. All agglomerated corks are produced with the same type of granules and therefore are characterized by almost the same cell wall thickness and hence the variations in density must be ascribed to a different degree of compaction of the planks, but not to micro morphological differences in the material. This clarify why NL10 and NL25 display a difference of only 33 % at 1 J and of 39.7 % at 2.5 J in the maximum force and justifies why all three agglomerated corks are characterized by the same perforation threshold, i.e. 5J. Regardless of density, all samples do not undergo perforation because of cork damage or collapse, but suffer perforation because of the appearance of an untimely intergranular fracture due to the failure of the interface between cork granules and the polymeric binder employed to join them together as also demonstrated by the damage mode in Figure 115.C and 115.D. The further examination of agglomerated cork damage scenario in Figure 115 reveals, once again, its outstanding dimensional recovery capability, in fact no permanent indentation can be detected for the samples impacted at 1 J and 2.5 J. The only type of damage that can be observed is an initial intergranular fracture in samples impacted at 2.5 J.
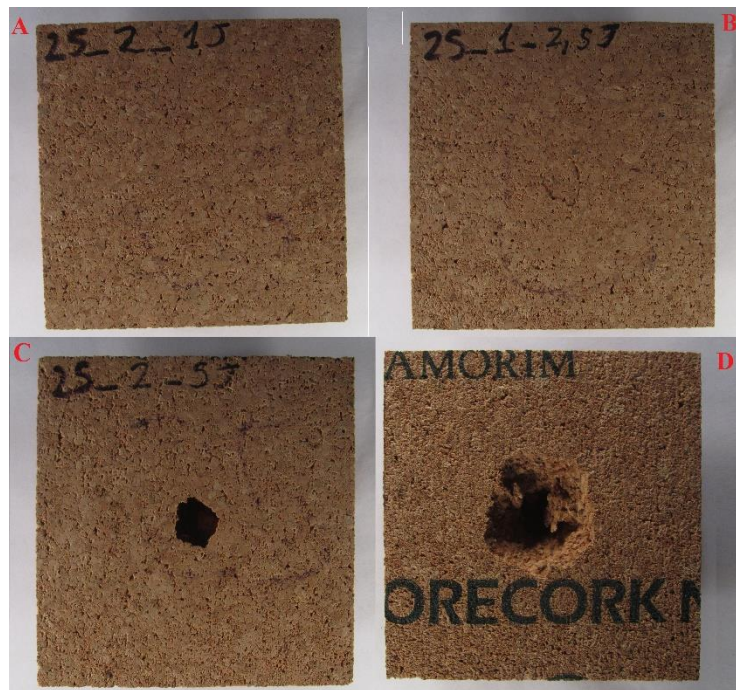
Figure 115: NL25 damage progression at 1 J (A), 2.5 J (B) and 5 J (C Front and D Back)

The investigation of density effect on PVC foams impact response leads to completely different conclusions, in fact changes in polymeric foam density must be ascribed to modifications in core microstructure. In particular, a foam with higher density is characterized by a lower air content and, as a consequence, by thicker cell walls as already acknowledged by Lim and Altstädt [159] and by Colloca et al. [160]. Due to these features, the densest foam presents the lower maximum displacement and the highest maximum force, in fact thicker cell walls exercise a higher reaction force being equal the impact energy. The profound differences that arise in HP130 and HP250 microstructure also explains why the variations in maximum force moving from the lower dense to the denser foam are much more pronounced than the ones in agglomerated cork. In particular, HP250 is characterized by a maximum force 46.4 % higher at 2.5 J and 55 % higher at 5 J than

HP130. Taking into account that thicker cell walls require a higher energy amount to collapse and fracture, microstructure discrepancies also justify the increase in perforation threshold for increasing foam densities. Remarkable differences between PVC foams and agglomerated corks can be recognized even in the damage progression as can be inferred from HP130 impacted samples shown in Figure 116. If agglomerated cork is able to dissipate conspicuous amounts of energy thanks to its pronounced viscoelastic behavior, the rigid PVC foams cell walls can dissipate energy only through bending and collapse thus leading necessarily to permanent indentation traces even for low impact energies. The damage generated by the impactor was quantified through profilometric analysis and the indentation depth values obtained for the three PVC foams as a function of impact energy are summarized in Figure 117. An increase in permanent indentation for increasing impact energies can be observed for all PVC foams and it ranges between 36 % and 39 % for HP130 and between 26 % and 32 % for HP250. Moreover, at the same impact energy, a higher density implies a lower permanent indentation, in fact HP130 suffers a permanent indentation between 42 % and 55 % higher than HP250. This is in perfect agreement with the remarks made on microstructure considering that thinner cell walls need a lower impact energy to reach the same deformation of thicker ones. Another important parameter to study when considering impact tests is the percentage absorbed energy whose values are gathered in Figure 118 for all six core materials and show how agglomerated corks, and particularly NL20 and NL25, are characterized by absorbing capabilities comparable to PVC foams ones in the low impact energies range. Based on the results obtained, it is possible to conclude that HP200 and HP250 foams are characterized by much higher mechanical properties than the corresponding agglomerated corks, as already demonstrated during the presentation of the results derived from the quasi-static characterization. Moreover, it can be concluded that NL25 is the most performing agglomerated cork and that only HP130 results seems to be suitably comparable with NL25 ones. In consideration of these conclusions, the lightest foam HP130 and the most performing agglomerated cork NL25 were selected to carry out the finite element analysis which will be presented in section 3.4.5 and which permits to numerical simulate the puncture response of these core materials.
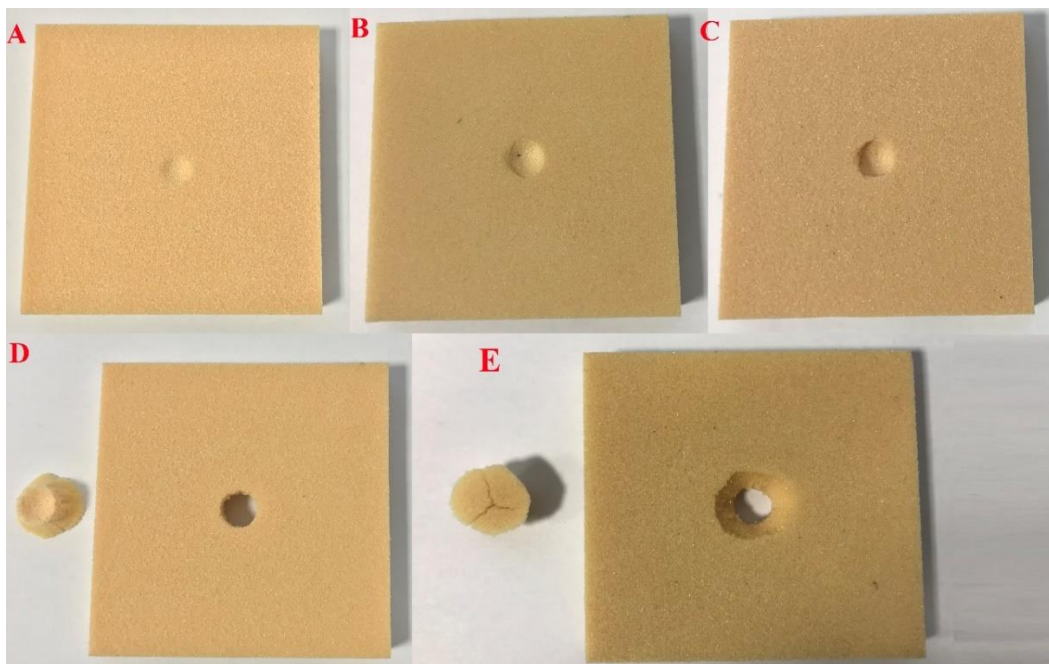
Figure 116: HP130 damage progression at 1 J (A), 2.5 J (B), 5 J (C) and 10 J (D Front and E Back)
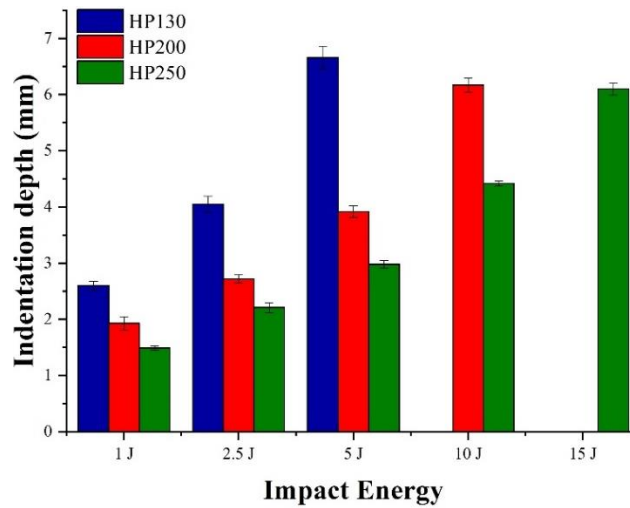
Figure 117: PVC foams residual indentation depth as a function of impact energy
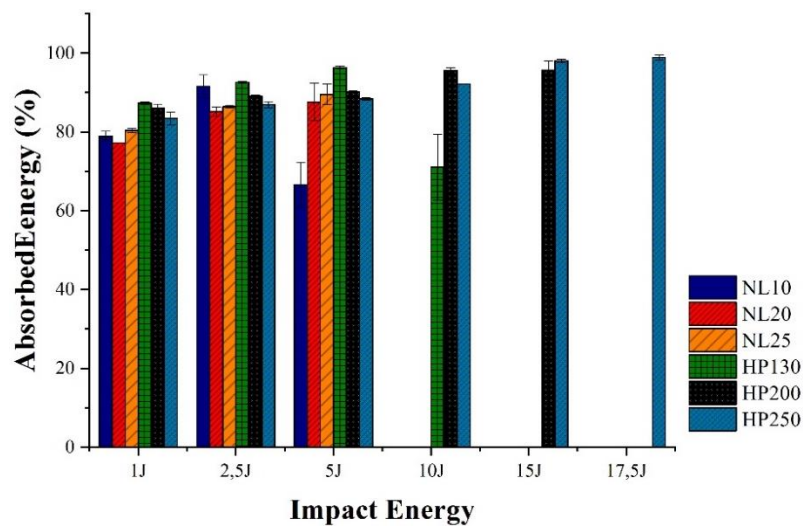
Figure 118: Percentage absorbed energy of the six cores as a function of impact energy

3.4.5 Puncture tests Finite Element Analysis (FEA)

The results obtained from the numerical simulations were compared with experimental ones in order to obtain a validation of the model. The comparison between the experimental and numerical load-displacement curves for NL25 cork at various impact energies is given in Figure 119 and, as it is possible to verify, the results obtained through the FE model are really close to experimental ones disclosing a good match of the curves. In light of the good validation achieved, the different energy contributions that intervene in the impacts, i.e. model total energy, internal energy, kinetic energy and the energy dissipated by damage and through frictional effects, were computed numerically and the resulting data are plotted in Figure 120. Focusing on the 5 J impact, namely the one at which agglomerated cork perforation occurs, it is possible to notice that the model allowed to dissipate almost 0.9 J through damage (Eroded IE), accounting for 17 % of the initial kinetic energy, and 0.2 J through friction and sliding. Contrary to the other impact conditions, the kinetic energy does not reach the zero value when the 5 J impact is modelled because the impactor still has a residual velocity that was not able to dissipate before specimen complete perforation took place.
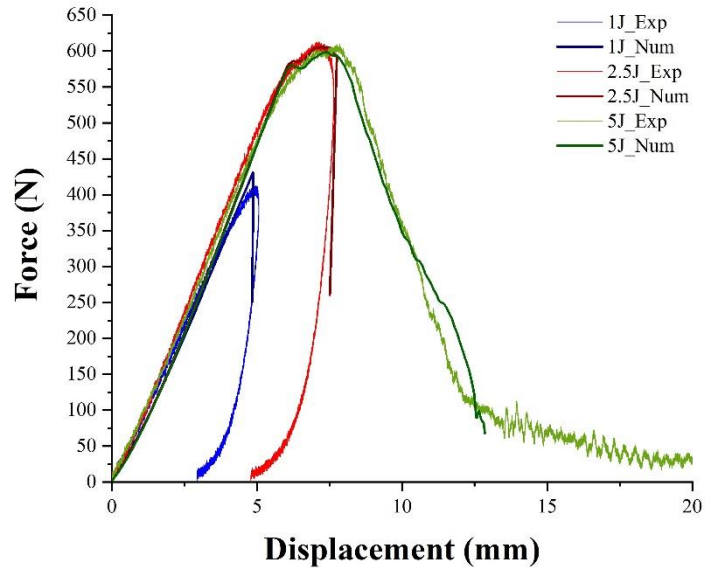
Figure 119: Experimental and numerical force-displacement curves for agglomerated cork NL25 at all impact energies
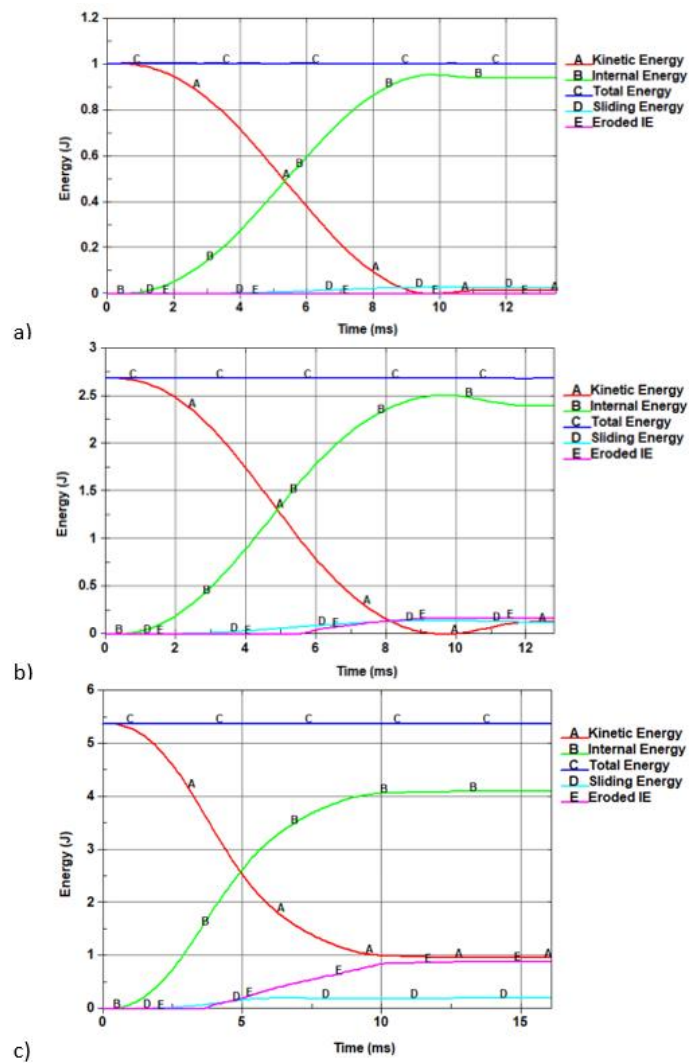
Figure 120: Various energy contributions measured numerically throughout the impacts at 1J (a), 2.5J (b), and 5J (c)

For the other two impact energy conditions, the point where kinetic energy reaches the zero value corresponds to the moment in which impactor velocity nullify and the rebound phase starts. In all cases, when the kinetic energy reaches its minimum, the internal and the damage dissipation energies reach their maximum as expected. It is noteworthy that, even if the amount of energy dissipated through friction is low when compared to the other contributions, it actually contributes to energy dissipation in this model. The comparison between experimental and numerical curves was carried out even for the PVC foam HP130 and is shown in Figure 121. Even in this case, the discrete model appears able to capture the main crushing phenomena and can be successfully validated. The peaks and valleys observable on the numerical curves are due to the element deletion for the failure criteria implemented. As demonstrated by the results in Figure 122, the addition of the erosion criteria in the model allows also to reproduce the internal damage suffered by the material leading to the progressive deletion of the elements to reproduce the penetration and the perforation.
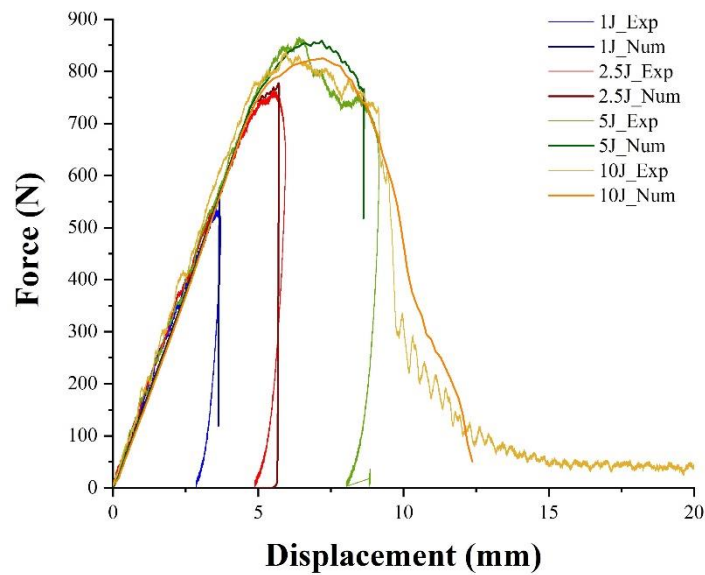
Figure 121: Experimental and numerical force-displacement curves for agglomerated cork HP130 at all impact energies
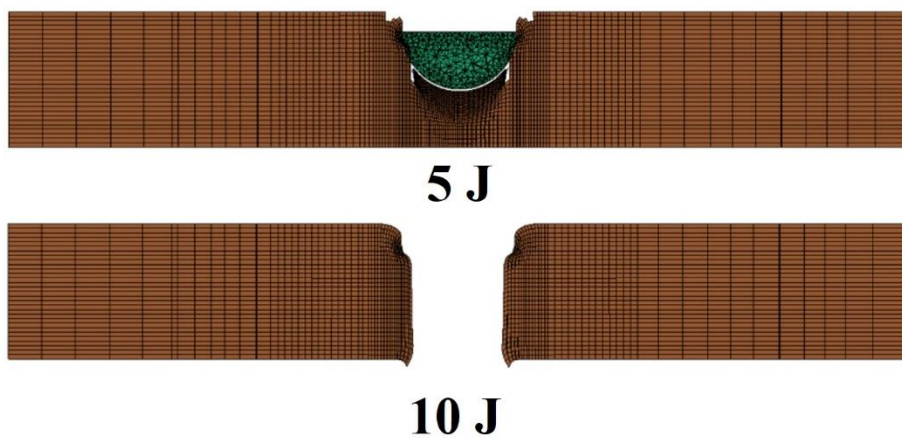
Figure 122: Numerical crushing of HP130 foam at 5 J and 10 J impact energy

3.4.6 Puncture Multiple-Impacts tests

As already stated in section 3.4.4 where core materials puncture impact response was investigated and their perforation thresholds were pinpointed, synthetic foams performances are clearly superior to agglomerated corks ones considering that the latter are also hindered by the untimely intergranular fractures responsible for samples perforation. The execution of puncture multiple-impacts at 1.25 J and 2.5 J confirmed the undoubted supremacy of HP200 and HP250, but strengthened the similarities in the mechanical performances between NL25 and HP130 observed until this point. Looking at the data reported in Table 28, which summarizes the impacts number that each core material can bear before undergoing perforation, and in Figure 123 and 124, which displays the evolution of the maximum force and of the maximum displacement as a function of the number of impacts at 1.25 J and 2.5 J respectively, it is possible to find confirmations to these statements. HP200 and HP250 foams are characterized by a superior stiffness and strength responsible for the higher maximum reaction force and for the lower maximum displacement which disclose a lower tendency to bend and deform. The ability to withstand more than 10 impacts at both 1.25 J and 2.5 J without undergoing perforation is another sign of the higher mechanical properties of the denser foams considering that the other core materials are not able to achieve the same performances. Focusing on NL25 and HP130, it is possible to point out that, despite the intrinsic nature of the foam which makes it stiffer thus determining a lower maximum displacement and a higher reaction force, both cores are able to withstand the same number of impacts at 2.5 J and NL25 can tolerate a higher number of impacts at 1.25 J.

Table 28: Impacts number that each core material can withstand before undergoing perforation at 1.25J and 2.5 J

Core	Impacts number before perforation at 1.25 J	Impacts number before perforation at 2.5 J
NL10	5	2
NL20	>10	3
NL25	>10	4
HP130	10	4
HP200	>10	>10
HP250	>10	>10
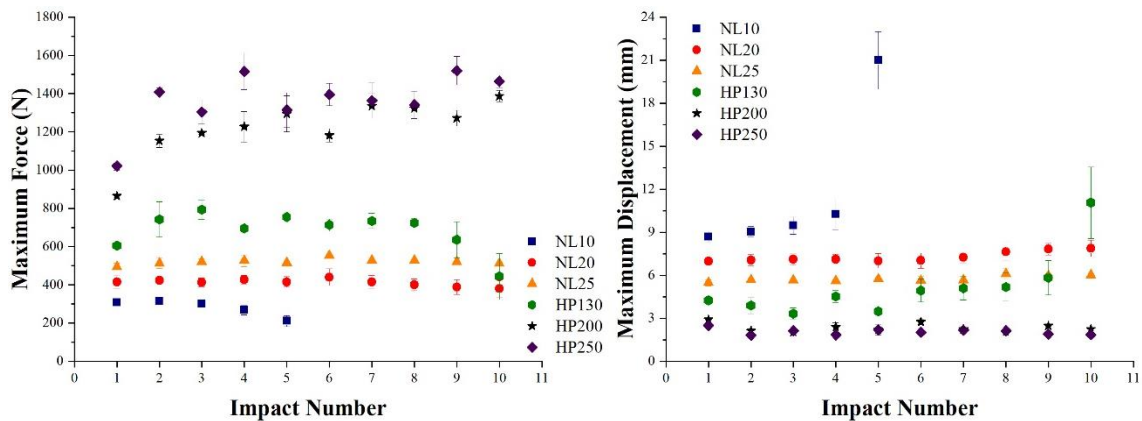
Figure 123: Maximum force and displacement of all six cores subjected to multiple-impacts at 1.25 J
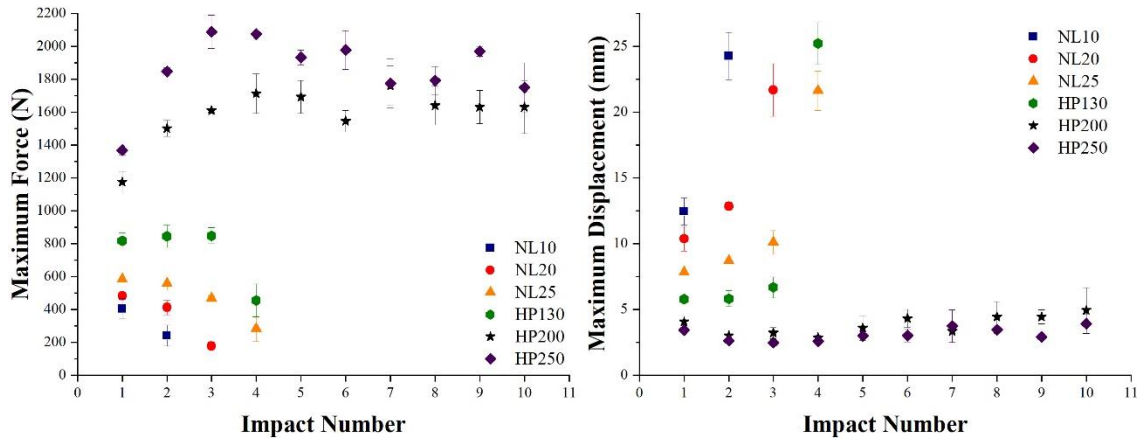
Figure 124: Maximum force and displacement of all six cores subjected to multiple-impacts at 2.5 J

A more accurate analysis of density effect on agglomerated corks behavior can be carried out considering the results plotted in Figure 125 and 126 that show the evolution of maximum force, maximum displacement and percentage absorbed energy as a function of impacts number for all agglomerated corks at 1.25 J and 2.5 J, respectively. The results in section 3.4.4 demonstrated that all bio-based core materials experience perforation at the same energy regardless of their density because of the intergranular fracture caused by the failure of cork granules and polymeric binder interface. When multiple-impacts are addressed, the situation changes and a certain influence of density can be detected. At 1.25 J, i.e. 25 % of perforation energy, the denser corks NL20 and NL25 show almost a constant behavior throughout the ten impacts which is only characterized by little oscillations in maximum force, maximum displacement and absorbed energy values. The situation is different for NL10 that undergoes perforation at the fifth impact following a parabolic tendency in maximum displacement increase and maximum force decrease, i.e. $R^2 = 0.999$ and $R^2 = 0.899$, respectively. As extensively said, a lower density implies a higher air content of the samples due to a lower compaction of the granules which in turn entails a reduction of the amount of material available to counteract the impact thus increasing the shear and bending loads to which is exposed the polymeric binder and determining the component failure. Moving to impacts performed at 2.5 J, i.e. 50 % of perforation energy, the impact response observed at 1.25 J for NL10 can be found even for NL20 and NL25 which display a parabolic decrease of the maximum force ($R^2 = 1$ and $R^2 = 0.999$) and a parabolic increase of the maximum displacement ($R^2 = 1$ and $R^2 = 0.963$). It was also observed that the lower the cork density the steeper the parabola curvature which even degenerates in a straight line in the case of NL10.
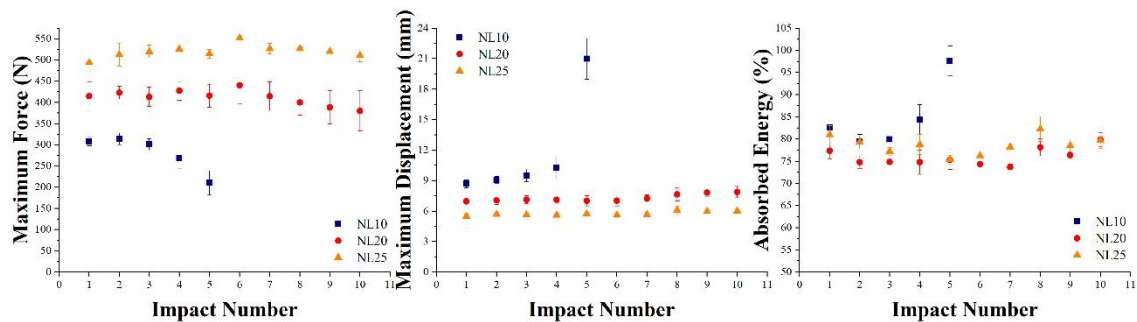
Figure 125: Agglomerated corks maximum force, maximum displacement and percentage absorbed energy evolution at 1.25 J

148
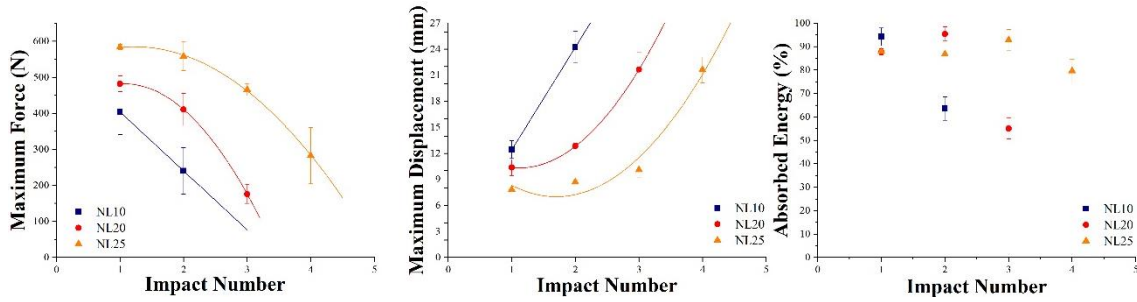
Figure 126: Agglomerated corks maximum force, maximum displacement and percentage absorbed energy evolution at 2.5 J

As previously established, the direct comparison of agglomerated corks and PVC foams impact response at 1.25 J and 2.5 J was not suitable due to the higher stiffness and strength of the latter. A more conceivable comparison can be obtained by the examination of core response at 25 % and 50 % of their own perforation energy (P.E.). The data necessary to perform this analysis are gathered in Table 29, which summarizes the number of impacts that each core material can withstand before reaching perforation at 25 % and 50 % of its perforation energy, and in Figures 127 and 128, which show the trend of maximum displacement and percentage absorbed energy for increasing number of impacts at 25 % and 50 % of cores perforation energy, respectively.

Table 29: Impacts number that each core material can withstand before undergoing perforation at 25 % and 50 % of its perforation threshold

Core	Impacts number before perforation at 25 % P.E.	Impacts number before perforation at 50 % P.E.
NL10	5	2
NL20	>10	3
NL25	>10	4
HP130	4	2
HP200	10	3
HP250	9	3
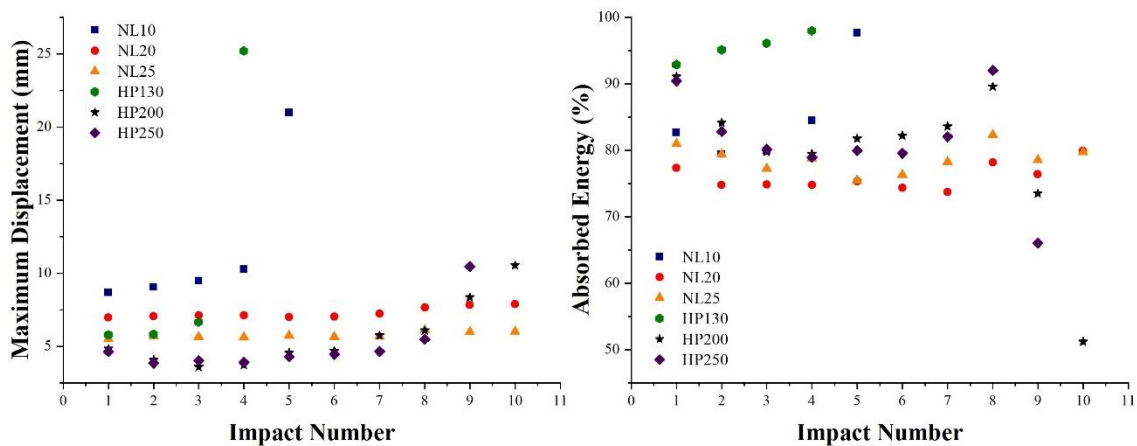
Figure 127: Direct comparison of the maximum displacement and the percentage absorbed energy evolution of the six cores at 25 % of their perforation energy

149
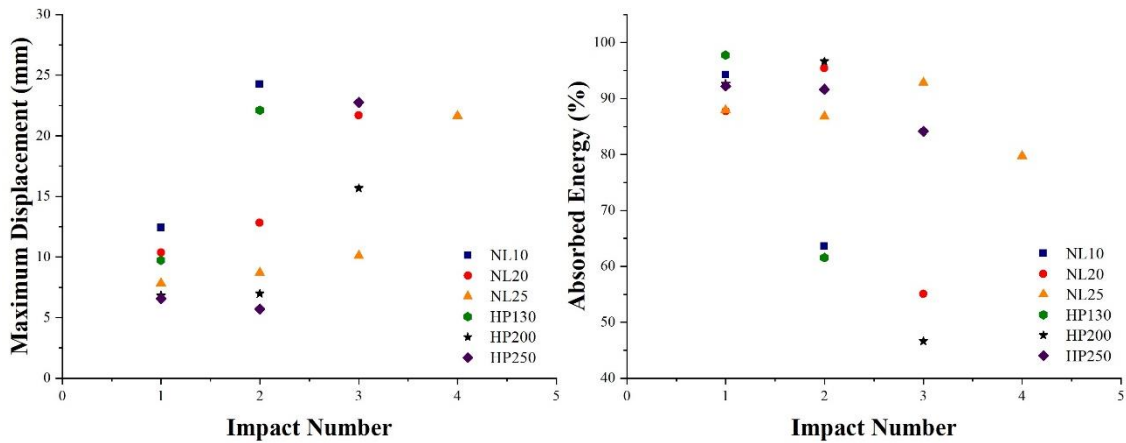
Figure 128: Direct comparison of the maximum displacement and the percentage absorbed energy evolution of the six cores at 50 % of their perforation energy

The direct comparison of the agglomerated cork with the PVC foam with the corresponding density reveals that the two different core types can endure a similar impacts number and actually agglomerated cork can withstand one or two impacts more than the corresponding foam. Moreover, the percentage absorbed energy and maximum displacement values are close and totally comparable. All the results presented above prove that HP130 is the only PVC foam comparable directly with the agglomerated corks in these impact conditions and that its puncture multiple-impact performances are really close to NL25 ones. In view of this, NL25 and HP130 are the two cores selected to pinpoint the differences that arise in the damage progression of these two class of materials. NL25 damage evolution for increasing number of impacts is shown in Figure 129 whereas HP130 one is represented in Figure 130. The natural cellular core NL25 does not display any permanent indentation thanks to the often mentioned high dimensional recovery that permits almost a complete restoration of the initial size of the granules. The only form of damage detectable before the complete perforation of the sample is a progressive detachment of cork granules caused by polymeric binder failure in correspondence of the impacted area. Completely different is HP130 damage mode which entails a significant indentation of the sample already after the first impact and its deepening for increasing number of impacts.
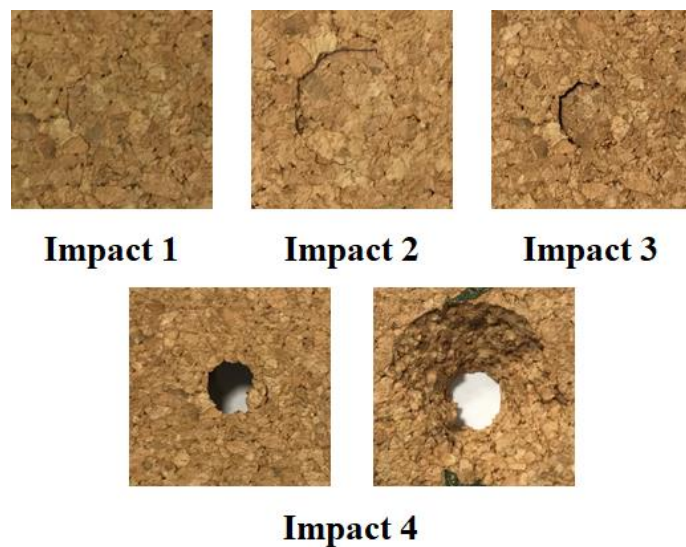
Figure 129: Damage progression of a NL25 specimen impacted at 2.5 J

150
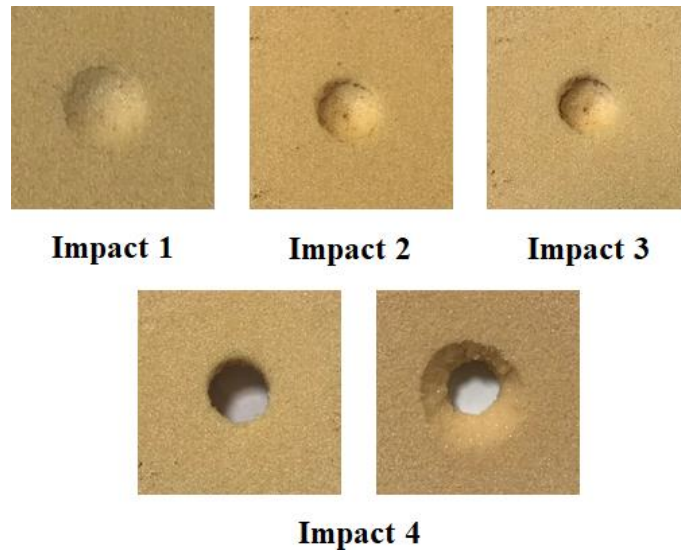
Figure 130: Damage progression of a HP130 specimen impacted at 2.5 J

If agglomerated cork has the possibility to store energy taking advantage of a reversible process, i.e. the increase of cell walls corrugation, that is progressively recovered after the impact, the rigid polymeric foam finds in cell walls fracture and cells collapse the only possible way to dissipate the energy of an impact thus entailing a permanent deformation of the material. For this reason, HP130, and more in general all PVC foams, show traces of the impactor fall already after the first impact. Considering the proneness to permanent indentation of the rigid PVC foams, interesting conclusions can be drawn investigating the evolution of this parameter as a function of impacts number as presented in Figure 131. The 1.25 J data highlight a parabolic trend in HP130 permanent indentation increase ($R^2 = 0.994$) and a logarithmic one for HP200 and HP250 ($R^2 = 0.996$ and $R^2 = 0.998$, respectively). Both trends imply a progressive deceleration of the permanent damage cause by the impactor, but parabolic one entails a more severe damage in the first stages thus leading to an earlier perforation of HP130. Similar outcomes can be observed for the 2.5 J impacts where HP200 and HP 250 are still characterized by a logarithmic evolution ($R^2 = 0.997$ and $R^2 = 0.998$, respectively), but with a steeper slope. HP130 evolution goes from a parabolic to a linear trend meaning that no deceleration intervenes in permanent deformation progression. As already pointed out the higher the density the thicker the cell walls and the higher the amount of energy that the core can dissipate before suffering fracture and cell collapse.
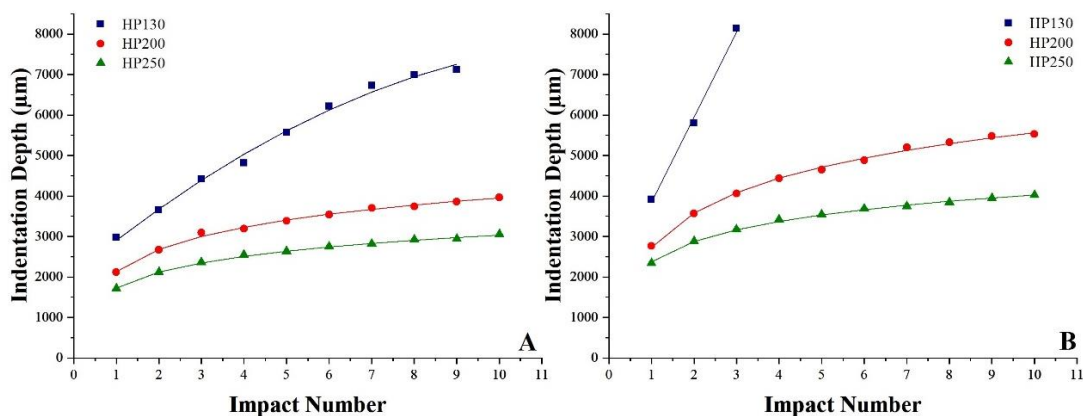
Figure 131: Evolution of the indentation depth of all PVC cores subjected to multiple-impacts at 1.25 J (A) and 2.5 J (B)

151

3.4.7 Impact tests with CAI support

The first step in the characterization of cores impact response with CAI constraints enabled the identification of the perforation threshold of each core material. The resulting values are summarized in Table 30 and are usefully compared with the ones obtained in puncture impact conditions. Considering that puncture constraints are more restrictive than CAI ones, it is not surprising that all core materials are characterized by a higher perforation threshold in this second configuration. The wider unsupported area allows the materials to deform more freely thus promoting the activation of further energy dissipation mechanisms, such as bending, that otherwise would be hindered or limited. PVC foams display a higher increase in perforation energy moving from the more restrictive puncture to CAI thus confirming the strong limitations of agglomerated cork due to the poor interface between the polymeric binder and cork granules that causes a premature failure of the specimen. By the way, the occurrence of further deformation mechanisms allows to detect slight differences in agglomerated cork impact resistance, i.e. different perforation energies, that could not be recognized in puncture impact conditions. The increase in core deformation makes more relevant the variations in material stiffness due to the differences in density. Once identified the perforation threshold, each core material was tested at 25 %, 50 %, 75 % and 100 % of perforation energy and the resulting impact curves are shown in Figure 132 for agglomerated corks and Figure 133 for the PVC foams. Moreover, in Figure 134 are displayed the maximum force, maximum displacement and percentage absorbed energy values of each core material as a function of impact energy. As a general analysis an increase in maximum force, maximum displacement and percentage absorbed energy can be observed in each core material for increasing impact energies.

Table 30: Comparison of the perforation energies of the six core materials in CAI and puncture impact conditions

Core	CAI Perforation Energy (J)	Puncture Perforation Energy (J)
NL10	5	5
NL20	6	5
NL25	7	5
HP130	13	10
HP200	25	15
HP250	30	17.5
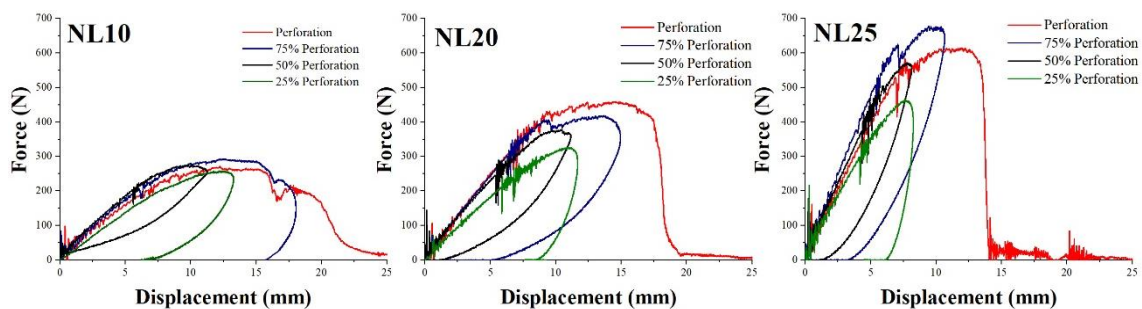
Figure 132: NL10, NL20 and NL25 CAI impact response curves at 25 %, 50 %, 75 % and 100 % of perforation energy
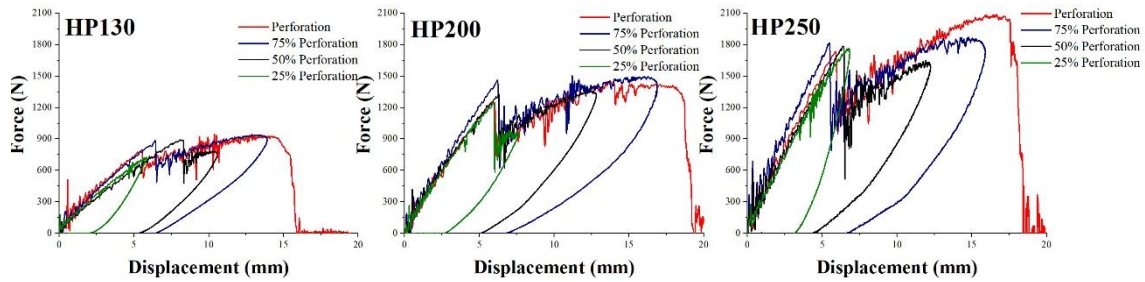
Figure 133: HP130, HP200 and HP250 CAI impact response curves at 25 %, 50 %, 75 % and 100 % of perforation energy
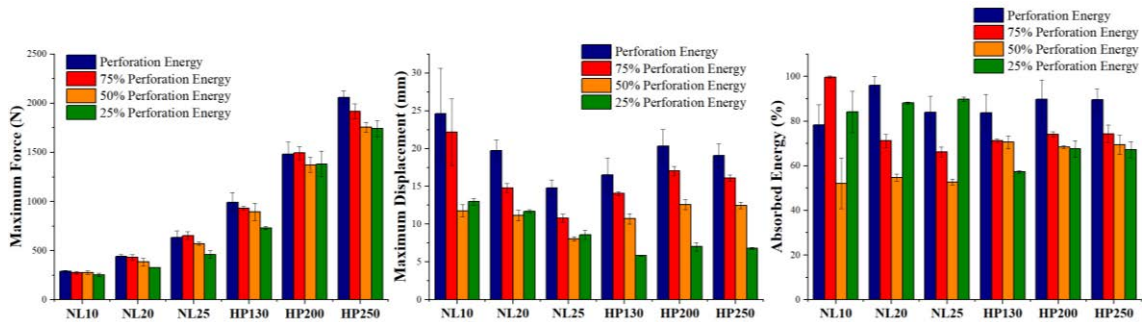
Figure 134: Maximum force, maximum displacement and absorbed energy of the six core materials at 25 %, 50 %, 75 % and 100 % of perforation energy

This is reasonable considering that a higher impact energy implies a higher deformation of the material and hence the involvement of a wider area of the sample that leads to an increase in the reaction force. The only exception to this analysis can be observed for the 25 % perforation energy impacts of agglomerated cork that display an increase in both maximum displacement and percentage absorbed energy with respect to the 50 % ones. This could be explained considering that the impact energy is so low, i.e. 1.25 J for NL10 and 1.75 J for NL25, that the impactor is not able to induce an overall bending of the sample, but concentrates the deformation in a limited area around the impacted zone in the form of compressive deformation thus leading to a local higher maximum displacement and to the inability of this small area to induce a significant rebound of the heavy impactor and hence to an increase in the amount of energy dissipated locally. This hypothesis is further corroborated by the observation of the impact response curves. The initial slope of the curves at 25 % of perforation energy is lower than the slope of the other curves and this is indicative of a lower stiffness of the material that can be justified considering that agglomerated cork is characterized by a flexural stiffness higher than compressive one, i.e. 9.24 – 37.3 MPa against 4.36 - 13.6 MPa, as shown in section 3.3.2 and 3.3.3. Moreover, 25 % curves display a higher residual deformation, but the impacted samples do not show any back fracture due to excessive bending as in the case of samples impacted at higher energies and this could entail a change in the deformation mode. Unfortunately a higher hypothetical penetration of the impactor at the time of the impact cannot be quantified due to the exceptional dimensional recovery of cork that promotes a conspicuous attenuation of impactor indentation already after few milliseconds from the impact as proved in drop weight tower dynamic compression tests in section 3.4.1. Once completed the room temperature analysis, CAI impact tests were carried out at 60 °C and -40 °C in order to investigate the effect of low and high operating temperatures on the impact response of the two families of core materials. The changes in cores perforation energy as a function of operating temperature are reported in Table 31.

Table 31: Comparison of the perforation energies of the six core materials as a function of testing temperature

Core	Perforation Energy at -40 °C (J)	Perforation Energy at Room Temperature (J)	Perforation Energy at 60 °C (J)
NL10	4	5	3
NL20	6	6	4
NL25	5	7	5
HP130	10	13	14
HP200	12	25	27
HP250	15	30	34

Concerning PVC foams, a constant trend can be detected and, in particular, an increase in perforation energy for increasing temperature can be observed. These results can be explained considering the DMA data presented in section 3.2.3. Even if all foams are well below their glass transition temperature in all testing conditions, meaning that they work always in a glassy state, the storage modulus trend displays a slight and progressive decrease for increasing temperature before the sharp drop at the glass transition. This means that the brittle behavior of these polymeric foams is only slightly mitigated at temperatures even beyond the glass transition. The situation is more complex for agglomerated corks that exhibit the highest performances at room temperature. Tests carried out at 60 °C show a reduction of 2 J in the perforation energy for all agglomerated corks due to the progressive softening of the polymeric binder whereas the decrease detected at -40 °C can be ascribed to the approach of the glass transition temperature of the polymeric binder, as proved by the DMA data, and hence to its embrittlement. A deeper understanding of the CAI impact behavior of the core materials as a function of temperature can be achieved from the response curves shown in Figure 135 for agglomerated corks and in Figure 136 for the PVC foams and from the data gathered in Figures 137 and 138 for agglomerated corks and PVC foams, respectively. Both synthetic and natural cores are characterized by an increment in the maximum displacement when test temperature increases but an opposite trend can be observed in the maximum force. In fact, PVC foams are characterized by an increase of this parameter and agglomerated corks by a decrease when operating temperature rises. Concerning agglomerated cork, this behavior can be explained considering that between 11 °C and 16 °C, depending on cork density as already seen in DMA results, suberin melting takes place [169] determining a sharp change in material storage modulus. This means that at -40 °C the material is working well below and at 60 °C well above this transition value moving from the glassy to the viscoelastic behavior in proximity of room temperature.
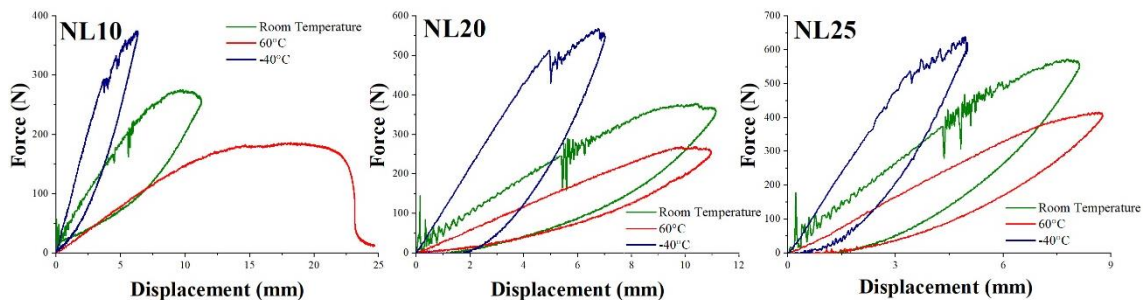
Figure 135: NL10, NL20 and NL25 CAI impact response curves 50 % of perforation energy as a function of operating temperature

Different is PVC foams condition because an increase of temperature in the glassy region causes a little decrease of material brittleness thus allowing an easier deformation and an easier approach of the densification region due to cell collapse that causes the increase in maximum force. This hypothesis is corroborated by the indentation depth data presented in Figure 139 that show clearly how the depth of the damage left by the impactor and measured through profilometric analysis increases for increasing test temperatures. These outcomes are strictly correlated to the almost general trend observed for the percentage absorbed energy that increases when test temperature rises thanks to the decrease in material brittleness that facilitates the core deformation.
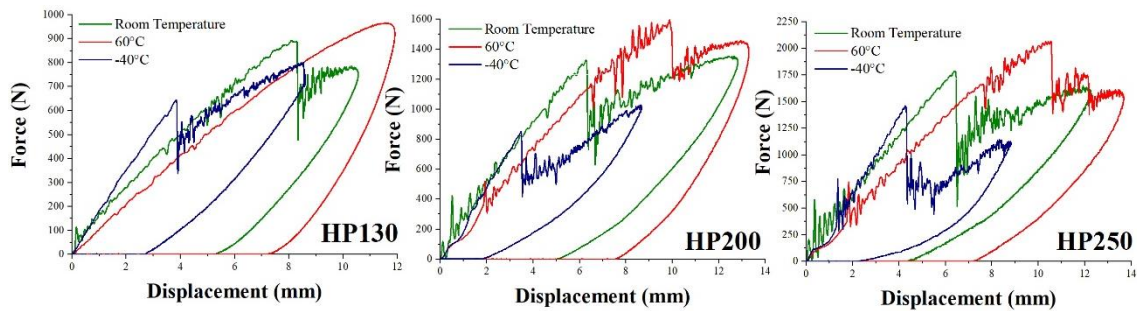
Figure 136: HP130, HP200 and HP250 CAI impact response curves 50 % of perforation energy as a function of operating temperature
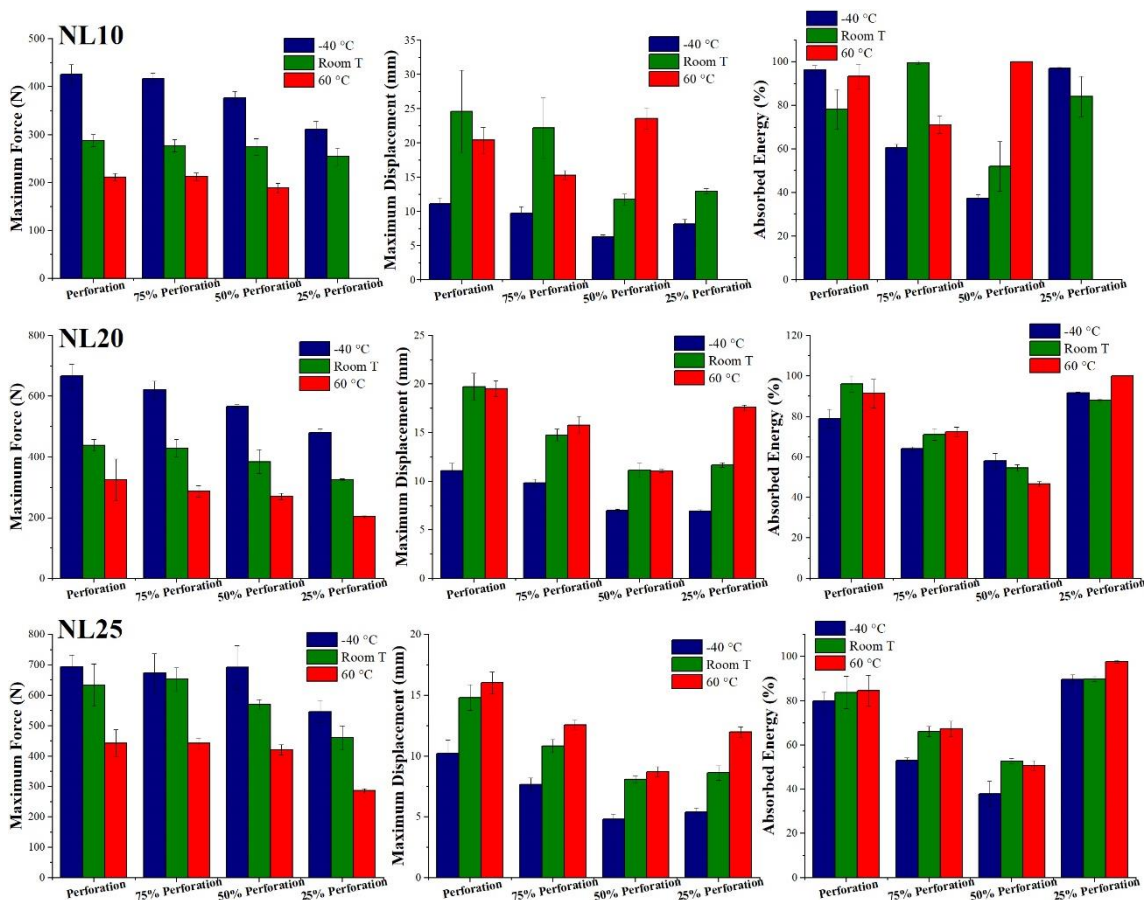
Figure 137: Maximum force, maximum displacement and absorbed energy of NL10, NL20 and NL25 at 25 %, 50 %, 75 % and 100 % of perforation energy as a function of operating temperature
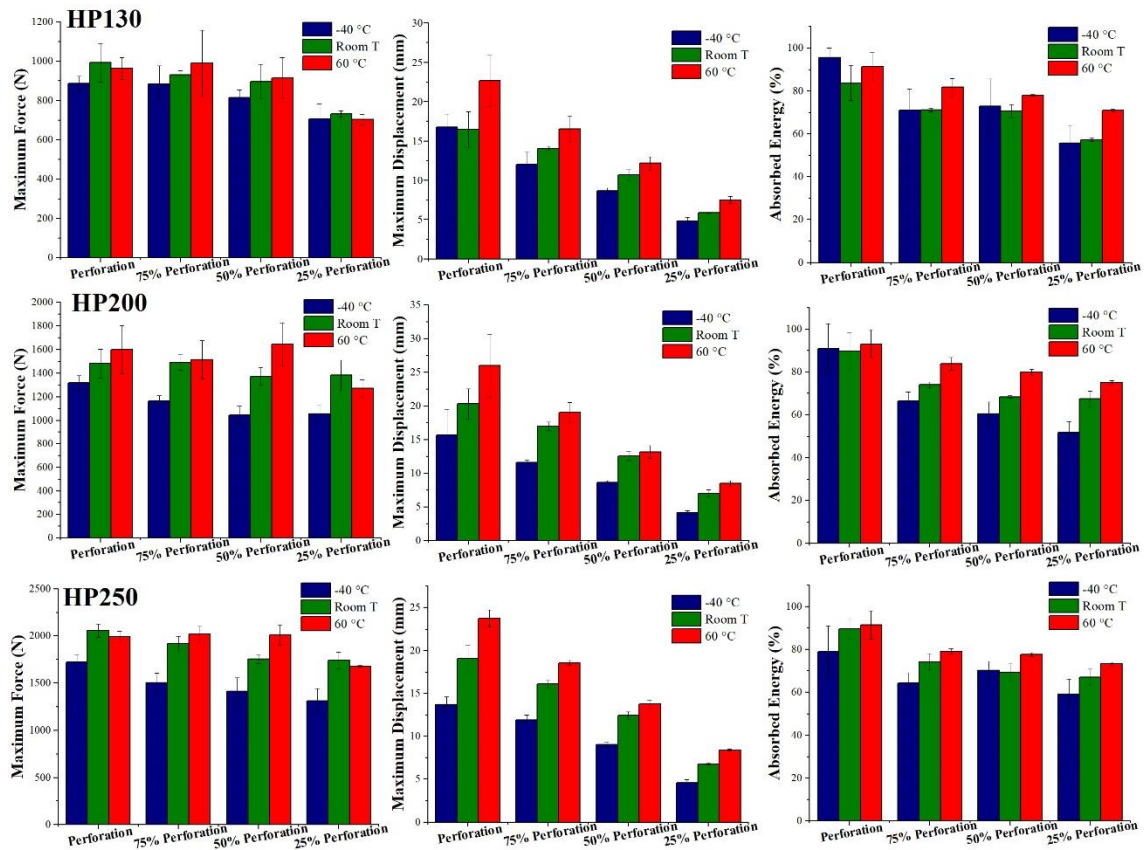
Figure 138: Maximum force, maximum displacement and absorbed energy of HP130, HP200 and HP250 at 25 %, 50 %, 75 % and 100 % of perforation energy as a function of operating temperature
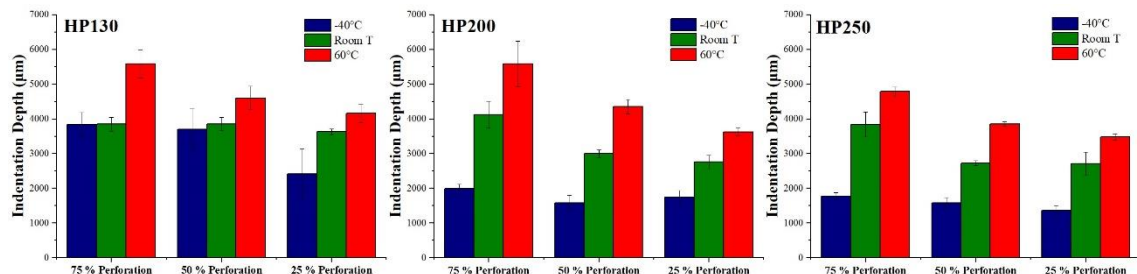
Figure 139: HP130, HP200 and HP250 permanent indentation depth as a function of impact energy and operating temperature

The observation of PVC foams curves allows to detect a first peak force followed by a sharp drop that must be ascribed to the formation of a brittle fracture on the back side of the sample as a consequence of the bending deformation suffered by the material. The same type of damage can be observed in all agglomerated corks but the identification of this phenomenon on the impact curves is not always possible because it is due to the failure of the weak interface at granules boundaries. Considering this common damage feature, an analysis of crack extension as a function of impact energy and test temperature was carried out on both core types. Figures 140 and 141 show the evolution of crack extension for NL25 agglomerated cork and HP130 PVC foam, respectively, whereas in Figures 142 and 143 are summarized the measurements of crack lengths for agglomerated corks and PVC foams, respectively. The results prove unequivocally the

embrittlement effect played by a decrease in temperature displaying an increase of the back-side fracture. For agglomerated cork the transition from the viscoelastic to the glassy state implies a reduction of cell walls deformability and hence an overloading of the polymeric binder that becomes maximum at -40 °C when the latter approaches its glass transition temperature and hence its glassy state.
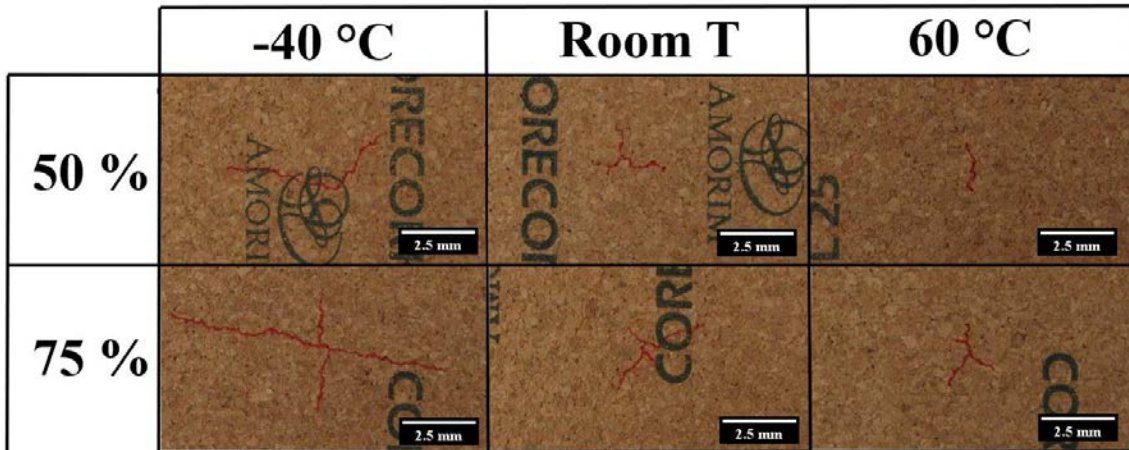
Figure 140: Crack extension evolution as a function of impact energy and temperature in NL25 samples
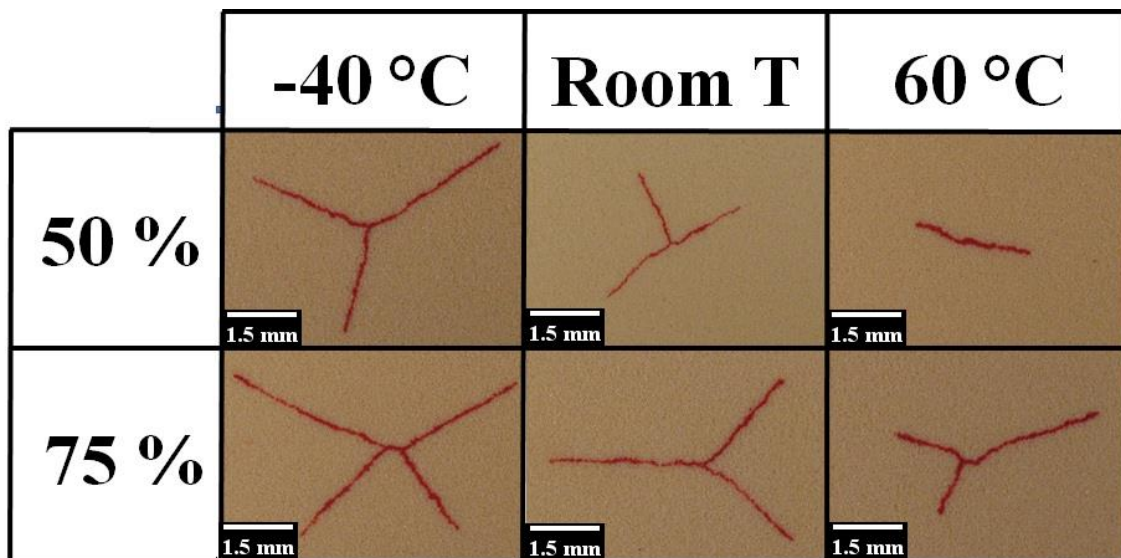
Figure 141: Crack extension evolution as a function of impact energy and temperature in HP130 samples
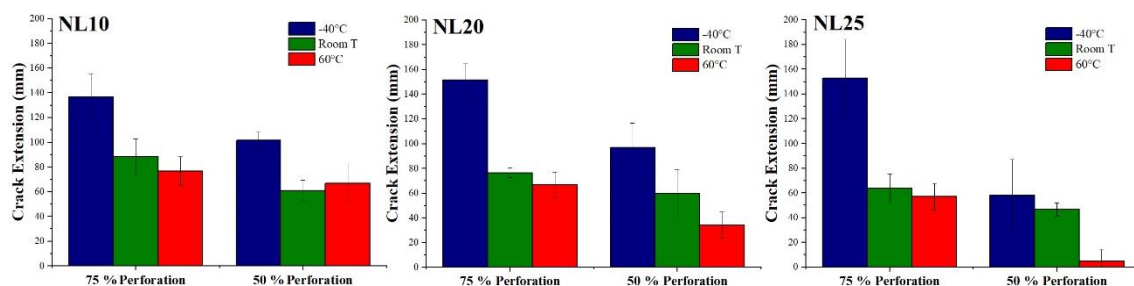
Figure 142: Crack extension as a function of impact energy and temperature for the three agglomerated corks

157
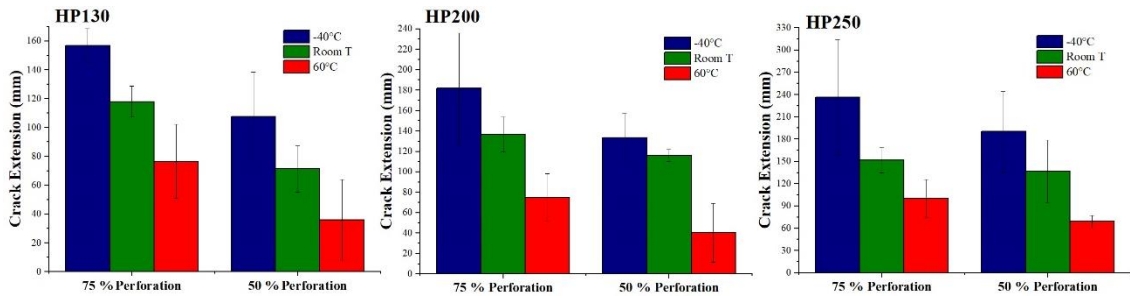
Figure 143: Crack extension as a function of impact energy and temperature for the three PVC foams

This is confirmed by the fact that for impacts performed at 75 % of the perforation energy the differences in cracks extension between 60 °C and room temperature ranges only between 10.8 % and 13 % and rises up to 35.4 %-58.3 % between room temperature and -40 °C. In the case of the PVC foams the increase in crack extension is connected with the reduction in permanent indentation depth, as previously shown in Figure 139. In fact, if energy dissipation phenomena like foam densification are hindered or limited, the only way for the material to dissipate the impact energy is through crack propagation.

3.4.8 Ballistic impact test

The execution of ballistic tests allowed to study the evolution of the projectile residual velocity as a function of the impact velocity as shown in the curves in Figure 144 for agglomerated corks and in Figure 145 for PVC foams. These experimental data set were employed to identify the ballistic limit of all core materials taking advantage of the Lambert-Jonas interpolation implemented with the help of the software Kaleida graph and the resulting values are summarized in Figure 146. As already observed in the previous sections, PVC foams are always characterized by the best mechanical performances, in fact all PVC foams display a ballistic limit higher than agglomerated corks ones regardless of density. Both core types exhibit an increase in the ballistic limit for increasing density, but the trend that describes this incrementation is completely different. PVC foams experiences a linear increase of the ballistic limit for increasing core densities ($R^2 = 0.995$) whereas agglomerated corks go through an increase characterized by a progressive parabolic deceleration ($R^2 = 1$). As previously explained, an increase in PVC foams density is due to a lower air content and hence to thicker cell walls thus implying a higher number of covalent bonds to break and a higher dissipated energy before reaching perforation. This is not true for agglomerated corks whose Achille's heel can be always identified in the weak polymeric binder-cork granules interface which is responsible for the premature intergranular fracture of the material. This means that even if a denser cork can exert a marginally higher resistance to projectile penetration thus increasing slightly core ballistic limit thanks to a higher compactness of the granules, the improvement of this parameter is however limited by the previously mentioned bottle neck that delimits the upper limit achievable with the bio-based cores. The observations made to explain the discrepancies in PVC foams and agglomerated corks ballistic limits are also useful to justify the differences observed in the damage mode of the two types of core. Figure 147 shows the typical intergranular fracture with conical shape that characterizes all agglomerated corks whereas Figure 148 shows the plugging damage mode typical for all PVC foams. Agglomerated cork displays a conoid fracture that origins in the area impacted by the projectile and increases its extension throughout sample thickness. This damage mode can be ascribed to two main reasons.
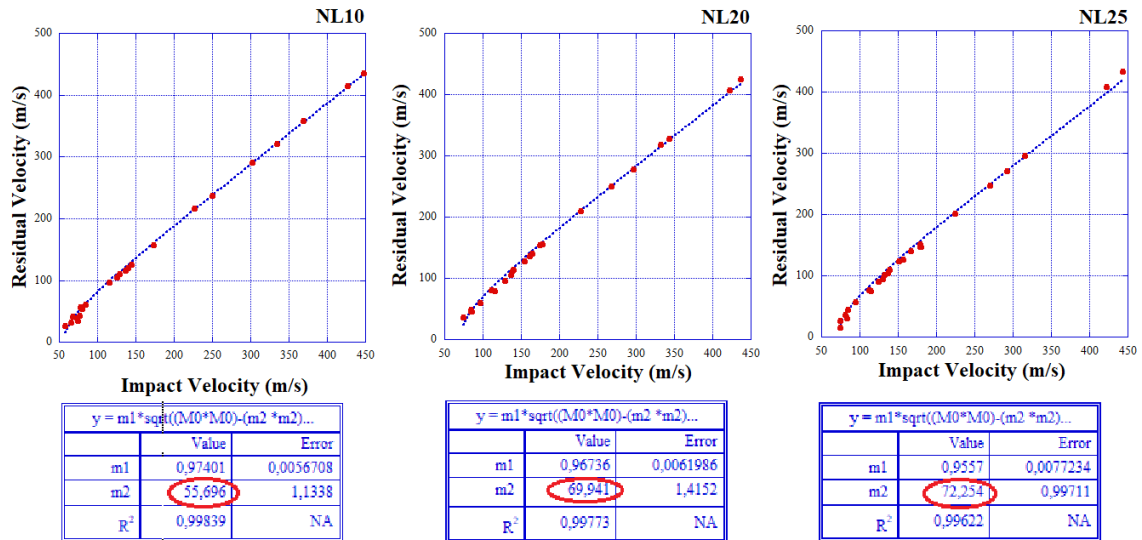
Figure 144: NL10, NL20 and NL25 experimental data and interpolation curves obtained implementing the Lambert-Jonas equation in the software Kaleida graph
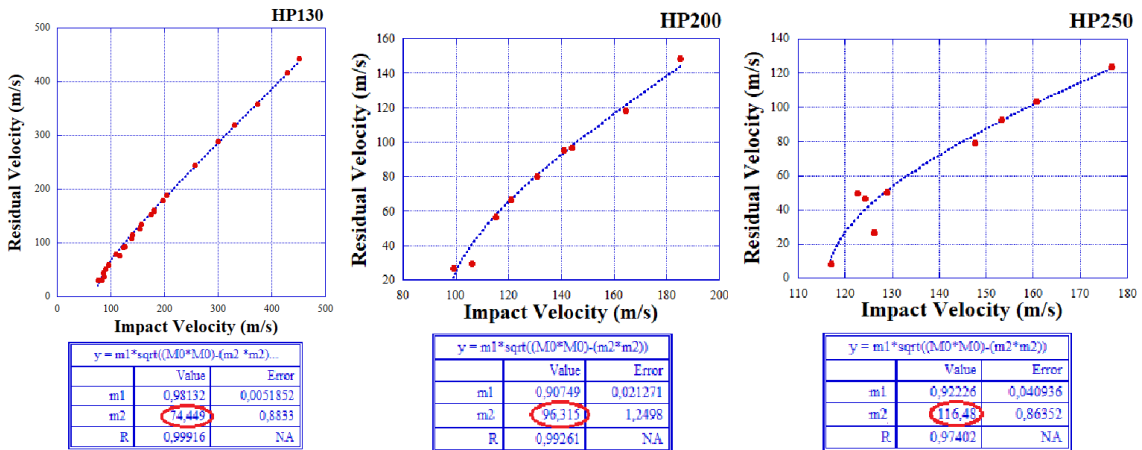
Figure 145: HP130, HP200 and HP250 experimental data and interpolation curves obtained implementing the Lambert-Jonas equation in the software Kaleida graph
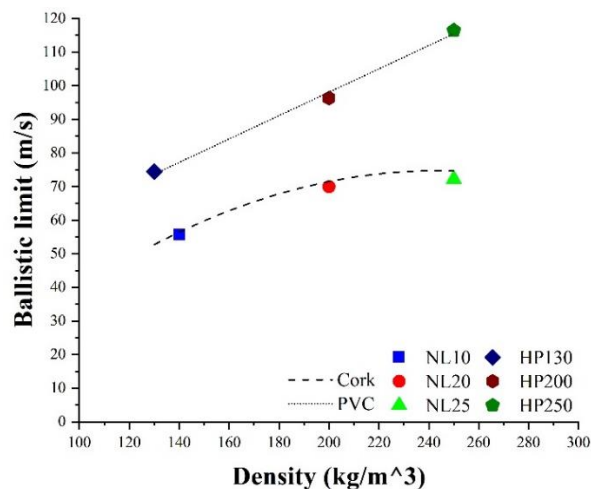
Figure 146: Ballistic limits of the six core materials calculated through the Lambert-Jonas equation

159
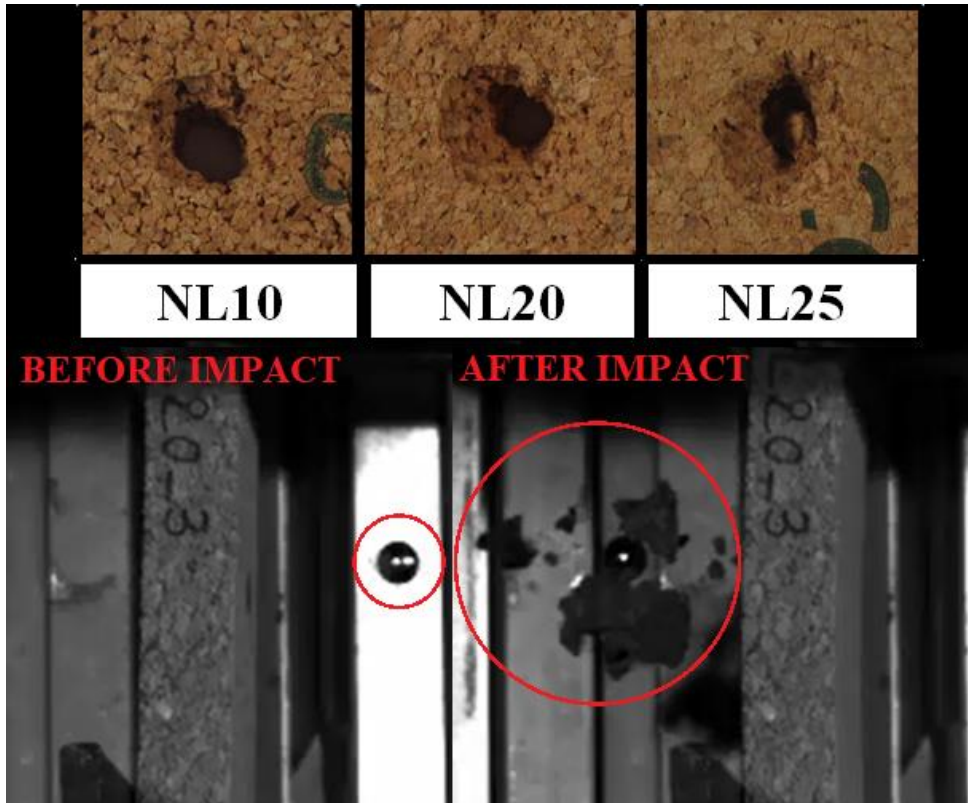
Figure 147: Conical intergranular fracture typical of agglomerated corks
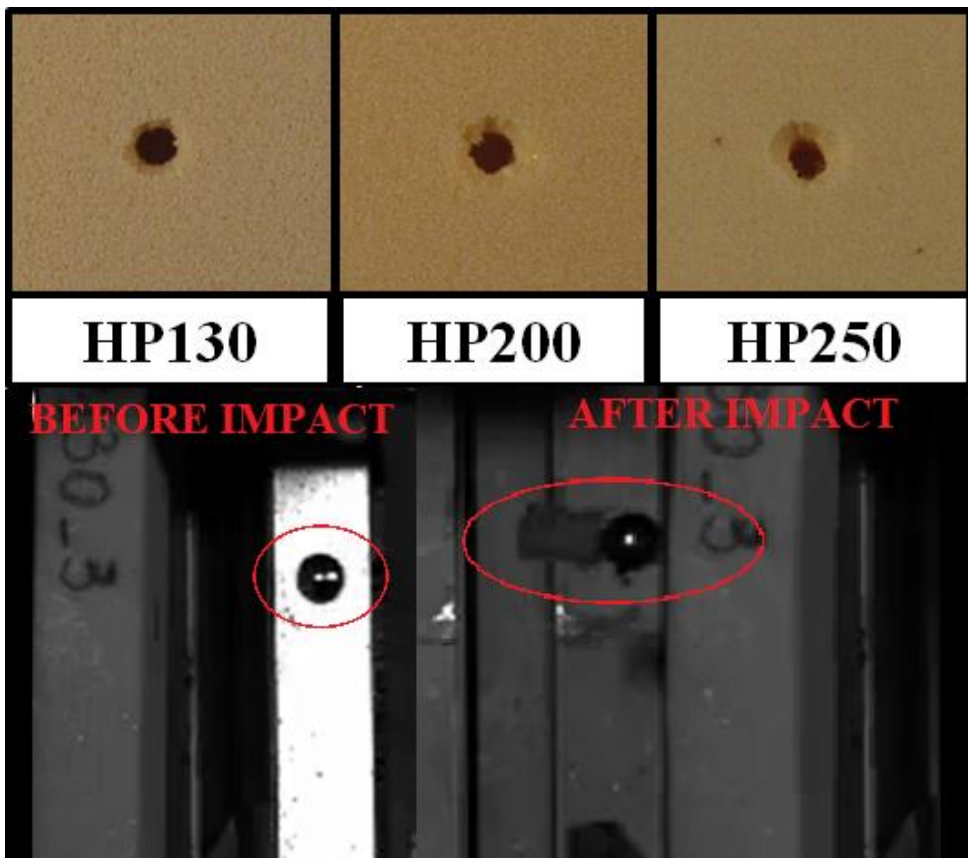
Figure 148: Plugging damage mode typical of PVC foams

The first reason is the, already mentioned, weak granules-binder interface which acts as a preferential path for crack propagation being the less energy consuming. This means that the crack changes its path every time that encounters a cork granule instead of a boundary region thus leading to a progressive increase of the detached area. The second reason can be found in the low solid mass volume fraction, approximately 10 %, that characterizes natural cork as reported by Pereira [37]. This value is certainly higher for agglomerated cork due to the presence of the polymeric binder, but it is reasonable to expect it low by the way. This means that cork granules interfaces can be recognized as the areas were material mass concentrates thus acting as a preferential path for shock wave propagation. Different is PVC foams damage mode that is more localized and is characterized by a cylindrical shape. This damage mode is called plugging and arises as a consequence of an excessive localized plasticity and to the excess of material shear strength. This is not surprising considering that all chemical bonds in PVC backbone are characterized by the same strength and hence a cylindrical rupture is the less energy consuming path for crack propagation. Further studies on core damage were carried out evaluating the damage area extension as a function of impact velocity and the resulting data are shown in Figure 149. All cores regardless of their nature and density are characterized by a decrease in back damage extension for increasing impact velocities. This behavior was already acknowledged by Buitargo et al. [191], by López-Puente et al. [192] and by Amaro et al. [193] in their study on glass/polyester, carbon/epoxy and Kevlar/cork powder/epoxy composites, respectively. In ballistic impacts the interaction time between the sample and the projectile is definitely low, but when a material is close to its ballistic limit this interaction time is higher as indeed material reaction time. This means that a higher portion of the sample is affected by deformation leading to a less localized damage. In particular agglomerated corks show a reduction in back damage extension between 72.2 % and 88.4 % whereas PVC foams a reduction between 92 % and 96 %. All cores are characterized by a lower limit below which they cannot go that is around 90 mm^2 for agglomerated corks and 10 mm^2 for the PVC foams.
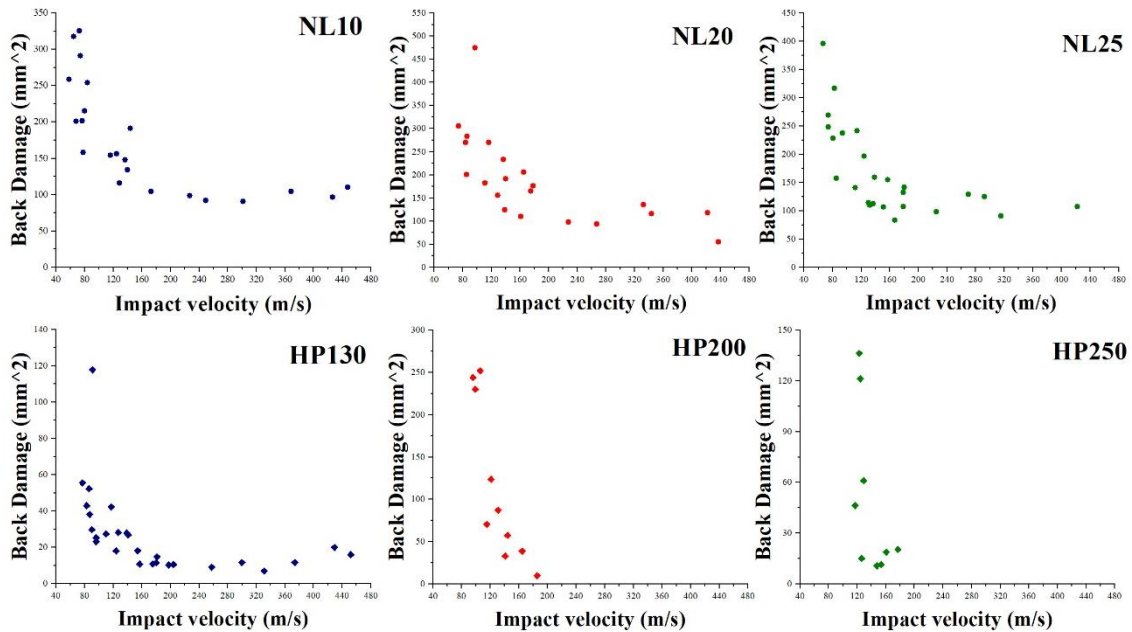
Figure 149: Evolution of back damage area extent as a function of impact velocity for the six core materials

Chapter 4: Skin Characterization

4.1 Quasi-Static Characterization

4.1.1 Thermal analysis

Thermal analysis, i.e. Thermogravimetric analysis (TGA) and Differential Scanning Calorimetry (DSC), were carried out on PP and PPC skins in order to obtain useful information to better understand the evolution of composite mechanical behavior as a function of temperature. Figure 150 shows sample weight and derivative sample weight evolution as a function of temperature. Both skin types display a similar trend and, in particular, an initial mass decrease of 1.5 % due to moisture removal between 40 °C and 115 °C which is followed by two major drops. Samples are subjected to a mass loss of 5 % at 310 °C which can be identified as the temperature of degradation beginning. The first mass drop occurs between 320 °C and 380 °C and causes a reduction of almost 25 % due to flax fibers thermal degradation whereas the second mass drop of 35 % takes place between 420 °C and 490 °C and must be ascribed to PP thermal degradation. These results are in perfect agreement with the ones reported by Khalfallah et al. [194] who identified flax thermal degradation between 270 °C and 380 °C, by Biagiotti et al. [195] who studied flax-polypropylene composites and detected flax degradation between 355 °C and 360 °C and PP degradation at 460 °C and by Russo et al. [196] who investigated the effect of carbon nanotubes and stearic acid treatment on flax-polypropylene composites and found out flax thermal degradation between 340 °C and 360 °C and PP degradation between 380 °C and 470 °C.
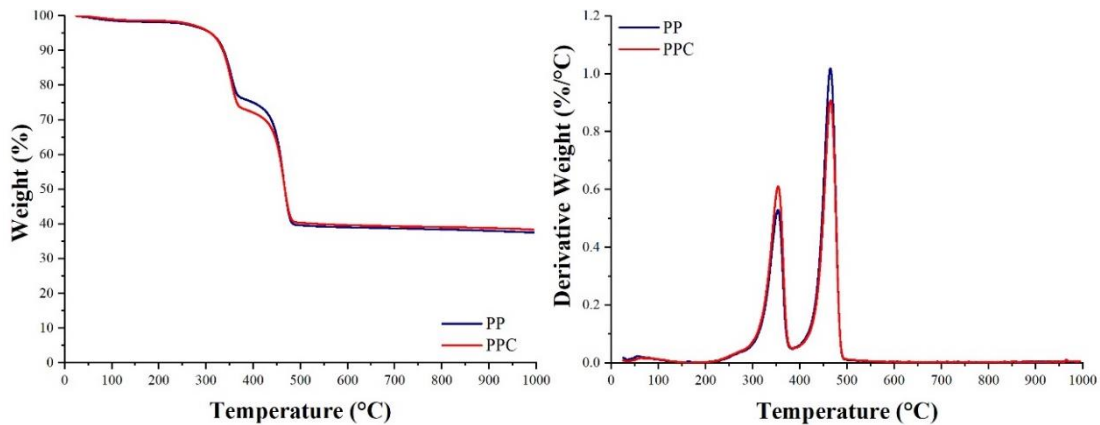
Figure 150: TGA and DTG curves of PP and PPC skins

DSC results for both PP and PPC skins are reported in Figure 151 and Table 32, in particular Figure 151 shows the curves of the first heating and cooling cycle for both PP and PPC skins, whereas Table 32 summarizes melting and crystallization temperatures and the degree of crystallinity calculated according to Equation (4.1):

$$X_c = \frac{\Delta H_m}{(1-w_f)\Delta H_{m100\%}} \tag{4.1}$$

162

where ΔH_m is the melting enthalpy, w_f is fiber weight percentage and $\Delta H_{m100\%}$ is the melting enthalpy for a 100 % crystalline PP which is equal to 207 J/g [197]. PP and PPC melting and crystallization temperatures are equal to 168 °C and 118 °C and these values are in perfect agreement with the ones obtained by Biagiotti et al. [195] who found out a melting temperature between 163 and 168 °C and a crystallization temperature between 104 °C and 109 °C. Analyzing more in depth the DSC curves, it is possible to observe a small peak in the heat flow at around − 12.5 °C, which points out the glass transition underwent by the polypropylene, and a larger one that extends up to 65 °C – 70 °C and includes moisture removal from flax fibers and flax glass transition that takes place at around 55.5 °C and 66 °C as already acknowledged by Dong et al. [198] and by Khalfallah et al. [194], respectively.
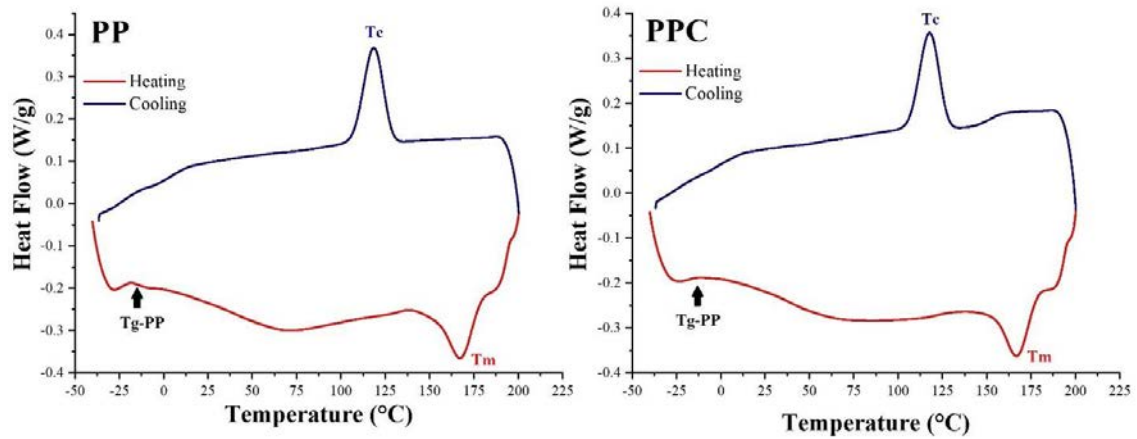
Figure 151: First heating and cooling DSC curves of PP and PPC skins

Table 32: Melting and crystallization temperatures and degree of crystallinity of PP and PPC skins calculated from DSC curves

Sample	Tm (°C)	Tc (°C)	Xc (%)
PP	169.1	117.6	37.9
PPC	167.1	118.6	31.6

4.1.2 Tensile tests

Skin tensile test results are shown in Figures 152 and 153, in particular Figure 152 displays the tensile curves as a function of fibers orientation and matrix type, i.e. PP or PPC, and Figure 153 summarizes the resulting tensile modulus and strength values. The first outcomes that can be pointed out are a higher tensile modulus along flax fibers direction and a higher tensile strength along basalt fibers direction being equal the matrix employed. Concerning the tensile modulus, the higher stiffness obtained along flax direction can be ascribed to the higher fiber volume fraction. Even if the hybrid fabric employed as skin reinforcement is perfectly balanced with a 50 wt. % of basalt and a 50 wt. % of flax, the much lower density of vegetable fibers leads to a higher volume fraction and hence to an improved stiffness according to the rule of mixture. The opposite situation detected for the tensile strength, which turned out to be higher along basalt direction, is due to the intrinsic higher mechanical properties of basalt compared to flax. The effect of the maleic anhydride coupling agent on the quasi-static tensile properties of the skins was examined.
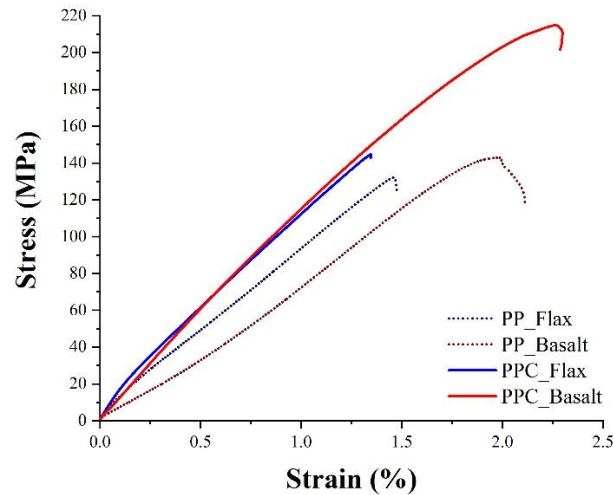
Figure 152: Tensile curves of PP and PPC along flax and basalt fibers direction
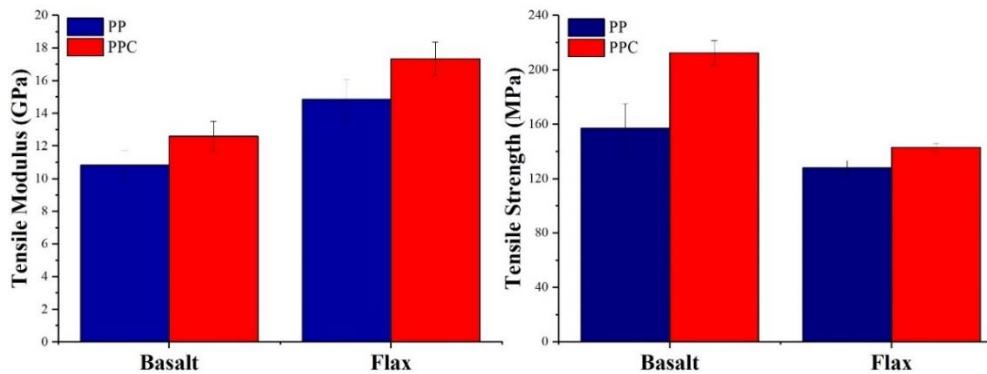
Figure 153: Tensile modulus and strength of PP and PPC skins along flax and basalt direction

An increase in both tensile modulus and strength was observed in all compatibilized composites regardless of fibers orientation. The improvement of fiber-matrix interface allows a better exploitation of reinforcement mechanical properties improving the load transfer from the weak matrix to the performing fibers. These results are in perfect agreement with the ones presented in previous studies like the ones proposed by Kiss et al. [199] and by Watanabe et al. [200] who investigated the enhancement obtained in glass fiber/polypropylene composites thanks to the addition of MA-g-PP, by Keener et al. [63] and by El-Sabbagh [201] who investigated the effect of this coupling agent on vegetable fiber composites and by Sarasini et al. [124], by Sergi et al. [125,202] and by Chen et al. [203] who investigated the effect of a maleic anhydride coupling agent on natural fiber hybrid composites, i.e. hemp/basalt, cellulose/basalt, wood/basalt, respectively. The enhancement of fiber-matrix interface can be inferred not only from the changes observed in samples damage mode as shown in Figure 154, but also from the micrographs shown in Figures 155 and 156, which display the fracture surfaces along basalt and flax directions, respectively. The examination of PP skins damage mode reveals a severe incompatibility between the fibers and the matrix being the former completely uncovered and detached from the polymer thus revealing the missed cooperation in bearing the tensile load. Opposite is the situation of PPC skins, characterized by a clean fracture that points out a good synergy between fibers and matrix and hence a better exploitation of fibers mechanical properties. These results are further corroborated by SEM micrographs. In Figures 155.A and 156.A the fracture surfaces of non-compatibilized composites are shown and a strong incompatibility between natural fibers and PP

164

matrix can be observed considering that the latter is present only in small traces on the surface of the formers. The possibility to identify clearly the neat basalt fibers and the flax bundle is a precise sign of the pull-out phenomena further confirmed by the pronounced imprints left on the matrix. Completely different are the PPC micrographs in Figures 155.B and 156.B which underline a better fiber-matrix interface as proved by the complete covering of the fibers by the matrix. The absence of debonding and discontinuities confirms how fibers and matrix were able to work synergistically to withstand the applied load.

Figure 154: PP and PPC samples damage mode along basalt and flax direction, respectively
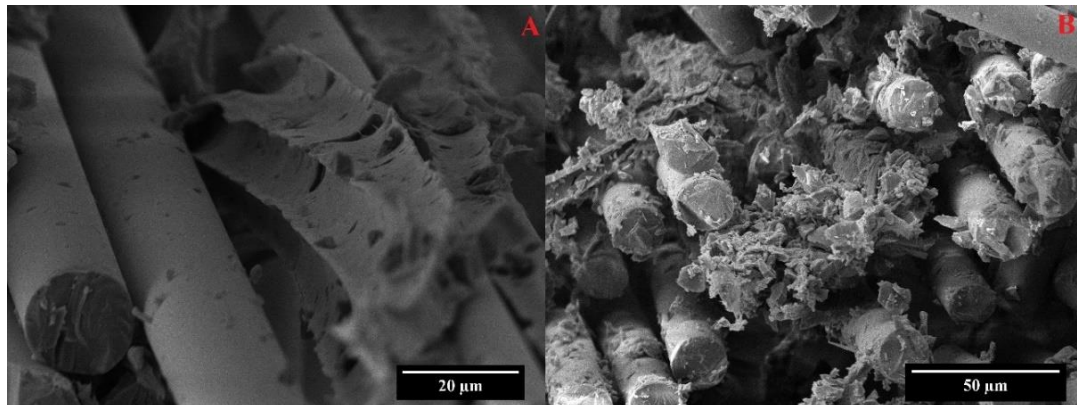
Figure 155: SEM micrographs of the fracture surface along basalt direction for PP (A) and PPC (B) skins
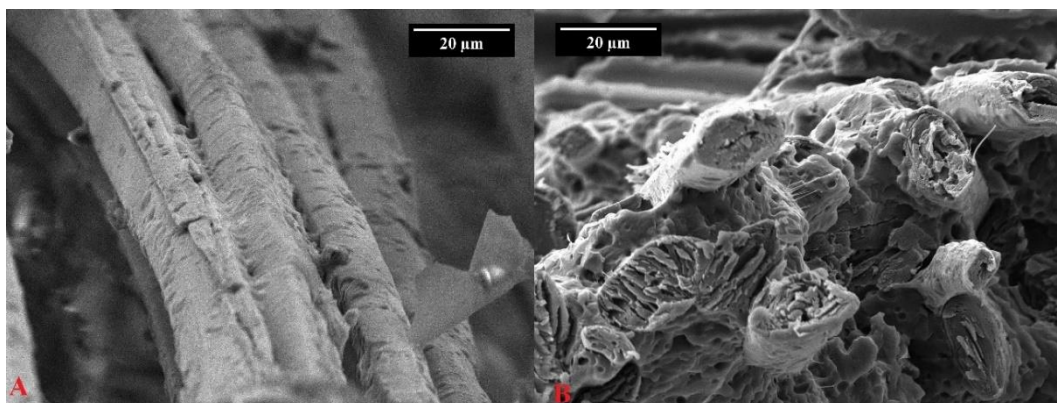
Figure 156: SEM micrographs of the fracture surface along flax direction for PP (A) and PPC (B) skins

4.1.3 Bending tests

Skin bending test results are shown in Figures 157 and 158, in particular Figure 157 displays the bending curves as a function of fibers orientation and matrix type, i.e. PP or PPC, and Figure 158 summarizes the resulting flexural modulus and strength values. The results obtained agree perfectly with tensile test ones presented in the previous section. Being equal the matrix, a higher flexural modulus is achieved along flax fibers direction and a higher flexural strength can be achieved along basalt fibers direction thanks to the higher fiber volume fraction and the intrinsic higher mechanical properties, respectively. Even in this case an increase in both flexural modulus and strength can be observed in all compatibilized composites regardless of fibers orientation thanks to the enhanced fiber-matrix interface. To confirm the paramount role played by MA-g-PP in skins mechanical properties improvement, further SEM analysis were performed on specimens failed in bending. Figures 159 and 160 show the fracture surfaces of basalt oriented and flax oriented samples, respectively. Figures 159.A and 160.A reveal a pronounced pull out of the fibers and a significant debonding from the matrix in the not compatibilized composites. Fiber-matrix debonding is proved by the deep grooves that can be detected at the base of the fibers. On the contrary, the PPC micrographs in Figures 159.B and 160.B show a better coverage of the fibers with the polymer matrix in the case of basalt fibers, and an absence of gaps at flax fiber/matrix interface.
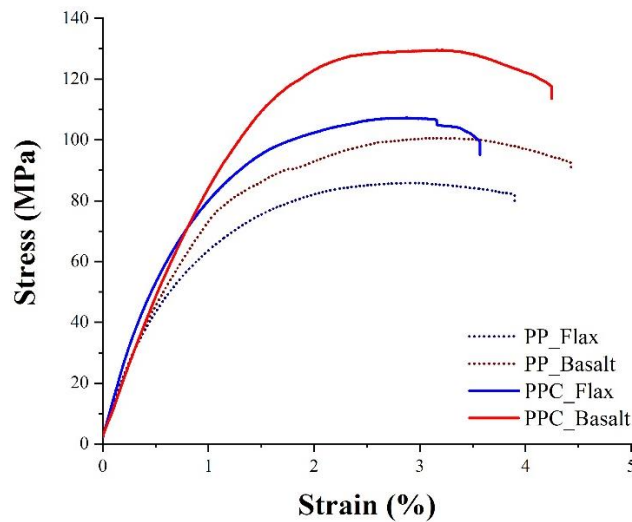
Figure 157: Bending curves of PP and PPC along flax and basalt fibers direction
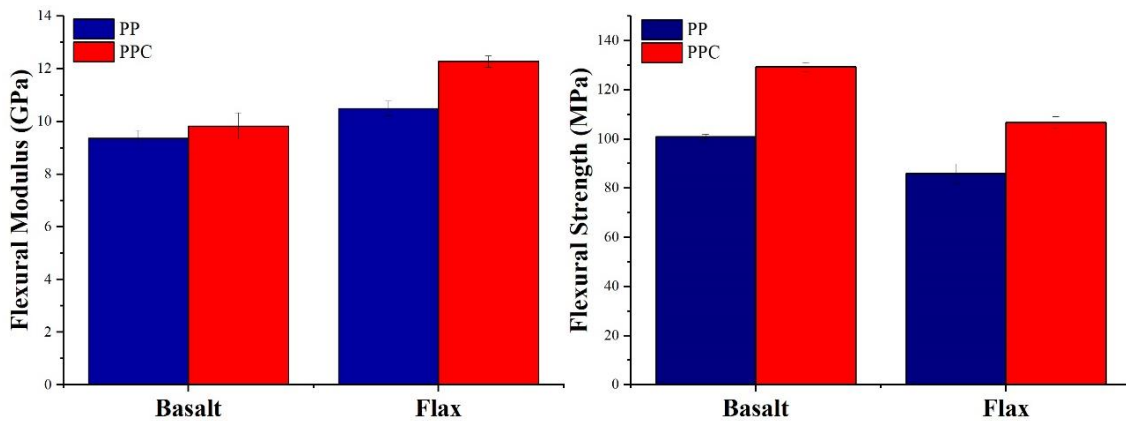
Figure 158: Flexural modulus and strength of PP and PPC skins along flax and basalt direction
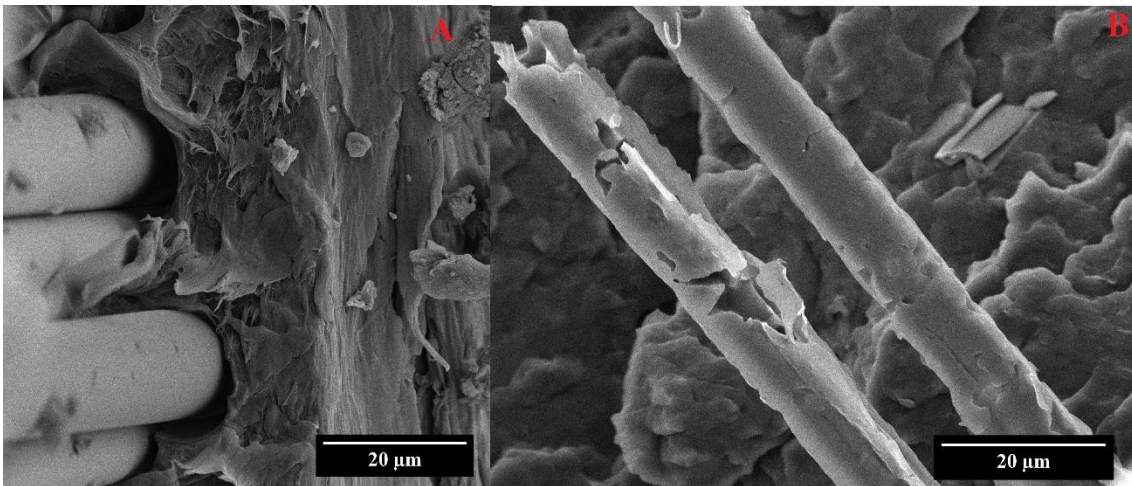
Figure 159: SEM micrographs of the fracture surface along basalt direction for PP (A) and PPC (B) skins
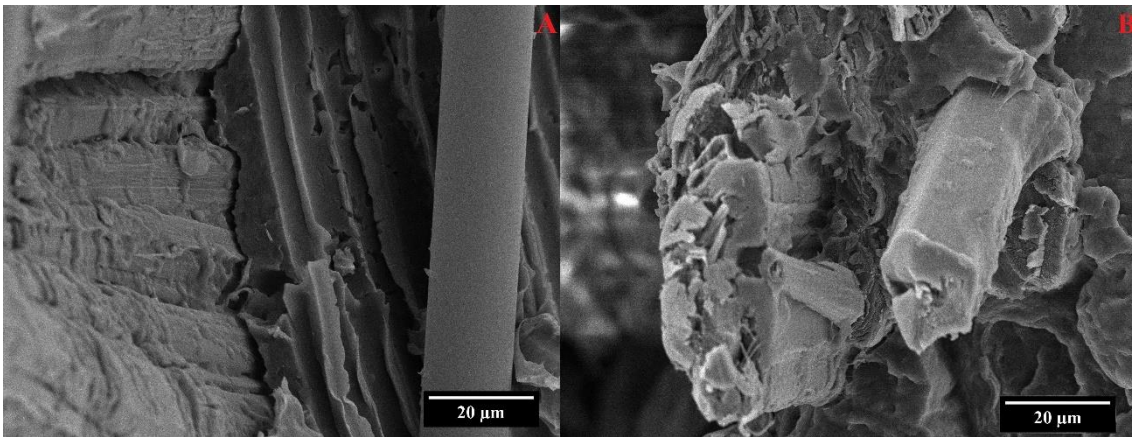
Figure 160: SEM micrographs of the fracture surface along flax direction for PP (A) and PPC (B) skins

4.2 Dynamic Characterization

4.2.1 Puncture impact tests

Once completed skin quasi-static characterization and once ascertained the positive effect played by the coupling agent on fiber-matrix interface, the experimental campaign progressed to investigate the effect of coupling agent on skin dynamic response. The results related to puncture impact tests are reported in Figures 161 and 162, which show PP and PPC impact response curves and maximum force, maximum displacement and percentage absorbed energy as a function of impact energy, respectively. The first outcome to point out is the higher perforation energy of PP skins compared to PPC. Indeed, PP skins can withstand a 30 J impact before undergoing perforation, whereas PPC skins can tolerate only a 20 J impact before perforation. This finding reveals a negative effect of coupling agent on the impact response of the composite laminates in perfect agreement with the results reported in previous works by Simeoli et al. [204], by Sorrentino et al. [205] and by Boccardi et al. [206], who investigates the effect played by coupling

agent on PP/ glass fiber composites. Composite laminates usually dissipate the energy of an impact through matrix and fibers breakage and delamination phenomena, but a weak fiber-matrix interface enables additional energy dissipation mechanisms such as fibers pull out, fiber-matrix friction and fiber/matrix debonding that allow to increase material impact strength and to preserve its integrity at higher impact energies before final failure occurs. Fibers slippage ensures a local rearrangement of the reinforcement in the matrix leaving to the latter the possibility to deform plastically thus promoting another energy dissipation mechanism. These mechanisms are hindered in PPC skins by the improved fiber-matrix interface, which prevents fibers local rearrangements and matrix capability to deform plastically thus inducing an embrittlement effect in material response. Looking at the data in Figure 162, it is possible to notice that both skin types reach almost the same maximum displacement, but PPC skins are characterized by a slightly higher maximum force and PP skins by a higher absorbed energy. These results are in agreement with the previous analysis, in fact being equal the maximum displacement and the impact energy, PPC enhanced interface provides the laminates with a higher reaction force, as observed in the quasi-static characterization, whereas PP weak interface promotes a better energy dissipation. The conclusions drawn are further corroborated by the analysis of skins damage mode. Figure 163 summarizes the permanent indentation depth data whereas Figure 164 displays the front and back damage progression of PP and PPC skins as a function of impact energy. Due to matrix plasticization, PP skins are able to dissipate locally the impact energy undergoing a higher permanent indentation. This is not possible for PPC skins due to the embrittlement effect played by the coupling agent. For this reason, the only way in which PPC skins can counteract the load applied by the impactor is to involve a wider during the impact event.
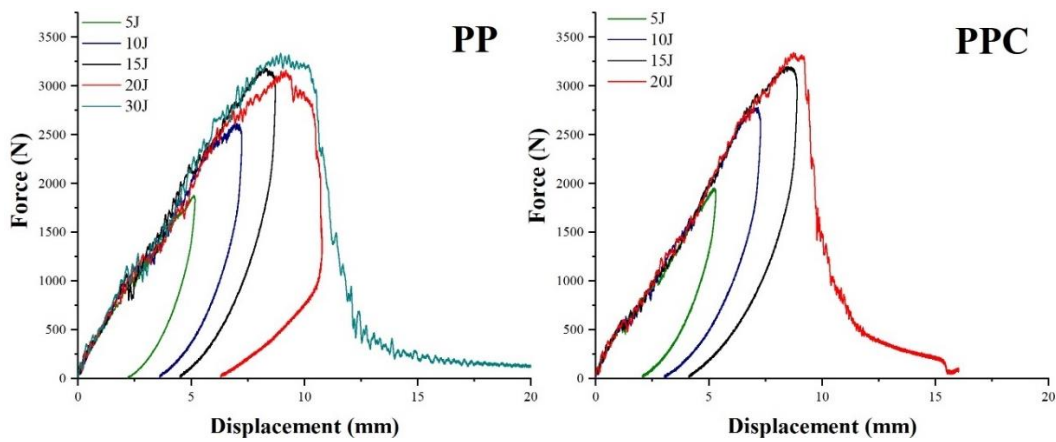
Figure 161: PP and PPC skins puncture impact response curves at different impact energies
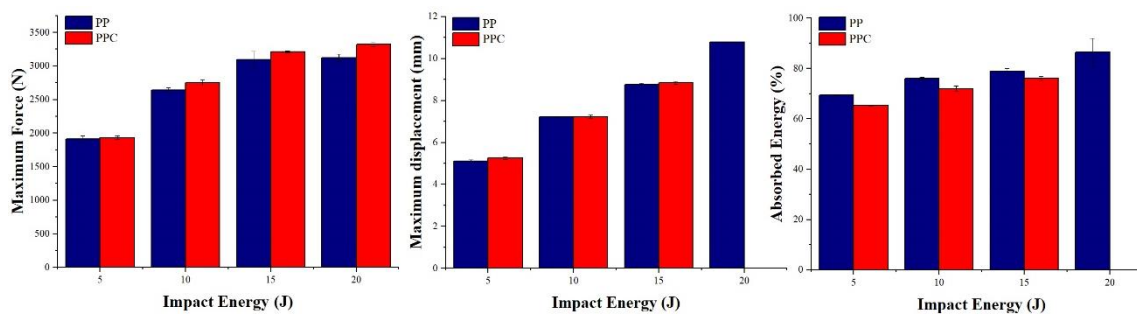
Figure 162: Maximum force, maximum displacement and percentage absorbed energy of PP and PPC skins as a function of impact energy

168

This hypothesis is confirmed by the observation of the damage progression of PPC skins shown in Figure 164, where large whitened areas can be recognized. The extension of these areas increases for increasing impact energies until reaching the edges of the specimen, proving the increasing amount of material interested by the impact.
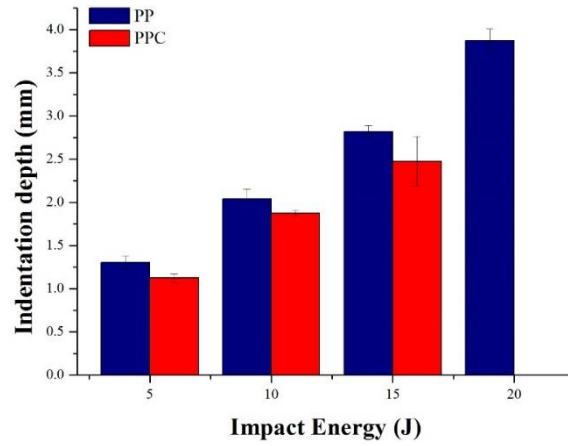
Figure 163: Permanent indentation depth measured through profilometry of PP and PPC skins as a function of impact energy
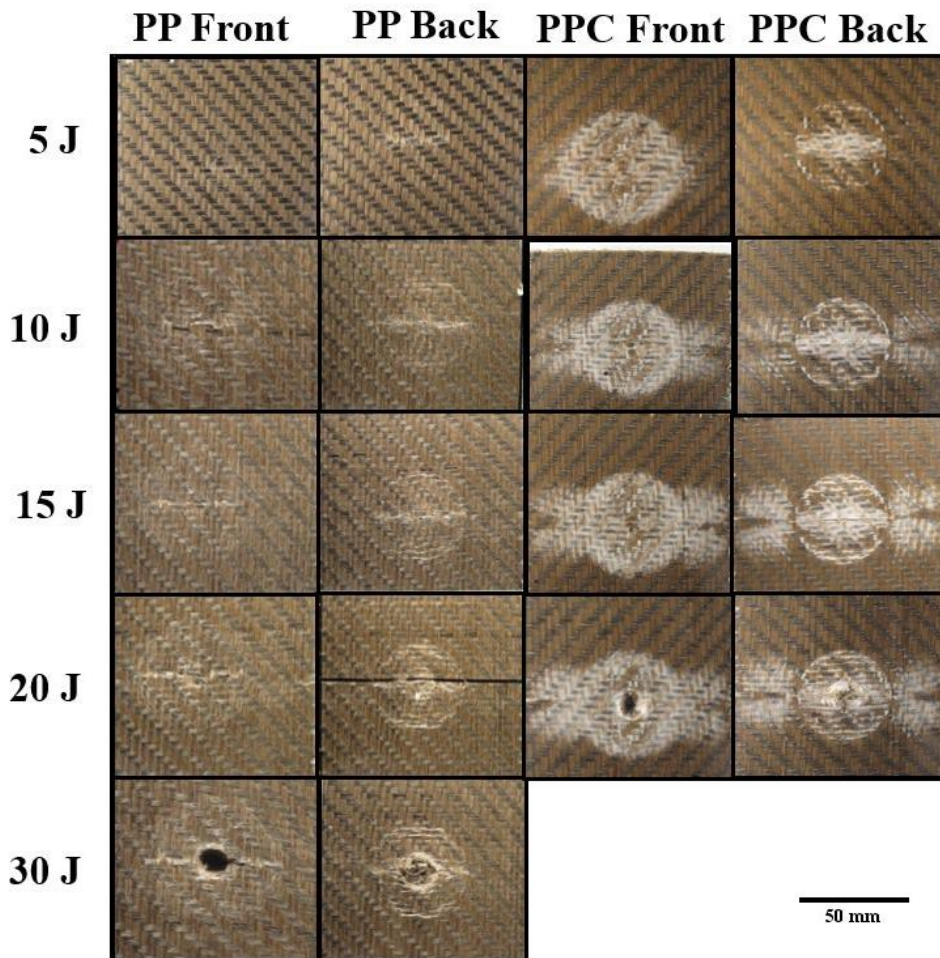
Figure 164: PP and PPC skins front and back damage progression as a function of impact energy

4.2.2 Impact tests with CAI support

As previously seen for core materials, the first step in the characterization of skin impact response with CAI constraints consists in the identification of the perforation threshold of each laminate and the resulting values are summarized in Table 33 and are compared with the ones obtained in puncture impact conditions. If for all core materials an increase in perforation energy was detected moving from the more restrictive puncture constraints to CAI ones, the situation is completely opposite for skin laminates that suffer a reduction in the perforation threshold. A higher degree of deformation freedom proved to be advantageous for the core materials that can be considered isotropic along the x-y plane and hence can exploit a higher amount of material to counteract the impact load. This is not true for the skins that are characterized by anisotropic properties along the x-y plane depending on flax and basalt fibers orientation and are negatively affected moving from the symmetric constraints of the puncture to the rectangular support of the CAI.

Table 33: Comparison of the perforation energies of PP and PPC skins in CAI and puncture impact conditions

Skin	CAI Perforation Energy (J)	Puncture Perforation Energy (J)
PP	20	30
PPC	18	20

It was previously mentioned that CAI constraints allow a notable bending of the sample and being the flax fibers oriented along the shortest side they will be characterized by a lower span length. The deflection δ (mm) of a sample in bending can be calculated according to Equation (4.2):

$$\delta = \frac{Ps^3}{48\,EI} \tag{4.2}$$

where P is the force necessary to reach that deformation, s is the span length, E material flexural modulus and I the moment of inertia that depends on sample thickness and width (b). Considering that during the impact the maximum deflection reached by flax and basalt fibers is equal it is possible to state that:

$$\frac{P_{Flax}\,s^3_{Flax}}{48\,E_{Flax}I_{Flax}} = \frac{P_{Bas}\,s^3_{Bas}}{48\,E_{Bas}I_{Bas}} \tag{4.3}$$

Starting from Equation (4.3) it is possible to obtain the relationship between the load borne by flax fibers and the one sustained by basalt ones according to Equation (4.4):

$$P_{Flax} = \left(\frac{s_{Bas}}{s_{Flax}}\right)^3 \frac{b_{Flax}}{b_{Bas}} \frac{E_{Flax}}{E_{Bas}}\,P_{bas} \tag{4.4}$$

Assuming that $b_{Flax} = s_{Bas}$ and $b_{Bas} = s_{Flax}$ Equation (4.4) converts into Equation (4.5):

$$P_{Flax} = \left(\frac{s_{Bas}}{s_{Flax}}\right)^4 \frac{E_{Flax}}{E_{Bas}}\,P_{bas} \tag{4.5}$$

It is known that materials flexural modulus depends on the span length employed. In the case of flax fiber direction, the span length during a CAI impact is equal to 75 mm that is close to the one employed in skin bending tests which was 80 mm. This is not true for basalt fiber direction where the span length during a CAI impact is equal to 125 mm. In their work on span length effect on the flexural properties of carbon and glass reinforced epoxy laminates, Mehndiratta et al. [207] found out that for both unidirectional and bidirectional composites the flexural modulus reaches its maximum value in a span length between 50 and 80 mm and decrease for higher values. In light of these findings, employing a basalt flexural modulus equal to the ones obtained during bending tests permit to consider the more optimistic situation. Inserting all the mentioned values in Equation (4.5) it turns out that the load applied on flax fibers is 8.5 times higher than the one sustained by basalt fibers. The proposed calculation is only an approximation, considering that in a bending test sample extremity are sustained and not pinned and that two side of the sample are completely free, and does not mean to be explicative of the mechanisms that take place during the impact, but it is a valid support to explain the results obtained. Indeed, the lower span length along flax fibers direction causes an overload of these vegetable fibers, that being characterized by a lower flexural strength than basalt ones, are not able to withstand the impact load thus leading to a premature failure of the laminate with a consequent decrease in the perforation threshold. It is also necessary to highlight that the premature failure due to the missed exploitation of basalt fibers strength does not allow to take full advantage of matrix plasticization that is one of the main dissipation mechanisms in PP laminates determining a sharper decrease in the perforation threshold of this type of composite. All these statements are corroborated by the analysis of skins damage at perforation shown in Figure 165. If in puncture impact conditions PP and PPC skins displayed a clear hole left by the impactor, this is not true in CAI conditions where only a small fissure can be detected together with a long crack that expands transversally to flax fibers. This crack proves the overloading experienced by flax fibers and allows the impactor perforating the sample avoiding the more resistant basalt fibers. Despite the stronger decrease in perforation energy experienced by PP skins, they still prove to be better than PPC ones for impact purposes confirming the detrimental effect of the coupling agent on composite energy dissipation.
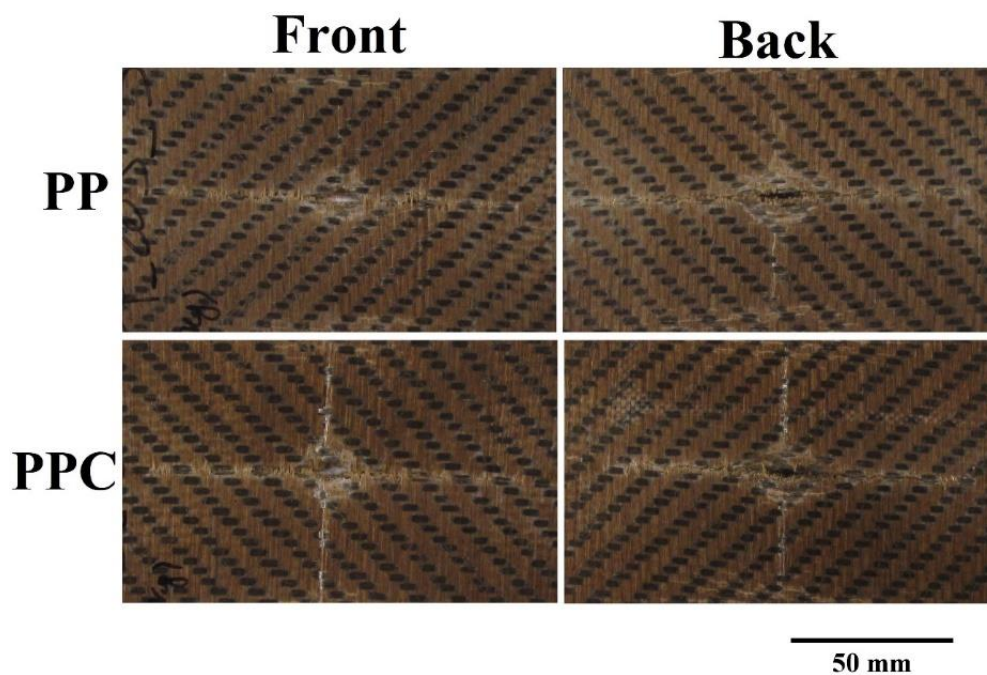
Figure 165: PP and PPC skins front and back damage at perforation

Once identified the perforation energy, each skin was tested at 25 %, 50 %, 75 % and 100 % of this value and the resulting curves and the correlated results are shown in Figures 166 and 167, respectively. As a general analysis, PP and PPC skins display similar impact response curves that underline a perfect elastic behavior of the laminates when impacted at 25 % and 50 % of perforation energy and an elastic response of the samples impacted at 75 % of perforation energy after experiencing a significant drop in the maximum force. The shape of the response curves is strictly correlated to laminates damage mode as can be inferred from observing PP and PPC front and back damages as a function of impact energy shown in Figure 168. For every impact energy, the formation of a crack transversal to the overloaded flax fibers is the main damage mechanism for both skin types and hence the main energy dissipation process. In consideration of this, the higher the impact energy the higher crack extension that becomes maximum at 75 % of perforation energy when it reaches the edges of the CAI support. The approach of the crack to sample extremity explains the response curve at 75 % of perforation energy, in fact the crack propagates quickly causing the sharp drop in sample reaction force and when it stops at the constraint the elastic rebound occurs. Concerning the analysis of the impact parameters in Figure 167, an increase in maximum force, maximum displacement and percentage absorbed energy can be observed in both PP and PPC skins for increasing impact energies and this is reasonable considering that the higher the impact energy the higher the deformation imposed to the material and hence the reaction force that it exerts.
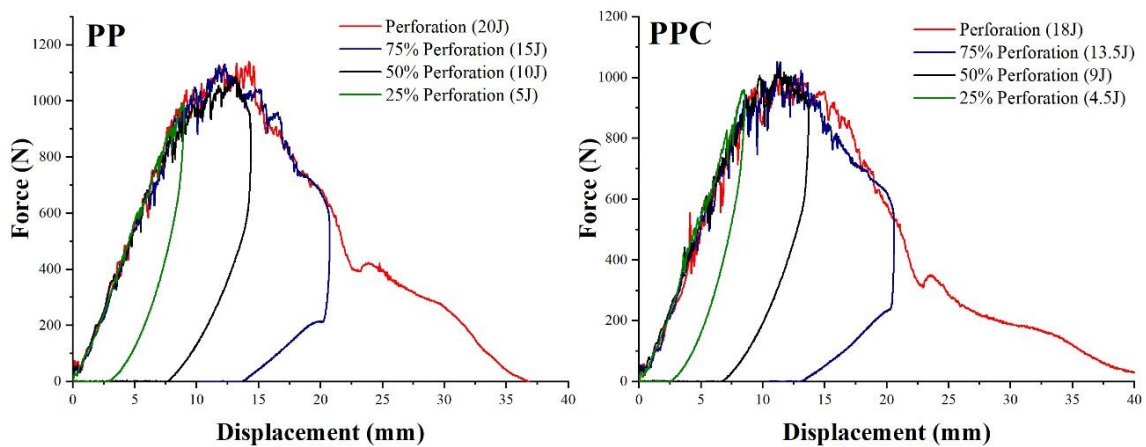
Figure 166: PP and PPC skins CAI impact response curves at 25 %, 50 %, 75 % and 100 % of perforation energy
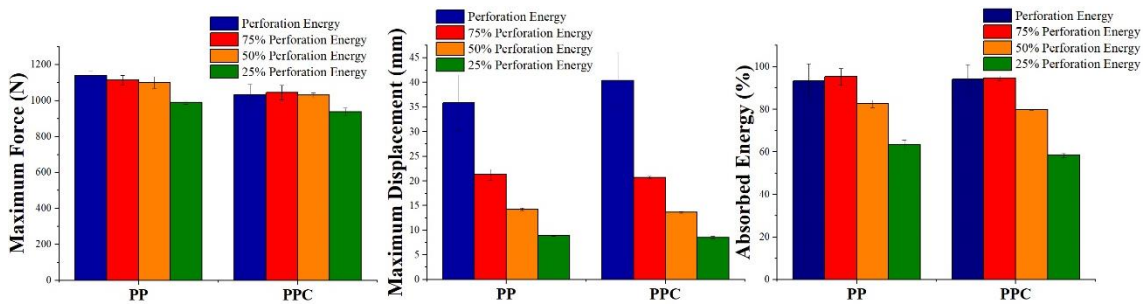
Figure 167: Maximum force, maximum displacement and absorbed energy of PP and PPC skins at 25 %, 50 %, 75 % and 100 % of perforation energy
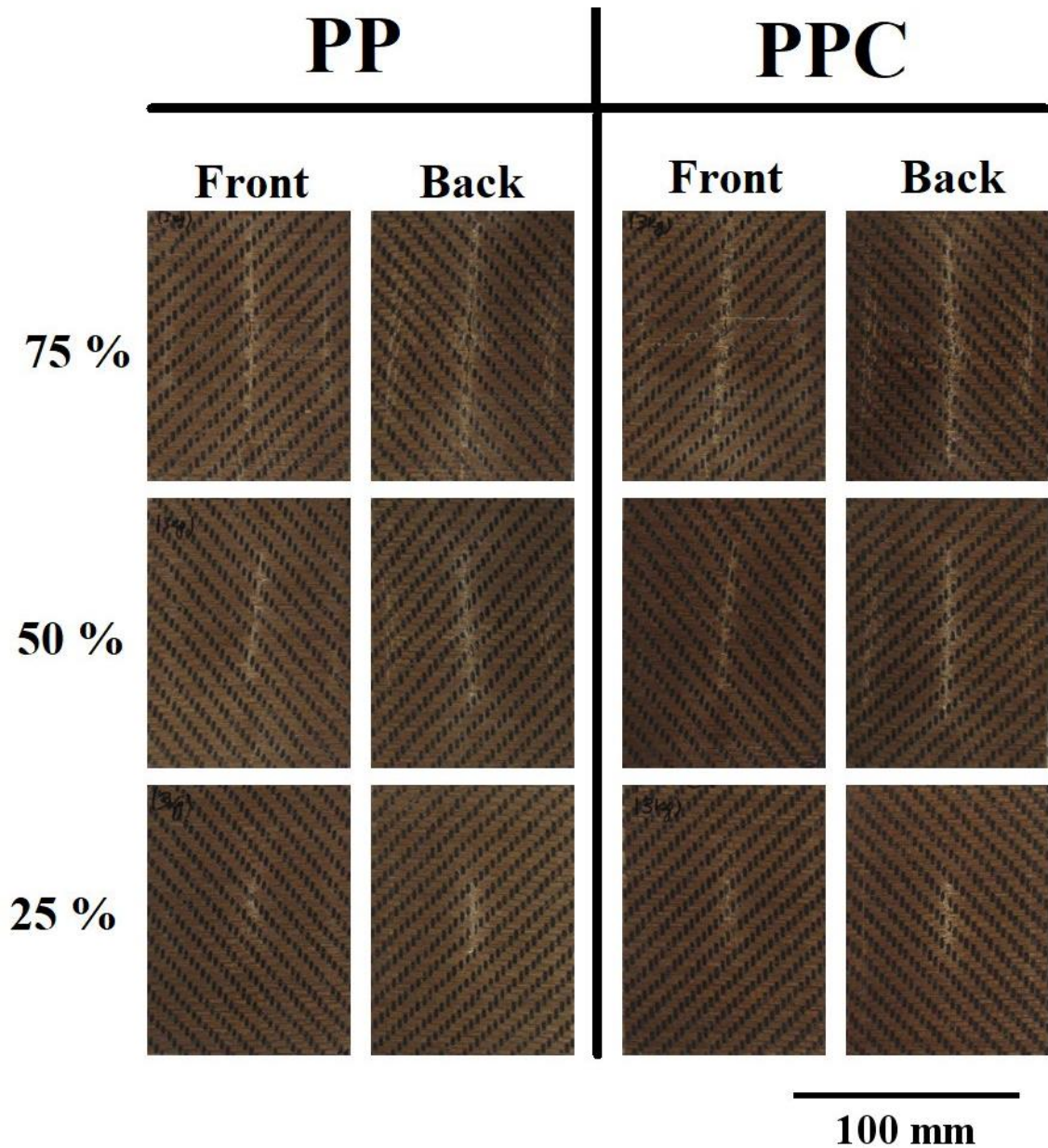
Figure 168: PP and PPC skins front and back damage at 75 %, 50 % and 25 % of perforation energy

In light of the results obtained at room temperature, it is possible to conclude that the role played by the coupling agent is less critical compared to what observed in puncture impact conditions due to the changes in laminates deformation mode. The situation is more complex and scattered when tests at -40 °C and 60 °C are considered. Table 34 summarizes PP and PPC perforation energy at -40 °C, room temperature and 60 °C. At -40 °C both PP and PPC skins show a decrease of 3 J in the perforation threshold and this can be explained considering the DSC data shown in section 4.1.1, where PP glass transition temperature was detected at around -12.5 °C. At this operating temperature the laminates are working in the glassy state displaying a brittle response to the impact. In these conditions, the differences that arise between PP and PPC skins are small because they are not due to matrix plasticization, but must be ascribed to the possibility of fibers to slip freely into the matrix, thanks to the weaker interface, thus dissipating a slightly higher energy through friction and rearrangement. At 60 °C both PP and PPC skins display an increase

in their perforation energy thanks to the exceeding of flax glass transition temperature as shown in section 4.1.1 and to the fact that the matrix is working well far from its glass transition temperature being able to fully exploit plasticization phenomena. This statement is further confirmed by the observation of the response curves at 25 % of perforation energy shown in Figure 169 that display a strong reduction in laminates stiffness. The complete activation of plasticization phenomena makes evident the strong differences between PP and PPC skins, in fact the good fiber-matrix interface achieved in compatibilized composites keeps unchanged laminates deformation mode implying a continuous overload of flax fibers. Instead, the poor fiber-matrix interface in PP composite allows to spread the load over a wider area of the composite making more significant basalt fibers contribution as can be inferred also by the observation of skins damage progression reported in Figure 170. More information about skins CAI impact response as a function of operating temperature can be obtained analyzing PP and PPC maximum force, maximum displacement and percentage absorbed energy data summarized in Figures 170 and 171, respectively. The first outcome that can be pointed out is that for both PP and PPC skins, tests performed at 60 °C are characterized by the higher maximum displacement and the highest percentage absorbed energy and this is due to the strong ductility acquired by the matrix that can undergo large deformations thus consuming a highest amount of energy especially for neat PP skins. The latter are also characterized by a common trend in maximum force and maximum displacement: in fact, room temperature samples are characterized by the highest maximum force and the lowest maximum displacement whereas samples tested at -40 °C are characterized by the lower maximum force. The difference in the maximum displacement between room temperature and -40 °C can be explained considering that at room temperature the matrix has moved to its viscoelastic state and the material needs to deform less to dissipate the impact energy considering that the perforation thresholds are close.

Table 34: Comparison of the perforation energies of PP and PPC skins as a function of operating temperature

Core	Perforation Energy at -40 °C (J)	Perforation Energy at Room Temperature (J)	Perforation Energy at 60 °C (J)
PP	17	20	40
PPC	15	18	20
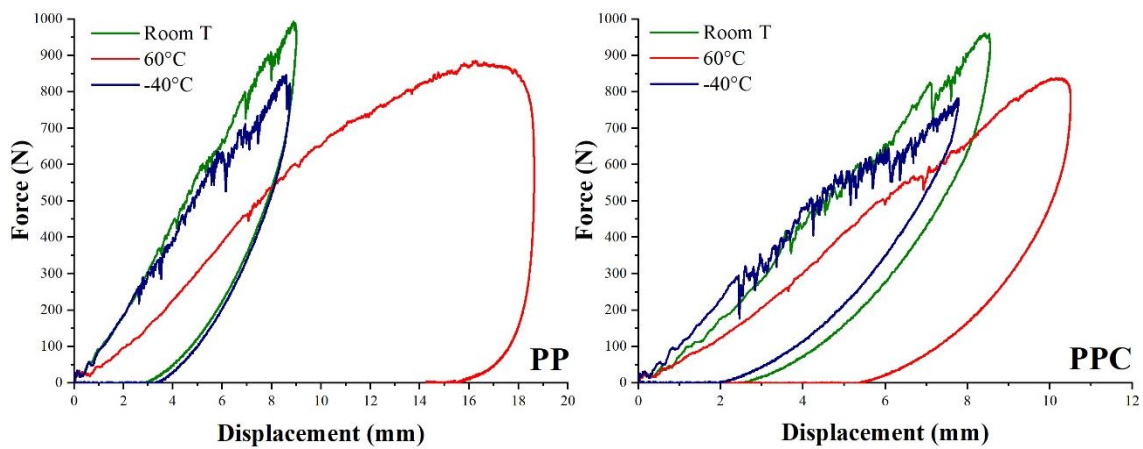
Figure 169: PP and PPC CAI impact response curves at 25 % of perforation energy as a function of operating temperature

Concerning the highest maximum force, it must be considered that it is reached in correspondence of the occurrence of the bending cracks on the bottom face of the laminate that appears earlier in -40 °C samples being more brittle. Moving from room temperature to 60 °C, there is a decrease in the maximum force due to the further softening of the matrix. Different is the situation for PPC skins where the increase in operating temperature plays a role similar to the one observed in PP skins, but where the good fiber-matrix interface makes the laminate behave in a brittle way even at 60 °C as can be inferred from the curves in Figure 169. That is the reason why for PPC skins maximum displacement increases moving from -40 °C to room temperature because even in the latter condition the material still behaves in a brittle way.
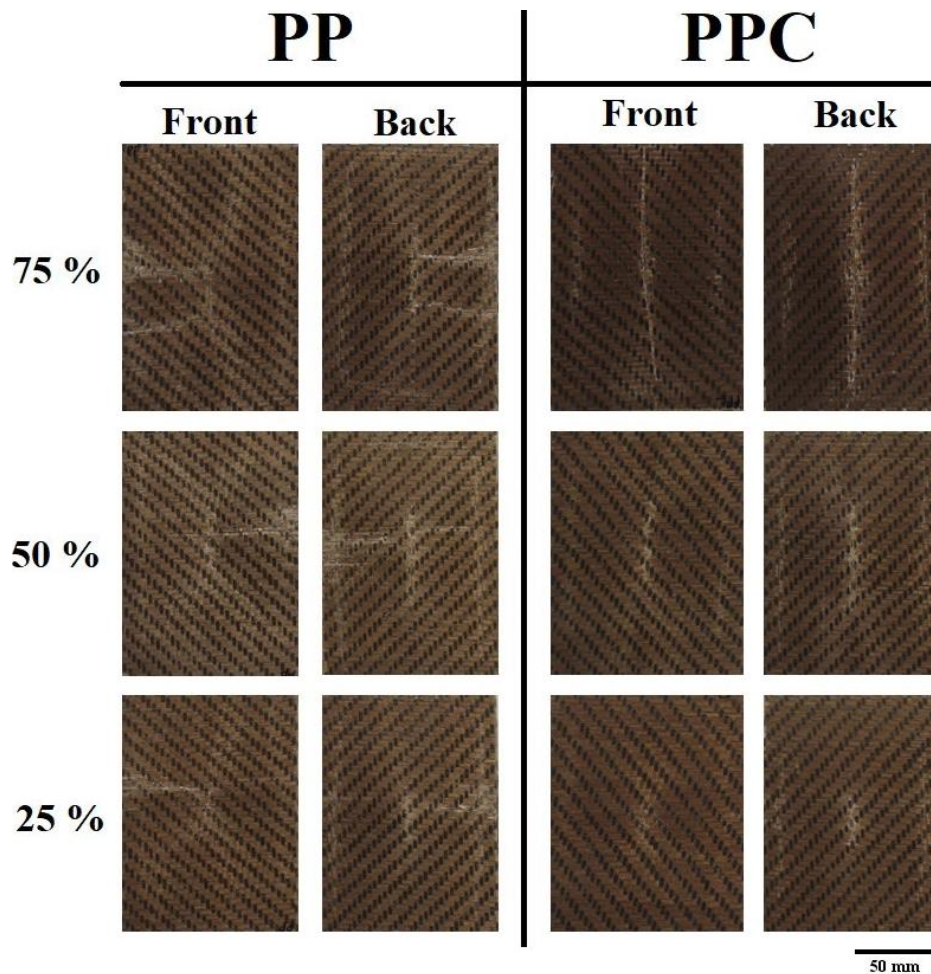
Figure 170: PP and PPC skins front and back damage at 75 %, 50 % and 25 % of perforation energy at 60 °C
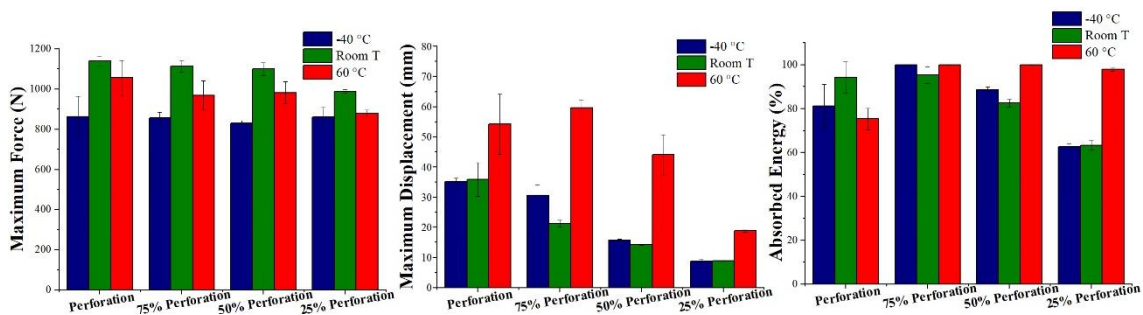
Figure 171: Maximum force, displacement and absorbed energy of PP skins at 25 %, 50 %, 75 % and 100 % of perforation energy as a function of testing temperature

175
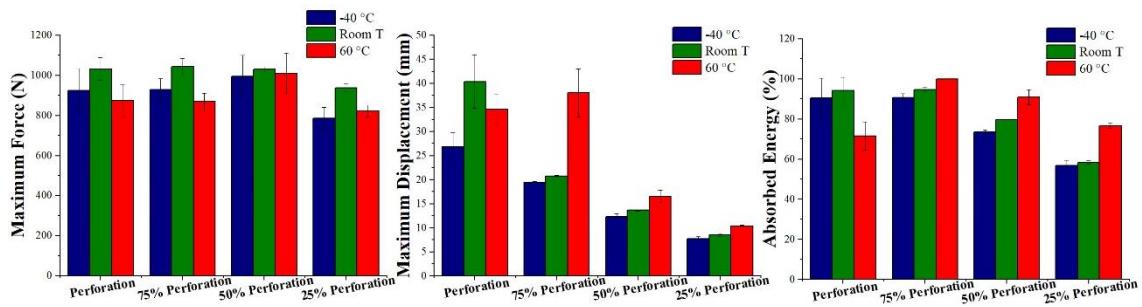
Figure 172: Maximum force, displacement and absorbed energy of PPC skins at 25 %, 50 %, 75 % and 100 % of perforation energy as a function of testing temperature

4.2.3 Ballistic impact test

The evolution of the projectile residual velocity as a function of impact velocity was investigated through ballistic impact tests as shown in the curves in Figure 173 for both PP and PPC skins. The application of Lambert-Jonas interpolation to the data set allowed to evaluate laminates ballistic limit that turned out to be equal to 101.16 m/s for PP and to 100.34 m/s for PPC. Contrary to what observed in low velocity impacts, no significant differences can be observed between neat and compatibilized skins. The extremely low reaction time given to the composite, i.e. microseconds, entails a strong localization of the impact and hence of the sample area involved in the process. This means that the improvement in fiber-matrix interface provided by the coupling agent does not play a significant role contrary to low velocity impact where the reaction time is in the order of the milliseconds and allows the sample to deform and react globally to the impact. This is confirmed by the observation of the damage mode of the two skin types shown in Figure 174. The front side is characterized by a clear circular hole that allows to identify the projectile entrance point whereas the back side displays a crack due to the breakage of the less resistant flax fibers. For both PP and PPC composites, basalt fibers did not undergo fracture and were simply pulled out from the matrix to leave the projectile the possibility to slip between them. It appears evident that basalt fibers breakage would have been more energy consuming for the projectile that found in their pull out a preferential path.
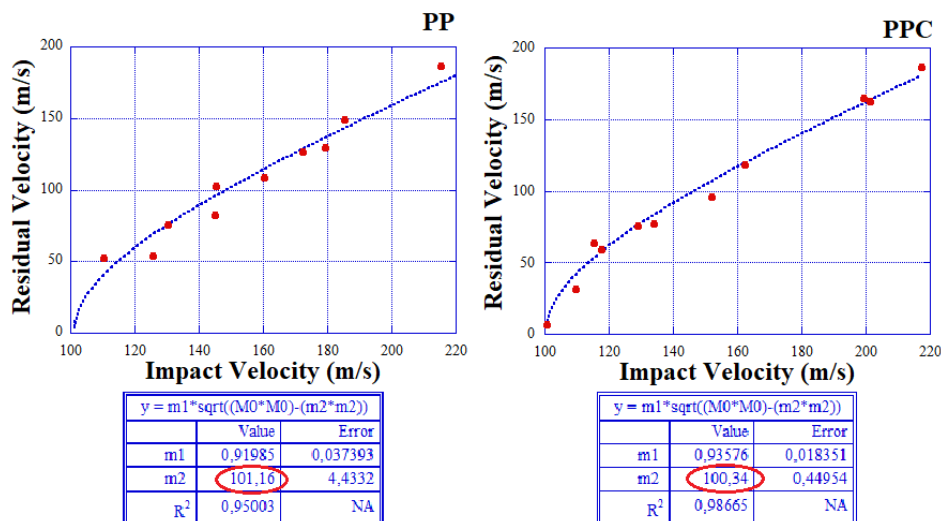
Figure 173: PP and PPC experimental data and interpolation curves obtained implementing the Lambert-Jonas equation in the software Kaleida graph
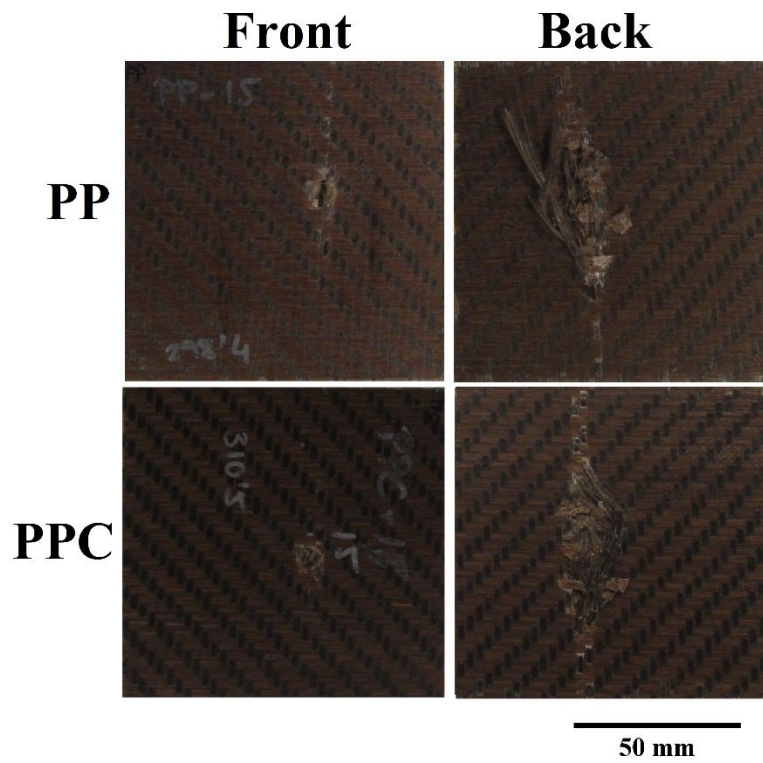
Figure 174: Front and back damage suffered by PP and PPC samples when subjected to ballistic impact at 290 and 300 m/s, respectively.

Chapter 5: Sandwich Characterization

5.1 Quasi-Static Characterization

5.1.1 Bending tests

All the bio-based and petroleum-based cores under study were employed to produce sandwich samples to be tested in bending in order to evaluate the effect of core type, core density and skin type on their overall quasi-static performance. Sandwich structures bending tests results are shown in Figure 175 that summarizes the resulting flexural modulus and strength values. The first outcomes that can be pointed out are the superior flexural properties of PVC foam structures compared to agglomerated cork ones both as flexural modulus and as maximum strength. Not only PVC foams allow to obtain better flexural properties than the agglomerated cork with the corresponding density, but all PVC foams allow to obtain better performances than all agglomerated corks displaying a much stiffer behavior. Only NL25 sandwich composites approach the flexural properties achievable with HP130 ones, especially when maximum strength is considered. Another important finding connected with core type is the evolution of flexural properties as a function of core density. In PVC foam sandwiches flexural modulus and strength tend to increase linearly with core density (R^2=0.986 and R^2=0.976, respectively) whereas in agglomerated cork sandwiches the increase in flexural properties is characterized by a parabolic trend (R^2=1). This means that moving from NL10 to NL20 the improvement is much less significant than the one achievable with NL25.
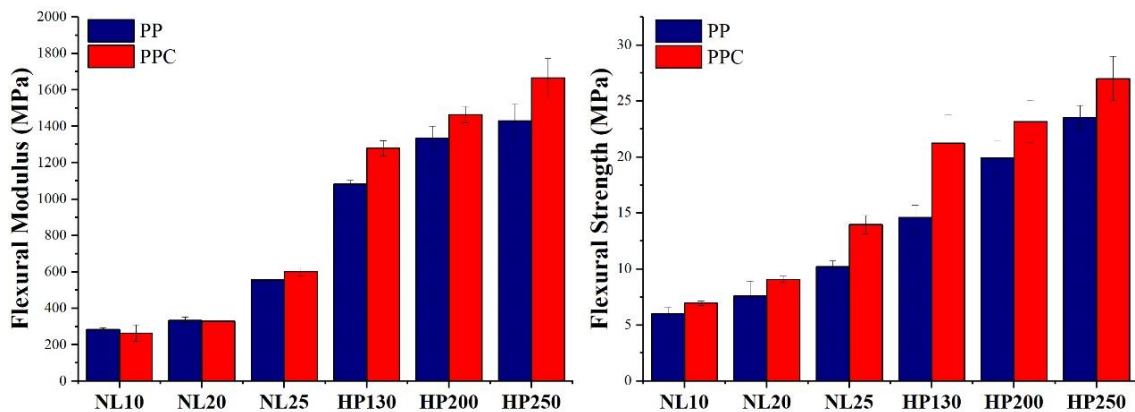
Figure 175: Flexural modulus and strength of all sandwich configurations with both PP and PPC skins

Moving to the analysis of skin type effect, it is possible to notice that the results obtained agree perfectly with the ones presented in section 4.1.3 for the sole skin where an increase in both flexural modulus and strength can be observed in all compatibilized composites thanks to the enhanced fiber-matrix interface. In light of the results obtained with sandwiches bending tests and the results obtained with cores in quasi-static and dynamic characterizations only three cores were selected for the dynamic characterization of the sandwiches, i.e. NL10, NL25 and HP130. HP130 is the only synthetic foam which can be compared with agglomerated corks considering that

HP200 and HP250 are much more performing. Concerning the natural cores, NL25 was selected being the more performing agglomerated cork and being the only one that can be usefully compared with HP130, whereas NL10 was selected in order to have a direct comparison of structures with the same core density.

5.2 Dynamic Characterization

5.2.1 Puncture Impact tests

Puncture impact tests were carried out on PP and PPC sandwich composites with NL25 and HP130 as core materials to evaluate the effect of coupling agent and core type on the impact response of the overall structure. The resulting impact curves are reported as a function of impact energy in Figure 176 for NL25 composites and in Figure 177 for HP130 ones. Regardless of core and skin type, all sandwich structures are characterized by the same evolution in impact curves shape when impact energy increases. At low impact energies, i.e. 20 J - 30 J for PP structures and 20 J for PPC structures, the curves display the typical shape that characterizes an impact with elastic rebound because the impactor interacts only with the upper skin of the structure. Moving to medium impact energies, i.e. 40 J for PP and 30 J for PPC based sandwich, the impactor penetrates into the structure and the first peak obtained as a consequence of impactor-skin interaction is followed by a plateau region originated by the interaction of the impactor with the core. This region is characterized by a lower reaction force due to the lower mechanical properties of the cores respect to skins. Finally, for higher impact energies, i.e. 60 J - 80 J for PP and 40-60 J for PPC, a second peak force follows the plateau region as a consequence of core total perforation and impactor interaction with the second skin. Another conclusion can be drawn looking at impact curves, in fact PP structures produced with both core types are characterized by a perforation energy of 80 J that is significantly higher than PPC composites one that is 60 J. These results are in perfect agreement with the ones reported in skins puncture impact response in section 4.2.1. The lack of energy dissipation mechanisms, such as fibers slippage and rearrangement, matrix plasticization and fiber-matrix friction, due to fiber-matrix interface enhancement induces a deterioration of the impact response not only of the sole skins but also of the overall sandwich structure produced with them.
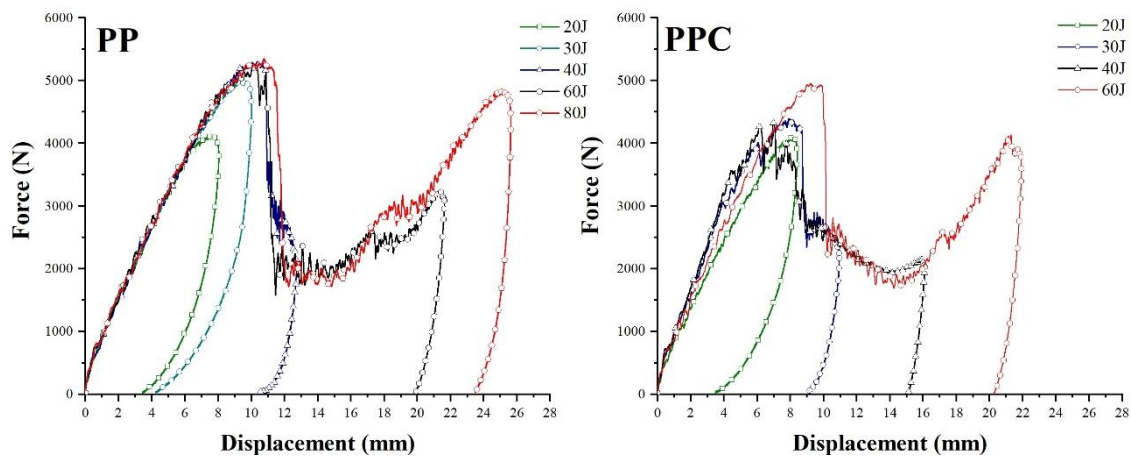
Figure 176: Impact curves of PP and PPC NL25 sandwiches at different impact energies
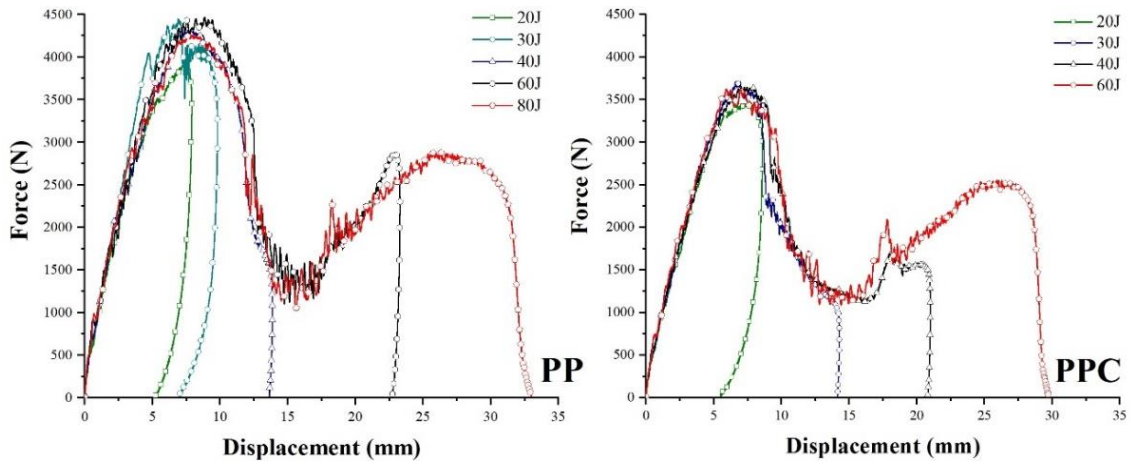
Figure 177: Impact curves of PP and PPC HP130 sandwiches at different impact energies

To go more into detail the maximum force, maximum displacement and percentage absorbed energy values of PP and PPC composites are summarized in Figures 178 and 179 for NL25 core and HP130 core, respectively. Regardless of the core employed, the three mentioned parameters display the same trend. PPC sandwich composites are always characterized by a lower maximum force than PP ones and this is due to PP skins lower stiffness. When the sole skins were investigated, PPC laminates displayed the higher maximum force thanks to the superior flexural properties that allowed to reach a higher reaction force being equal the maximum displacement. The situation is dramatically different in the case of sandwich composites where the skins are constrained to the core and are not able to bend freely. This leads to a high stress concentration in a restricted area with a consequent more severe penetration of the impactor.
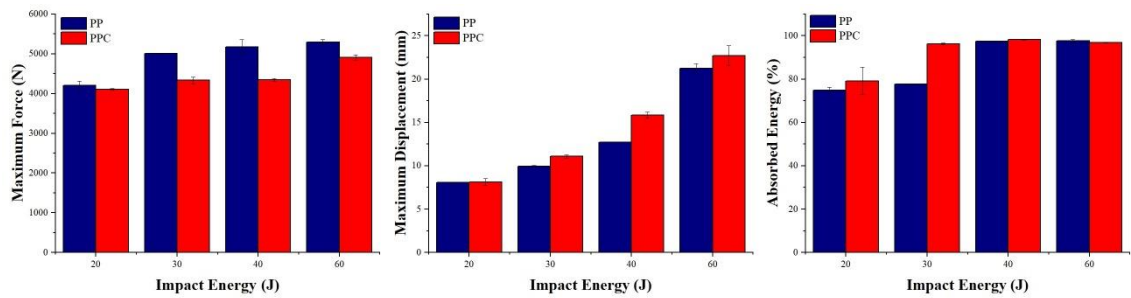
Figure 178: Maximum force, displacement and percentage absorbed energy of PP and PPC-NL25 sandwiches as a function of impact energy
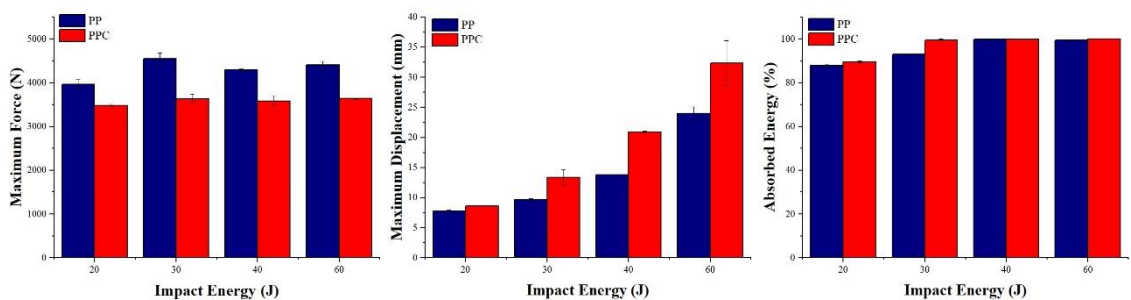
Figure 179: Maximum force, displacement and percentage absorbed energy of PP and PPC-HP130 sandwiches as a function of impact energy

180

Skin constraint is less severe for PP structures thanks to the lower flexural stiffness of the skins, as shown in sections 4.1.1 and 4.1.2, which ensures their easier deformation and hence the possibility to spread the impact load over a wider area thus increasing the volume of core that acts as a support and leading to a higher maximum reaction force. Maximum displacement and percentage absorbed energy are two other fundamental parameters and are strongly interconnected. PP and PPC structures are always characterized by comparable absorbing capabilities but PPC skins experience a higher maximum displacement to reach the same absorption performances. Indeed, thanks to the higher number of energy dissipation mechanisms, PP structures need to withstand a lower deformation to dissipate the same amount of energy of PPC ones. The only significant difference in the absorbing behavior of PP and PPC sandwich structures can be detected at 30 J where PP composites display a lower energy absorption capability than PPC. This discrepancy can be easily explained observing the impact curves previously introduced in Figures 176 and 177: in fact, if PPC composites have already experienced penetration by the impactor and hence core damage, which allows to dissipate a conspicuous amount of energy, PP composites are still working in the elastic rebound regime. In addition to coupling agent effect also core type effect on sandwich impact response was addressed and in Figures 180 and 181 are summarized NL25 and HP130 maximum force, displacement and percentage absorbed energy for PP and PPC skins, respectively. Regardless of the impact energy employed, both NL25 and HP130 sandwich composites reach the maximum value of force as a result of the interaction of the impactor with the upper skin of the structure and NL25 composites are always characterized by a higher maximum force than HP130 ones. This latter outcome can be explained considering the differences in core material density, but also the typical three-steps curve that characterizes cellular core compressive behavior and focusing on the densification region where opposite cell walls start to touch each other determining significant increase in material reaction force for little increase in the applied deformation.
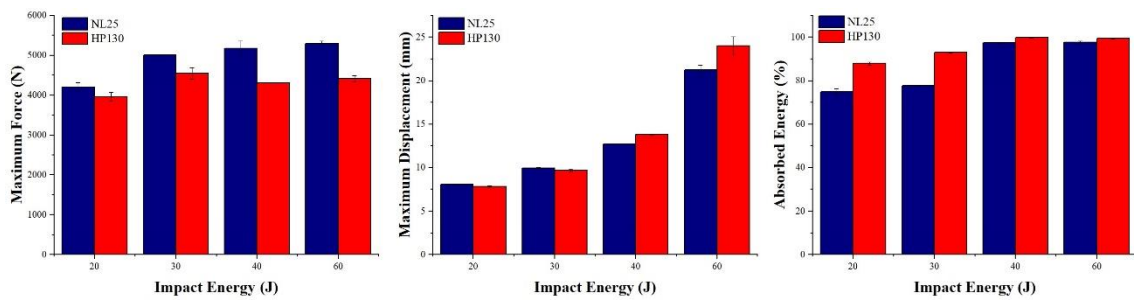
Figure 180: Maximum force, displacement and percentage absorbed energy of PP-NL25 and HP130 sandwiches as a function of impact energy
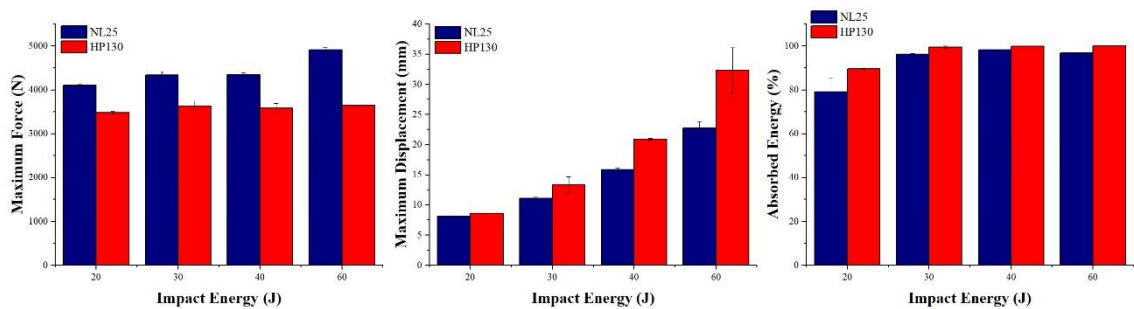
Figure 181: Maximum force, displacement and percentage absorbed energy of PPC-NL25 and HP130 sandwiches as a function of impact energy

181

Considering that at the lower impact energies, i.e. 20 J -30 J for PP composites and 20 J for PPC composites, the only interaction of the structures with the impactor takes place through the upper skin and that both NL25 and HP130 panels show comparable displacements, it is possible to conclude that a denser material approaches earlier the densification region being equal the displacement, thus providing a stiffer support to the upper skin. Concerning the energy absorption performances, HP130 structures display a higher energy absorption capability than NL25 at the lower impact energies, i.e. 20 J -30 J for PP composites and 20 J for PPC composites, and this can be ascribed to the different energy absorption mechanisms exploited by the two core types. Even if the bio-based and the synthetic cellular materials experience almost the same displacement, agglomerated cork absorbs energy mainly in a viscoelastic way whereas the polymeric foam undergoes permanent indentation and damage. At higher impact energies, the absorbing capacities of the two structures become comparable and range between 96 % and 100 %. This change is due to the penetration of the impactor in the cores that dissipate all impact energy through cell walls bending and collapse and intergranular fracture in the case of agglomerated cork and cell wall crushing in the case of the PVC foam. In these conditions the maximum displacement suffered by HP130 structures is higher than NL25 ones because of the more brittle nature of the PVC foam and hence of the higher difficulties in energy dissipation. All the conclusions drawn are supported by the results obtained through the post impact analysis which are shown in Figures 182 and 183. In particular, Figure 182 displays the cross section of the impacted area as a function of impact energy for all composite types to evaluate the damage extension in the inner parts of the panels and Figure 183 reports the permanent indentation depth measured through profilometry. This analysis technique was employed only on samples impacted at 30 J or lower because of the laser scanning limits that do not allow to detect deeper indentation. Concerning coupling agent effect, PPC structures display a higher damage extension and a higher permanent indentation with respect to the corresponding PP composites, thus proving that fiber-matrix interface enhancement is advantageous for structure quasi-static performances but plays a detrimental role in the impact response hindering energy dissipation.
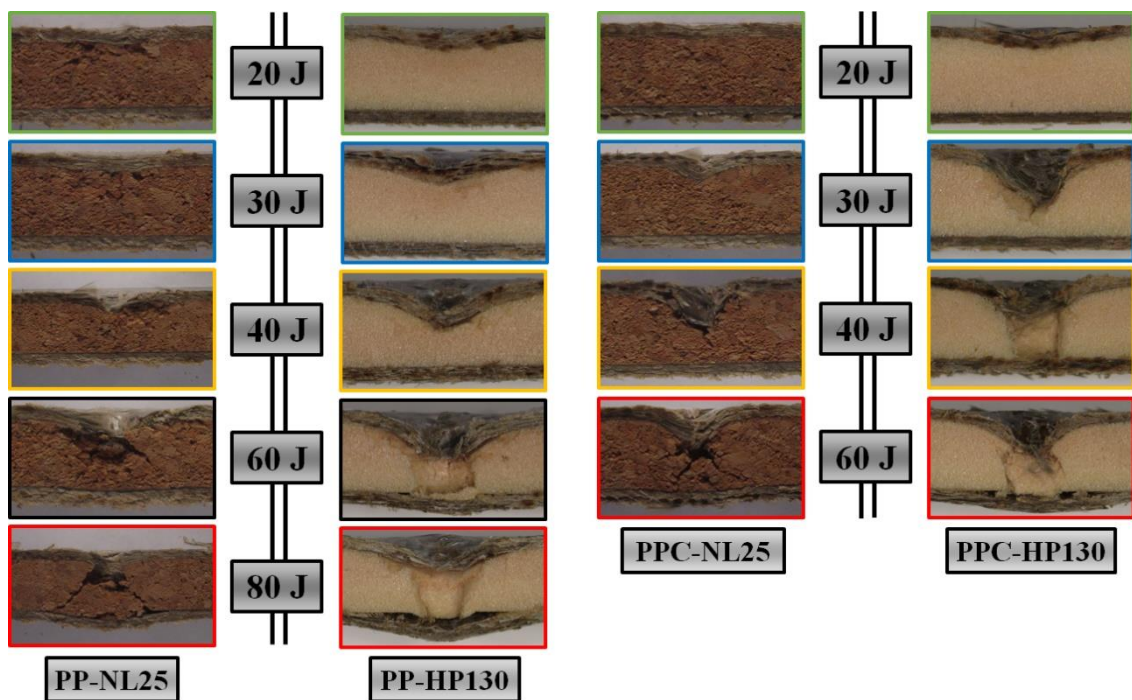
Figure 182: Samples damage progression as a function of sandwich type and impact energy
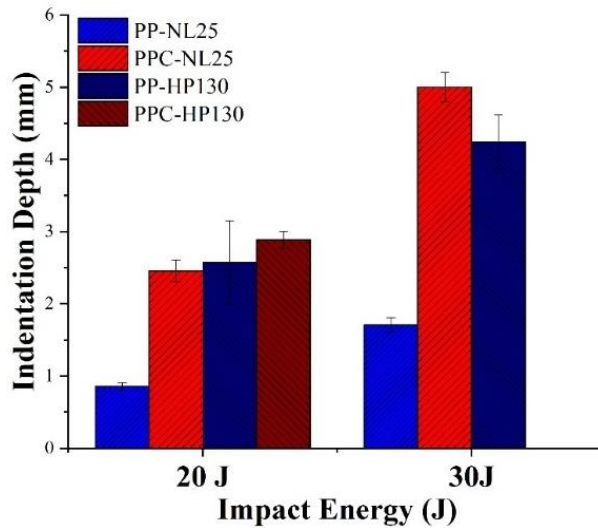
Figure 183: Permanent indentation depth of the four different types of sandwich structures at 20 and 30 J

Moving to core type effect on sandwich impact response, it is possible to observe and conclude that NL25-based structures are characterized by a lower damage extension and by a lower permanent indentation than HP130 ones, meaning that NL25 is able to provide a better damage tolerance to the structure. When tested as sole core, NL25 is characterized by a lower perforation energy than HP130 due to the premature intergranular fracture that leads to material plug detachment. Indeed, when integrated in the structure and embedded between the two skins, this detachment is prevented and cork damping and absorbing capacities can be fully exploited.

5.2.2 Impact tests with CAI support

As already seen for core materials and skin laminates, the CAI perforation thresholds of each sandwich structure configuration were identified and are compared with the ones obtained in puncture impact conditions in Table 35. The first point to underline is that the negative effect played by CAI support on skins impact response due to the excessive bending that induces an overload on flax fibers is cancelled when the skins are combined with the core to obtain the overall structure. The constraint created by the core and the increase in flexural stiffness due to the sandwich configuration allow to obtain a perforation energy equal, in the case of HP130 panels, or superior, in the case of NL25 panels, to puncture impact one. The difference that arises in the perforation threshold of HP130 and NL25 structures can be ascribed to the different flexural stiffness of the two sandwiches. The bending test results presented in section 5.1.1 revealed that HP130 structures are characterized by a flexural modulus two times higher than NL25 ones and this means that the impactor struggles to deform the sample thus leading to a concentration of the impact load in the impacted area as happens in puncture impact conditions. As already observed in puncture tests, when tested as sole cores NL10 and NL25 agglomerated corks are characterized by a perforation energy in CAI support condition much lower than HP130 one due to the poor interface between cork granules that prevent the exploitation of cork absorbing capabilities. Even in this case, when integrated in the overall structure, both NL10 and NL25 display much more compelling performances and, in particular, NL25 structures are characterized by a perforation threshold 20 J higher than HP130 ones for both PP and PPC skins and NL10 a perforation energy

of 5 J higher than HP130 one for PPC skins. These results are promising in view of the achievement of performing eco-friendly sandwiches for applications where impact resistance is one of the key design parameters.

Table 35: Comparison of the perforation energies of the six sandwich configurations in CAI and puncture impact conditions

Sandwich Composite	CAI Perforation Energy (J)	Puncture Perforation Energy (J)
PP_NL10	65	-
PPC_NL10	65	-
PP_NL25	100	80
PPC_NL25	80	60
PP_HP130	80	80
PPC_HP130	60	60

Another outcome that confirms the results previously obtained is the higher perforation threshold achievable with neat PP skins with respect to compatibilized ones. Figures 184, 185 and 186 show the impact response curves as a function of impact energy for NL10, NL25 and HP130 sandwich structures, respectively, whereas Figure 187 summarizes the maximum force, maximum displacement and percentage absorbed energy values. As already acknowledged in puncture impact tests, all sandwich composites are characterized by the same evolution in impact curves shape for increasing impact energies regardless of core and skin type. At 25 % of perforation energy, all structures display the typical curve of an elastic rebound that discloses the interaction of the impactor with the sole upper skin. Moving to 50 % of perforation energy, the interaction of the impactor with the core due to penetration and in PP-HP130 case the initial reaction force exerted by the second skin can be detected in the graphs. The only exception is observed for PP-NL10 sandwich composites that are still working in the elastic regime. This is reasonable considering that PP and PPC NL 10 structures are characterized by the same perforation threshold, but PP skins allow a better energy dissipation delaying impactor penetration. Finally, at 75 % of perforation energy, all sandwich impact curves display the second peak force due to the direct interaction or the indirect loading of the back skin of the structure.
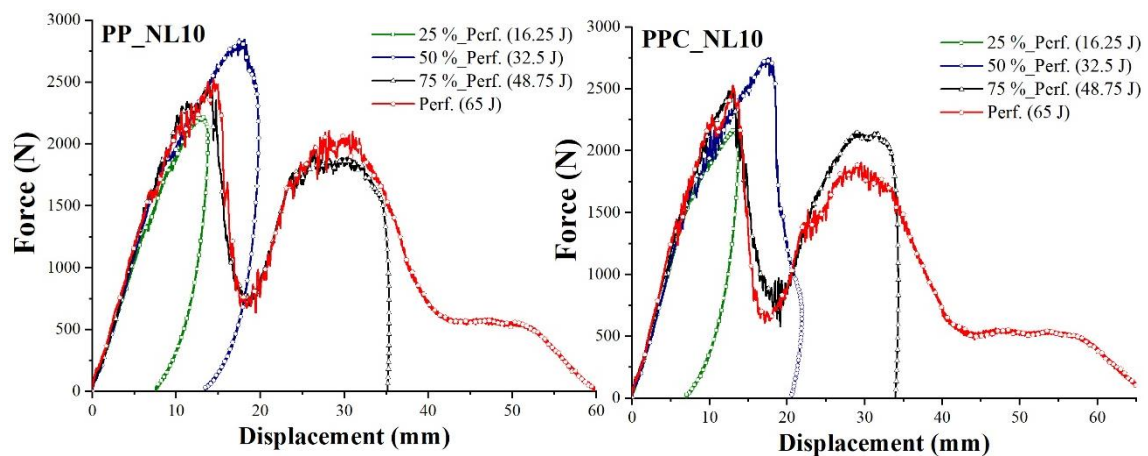
Figure 184: PP and PPC NL10 cored sandwich structures impact response curves as a function of impact energy
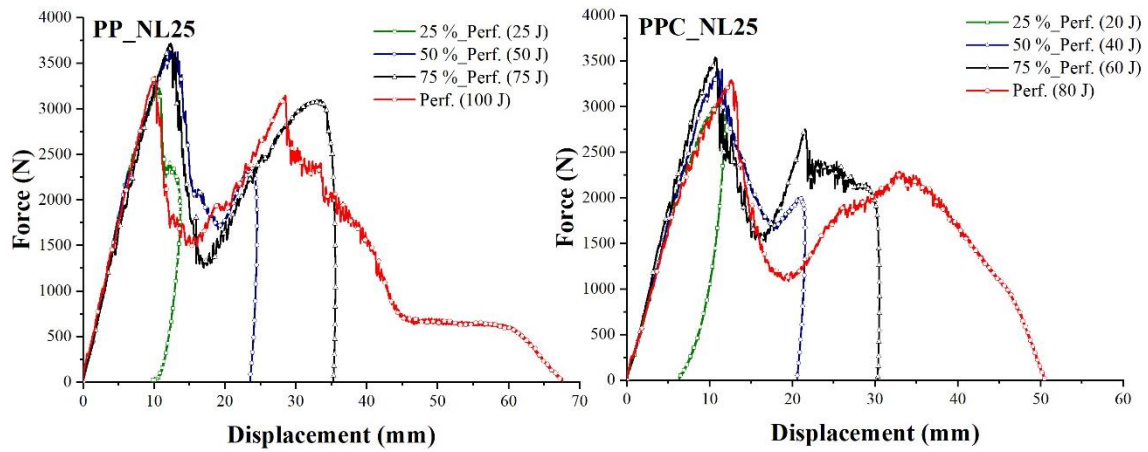
Figure 185: PP and PPC NL25 cored sandwich structures impact response curves as a function of impact energy
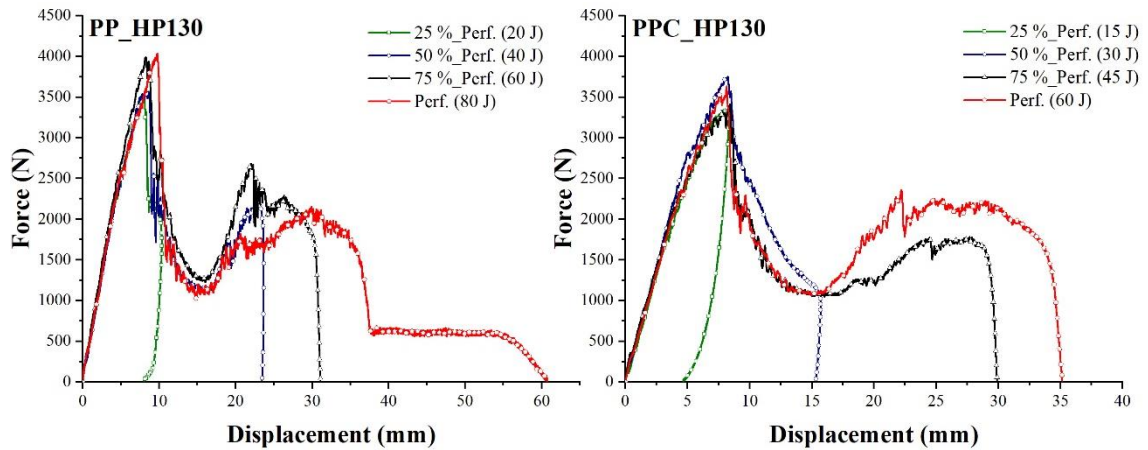
Figure 186: PP and PPC HP130 cored sandwich structures impact response curves as a function of impact energy

Moving to the analysis of the single impact parameters, a general increase in maximum force, maximum displacement and percentage absorbed energy can be observed for increasing impact energies in all sandwich configurations. All structures reach the maximum value of force at the first peak and hence as a consequence of the interaction of the impactor with the upper skin of the structure. These results agree with the ones observed in puncture impact tests, but contrary to the latter, in CAI support conditions the highest maximum force is reached by HP130 structures and not by NL25 ones being equal the skin type. This can be explained considering that in puncture impact conditions composite deformation is hindered, thus leading to a localization of the impact load and allowing a denser material to approach earlier the densification region providing a stiffer support to the upper skin. This is not true in CAI support impacts where a certain bending of the sample is allowed and hence the stiffer the structure the higher the reaction force exerted. This hypothesis is corroborated by looking at 25 % of perforation energy impacts, which are completely elastic as previously illustrated, and considering together maximum force and maximum displacement. HP130 structures are characterized by the lowest maximum displacement and the highest maximum force due to the stiffer nature already observed in section 5.1.1. It is useful to underline that all sandwich structures display comparable energy absorption capabilities for 50 %, 75 % and 100 % perforation energy impacts with a percentage absorbed

energy that ranges between 98 % and 100 %. This is due to the interaction of the impactor with the core materials that is the damping component of the structure. Thanks to sample damage progressions as a function of impact energy shown in Figures 188, 189 and 190 for NL10, NL25 and HP130, respectively, it is possible to carry out a post-impact analysis of the samples taking also advantage of the results obtained by the profilometric analysis and reported in Figure 191. The first thing that can be pointed out, and is actually true also for puncture tests, is the different damage mode that characterizes the different inner core materials and that is comparable to the one observed for the sole cores in ballistic impacts. In particular both NL10 and NL25 agglomerated corks show a conical crack due to the damage propagation through the polymeric binder, but contrary to what happens for the sole core, no plug detachment occurs thanks to the second skin that holds the piece that can experience compression and energy dissipation. Instead, HP130 PVC foam displays a more localized damage like the plugging mode observed in the sole core ballistic impacts.
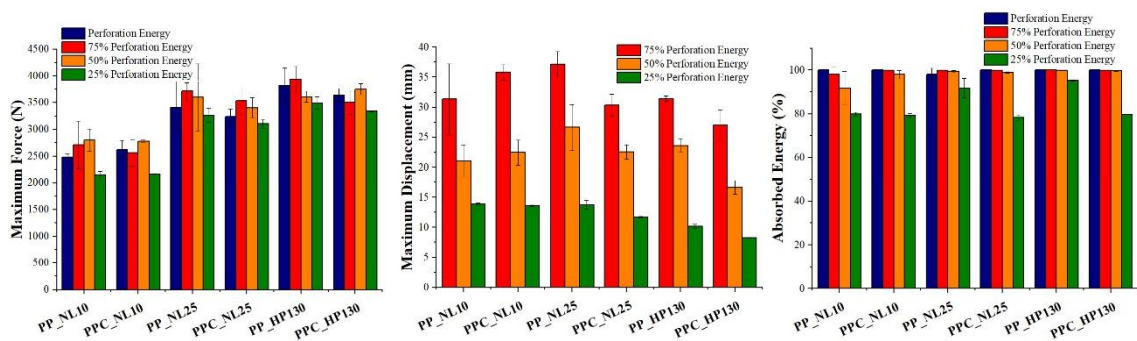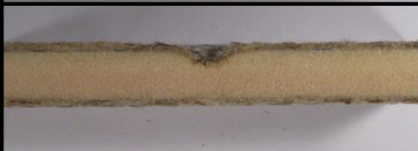
Figure 187: Maximum force, displacement and absorbed energy of all six sandwich structure configurations at 25 %, 50 %, 75 % and 100 % of perforation energy
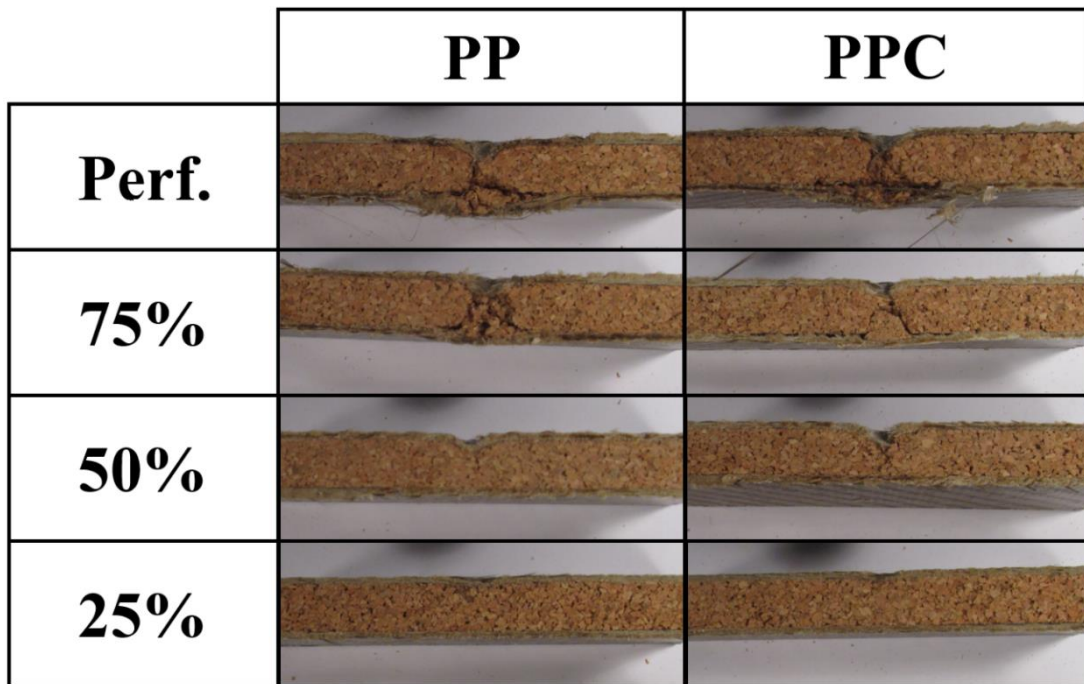
Figure 188: Damage progression in PP and PPC NL10 sandwich structures as a function of impact energy

Figure 189: Damage progression in PP and PPC NL25 sandwich structures as a function of impact energy

Figure 190: Damage progression in PP and PPC HP130 sandwich structures as a function of impact energy

As a general comment, it is possible to observe that PVC foam structures display a much more pronounced permanent indentation with respect to agglomerated cork ones at 50 % and 75 % of perforation energy and this means that they will likely suffer a higher reduction in the residual

flexural properties. This concentration of the damage and hence the higher permanent indentation can be mainly ascribed to the stiffer nature of the structures that causes a concentration of the impact load in a limited area as observed in puncture impacts. This suggests that agglomerated cork core structures are characterized by a higher damage tolerance especially if it is considered that PPC-HP130 and PP- and PPC-NL10 sandwiches were impacted at similar impact energies and that PP-HP130 and PPC-NL25 composites were impacted at the same impact energies. From the permanent indentation data in Figure 191 is also interesting to notice how at 25 % of perforation energy PP sandwiches are always characterized by a higher permanent indentation than the corresponding PPC ones. This is due to the fact that all structures are still working in the elastic regime and the permanent indentation suffered by the structure depends on the stiffness of the upper skin, that is higher for PPC skins, and by the higher impact energy applied to PP structures. The situation changes at 50 % of perforation energy where the penetration of the impactor due to the collapse of the upper skin occurs. Considering the higher energy dissipation capability of the neat PP skins thanks to matrix plasticization, a lower penetration of the impactor in the core is needed.
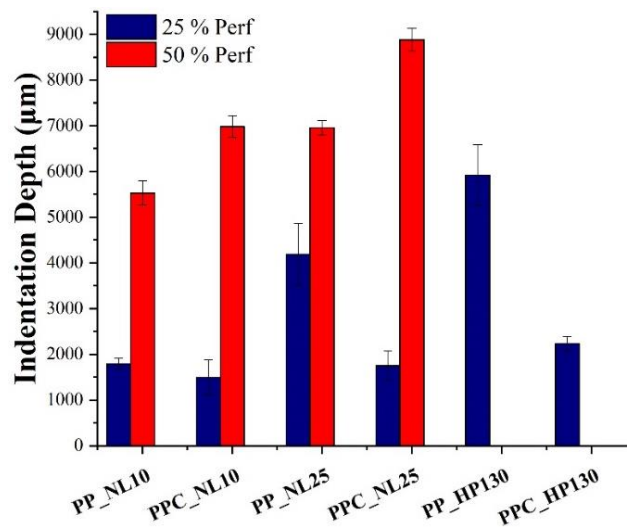
Figure 191: Permanent indentation depth of the six sandwich configurations at 25 % and 50 % of perforation threshold

Moving to the impact tests carried out at low and high temperatures, it is necessary to highlight that, if for samples tested at -40 °C it was possible to identify the perforation energy and to test the samples at 75 %, 50 % and 25 % of this value, this was not possible for samples tested at 60 °C. Indeed, the higher operating temperature led to a significant increase of the perforation threshold of agglomerated cork PP sandwiches which could not be perforated even increasing the impactor mass from 12.055 kg to 17.055 kg to reach impact energies of 170 J and 180 J, as shown in Figure 192. The strong plasticization of the matrix and the poor fiber-matrix interface allow to spread the impact load over a wider area involving a significant bending of the sample and preventing perforation. In light of the inability of reaching the perforation threshold of these composites and in order to work with the same impactor mass employed at room temperature and at -40 °C, all six sandwich configurations were tested at 130 J and at 75 %, 50 % and 25 % of this value which is the highest achievable with this impactor mass and actually coincides with PPC NL10 and NL25 sandwiches perforation energy. In this way it was possible to obtain a direct comparison of samples impact response being equal the impact energy.
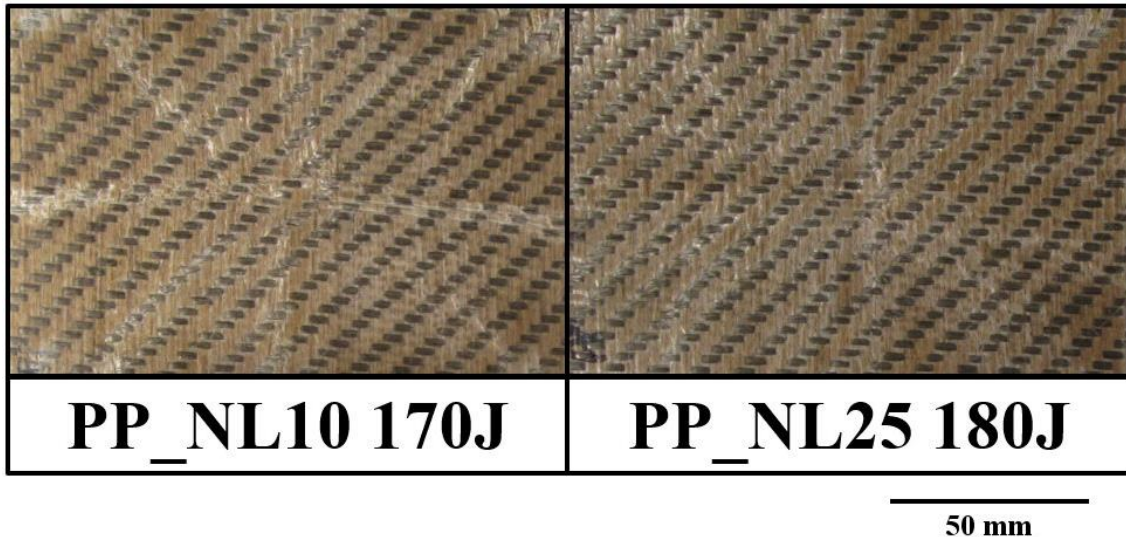
Figure 192: PP NL10 and NL25 samples tested at 170 J and 180 J with an overall mass of 17.055 kg.

Starting with the comparison of the results at room temperature and -40 °C, Table 36 summarizes the perforation energy values of the six types of sandwich composites as a function of operating temperature, Figure 193 displays the impact response curve at 75 % of perforation energy and Figures 194, 195 and 196 show the maximum force, maximum displacement and percentage absorbed energy values of NL10, HP130 and NL25 sandwich structures, respectively. All sandwich structures underwent a strong reduction in their perforation threshold moving from room temperature to -40 °C due to the embrittlement effect suffered especially by the skins which move from the viscoelastic to the glassy state and are not able to dissipate energy through plasticization anymore. This hypothesis is further confirmed noticing that PP sandwiches suffer a reduction of their perforation energy between 15 J and 40 J whereas PPC composites only between 10 J and 20 J. This is reasonable considering that the improved fiber-matrix interface of PPC composites tends to play itself an embrittlement effect and hence the effect of temperature on composites impact response appears more evident on PP skin composites that, by losing matrix plastic deformation contribution, start to act similarly to PPC ones. This is also proved by the fact that at -40 °C both PP and PPC composites are characterized by the same perforation energy. Concerning core type, it is possible to notice that NL10 is able to provide the same impact resistance of HP130 not only with PPC skins, as happens at room temperature, but also with PP skins, whereas NL25 still provides a higher impact resistance with a 10 J higher perforation energy. The more brittle behavior of -40 °C samples can be also inferred from the curves shown in Figure 193 and from the data in Figures 194, 195 and 196 which exhibit a higher maximum reaction force and a lower deformation of the composite. If for the sole skin laminates room temperature samples were characterized by a higher maximum force and by lower maximum displacement because the material was free to bend and PP laminates needed to deform less to dissipate the impact energy and were able to delay the occurrence of the bending cracks on the bottom face of the laminate providing a higher maximum force, the situation changes in the case of sandwich structures where the skins are constrained by the core. The higher maximum force is always reached at the perforation of the first skin, but in this case, it is not due to the premature occurrence of cracks on the bottom face of the laminate and the skin is able to exert completely its reaction force. The embrittlement effect played by the temperature can be also noticed from the increased stiffness of the samples confirmed by the higher slope of the impact response curve.

Table 36: Comparison of the perforation energies of the six sandwich configurations as a function of operating temperature

Sandwich Composite	CAI Perforation Energy at -40 °C (J)	CAI Perforation Energy at Room Temperature (J)
PP_NL10	50	65
PPC_NL10	50	65
PP_NL25	60	100
PPC_NL25	60	80
PP_HP130	50	80
PPC_HP130	50	60

Moving to the analysis of the percentage absorbed energy, it is necessary to introduce Figures 197, 198 and 199 which present the evolution of the damage at -40 °C and as a function of impact energy in NL10, NL25 and HP130 sandwich composites, respectively.
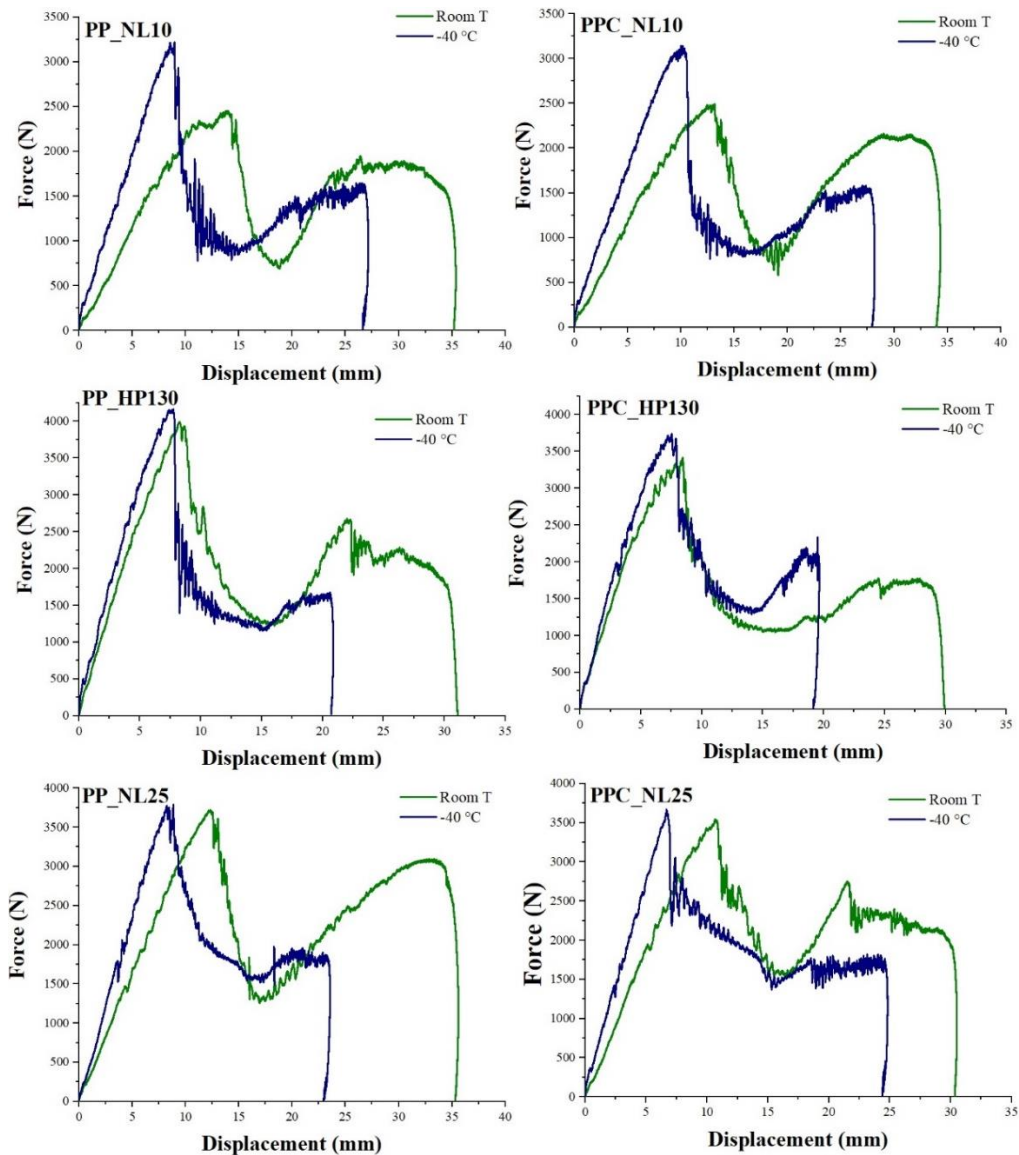
Figure 193: CAI impact response curves of the six sandwich configurations at 75 % of perforation energy and as a function of operating temperature, i.e. room temperature and -40 °C

At 75 % of perforation energy, room temperature and -40 °C samples are characterized by equal absorbing capabilities because impactor penetration occurs preventing the rebound and inducing a whole absorption of the impact energy. Similar results were obtained at 50 % of perforation energy with the exception of PP-NL10 samples which are characterized by a lower percentage absorbed energy at room temperature because the sample provides a perfectly elastic rebound without undergoing any penetration thus absorbing a lower amount of energy as also confirmed by the curves in Figure 186 and the damage progression in Figure 188. Moving to 25 % of perforation energy, where all sandwich structures react elastically to the impact, it is possible to notice that PP skin composites at room temperature are characterized by a higher percentage absorbed energy. The viscoelastic response of the PP matrix increases the damping capability of the structure.
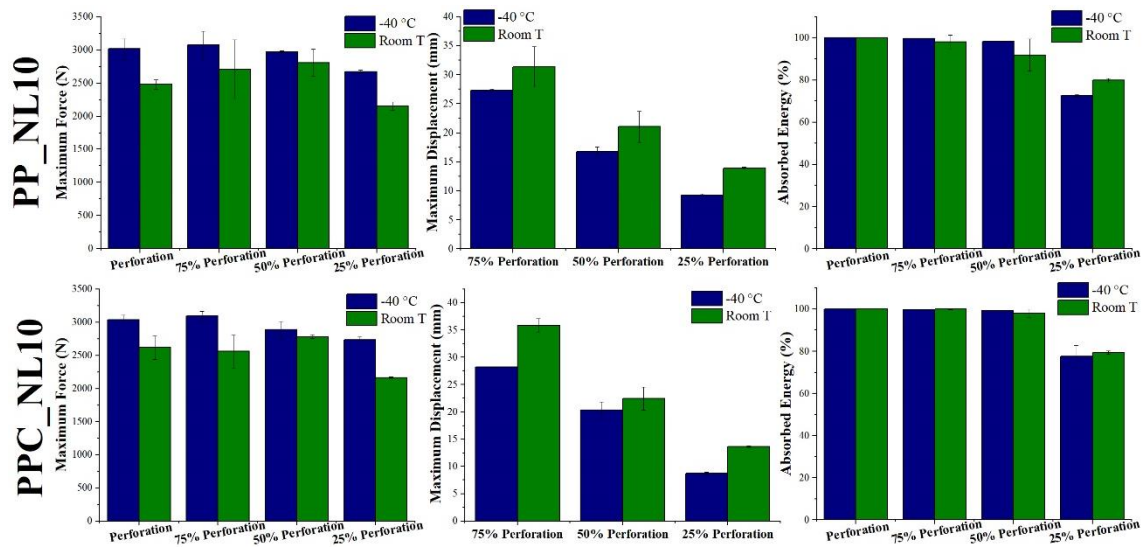
Figure 194: Maximum force, displacement and percentage absorbed energy of PP and PPC NL10 sandwiches at 25 %, 50 %, 75 % and 100 % of perforation energy as a function of testing temperature, i.e. room temperature and -40 °C
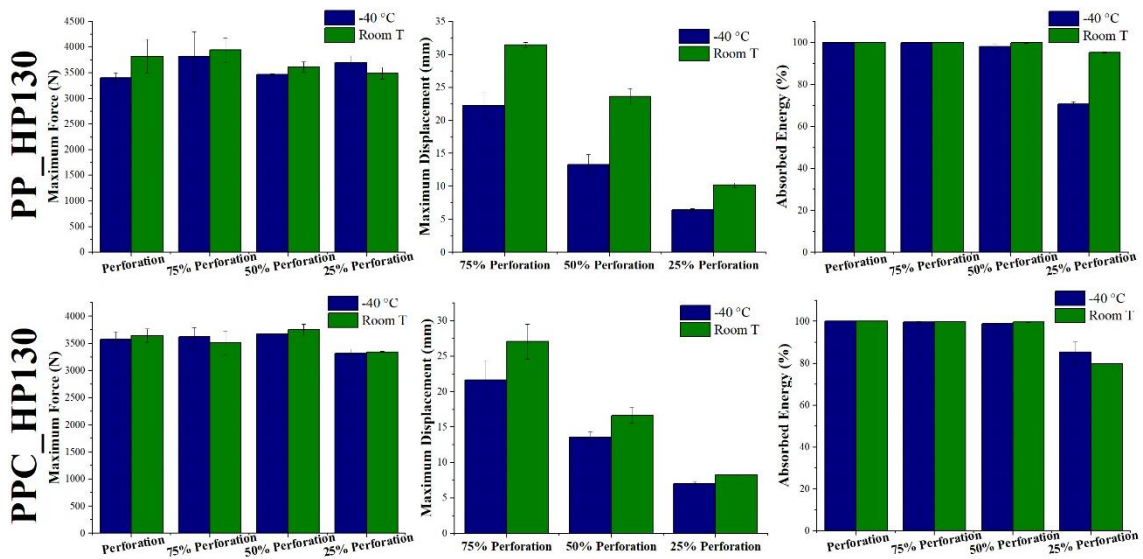
Figure 195: Maximum force, displacement and percentage absorbed energy of PP and PPC HP130 sandwiches at 25 %, 50 %, 75 % and 100 % of perforation energy as a function of testing temperature, i.e. room temperature and -40 °C
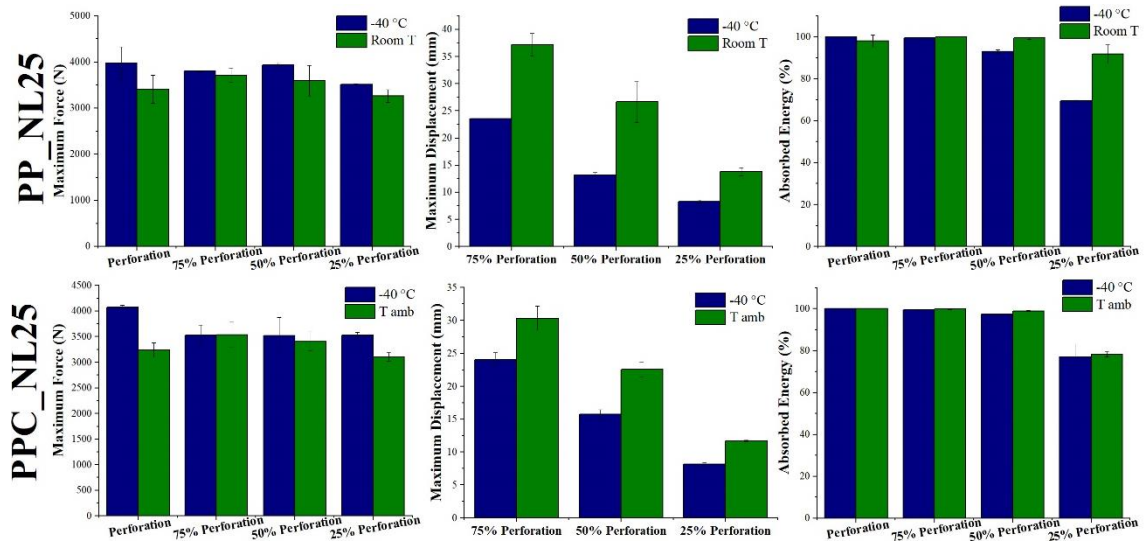
Figure 196: Maximum force, displacement and percentage absorbed energy of PP and PPC NL25 sandwiches at 25 %, 50 %, 75 % and 100 % of perforation energy as a function of testing temperature, i.e. room temperature and -40 °C
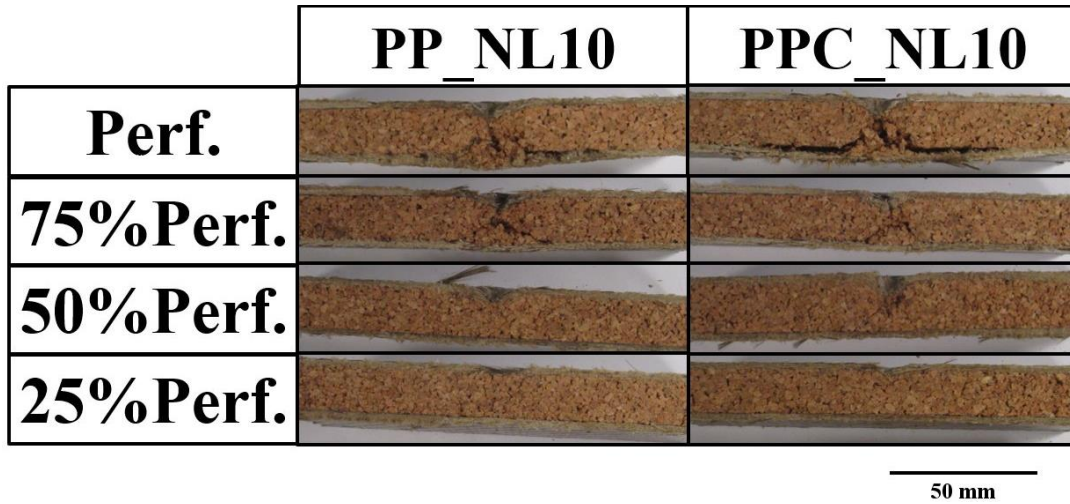
Figure 197: Damage progression in PP and PPC NL10 sandwich structures as a function of impact energy at -40 °C
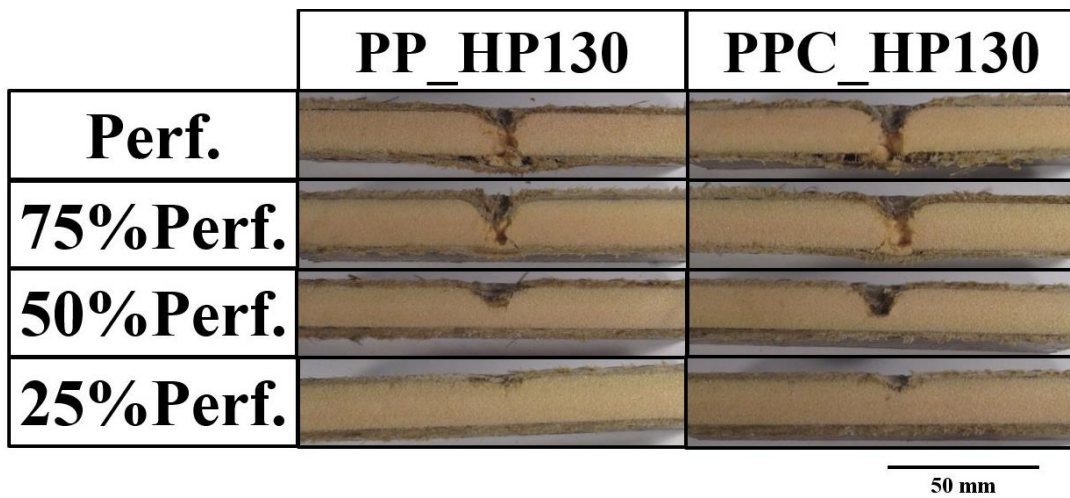
Figure 198: Damage progression in PP and PPC HP130 sandwich structures as a function of impact energy at -40 °C

	PP_NL25	PPC_NL25
Perf.		
75%Perf.		
50%Perf.		
25%Perf.		

50 mm
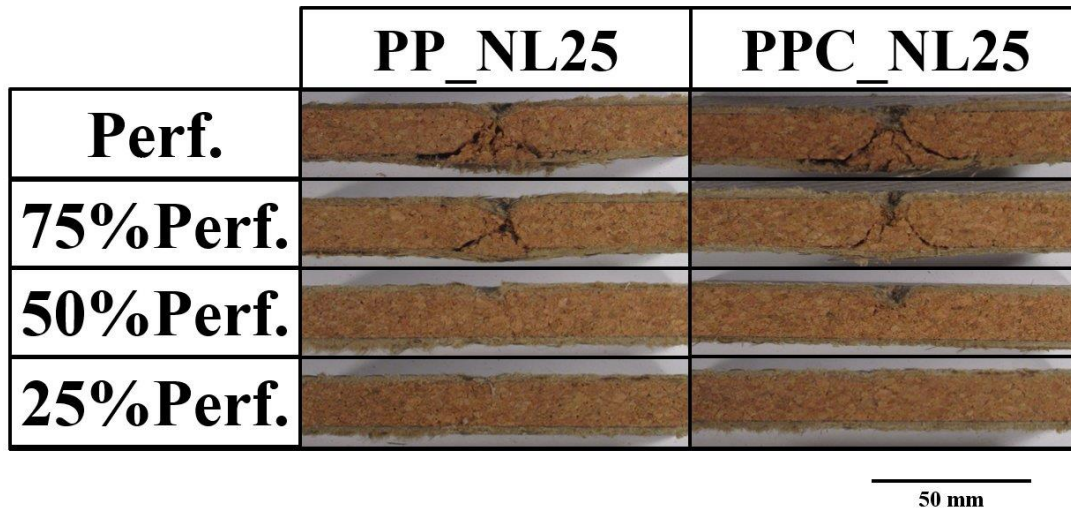
Figure 199: Damage progression in PP and PPC NL25 sandwich structures as a function of impact energy at -40 °C

Concerning the damage progression, it is possible to notice that, even if NL10 and HP130 composites are characterized by the same perforation energy, HP130 structures suffer a higher localization of the damage especially at 75 % and 50 % of perforation energy that can severely compromise the damage tolerance and the residual mechanical properties of the structures. This is true even when comparing HP130 and NL25 even if the latter is tested at higher impact energies thanks to its higher perforation threshold.

Moving to the analysis of 60 °C impact test results, a direct comparison with the results at room temperature and -40 °C is not possible due to the complications previously mentioned, but a direct comparison of the different sandwich configurations can be made and some conclusions on the effect of a higher operating temperature can be drawn. The resulting impact curves are shown in Figure 200 and the related data are summarized in Figure 201, whereas Figures 202, 203 and 204 display the damage progression of NL10, HP130 and NL25 composites, respectively. The first conclusion that can be drawn is that moving from room temperature to 60 °C there is an increase in composite perforation threshold. Indeed, even if PP NL10 and NL25 perforation energy could not be detected, their impact resistance is certainly higher than room temperature one where they underwent perforation at 65 J and 100 J, respectively. This is also confirmed by PPC NL10 and NL25 composites that display a perforation energy of 130 J at 60 °C which is definitely higher than 65 J and 80 J obtained at room temperature. The improved impact resistance of these structures must be ascribed to the combination of the strong ductility acquired by the matrix, especially in the case of PP skins, and the capability of agglomerated cork to adapt to the imposed deformation involving a wider area of the samples and avoiding local stress concentrations. This is not true for HP130 structures that, despite the improved matrix ductility, undergo perforation even at 97.5 J with both PP and PPC skins. The higher stiffness of the polymeric core and its brittle behavior, due to its glass transition temperature higher than 60 °C, do not allow to reach high deformation in bending and to spread the impact load all over the sample thus inducing a stress concentration in the impacted zone. By the way a certain improvement in the impact resistance thanks to the increased temperature can be observed even for this type of structures. In fact, PPC-HP130 sandwiches undergo perforation at 60 J when impacted at room temperature whereas at 60 °C display only a severe indentation when impacted at 65 J as shown in Figure 203. Looking at the data in Figure 201, it is possible to observe that all sandwich configurations are

characterized by a decrease in maximum force, maximum displacement and percentage absorbed energy with decreasing impact energies as already acknowledged at room temperature. NL10 composites are characterized by the lowest maximum force and the highest maximum displacement due to the lower stiffness of the overall structure whereas NL25 and HP130 ones display comparable results but a completely different damage mode. PP structures produced with agglomerated cork cores display a negligible indentation for each impact energy and almost a constant spacing of the skin meaning that the residual flexural properties of the structures should not be affected significantly. This is not true for PP HP130 structures that undergo perforation at both 130 J and 97.5 J thus suffering undoubtedly a sharp reduction in their load bearing capability. Similar conclusion can be drawn for PPC composites where the stress concentration suffered by HP130 sandwich structures leads to a severe indentation even at 65 J and 32.5 J. The more brittle behavior of PPC skins due to the improved fiber-matrix interface causes a relevant damage even in agglomerated cork structures but only until 97.5 J, as at 65 J and 32.5 J the excellent damping capabilities of cork allow to prevent core penetration.
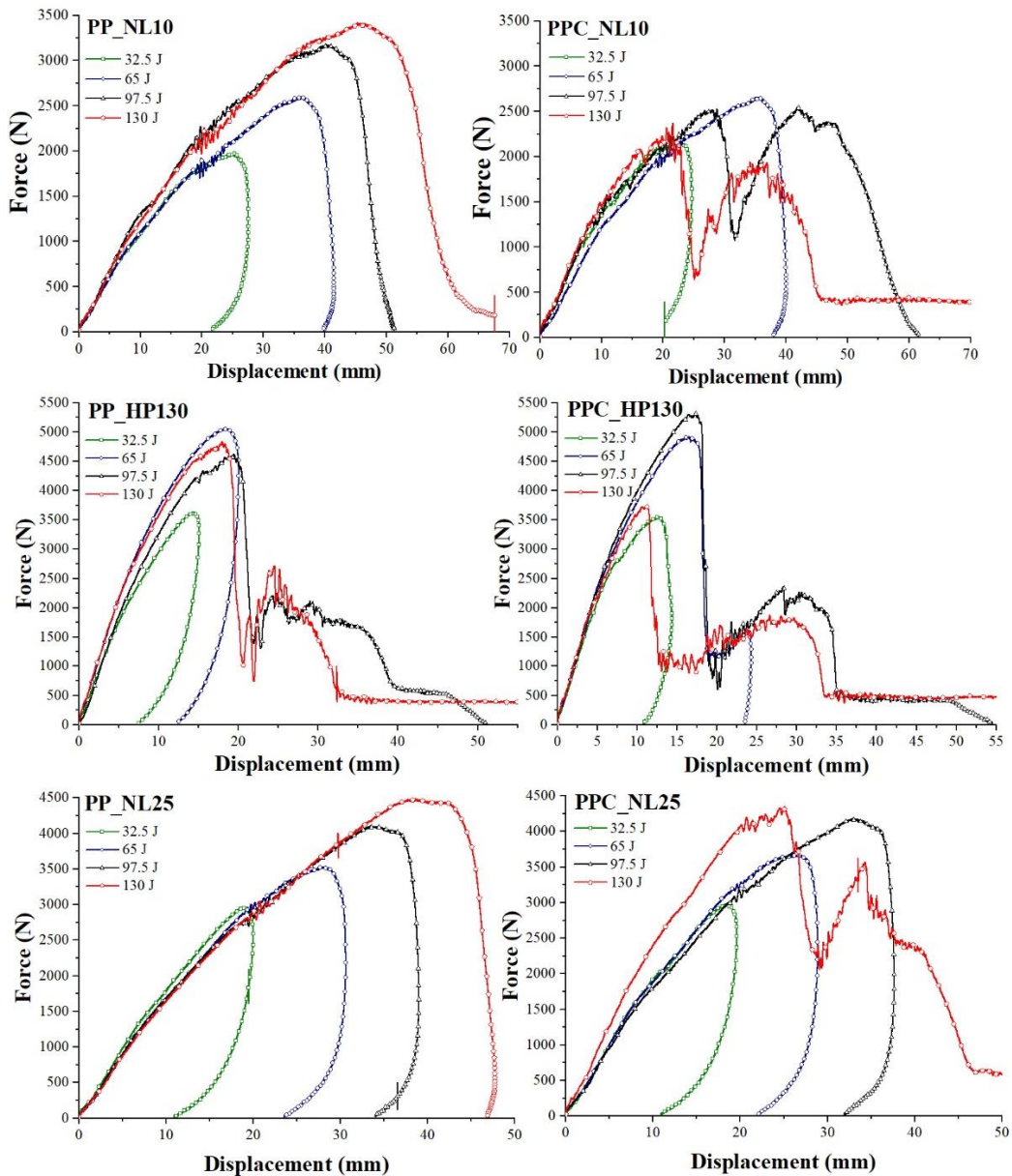
Figure 200: CAI impact response curves of the six sandwich configurations at 60 °C

194
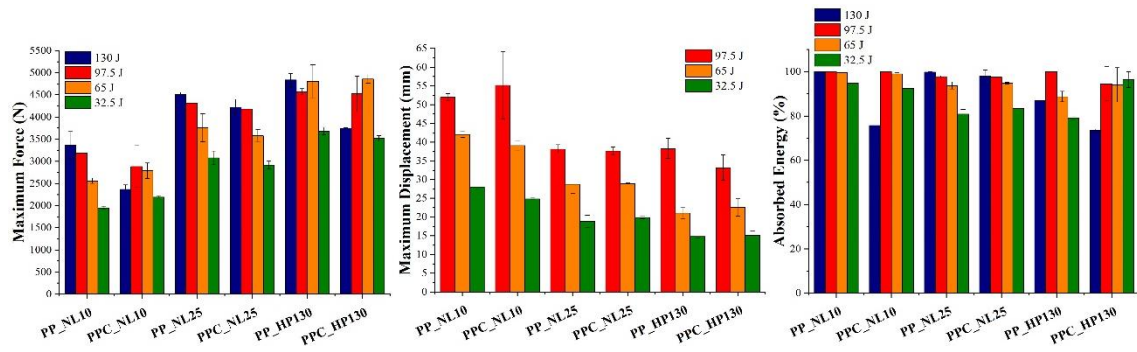
Figure 201: Maximum force, displacement and absorbed energy of all six sandwich structures configurations tested at 60 °C and at 32.5 J, 65 J, 97.5 J and 130 J
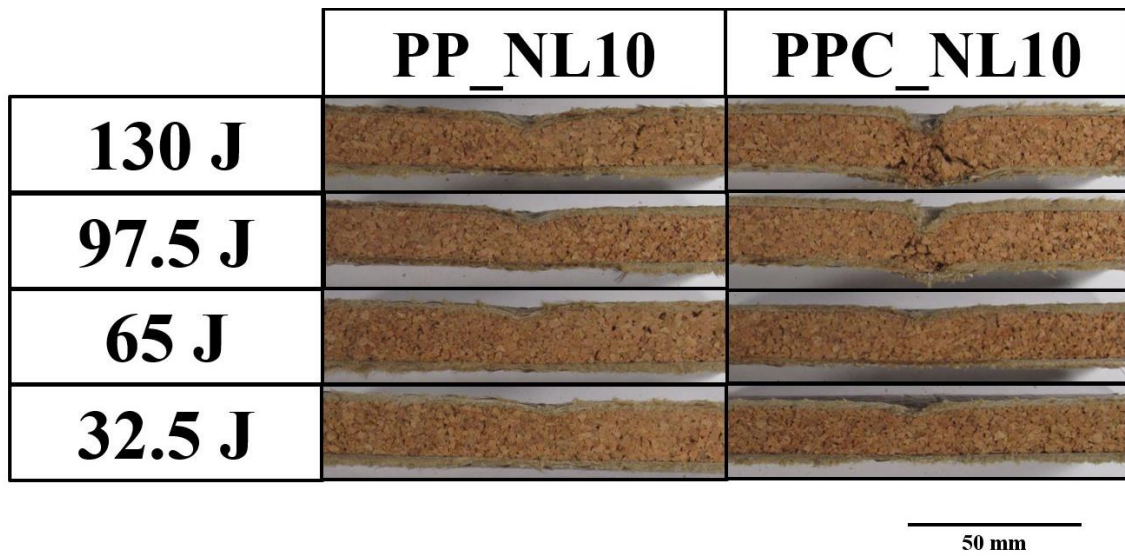
Figure 202: Damage progression in PP and PPC NL10 sandwich structures as a function of impact energy at 60 °C
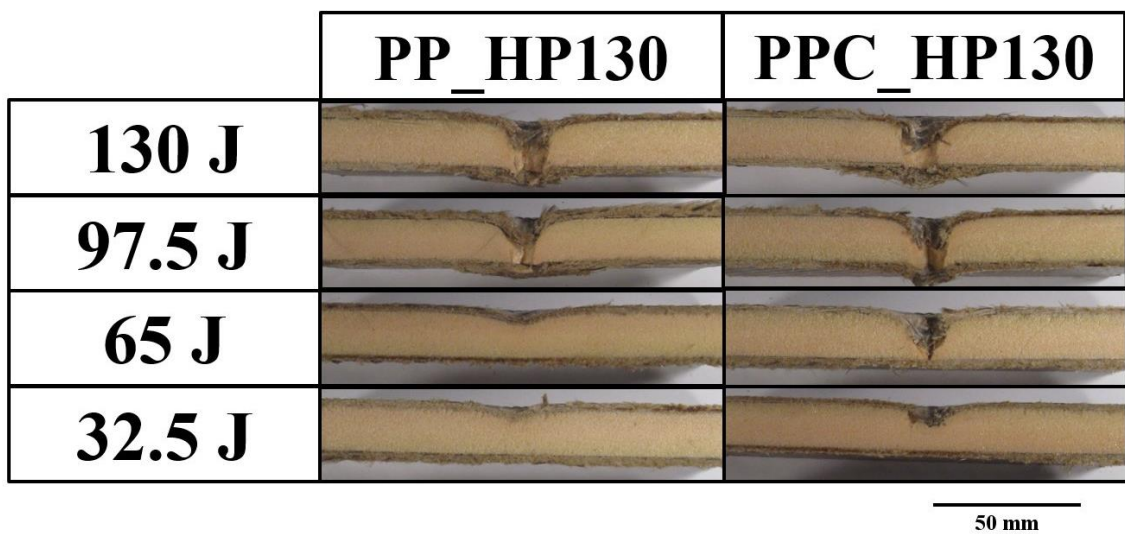
**Figure 203:** Damage progression in PP and PPC HP130 sandwich structures as a function of impact energy at 60 °C

195
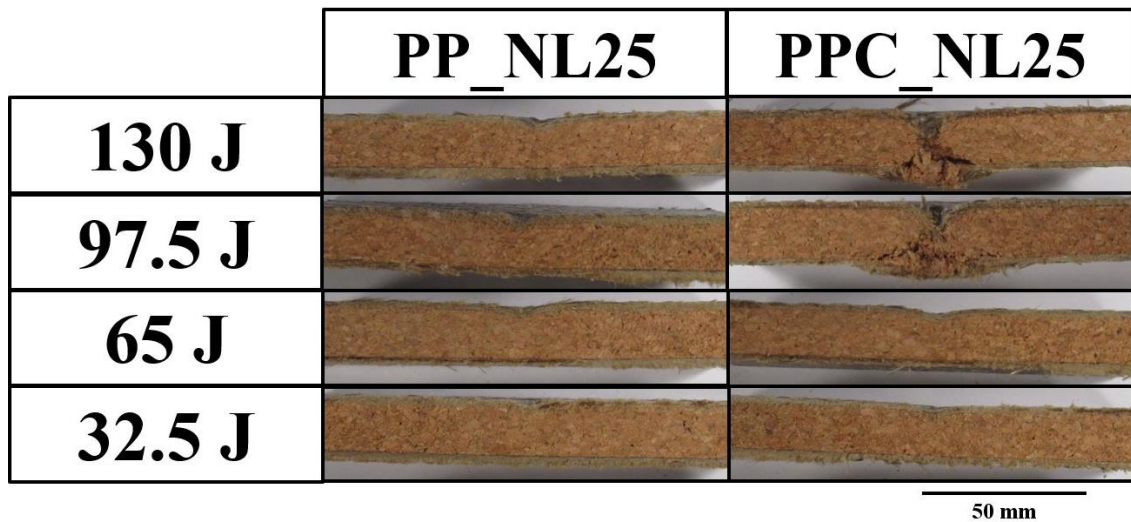
Figure 204: Damage progression in PP and PPC NL25 sandwich structures as a function of impact energy at 60 °C

5.2.3 Ballistic impact test

The application of Lambert-Jonas interpolation to the data set obtained measuring projectile impact and residual velocity allowed to evaluate the ballistic limits of the six sandwich configurations that are summarized in Table 37 and whose calculation is shown in Figure 205. The ballistic impacts carried out on the sole cores proved that all PVC foams are characterized by a higher ballistic limit than all agglomerated corks. However, as already observed for the low velocity impacts, the integration of agglomerated cork between the two skins to obtain the complete structure allows to prevent the premature detachment of sample pieces due to the occurrence of the intergranular fracture thus overturning the results obtained. Indeed, HP130 and NL10 structures which are characterized by core with the same density display comparable ballistic limits whereas NL25 structures are even characterized by a higher one. In section 4.2.3 it was pointed out that no significant differences could be observed between PP and PPC skins due to the low reaction time given to the composite and that induces a severe localization of the impact. This proved to be true even for HP130 structures where the severe localization of the impact assisted by the typical damage mode of the foam and the higher stiffness of the composite do not allow to detect any difference in sandwich ballistic response. This is confirmed by the damage evolution for a 175 m/s and a 420 m/s impact shown in Figure 206 and 207, respectively. The situation is slightly different for NL10 and NL25 composites that display a slight increase in the ballistic limit of 6.5 m/s and 10 m/s, respectively, moving from the PPC to the PP configuration.

Table 37: Ballistic limits of the six sandwich structures under study

Sandwich	Ballistic limit (m/s)
PP_NL10	171.6
PPC_NL10	165.1
PP_NL25	187
PPC_NL25	177.6
PP_HP130	171.1
PPC_HP130	172.3

PP_NL10

y = m1*sqrt((M0*M0)-(m2*m2))		
	Value	Error
m1	0,97145	0,0054322
m2	171,62	0,99609
R²	0,99871	NA

PPC_NL10

y = m1*sqrt((M0*M0)-(m2*m2))		
	Value	Error
m1	0,9616	0,005626
m2	165,13	1,3036
R²	0,99867	NA

PP_NL25

y = m1*sqrt((M0*M0)-(m2*m2))		
	Value	Error
m1	0,956	0,011377
m2	187,03	1,4554
R²	0,99448	NA

PPC_NL25

y = m1*sqrt((M0*M0)-(m2*m2))		
	Value	Error
m1	0,95054	0,0048253
m2	177,57	1.2786
R²	0,99898	NA

PP_HP130

y = m1*sqrt((M0*M0)-(m2*m2))		
	Value	Error
m1	0,97318	0,0068265
m2	171,11	1,5448
R²	0,99782	NA

PPC_HP130

y = m1*sqrt((M0*M0)-(m2*m2))		
	Value	Error
m1	0,98125	0,0094275
m2	172,35	1.0828
R²	0,99619	NA

Figure 205: All sandwich configurations experimental data and interpolation curves obtained implementing the Lambert-Jonas equation in the software Kaleida graph

197
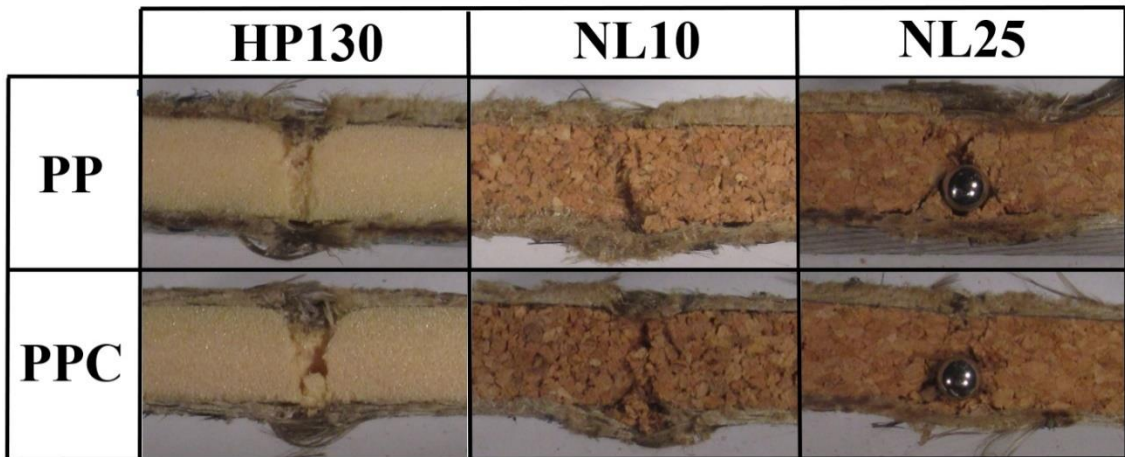
Figure 206: Damage experienced by the six sandwich configurations for a 175 m/s impact
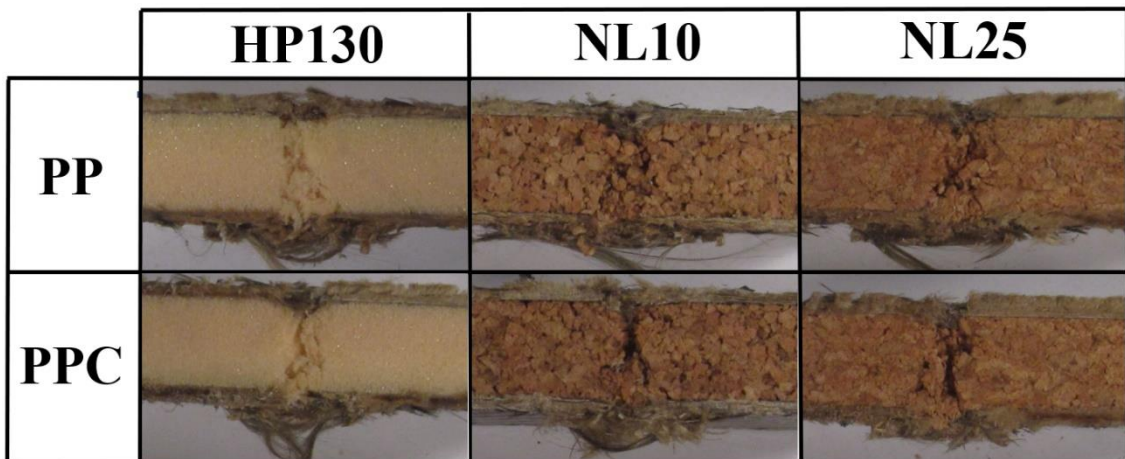
Figure 207: Damage experienced by the six sandwich configurations for a 420 m/s impact

Even if this increment is minimal, it can be ascribed to the different damage mode of agglomerated cork with respect to the foam. The intergranular fracture that arises in the bio-based core tends to evolve with a conical shape, as confirmed by Figures 206 and 207 and as already acknowledged in section 3.4.8, meaning that it is characterized by a wider area in the exit side respect to the enter side. This allows to progressively increase the area of the sample that react to the impact especially in correspondence of the ballistic limit. This means that the area of the bottom skin interested by the impact may be extended to such an extent to induce small differences between neat and compatibilized skins.

Chapter 6: Conclusions and Future Work

In the present work the feasibility of agglomerated cork as an eco-friendly core material to produce bio-based sandwich structures was evaluated and to legitimate its validity as an effective green core, all the experimental campaign was also carried out on more traditional PVC foams employed as benchmark. In order to keep the environmentally friendly character of the composite, skins were produced with a polypropylene matrix reinforced with a flax/basalt hybrid fabric. Due to the poor fiber-matrix interface between the hydrophilic vegetable fibers and the hydrophobic polyolefin matrix the effect of a maleic anhydride grafted polypropylene as coupling agent on skin quasi-static and dynamic properties was also investigated. Considering the susceptibility of sandwich structures to impact events, which can jeopardize their structural integrity and their residual mechanical properties, the present work aimed to address the Achille's heel of the novel bio-based structures under consideration.

The first part of the experimental campaign focused on the sole cores and allowed to identify similarities and differences between the two core types and to point out their weaknesses and their strengths. Both natural and synthetic cores displayed a hydrophobic nature and a closed-cell alveolar structure responsible for their lightness and their good thermal insulation capacity. This characteristic is particularly appealing in the field of buildings and construction to improve the energy efficiency and reduce the squandering. For this reason, an in-depth analysis of this feature through a modified transient plane source allowed to conclude that, even if the PVC foams are characterized by a slightly lower thermal conductivity, the insulation capability of a material depends also on other heat transfer contributions, i.e. convection and radiation, and the smaller cork cells dimensions allow to reduce the radiation effect leading to a lower thermal diffusivity and hence to a slower propagation of the heat throughout the material. A strict correlation between core materials morphology and their mechanical properties was also detected. Despite their intrinsic superior mechanical properties, PVC foams are characterized by rigid and brittle cell walls that tend to crack and fracture when subjected to an excessive compressive load thus leading to a permanent deformation of the material. On the contrary, cork cell walls corrugation and chemical composition, i.e. the conspicuous amount of flexible suberin macromolecules, allow a complete folding of the walls without undergoing fracture or permanent damage and leading to incomparable dimensional recovery capabilities. When subjected to a compressive deformation of 95 %, agglomerated cork displays a permanent deformation of only 10 – 15 % which is significantly lower than 55 – 65 % suffered by the polymeric foam. This aspect is fundamental to guarantee a higher dimensional stability to the sandwich structure and a higher regularity in its flexural properties. Indeed, if the inherent higher mechanical properties of the PVC foams can provide higher flexural performances to the sandwich composites produced with them, it is also true that sandwich flexural properties depend strongly on skin distancing and a reduction of their spacing during the life cycle of the component can cause a critical decrease in the mechanical performances thus leading to a premature failure. Moreover, the maintenance of the original shape is fundamental for some structures like wind turbine blades where an alteration of the geometry could change the air flow on the blade reducing the conversion efficiency of wind power in electrical energy. The stunning recovery capabilities of cork are extremely appealing even for multiple-impact events resistance purposes reducing the accumulation of damage over time and preventing the deterioration of structural efficiency. This feature could be exploited in safety

devices like helmets that prevent brain injuries and skull fracture by decelerating the head during an impact through the inner liner that absorbs the impact energy and reduces the impact force through cell walls crushing. The employment of agglomerated cork would allow to reduce the permanent deformation and the alteration of the microstructure thus ensuring a good protection to the user even after the first impact thanks to a controlled increase of the maximum force, i.e. logarithmic increase, and a restoration of liner initial height.

Cores characterization in compression allowed to disclose also a strong strain rate sensitivity of both core types due to their viscoelastic nature and a certain anisotropy due to the production process. Concerning the strain rate sensitivity, both cellular materials experience an increase of their compressive properties for increasing strain rate, but this increment is not constant throughout the whole strain rate working range: in fact, a more pronounced strain rate sensitivity was detected in the high-medium strain rate range. Concerning material anisotropy, the elongation of PVC foam cells along the z-axis due to the inflating production process leads to out of plane properties higher than in plane ones, whereas the residual stresses induced by the employment of pressure in the agglomeration process cause a decrease in agglomerated corks out of plane properties that are more pronounced for the denser cork.

The quasi-static characterization in shear of agglomerated cork revealed an intergranular fracture at the cork granules/polymeric binder interface as main damage mode. This type of damage is the main weak point of agglomerated cork because it arises in all impact conditions, i.e. puncture, CAI support and ballistic, and leads to the premature failure of the component causing the detachment of a conical plug and preventing the full exploitation of cork energy absorbing and damping capabilities, thus increasing the gap with the more performing PVC foams. This is confirmed by the tests in puncture impact conditions, where agglomerated cork perforation threshold does not vary with density in contrast to PVC foams that show an increase in perforation energy for increasing density, and by ballistic impact tests, where PVC foams ballistic limit tends to increase linearly with density whereas agglomerated cork one displays an increase characterized by a progressive parabolic deceleration. The execution of drop weight tower dynamic compression tests and impact tests with CAI support at high and low temperatures, i.e. 60 °C and -40 °C, allowed to highlight the embrittlement effect played by a decrease in operating temperature and the resulting detrimental effect on the energy absorbing capabilities of both natural and synthetic cores. The puncture impact tests performed on one agglomerated cork, i.e. NL25, and one PVC foam, i.e. HP130, were numerically modelled through the finite element software LS-DYNA employing the MAT63-CRUSHABLE_FOAM material model. A good fitting between the experimental and the numerical simulation curves was achieved providing a valuable tool to predict the dynamic impact response of these two core materials. The sole cores rather than the whole sandwich structures were numerically modelled in order to obtain a simulation efficient even with other skins and other sandwich configurations and not only for the present work purposes.

The second part of the experimental campaign focused on the sole skins in order to address fiber orientation and coupling agent effect on the quasi-static and dynamic properties of the laminates. The quasi-static characterization in tension and bending confirmed the higher maximum strength achievable along basalt fibers direction thanks to their intrinsic superior mechanical properties and revealed an improved stiffness along flax fibers direction thanks to the higher volume fraction. The maleic anhydride coupling agent allows to enhance significantly fiber-matrix interface leading to a better load transfer and hence to an improved strength and stiffness of the composite. If the improvement in fiber-matrix interface plays a positive role on the quasi-static performances of the hybrid laminates, it has a detrimental effect on their low velocity impact

response leading to a decrease of 10 J in the perforation energy in puncture impact conditions and a decrease of 2 J at -40 °C and at room temperature and of 20 J at 60 °C in CAI supported impact tests. Compatibilized composites tend to be more brittle and to dissipate the energy of an impact through matrix and fibers breakage and delamination phenomena, whereas the weak fiber-matrix interface of neat composites enables additional energy dissipation mechanisms such as fiber pull out, fiber-matrix friction, fiber slippage and matrix plastic deformation that allow to preserve composite integrity at higher impact energies before final failure occurs. In compatibilized composites, the improved interface hinders fiber slippage and rearrangement thus preventing matrix plastic deformation, inducing an embrittlement effect in material response and reducing the energy dissipation mechanisms. Operating temperature proved to play a significant role on the low velocity impact response in CAI supported tests of the skins. In particular, at -40 °C, polypropylene reached its glassy state and behaved in a brittle way as compatibilized composites do, whereas at 60 °C polypropylene is well above its glass transition temperature and neat composites are able to exploit completely matrix plasticization increasing the gap with the more brittle compatibilized skins. The effect of coupling agent is negligible in ballistic conditions where the extremely low reaction time given to the composite causes a strong localization of the impact and prevents the global reaction of the sample. The reduced area of the sample involved ensures that the improvement in fiber-matrix interface provided by the coupling agent does not play a significant role.

The final step of the experimental campaign entails the production and testing of the bio-based sandwich structures that, on the basis of the results obtained in the two previous step and the ones obtained with the bending tests performed on all possible sandwich configurations, were produced employing NL10 (ρ = 140 kg/m^3) and NL25 (ρ = 250 kg/m^3) agglomerated corks and HP130 (ρ = 130 kg/m^3) PVC foam. The latter is the only synthetic foam which can be compared with agglomerated corks considering that HP200 and HP250 are much more performing, whereas NL25 was selected being the most performing agglomerated cork and NL10 was selected in order to have a direct comparison of structures with the same core density. Concerning skin types, the presence of coupling agent confirmed to be detrimental for the impact performances of the structures causing a reduction of 20 J in the perforation energy in both puncture and CAI supported impact conditions at room temperature for both NL25 and HP130 sandwiches. This discrepancy is negligible at -40 °C in CAI supported conditions due to the transition to the glassy state of the neat polypropylene but is intensified at 60 °C where the difference becomes higher than 50 J for NL10 and NL25 composites. Before addressing the effect of core type, it is necessary to highlight that the integration of agglomerated cork between the two skins allows to prevent its premature intergranular failure and the detachment of the conical plug thus ensuring the complete exploitation of its absorbing capacities and the attenuation of its weak point. Concerning NL25 structures, they are always characterized by performances comparable or higher than HP130 ones. In particular, they display the same perforation threshold in puncture conditions, a 20 J higher perforation energy in CAI impact tests at room temperature, a 10 J higher perforation energy at -40 °C and a more than 30 J higher perforation energy for PPC composites and more than 80 J for PP composites at 60 °C. Concerning NL10 structures, they display the same perforation energy of HP130 structures at -40 °C in CAI impact conditions, a perforation threshold 5 J higher for PPC composites but 15 J lower for PP composites at room temperature and a more than 30 J higher perforation energy for PPC composites and more than 80 J for PP composites at 60 °C. Moreover, HP130 sandwiches are generally characterized by a higher concentration of the damage and by a higher permanent indentation due to their stiffer nature that implies a higher impairment of the structural integrity and hence a more significant deterioration of the residual

mechanical properties. Concerning ballistic impacts, NL10 and HP130 structures are characterized by comparable ballistic limits whereas NL25 composites are characterized by a 10 m/s higher ballistic limit.

In conclusion, NL10 sandwich structures are able to provide an impact resistance perfectly comparable with HP130 one, with an increase of only 5 % in structures weight and a total recyclability and a partial biodegradability of the component at the end of its life cycle. Unfortunately, the flexural performances of these composites are well far from HP130 ones, meaning that this green solution is valid only if impact resistance is one of the main design parameters and eco-friendliness must be favored with respect to the flexural performances. Different is the situation for NL25 composites that are characterized by an improved impact resistance and damage tolerance and by a flexural strength closer to HP130 ones. PPC NL25 structures display the same flexural strength of PP HP130 ones and, in CAI impact conditions, the same perforation energy at room temperature and an improved perforation threshold at both - 40 °C and 60 °C. The only drawback is an increase of 20 % in structure weight. Agglomerated cork NL25 proved to be a feasible and valid alternative to HP130 to obtain a green sandwich structure with an improved impact resistance, damage tolerance, dimensional stability and eco-compatibility for all those applications that can tolerate a slight increase in structure weight.

Concerning the future work and developments connected with the present PhD thesis, the following items will be likely addressed:

- Numerical simulation and finite element analysis of the impact response of the skins. Due to the thermoplastic matrix employed, the numerical modelling of the laminates cannot be performed with traditional composite damage models like Hashin, used to simulate the behavior of elastic-brittle composites, but appropriate subroutines need to be developed to account for matrix plastic deformation that is one of the main energy dissipation mechanisms and cannot be neglected.
- The impact resistance of the sandwich structures proposed was investigated in the present study. The following step is the quantification of their damage tolerance. The residual mechanical properties of the impacted samples are going to be evaluated in bending and the reduction experienced by their flexural properties will allow to quantify their damage tolerance.
- The effect of salt fog exposure on the compressive properties of the sole cores was investigated in the present study. The next step is the exposure of the overall sandwich structure to this accelerated ageing in order to evaluate its effect on the impact response of the composites and, potentially, to legitimate their feasibility in marine applications or in other applications in maritime localities.
- Finally, a study on the fatigue behavior of these structures is going to be performed in order to evaluate if the good damping capabilities of cork are actually able to play an effect on the long-term performances of the composites.

Capítulo 6: Conclusiones y Trabajos Futuros

La presente Tesis Doctoral se ha enfocado en el estudio del corcho aglomerado y en la evaluación de su viabilidad como núcleo para la fabricación de estructuras sándwich respetuosas con el medio ambiente. Los estudios realizados sobre el núcleo de corcho aglomerado se han contrastado con espumas poliméricas de PVC, que han sido empleadas a modo de referencia. Para mantener la naturaleza eco-sostenible de la estructura sándwich, las pieles fueron fabricadas con un laminado de tejido híbrido de fibras de basalto y lino en una matriz de polipropileno. Debido a la mala adherencia en la interfaz entre las fibras naturales hidrófilas y la matriz hidrófoba, se ha considerado oportuno estudiar el efecto de un agente de acoplamiento a base de polipropileno combinado con anhídrido maleico sobre las propiedades cuasi-estáticas y dinámicas de los laminados de las pieles de forma aislada y de las estructuras sándwich completas. Debido a la gran sensibilidad frente a impacto de las estructuras sándwich, que puede reducir de forma significativa su capacidad resistente, la presente Tesis se centra en el estudio de este aspecto de las estructuras propuestas por poderse considerar crítico.

La primera parte del trabajo se ha enfocado en el estudio de los núcleos de forma aislada para determinar las diferencias y similitudes entre el comportamiento de los dos tipos de núcleo: corcho aglomerado y espuma polimérica de PVC. De este modo se han podido determinar las fortalezas y debilidades de cada uno de ellos. Tanto los núcleos naturales como los núcleos sintéticos exhiben una naturaleza hidrófoba y están caracterizados por una estructura alveolar con celdas cerradas responsable de su ligereza y sus buenas capacidades de aislamiento térmico. Esta calidad resulta particularmente útil en el campo de las construcciones para mejorar la eficiencia energética de los edificios y reducir el gasto energético. Por esta razón, un análisis minucioso de esta característica a través de una fuente transitoria plana modificada, ha permitido deducir que a pesar de la conductividad térmica ligeramente inferior de las espumas de PVC, y dado que las capacidades aislantes de un material dependen también de otros fenómenos de transporte de calor, i.e. convección e irradiación, el menor tamaño de las celdas de corcho permite reducir el efecto de irradiación y la difusividad térmica ralentizando la propagación del calor a través del material.

Se ha observado también una estrecha conexión entre la morfología de los núcleos y sus propiedades mecánicas. A pesar de que poseen mayores propiedades mecánicas intrínsecas, las espumas de PVC están compuestas por paredes celulares rígidas y frágiles que suelen romperse y quebrarse si son sometidas a cargas de compresión excesivas causando una deformación permanente del material tras la aplicación de la carga. Al contrario, la corrugación y la composición química, i.e. la ingente cantidad de macromoléculas de suberina flexible, de las paredes celulares del corcho permiten una flexión total de las celdas sin sufrir ruptura o daños permanentes y asegurando una excelente capacidad de recuperación dimensional. Una vez sometido a una deformación en compresión del 95 %, el corcho aglomerado exhibe una deformación permanente solamente del 10 – 15 %, claramente inferior al 55 – 65 % sufrido por las espumas de PVC. Esto permite garantizar una mayor estabilidad dimensional de la estructura sándwich y, como consecuencia, asegurar que la rigidez a flexión de la estructura se mantiene después de aplicar una carga transversal. Así, aunque las propiedades mecánicas de las espumas de PVC son mayores que las del núcleo de corcho aglomerado, debido a que tras la aplicación de una carga se puede producir una disminución del espesor del núcleo, la resistencia y la rigidez de

una estructura sándwich con núcleo de espuma de PVC puede disminuir considerablemente durante la vida del componente e incluso producir la rotura prematura de la misma.

Además, el mantenimiento de la forma original del componente es fundamental en estructuras como las turbinas eólicas donde la modificación del perfil aerodinámico de la pala puede afectar a las fuerzas que se ejercen sobre la estructura e incidir en la generación de energía de la turbina.

La excepcional capacidad de recuperación dimensional del corcho es muy interesante también en todas aquellas aplicaciones que requieren una buena resistencia a fenómenos de impacto repetido. Este material permite reducir el daño acumulado con el paso del tiempo y limitar la reducción de la eficiencia de la estructura. Esta característica es muy útil para los dispositivos de protección individual como los cascos que evitan lesiones en el cerebro o fracturas del cráneo durante un impacto, reduciendo la desaceleración de la cabeza ya que el revestimiento interno que adsorbe la energía del impacto y reduce su fuerza a través del aplastamiento de sus celdas. El empleo de corcho aglomerado permitiría reducir la deformación permanente del revestimiento interno y la alteración de su microestructura asegurando una buena protección al usuario en impactos sucesivos gracias a un aumento controlado de la fuerza, i.e. incremento logarítmico, y a una restauración casi total de la altura inicial del revestimiento.

La caracterización en compresión de los núcleos ha permitido determinar que ambos presentan una fuerte sensibilidad a la velocidad de deformación a causa se du naturaleza viscoelástica, así como una cierta anisotropía debida al proceso de fabricación. También presentan un incremento de propiedades en compresión al aumentar la velocidad de deformación. Este incremento no es constante a lo largo de todo el rango de velocidades estudiadas y resulta más marcado a velocidades medias-altas. En relación a la anisotropía, el alargamiento de las celdas de espuma de PVC a lo largo del eje z, causado por el soplado en el proceso de fabricación, produce un incremento de las propiedades fuera del plano, mientras que las tensiones residuales inducidas por la presión empleada en el proceso de aglomeración del corcho llevan a una disminución de las propiedades fuera del plano con efecto mayor sobre el corcho más denso.

La caracterización cuasi-estática a cortadura del corcho aglomerado ha mostrado que se produce una fractura intergranular en la interfaz entra los gránulos de corcho y el *binder* polimérico. Este tipo de daño es el punto débil del corcho aglomerado y aparece en todas las configuraciones de impacto, i.e. ensayos de punzonamiento, impacto a baja velocidad con soporte tipo CAI e impacto balístico. Eso lleva a una ruptura prematura del componente con desprendimiento de un tapón con forma cónica de la probeta que impide desarrollar todas las capacidades de absorción de la energía y de amortiguación del corcho incrementando aún más la diferencia con las espumas de PVC. Este fenómeno se ha puesto de manifestó en los ensayos de punzonamiento donde el umbral de perforación del corcho aglomerado no varía con su densidad al contrario de lo que ocurre con las espumas que muestran un incremento de la energía de perforación con la densidad. Este comportamiento hace que en los ensayos balísticos la velocidad de perforación de las espumas de PVC se incrementa linealmente con la densidad mientras que la del corcho aglomerado está caracterizada por un incremento parabólico decreciente.

Los ensayos de compresión dinámica en torre de caída de peso y los ensayos de impacto con soporte CAI en condiciones de alta (60 °C) y baja temperatura (-40 °C), han permitido observar un efecto de fragilización debido a la disminución de la temperatura de servicio y un efecto negativo en las capacidades de absorción de energía de ambos núcleos. Los ensayos de punzonamiento hechos sobre el corcho aglomerado NL25 y sobre la espuma polimérica HP130 fueron reproducidos a través de una modelización numérica de elementos finitos con el programa LS-DYNA empleando el modelo de material MAT63-CRUSHABLE_FOAM. Se ha conseguido

un buen ajuste entre las curvas experimentales y las simulaciones numéricas. Esta modelización se ha demostrado como una herramienta útil para predecir la respuesta a impacto de estos materiales. La elección de modelizar solamente los núcleos y no la estructura sándwich global es debida a la voluntad de conseguir una simulación eficiente y empleable también con otras pieles y otras configuraciones de sándwich y no restringir el modelo a la estructura empleada en este trabajo.

La segunda parte del estudio se ha enfocado en la caracterización de las pieles para evaluar el efecto de la orientación de las fibras y del agente de acoplamiento sobre las propiedades cuasi-estáticas y dinámicas de los laminados. La caracterización cuasi-estáticas en tracción y flexión ha confirmado la mayor resistencia mecánica alcanzable a lo largo de la dirección de las fibras de basalto gracias a sus mejores propiedades mecánicas y ha mostrado una mayor rigidez a lo largo de la dirección de las fibras de lino gracias a la mayor fracción en volumen. La incorporación del agente de acoplamiento lleva a una significativa mejora de la adhesión en la interfaz entre fibras y matriz y a un incremento de la resistencia y de la rigidez del laminado. Si la mejora de la interfaz resulta positiva para las prestaciones cuasi-estáticas del laminado, esta ejerce un efecto prejudicial sobre la respuesta a impacto a baja velocidad, causando una disminución de 10 J en la energía de perforación en los ensayos de punzonamiento. En los ensayos de impacto con soporte CAI, la disminución es de 2 J a -40 °C y a temperatura ambiente, y de 20 J a 60 °C. Un laminado con agente de acoplamiento se comporta de manera más frágil disipando la energía de impacto a través de fenómenos de delaminación y de ruptura de las fibras y de la matriz. En cambio, la débil adhesión entre fibra y matriz de los compuestos no compatibilizados permite activar más mecanismos de disipación de la energía como el *pull out* y el deslizamiento de las fibras, el rozamiento entre fibra y matriz y la deformación plástica de la matriz que permiten preservar la integridad del compuesto para energías de impacto mayores. En los compuestos con agente de acoplamiento la mejor adhesión interfacial impide el deslizamiento y el reordenamiento de las fibras y como consecuencia inhibe la deformación plástica de la matriz reduciendo los mecanismos de disipación de la energía y ejerciendo un efecto de fragilización.

La temperatura de servicio es otro parámetro que afecta considerablemente al comportamiento a impacto a baja velocidad de las pieles. En condiciones de impacto con soporte CAI a -40 °C, el polipropileno alcanza su estado vitreo comportándose de manera frágil como los compuestos con agente de acoplamiento. A 60 °C el polipropileno se encuentra lejos de su temperatura de transición vítrea y por lo tanto los compuestos sin agente de acoplamiento pueden aprovechar plenamente la plasticidad de la matriz incrementando mucho la diferencia con las pieles con agente de acoplamiento. El efecto del agente de acoplamiento es despreciable en condiciones de impacto balístico donde el pequeño tiempo característico del fenómeno implica una extrema localización del impacto inhibiendo una reacción global de la estructura. Dado que la zona de probeta afectada por las tensiones originadas por el impacto es pequeña, la mejora de la adhesión en la interfaz producida por el agente de acoplamiento no ejerce un papel relevante.

La última fase del estudio se centra en la fabricación y ensayos de las estructuras sándwich completas. En base a los resultados conseguidos en las etapas previas y aquellos conseguidos con los ensayos de flexión sobre todas las posibles configuraciones de sándwich, se han elegido como núcleos los corchos aglomerados NL10 ($\rho = 140$ kg/m^3) y NL25 ($\rho = 250$ kg/m^3) y la espuma de PVC HP130 ($\rho = 130$ kg/m^3). Esta es la única espuma sintética que se puede comparar razonablemente con los corchos estudiados dado que las espumas HP200 y HP250 tienen prestaciones muchos mayores. El NL25 fue seleccionado por ser el corcho con mejores propiedades mecánicas mientras que el NL10 fue seleccionado para poder realizar una comparación directa entre estructuras sándwich con la misma densidad. Por lo que concierne al

tipo de piel, la adición del agente de acoplamiento ha confirmado ser perjudicial para las prestaciones a impacto de las estructuras causando una reducción de 20 J en la energía de perforación de las estructuras sándwich con NL25 y HP130 en condiciones de punzonamiento y de impacto con soporte CAI a temperatura ambiente. Esta diferencia entre las pieles de PP y PPC, se anula a -40 °C a causa de la transición del polipropileno al estado vitreo, pero se intensifica a 60 °C donde se evidencia una diferencia de más de 50 J en todas las estructuras fabricadas con NL10 y NL25.

Antes de examinar el efecto ejercido por tipo de núcleo, es oportuno remarcar que la inclusión del corcho aglomerado entre las dos pieles permite prevenir la aparición de la fractura prematura intergranular asegurando un completo aprovechamiento de las capacidades de absorción de la energía de este núcleo y una reducción de su mayor punto débil. Las estructuras con núcleo de NL25 presentan prestaciones a impacto iguales o mayores de las alcanzables por las estructuras con HP130, teniendo el mismo umbral de perforación en los ensayos de punzonamiento y una energía de perforación mayor de 20 J en condiciones de impacto con soporte CAI a temperatura ambiente, de 10 J a -40 °C y mayor de más de 30 J y más de 80 J a 60 °C para laminados PP y PPC respectivamente. Las estructuras con núcleo NL10 tienen, en condición de impacto con soporte CAI, la misma energía de perforación que las estructuras con núcleo HP130 a -40 °C, una energía de perforación de 5 J mayor para las pieles de PPC y de 15 J menor para las pieles de PP a temperatura ambiente, y un umbral de perforación mayor de más de 30 J y más de 80 J a 60 °C para pieles PP y PPC respectivamente. Además, las estructuras sándwich con núcleo HP130 están caracterizadas generalmente por una mayor concentración del daño y una mayor indentación permanente por culpa de su mayor rigidez. Esto provoca una mayor reducción de la integridad estructural de la estructura y de sus propriedades mecánicas residuales. En lo relativo a los ensayos balísticos, la estructuras con núcleo NL10 y HP130 tienen límites balísticos perfectamente comparables y las estructuras con núcleo en NL25 muestran un límite balístico mayor de 10 m/s.

En conclusión, las estructuras sándwich con núcleo NL10 tienen una resistencia a impacto comparable a la de las estructuras con núcleo HP130, con un aumento de peso de la estructura de solo el 5 % y una total reciclabilidad y parcial biodegradabilidad del componente al final de su vida útil. Desafortunadamente las propiedades a flexión de estas estructuras son mucho menores de las alcanzables con el núcleo HP130 y por lo tanto esta estructura solo sería recomendable si la resistencia a impacto es uno de los parámetros principales del diseño y si el respecto del medio ambiente tiene un papel más relevante que las propriedades cuasi-estáticas. Diferente es la situación de las estructuras con núcleo NL25 que tienen una mayor resistencia al impacto y una mejor tolerancia del daño, pero también una resistencia a flexión similar a las del núcleo HP130. Las estructuras PPC-NL25 tienen la misma resistencia a flexión que las estructuras PP-HP130 y, frente a impacto con soporte CAI, muestran la misma energía de perforación a temperatura ambiente y un mayor umbral de perforación a -40 °C y 60 °C; siendo la única desventaja un incremento del 20 % del peso de la estructura. No obstante, el corcho aglomerado NL25 demostró ser una alternativa válida a la espuma HP130 para obtener estructuras sándwich más ecológicas, con una mayor resistencia a impacto, una mayor tolerancia al daño y una mayor estabilidad dimensional en todas aquellas aplicaciones que puedan tolerar un ligero incremento en el peso de la estructura.

En relación a los trabajos que se podrían llevar a cabo para continuar con el realizado en esta Tesis Doctoral, se proponen los siguientes:

♦ Modelización numérica del comportamiento frente a impacto de las pieles. Debido a que la matriz del laminado empleada en este trabajo es termoplástica (polipropileno), el

modelo constitutivo no puede ser simplemente un modelo lineal elástico hasta rotura, y requiere considerar el comportamiento elastoplástico de este tipo de materiales. La deformación plástica de la matriz es uno de los principales mecanismos de disipación de la energía y, por tanto, debe ser tenido en cuenta en la modelización. Este modelo, junto al desarrollado en la presente tesis permitiría modelizar el comportamiento frente a impacto de la estructura sándwich completa. Para validar el modelo, tanto el del laminado aislado como de la estructura sándwich completa se podrían utilizar los ensayos realizados en esta tesis.

♦ Análisis de la tolerancia al daño de las estructuras sándwich propuestas. Este trabajo sería complementario al estudio de la resistencia a impacto realizado en esta Tesis Doctoral. Las propiedades mecánicas residuales se deberían evaluar, tanto a flexión como compresión. Se han seleccionado estas condiciones de carga dado que en condiciones de compresión es donde es esperable una mayor reducción de la resistencia mecánica de la estructura dañada, y en flexión porque es el estado de carga más probable en condiciones de servicio de una estructura sándwich.

♦ Estudio del envejecimiento de la estructura sándwich completa para evaluar su efecto sobre el comportamiento frente a impacto y para validar, eventualmente, su aplicabilidad en aplicaciones marinas o en otras aplicaciones donde dichas condiciones aparezcan. Este trabajo completaría el estudio del efecto de una prolongada exposición en niebla salina sobre las propiedades a compresión de los núcleos llevado a cabo en la presente Tesis Doctoral

♦ Por último, estudio de la respuesta a fatiga de las estructuras sándwich propuestas para evaluar si las buenas propiedades de amortiguamiento de las vibraciones del corcho aglomerado pueden ejercer un papel positivo sobre las propiedades a largo plazo de las estructuras sándwich. Este estudio exigiría también analizar el comportamiento frente a fatiga del laminado híbrido empleado en esta Tesis para fabricar las pieles.

Capitolo 6: Conclusioni e Sviluppi Futuri

Il presente lavoro di tesi si è incentrato sul sughero agglomerato e sulla valutazione della sua applicabilità come materiale *core* ecosostenibile nella produzione di strutture sandwich a ridotto impatto ambientale. Per legittimare la sua validità l'intera campagna sperimentale è stata effettuata non solo sul sughero agglomerato, ma anche su più tradizionali schiume in PVC impiegate come riferimento. Per mantenere la natura ecocompatibile del composito, le pelli sono state prodotte con una matrice polimerica di polipropilene rinforzato con un tessuto ibrido in basalto e lino. A causa della scadente interfaccia che si viene a instaurare tra le fibre naturali idrofile e la matrice poliolefinica idrofoba, si è ritenuto opportuno studiare l'effetto esercitato da un agente accoppiante a base di polipropilene graffato con anidride maleica sulle proprietà quasi-statiche e dinamiche dei laminati impiegati come pelli nelle strutture sandwich. In considerazione della forte suscettibilità delle strutture sandwich ad eventi di impatto, che possono compromettere la loro integrità strutturale e le loro proprietà meccaniche residue, il presente lavoro mira ad affrontare questo punto critico delle nuove biostrutture proposte.

La prima parte della campagna sperimentale si è incentrata sullo studio dei soli *core* e ha consentito di individuare similitudini e differenze tra i due tipi di anima e di evidenziare le rispettive debolezze e punti di forza. Sia i *core* naturali che quelli sintetici sono caratterizzati da una natura idrofoba e presentano una struttura alveolare a celle chiuse responsabile della loro leggerezza e delle buone capacità di isolamento termico. Questa qualità risulta particolarmente interessante nel campo delle costruzioni e dell'edilizia per migliorare l'efficienza energetica e ridurre gli sprechi. Per tale ragione, un'approfondita analisi di tale caratteristica attraverso l'ausilio di una sorgente transitoria piana modificata ha consentito di concludere che, nonostante le schiume in PVC siano caratterizzate da una conducibilità termica leggermente inferiore, le capacità di isolamento di un materiale dipendono anche da altri fenomeni di trasporto del calore, come convezione e radiazione, e la minor dimensione delle celle di sughero consente di ridurre l'effetto di radiazione portando così ad una più bassa diffusività termica e di conseguenza a una più lenta propagazione del calore attraverso il materiale. È stata riscontrata una stretta correlazione anche tra la morfologia dei materiali *core* e le loro proprietà meccaniche. Nonostante le superiori proprietà meccaniche intrinseche, le schiume di PVC sono costituite da pareti cellulari rigide e fragili che tendono a rompersi e fratturarsi una volta sottoposte ad un eccessivo carico a compressione inducendo così una deformazione permanente del materiale. Al contrario, la corrugazione e la composizione chimica in termini di macromolecole flessibili di suberina delle pareti cellulari del sughero consentono un completo ripiegamento delle stesse senza che subiscano rottura o danni permanenti assicurando eccezionali capacità di recupero dimensionale. Una volta sottoposto ad una deformazione a compressione del 95 %, il sughero agglomerato presenta una deformazione permanente del solo $10 - 15\%$ che risulta decisamente inferiore al $55 - 65\%$ subito dalle schiume polimeriche. Questo aspetto risulta fondamentale per garantire una maggior stabilità dimensionale alle strutture sandwich e di conseguenza una maggior costanza e invariabilità delle loro proprietà flessionali. Infatti, se le intrinseche proprietà meccaniche delle schiume di PVC sono in grado di assicurare maggiori prestazioni flessionali alla struttura sandwich con esse prodotta, è altrettanto vero che le stesse proprietà dipendono fortemente dalla distanza tra le due pelli e un'eventuale riduzione di tale parametro durante la vita in servizio del componente potrebbe causare una diminuzione critica delle prestazioni meccaniche e una rottura

prematura del componente. Inoltre, il mantenimento della forma originale del componente risulta fondamentale in strutture come le pale eoliche in cui un'alterazione della geometria iniziale potrebbe modificare il flusso d'aria sulla pala causando una riduzione dell'efficienza di conversione del potere del vento in energia elettrica. Le sorprendenti capacità di recupero della forma del sughero risultano estremamente interessanti anche ai fini della resistenza ad eventi di impatto ripetuti, consentendo di ridurre il danno accumulato nel corso tempo e limitando il deterioramento dell'efficienza della struttura. Questa caratteristica potrebbe essere sfruttata, ad esempio, nei dispositivi di protezione individuale come i caschi i quali impediscono l'insorgenza di lesioni al cervello o fratture del cranio durante un impatto decelerando la testa grazie al ruolo svolto dal rivestimento interno che assorbe l'energia dell'impatto e riduce la forza dello stesso attraverso lo schiacciamento delle sue pareti cellulari. L'impiego del sughero agglomerato consentirebbe di ridurre la deformazione permanente del rivestimento interno e l'alterazione della sua microstruttura assicurando una buona protezione all'utilizzatore anche per eventi di impatto successivi grazie a un aumento controllato della forza massima con incremento logaritmico e ad un quasi totale ripristino dell'altezza iniziale del rivestimento.

La caratterizzazione in compressione dei *core* ha consentito di individuare, inoltre, una forte sensibilità alla velocità di deformazione di entrambi i tipi di anima a causa della loro natura viscoelastica e una certa anisotropia dovuta al processo produttivo. Per quanto riguarda la sensibilità alla velocità di deformazione, entrambi i materiali cellulari mostrano un aumento delle loro proprietà a compressione per velocità di deformazione crescenti. Tale incremento non è, però, costante lungo tutto l'intervallo di lavoro, ma risulta più marcato in corrispondenza di velocità di deformazione medio-alte. Per quanto riguarda invece l'anisotropia del materiale, l'allungamento delle celle di schiume in PVC lungo l'asse z, indotto dal processo produttivo di insufflaggio, comporta un aumento delle proprietà fuori dal piano, mentre le tensioni residue indotte dalla pressione impiegata nel processo di agglomerazione del sughero portano ad una diminuzione delle proprietà fuori dal piano con conseguenze più severe per il sughero più denso.

La caratterizzazione quasi statica a taglio del sughero agglomerato ha evidenziato, come modalità di danneggiamento principale, una frattura inter-granulare in corrispondenza dell'interfaccia tra i granuli di sughero e il *binder* polimerico. Questo tipo di danno è il maggior punto di debolezza del sughero agglomerato poiché si manifesta in tutte le configurazioni di impatto, impatto *puncture*, impatto con supporto CAI e impatto balistico, causando un cedimento prematuro del componente e il distacco di una porzione conica del campione che impedisce di sfruttare appieno le capacità di assorbimento dell'energia e di smorzamento del sughero aumentando ulteriormente il divario con le schiume di PVC. Ciò è confermato dai risultati dei test di impatto *puncture*, in cui la soglia di perforazione del sughero agglomerato non varia con la densità al contrario di quanto accade con le schiume in PVC che presentano una energia di perforazione crescente con la densità, e dai test di impatto balistico, in cui il limite balistico delle schiume aumenta linearmente con la densità mentre quello del sughero agglomerato presenta una crescita parabolica decrescente. L'esecuzione di test di compressione dinamica in torre a caduta di peso e di test di impatto con supporto CAI ad alte e basse temperature (60 °C e -40 °C) ha consentito di evidenziare un effetto infragilente dovuto alla diminuzione della temperatura operativa e un conseguente effetto deleterio sulle capacità di assorbimento dell'energia di entrambi i tipi di *core*. I test di impatto *puncture* effettuati su un sughero agglomerato, NL25, e su una schiuma polimerica, HP130, sono stati opportunamente riprodotti attraverso una modellizzazione numerica agli elementi finiti con il software LS-DYNA impiegando il modello di materiale MAT63-CRUSHABLE_FOAM. Si è ottenuto un buon fitting tra le curve sperimentali e le simulazioni numeriche fornendo così uno strumento utile a predire la risposta dinamica ad impatto

di questi due materiali. La scelta di modellizzare i soli *core* piuttosto che l'intera struttura sandwich è da attribuire alla volontà di ottenere una simulazione efficiente ed impiegabile anche con altre pelli e altre configurazioni sandwich e non finalizzata ai soli scopi del presente lavoro.

La seconda parte della campagna sperimentale si è incentrata sulla caratterizzazione delle sole pelli in modo tale da poter studiare l'effetto esercitato dall'orientazione delle fibre e dall'agente accoppiante sulle proprietà quasi statiche e dinamiche dei laminati. La caratterizzazione quasi statica a trazione e flessione ha confermato la maggior resistenza meccanica ottenibile lungo la direzione delle fibre di basalto grazie alle loro superiori proprietà meccaniche e ha evidenziato una maggior rigidezza lungo la direzione delle fibre di lino grazie alla loro maggior frazione in volume. L'aggiunta dell'agente accoppiante a base di anidride maleica ha portato ad un significativo miglioramento dell'interfaccia tra fibra e matrice e quindi ad un potenziamento del trasferimento del carico con conseguente incremento della resistenza e rigidezza del composito. Se è vero che il miglioramento dell'interfaccia tra fibra e matrice risulta positivo per le prestazioni quasi statiche del laminato ibrido, è altrettanto vero che esso gioca un effetto deleterio sulla risposta ad impatto a bassa velocità causando una diminuzione di 10 J nell'energia di perforazione nelle condizioni di impatto *puncture* e di 2 J a -40 °C e a temperatura ambiente e di 20 J a 60 °C nei test di impatto con supporto CAI. Un composito compatibilizzato tende a comportarsi in maniera più fragile dissipando l'energia di un impatto attraverso fenomeni di delaminazione e di rottura delle fibre e della matrice, mentre la debole interfaccia tra fibra a matrice di un composito non compatibilizzato consente di attivare meccanismi di dissipazione dell'energia addizionali come il *pull out* e lo slittamento delle fibre, l'attrito tra fibre e matrice e la deformazione plastica della matrice che consentono di preservare l'integrità del composito ad energie di impatto superiori prima dell'avvento della rottura finale. Nei compositi compatibilizzati la miglior interfaccia tra fibra e matrice impedisce lo slittamento e il riarrangiamento delle fibre e la conseguente deformazione plastica della matrice, riducendo così i meccanismi di dissipazione dell'energia ed esercitando un effetto infragilente. Anche la temperatura operativa si è dimostrata un parametro fortemente influente sulla risposta ad impatto a bassa velocità delle pelli in condizioni di supporto CAI. A -40 °C il polipropilene raggiunge lo stato vetroso comportandosi in maniera fragile come i compositi compatibilizzati, mentre a 60 °C il polipropilene si trova ben al di sopra della sua temperatura di transizione vetrosa perciò i compositi non compatibilizzati possono sfruttare appieno la plasticità della matrice incrementando ulteriormente il divario con le più fragili pelli compatibilizzate. L'effetto dell'agente accoppiante risulta trascurabile in condizioni di impatto balistico in cui il bassissimo tempo di reazione concesso al composito comporta una estrema localizzazione dell'impatto impedendo una reazione globale del campione. Essendo l'area del campione interessata dall'impatto estremamente ridotta il miglioramento dell'interfaccia tra fibra e matrice a carico dell'agente accoppiante non esercita un ruolo rilevante.

L'ultimo passo della campagna sperimentale si è occupato della produzione e dello studio dei biocompositi sandwich che, sulla base dei risultati ottenuti nei due step precedenti e di quelli ottenuti dai test a flessione effettuati su tutte le possibili configurazioni sandwich, sono stati prodotti impiegando come core il sughero agglomerato NL10 (ρ = 140 kg/m^3) e NL25 (ρ = 250 kg/m^3) e la schiuma in PVC HP130 (ρ = 130 kg/m^3). Quest'ultima è la sola schiuma sintetica che possa essere opportunamente comparata con il sughero agglomerato essendo l'HP200 e l'HP250 decisamente più performanti, mentre l'NL25 è stato selezionato essendo il sughero agglomerato più performante e l'NL10 per ottenere una comparazione diretta tra strutture con nucleo di medesima densità. Per quanto riguarda il tipo di pelle, la presenza dell'agente accoppiante si è confermata deleteria per le prestazioni ad impatto delle strutture causando una riduzione di 20 J nell'energia di perforazione dell'NL25 e dell'HP130 sia nelle condizioni di impatto *puncture* che

negli impatti con supporto CAI a temperatura ambiente. Questo divario si annulla a -40 °C in condizioni di impatto CAI a causa della transizione allo stato vetroso del polipropilene puro, ma si intensifica a 60 °C dove una differenza di oltre 50 J si manifesta nei compositi NL10 e NL25. Prima di affrontare l'effetto esercitato dal tipo di anima impiegato, è necessario evidenziare che l'inserimento del sughero agglomerato tra le due pelli consente di prevenire l'insorgenza della prematura frattura intergranulare assicurando il pieno sfruttamento delle capacità di assorbimento del sughero e attenuando così il suo maggior punto di debolezza. Per quanto riguarda le strutture con *core* in NL25, esse sono sempre caratterizzate da prestazioni uguali o superiori a quelle ottenibili con l'HP130. In particolare, esse presentano la stessa soglia di perforazione in condizioni di impatto *puncture*, una energia di perforazione in condizioni CAI superiore di 20 J a temperatura ambiente, di 10 J a -40 °C e > 30 J per compositi in PPC e > 80 J per compositi in PP a 60 °C. Per quanto riguarda le strutture con *core* in NL10, esse presentano, in condizioni di impatto CAI, la stessa soglia di perforazione delle strutture in HP130 a -40 °C, una energia di perforazione superiore di 5 J per i compositi in PPC, ma inferiore di 15 J per quelli in PP a temperatura ambiente e > 30 J per compositi in PPC e > 80 J per compositi in PP a 60 °C. Inoltre, a causa della maggior rigidezza, i sandwich in HP130 presentano generalmente una maggior concentrazione del danno e una maggior indentazione permanente che causano un maggior deterioramento dell'integrità strutturale del composito e quindi delle sue proprietà meccaniche residue. Per quanto riguarda i test di impatto balistico, le strutture composite in NL10 e HP130 sono caratterizzate da limiti balistici perfettamente confrontabili mentre le strutture in NL25 presentano un limite balistico superiore di circa 10 m/s.

In conclusione, le strutture sandwich in NL10 sono in grado di assicurare una resistenza ad impatto perfettamente confrontabile con quella ottenibile con le strutture in HP130, con un aumento del solo 5 % del peso della struttura e una totale riciclabilità e una parziale biodegradabilità del componente alla fine della sua vita utile. Sfortunatamente le prestazioni a flessione raggiungibili con questo tipo di compositi sono molto lontane da quelle ottenibili con l'HP130, pertanto la suddetta soluzione *green* risulta valida solamente se la resistenza ad impatto è uno dei parametri di progetto principali e se l'eco-compatibilità del composito risulta più importante delle sue prestazioni meccaniche quasi-statiche. Diversa è la situazione per i compositi realizzati con l'NL25 che sono caratterizzati da una miglior resistenza all'impatto e una superiore tolleranza del danno, ma anche da una resistenza a flessione vicina a quella dei compositi in HP130. Le strutture in NL25 con pelli compatibilizzate presentano la stessa resistenza a flessione delle strutture in HP130 con pelli non compatibilizzate e, in condizioni di impatto con supporto CAI, la stessa energia di perforazione a temperatura ambiente e una più alta soglia di perforazione a -40 °C e 60 °C. L'unico svantaggio è un aumento del 20 % nel peso della struttura. Il sughero agglomerato NL25 si è dimostrato una valida alternativa al HP130 nell'ottenimento di strutture sandwich più ecocompatibili e con una più alta resistenza all'impatto, tolleranza al danno e stabilità dimensionale per tutte quelle applicazioni che possono tollerare un leggero aumento nel peso della struttura.

Per quanto riguarda gli sviluppi futuri connessi al presente lavoro di tesi, è possibile dire che i seguenti temi verranno affrontati:

♦ Simulazione numerica agli elementi finiti del comportamento a impatto delle pelli. A causa dell'impiego della matrice termoplastica in polipropilene, la modellizzazione numerica dei laminati non può essere effettuata con i modelli di danno comunemente impiegati per i materiali compositi, come il criterio di Hashin impiegato per simulare il comportamento di compositi elastici-fragili, ma richiede lo sviluppo di un'apposita

subroutine che tenga conto della deformazione plastica della matrice che è uno dei principali meccanismi di dissipazione dell'energia e non può essere trascurato.

♦ Nel presente lavoro si è studiata la resistenza a impatto delle strutture sandwich proposte. Il passo successivo prevede di quantificare la tolleranza al danno delle stesse. Le proprietà meccaniche residue dei campioni impattati saranno valutate a flessione e il decremento subito dalle proprietà flessionali delle strutture consentirà di quantificare la tolleranza al danno di ognuna.

♦ Nel presente lavoro si è studiato l'effetto di una esposizione prolungata in nebbia salina sulle proprietà a compressione dei soli *core*. Il passo successivo prevede di esporre a tale invecchiamento accelerato l'intera struttura composita in modo tale da valutare l'effetto esercitato sul comportamento a impatto dei compositi e, eventualmente, di legittimarne l'applicabilità in applicazioni marine o in altre applicazioni in località marittime.

♦ Infine, le strutture sandwich proposte saranno sottoposte a uno studio a fatica in modo tale da poter valutare se le ottime proprietà di smorzamento delle vibrazioni del sughero sono in grado di giocare un effetto positivo sulle proprietà a lungo termine dei compositi.

Bibliography

[1]   Vinson R. J. The behavior of sandwich structures of isotropic and composite materials. Technomic publishing CO.,INC.; 1999.

[2]   D. Zenkert. The handbook of sandwich construction. Engineering Materials Advisory Services Ltd; 1997.

[3]   Birman V, Kardomatea GA. Review of current trends in research and applications of sandwich structures. Compos Part B 2018. doi:10.1016/j.compositesb.2018.01.027.

[4]   Quaresimin M. Structural design of composite sandwich. Via Mare By Sea 2004:19–25.

[5]   Xiong J, Du Y, Mousanezhad D, Asl ME, Norato J, Vaziri A. Sandwich Structures with Prismatic and Foam Cores : A Review. Adv Eng Mater 2019;21:1–19. doi:10.1002/adem.201800036.

[6]   Lakreb N, Knapic S, Machado JS, Bezzazi B, Pereira H. Properties of multilayered sandwich panels with an agglomerated cork core for interior applications in buildings. Eur J Wood Wood Prod 2018;76:143–53. doi:10.1007/s00107-017-1198-3.

[7]   Mouritz AP, Gellert E, Burchill P, Challis K. Review of advanced composite structures for naval ships and submarines. Compos Struct 2001;53. doi:10.1016/S0263-8223(00)00175-6.

[8]   Sargianis J, Kim H, Suhr J. Natural Cork Agglomerate Employed as an Environmentally Friendly Solution for Quiet Sandwich Composites. Sci Rep 2012;2:403. doi:10.1038/srep00403.

[9]   Jensen JF, Schultz JP, Berggreen C, Branner K. Application of Load Carrying Sandwich Elements in Large Wind Turbine. Sandw. Struct. 7 Adv. with Sandw. Struct. Mater., 2005. doi:10.1007/1-4020-3848-8.

[10]   Sommer MM, M. Päßler, Schledjewski R, Stack M. Thermoplastic Composite Sandwich Structure for Sportive Applications. Sandw. Struct. 7 Adv. with Sandw. Struct. Mater., 2005, p. 957–66.

[11]   Borsellino C, Calabrese L, Passari R, Valenza A. Study of Snowboard Sandwich Structures. Sandw. Struct. 7 Adv. with Sandw. Struct. Mater., 2005. doi:10.1007/1-4020-3848-8.

[12]   Chai GB, Zhu S. A review of low-velocity impact on sandwich structures. Proc Inst Mech Eng Part L J Mater Des Appl 2011;225:207–30. doi:10.1177/1464420711409985.

[13]   Olsson R. Engineering Method for Prediction of Impact Response and Damage in Sandwich Panels. J Sandw Struct Mater 2002;4. doi:10.1106/109963602023192.

[14]   Olsson R. Methodology for predicting the residual strength of impacted sandwich panels. 1997.

[15]   James D, Speight G. Chapter Eight - Environmental Regulations. Environ. Inorg. Chem. Eng., 2017, p. 383–426. doi:10.1016/B978-0-12-849891-0.00008-4.

[16]   Borrega M, Gibson LJ. Mechanics of balsa (Ochroma pyramidale) wood. Mech Mater 2015;84:75–90. doi:10.1016/j.mechmat.2015.01.014.

[17]   Silva A Da, Kyriakides S. Compressive response and failure of balsa wood. Int J Solids Struct 2007;44:8685–717. doi:10.1016/j.ijsolstr.2007.07.003.

[18] Borrega M, Ahvenainen P, Serimaa R, Gibson L. Composition and structure of balsa (Ochroma pyramidale) wood. Wood Sci Technol 2015;49:403–20. doi:10.1007/s00226-015-0700-5.

[19] Fletcher MI. Balsa--Production and Utilization. Econ Bot 1951;5:107–25. doi:10.1007/BF02984770.

[20] Easterling KE, Harrysson R, Gibson LJ, Ashby MF. On the Mechanics of Balsa and Other Woods. Proceeding R Soc A 1982;383:31–41. doi:10.1098/rspa.1982.0118.

[21] Bledzki AK, Gassan J. Composites-reinforced-with-cellulose-based-fibres_1999_Progress-in-Polymer-Science.pdf. Prog Polym Sci 1999;24:221–74. doi:10.1016/S0079-6700(98)00018-5.

[22] Nallagula S. University of New Orleans, Behavior and Flexure Analysis of Balsa Wood Core Sandwich Composites : Experimental , Analytical and Finite Element Approaches. 2006.

[23] Kaboglu C, Pimenta S, Morris A, Dear JP. The effect of different types of core material on the flexural behavior of sandwich composites for wind turbine blades. J Therm Eng 2017;3:1102–9. doi:10.18186/thermal.298608.

[24] Li X, Liu W, Fang H, Huo R, Wu P. Flexural creep behavior and life prediction of GFRP-balsa sandwich beams. Compos Struct 2019;224. doi:10.1016/j.compstruct.2019.111009.

[25] Sadler RL, Sharpe M, Panduranga R, Shivakumar K. Water immersion effect on swelling and compression properties of Eco-Core , PVC foam and balsa wood. Compos Struct 2009;90:330–6. doi:10.1016/j.compstruct.2009.03.016.

[26] Osei-antwi M, Castro J De, Vassilopoulos AP, Keller T. Shear mechanical characterization of balsa wood as core material of composite sandwich panels. Constr Build Mater 2013;41:231–8. doi:10.1016/j.conbuildmat.2012.11.009.

[27] Zaharia SM, Morariu CO, Nedelcu A, Pop MA. Experimental Study of Static and Fatigue Behavior of CFRP-Balsa Sandwiches under Three-point Flexural Loading Sebastian. BioResources 2017;12:2673–89. doi:10.15376/biores.12.2.2673-2689.

[28] Monti A, Mahi AEL, Jendli Z, Guillaumat L. Quasi-static and fatigue properties of a balsa cored sandwich structure with thermoplastic skins reinforced by flax fibres. Jorunal Sandw Struct Mater 2018;21:2358–81. doi:10.1177/1099636218760307.

[29] Daniel IM, Abot JL, Schubel PM, Luo J. Response and Damage Tolerance of Composite Sandwich Structures under Low Velocity Impact. Exp Mech 2012;52:37–47. doi:10.1007/s11340-011-9479-y.

[30] Atas C, Sevim C. On the impact response of sandwich composites with cores of balsa wood and PVC foam. Compos Struct 2010;93:40–8. doi:10.1016/j.compstruct.2010.06.018.

[31] Vural M, Ravichandran G. Dynamic response and energy dissipation characteristics of balsa wood : experiment and analysis. Int J Solids Struct 2003;40:2147–70. doi:10.1016/S0020-7683(03)00057-X.

[32] Jover N, Shafiq B, Vaidya U. Ballistic impact analysis of balsa core sandwich composites. Compos PART B 2014;67:160–9. doi:10.1016/j.compositesb.2014.07.002.

[33] Abdalslam S. Wayne State University: Impact Damage Analysis Of Balsa Wood Sandwich Composite Materials. 2013.

[34] Baran I, WeiJermars W. Residual bending behaviour of sandwich composites after impact. J Sandw Struct Mater 2018:1–21. doi:10.1177/1099636218757164.

[35] Knapic S, Oliveira V, Machado JS, Pereira H. Cork as a building material: a review. Eur J Wood Wood Prod 2016;74:775–91. doi:10.1007/s00107-016-1076-4.

[36] Silva SP, Sabino MA, Fernandes EM, Correlo VM, Boesel LF, Reis RL. Cork: properties, capabilities and applications. Int Mater Rev 2005;50. doi:10.1179/174328008X353529.

[37] Pereira H. The rationale behind cork properties: A review of structure and chemistry. BioResources 2015;10:1–23. doi:10.15376/biores.10.3.Pereira.

[38] Gibson LJ, Easterling KE, Ashby MF. The Structure and Mechanics of Cork. Proc R Soc A Math Phys Eng Sci 1981;377:99–117. doi:10.1098/rspa.1981.0117.

[39] Gil L. Cork composites: A review. Materials (Basel) 2009;2:776–89. doi:10.3390/ma2030776.

[40] Reis L, Silva A. Mechanical behavior of sandwich structures using natural cork agglomerates as core materials. J Sandw Struct Mater 2009;11:487–500. doi:10.1177/1099636209104523.

[41] Soares B, Reis L, Silva A. Testing of sandwich structures with cork agglomerate cores. Eighth Int Conf Sandw Struct (ICSS 8), Porto 2008:451–62.

[42] Castro O, Silva JM, Devezas T, Silva A, Gil L. Cork agglomerates as an ideal core material in lightweight structures. Mater Des 2010;31:425–32. doi:10.1016/j.matdes.2009.05.039.

[43] Wang H, Ramakrishnan KR, Shankar K. Experimental study of the medium velocity impact response of sandwich panels with different cores. Mater Des 2016;99:68–82. doi:10.1016/j.matdes.2016.03.048.

[44] Bernard LA. Low Velocity Impact Testing of Sandwich Panels with Polymeric Cores. 2011.

[45] Arteiro A, Reis ALMA, Nóvoa PJRO, Silva LFM, Zupan M, Marques AT. Low velocity impact and flexural performance of sandwich structures with cork and polymer foam cores. Cienc e Tecnol Dos Mater 2013;25:79–84. doi:10.1016/j.ctmat.2014.03.003.

[46] Hoto R, Furundarena G, Torres JP, Muñoz E, Andrés J, García JA. Flexural behavior and water absorption of asymmetrical sandwich composites from natural fibers and cork agglomerate core. Mater Lett 2014;127:48–52. doi:10.1016/j.matlet.2014.04.088.

[47] Mancuso A, Pitarresi G, Tumino D. Mechanical Behaviour of a Green Sandwich Made of Flax Reinforced Polymer Facings and Cork Core. Procedia Eng 2015;109:144–53. doi:10.1016/j.proeng.2015.06.225.

[48] Hachemane B, Zitoune R, Bezzazi B, Bouvet C. Sandwich composites impact and indentation behaviour study. Compos Part B Eng 2013;51:1–10. doi:10.1016/j.compositesb.2013.02.014.

[49] Garlotta D. A Literature Review of Poly (Lactic Acid). J Polym Environ 2001;9:63–84. doi:10.1023/A:1020200822435.

[50] Thorat-Gadgil BS, Killi N, Rathna GV. Polyhydroxyalkanoates as biomaterials. Med Chem Commun 2017;8:1774–87. doi:10.1039/C7MD00252A.

[51] Diez-Pascual AM. Synthesis and Applications of Biopolymer Composites. Int J Mol Sci 2019;20. doi:10.3390/ijms20092321.

[52] Witten E, Avk VM. The Market for Glass Fibre Reinforced Plastics (GRP) in 2019 2019.

[53] Pickering KL, Efendy MGA, Le TM. A review of recent developments in natural fibre composites and their mechanical performance. Compos Part A Appl Sci Manuf 2016;83:98–112. doi:10.1016/j.compositesa.2015.08.038.

[54] Jawaid M, Abdul Khalil HPS. Cellulosic/synthetic fibre reinforced polymer hybrid composites: A review. Carbohydr Polym 2011;86:1–18. doi:10.1016/j.carbpol.2011.04.043.

[55] Hao LC, Sapuan SM, Hassan MR, Sheltami RM. 2. Natural fiber reinforced vinyl polymer composites. Elsevier Ltd; 2018. doi:10.1016/B978-0-08-102160-6.00002-0.

[56] Kogan FM, Nikitina O V. Solubility of Chrysotile Asbestos and Basalt Fibers in Relation to their Fibrogenic and Carcinogenic Action. Environ Health Perspect 1994;102:205–6. doi:10.1289/ehp.94102s5205.

[57] Ku H, Wang H, Pattarachaiyakoop N, Trada M. A review on the tensile properties of natural fiber reinforced polymer composites. Compos Part B Eng 2011;42:856–73. doi:10.1016/j.compositesb.2011.01.010.

[58] Faruk O, Bledzki AK, Fink HP, Sain M. Biocomposites reinforced with natural fibers: 2000-2010. Prog Polym Sci 2012;37:1552–96. doi:10.1016/j.progpolymsci.2012.04.003.

[59] Thomas S, Paul SA, Pothan LA, Deepa B. Natural Fibres : Structure , Properties and Applications. Cellul. Fibers Bio- Nano-Polymer Compos., 2011, p. 3–42. doi:10.1007/978-3-642-17370-7.

[60] Liu K, Takagi H, Osugi R, Yang Z. Effect of physicochemical structure of natural fiber on transverse thermal conductivity of unidirectional abaca / bamboo fiber composites. Compos Part A Appl Sci Manuf 2012;43:1234–41. doi:10.1016/j.compositesa.2012.02.020.

[61] Monteiro SN, Calado V, Rodriguez RJS, Margem FM. Thermogravimetric behavior of natural fibers reinforced polymer composites-An overview. Mater Sci Eng A 2012;557:17–28. doi:10.1016/j.msea.2012.05.109.

[62] Xie Y, Hill CAS, Xiao Z, Militz H, Mai C. Silane coupling agents used for natural fiber/polymer composites: A review. Compos Part A Appl Sci Manuf 2010;41:806–19. doi:10.1016/j.compositesa.2010.03.005.

[63] Keener TJ, Stuart RK, Brown TK. Maleated coupling agents for natural fibre composites. Compos Part A Appl Sci Manuf 2004;35:357–62. doi:10.1016/j.compositesa.2003.09.014.

[64] Seghini MC, Touchard F, Sarasini F, Chocinski-arnault L, Tirillò J, Bracciale MP, et al. Effects of oxygen and tetravinylsilane plasma treatments on mechanical and interfacial properties of flax yarns in thermoset matrix composites. Cellulose 2019;27:511–30. doi:10.1007/s10570-019-02785-3.

[65] Seghini MC, Touchard F, Sarasini F, Cech V, Chocinski-arnault L, Mellier D, et al. Engineering the interfacial adhesion in basalt / epoxy composites by plasma polymerization. Compos Part A 2019;122:67–76. doi:10.1016/j.compositesa.2019.04.013.

[66] Petroudy SRD. 3 - Physical and mechanical properties of natural fibers. Adv. High Strength Nat. Fibre Compos. Constr., Elsevier Ltd; 2017, p. 59–83. doi:10.1016/B978-0-08-100411-1.00003-0.

[67] Sahu P, Gupta MK. A review on the properties of natural fibres and its bio-composites :

Effect of alkali treatment. J Mater Des Appl 2019;234:198–217. doi:10.1177/1464420719875163.

[68] Rowell RM. Acetylation of Natural Fibers to Improve Performance. Mol Cryst Liq Cryst 2004;418:153–64. doi:10.1080/15421400490479244.

[69] Bledzki AK, Mamun AA, Lucka-Gabor M, Gutowski VS. The effects of acetylation on properties of flax fibre and its polypropylene composites. EXPRESS Polym Lett 2008;2:413–22. doi:10.3144/expresspolymlett.2008.50.

[70] Gudayu AD, Steuernagel L, Meiners D, Gideon R. Effect of surface treatment on moisture absorption , thermal , and mechanical properties of sisal fiber. J Ind Text 2020;0:1–21. doi:10.1177/1528083720924774.

[71] Zei FWW, Debnath S, Mahmood A, Abdullah AH. Enhancing Mechanical Performance of Bagasse Fiber-Epoxy Composite by Surface Treatment. Solid State Phenom 2020;305:8–17. doi:10.4028/www.scientific.net/SSP.305.8.

[72] Zaman HU, Khan RA. Acetylation used for natural fiber/polymer composites. J Thermoplast Compos Mater 2019:1–21. doi:10.1177/0892705719838000.

[73] Senthilraja R, Sarala R, Antony AG, Seshadhri. Effect of acetylation technique on mechanical behavior and durability of palm fibre vinyl-ester composites. Mater Today Proc 2020;21:634–7. doi:10.1016/j.matpr.2019.06.729.

[74] Hossen MM, Feng J, Yuxiang Y, Jiang W. Preparation and evaluation mechanical , chemical and thermal properties of hybrid jute and coir fibers reinforced bio-composites using poly-lactic acid and poly-caprolactone blends. Mater Res Express 2020;7. doi:10.1088/2053-1591/ab952b.

[75] Chandekar H, Chaudhari V, Waigaonkar S, Mascarenhas A. Effect of chemical treatment on mechanical properties and water diffusion characteristics of jute-polypropylene composites. Polym Compos 2019:1–15. doi:10.1002/pc.25468.

[76] Kusmono, Hestiawan H, Jamasri. The water absorption , mechanical and thermal properties of chemically treated woven fan palm reinforced polyester composites. Journals Mater Res Technol 2020;9:4410–20. doi:10.1016/j.jmrt.2020.02.065.

[77] Peças P, Carvalho H, Salman H, Leite M. Natural Fibre Composites and Their Applications : A Review. J Compos Sci 2018;2:1–20. doi:10.3390/jcs2040066.

[78] Mohammed L, Ansari MNM, Pua G, Jawaid M, Islam MS. A Review on Natural Fiber Reinforced Polymer Composite and Its Applications. Int J Polym Sci 2015;2015. doi:10.1155/2015/243947.

[79] Shahzad A. Hemp fiber and its composites - A review. J Compos Mater 2012;46:973–86. doi:10.1177/0021998311413623.

[80] Joshi SV, Drzal LT, Mohanty AK, Arora S. Are natural fiber composites environmentally superior to glass fiber reinforced composites ? Compos Part A 2004;35:371–6. doi:10.1016/j.compositesa.2003.09.016.

[81] Fiore V, Scalici T, Di Bella G, Valenza A. A review on basalt fibre and its composites. Compos Part B Eng 2015;74:74–94. doi:10.1016/j.compositesb.2014.12.034.

[82] Militký J, Kovačič V, Rubnerová J. Influence of thermal treatment on tensile failure of basalt fibers. Eng Fract Mech 2002;69:1025–33. doi:10.1016/S0013-7944(01)00119-9.

[83] Deák T, Czigány T. Chemical Composition and Mechanical Properties of Basalt and Glass

Fibers : A Comparison. Text Res J 2009;79:645–51. doi:10.1177/0040517508095597.

[84]   Sathishkumar TP, Satheeshkumar S, Naveen J. Glass fiber-reinforced polymer composites- A review. J Reinf Plast Compos 2014;33:1258–75. doi:10.1177/0731684414530790.

[85]   Li Z, Ma J, Ma H, Xu X. Properties and Applications of Basalt Fiber and Its Composites. IOP Conf Ser Earth Environ Sci 186 2018;186. doi:10.1088/1755-1315/186/2/012052.

[86]   Wei B, Cao H, Song S. Tensile behavior contrast of basalt and glass fibers after chemical treatment. Mater Des 2010;31:4244–50. doi:10.1016/j.matdes.2010.04.009.

[87]   Fiore V, Di Bella G, Valenza A. Glass-basalt/epoxy hybrid composites for marine applications. Mater Des 2011;32:2091–9. doi:10.1016/j.matdes.2010.11.043.

[88]   Balaji K V, Shirvanimoghaddam K, Rajan GS, Ellis A V, Naebe M. Surface treatment of Basalt fiber for use in automotive composites. Mater Today Chem 2020;17. doi:10.1016/j.mtchem.2020.100334.

[89]   Militký J, Mishra R, Jamshaid H. Basalt Fibers. Handb. Prop. Text. Tech. Fibres, 2018, p. 805–40. doi:10.1016/B978-0-08-101272-7.00020-1.

[90]   Lilli M, Sarasini F, Di Fausto L, González C, Fernández A, Lopes CS, et al. Chemical Regeneration of Thermally Conditioned Basalt Fibres. Appl Sci 2020;10. doi:10.3390/app10196674.

[91]   Ralph C, Lemoine P, Archer E, Mcilhagger A. Mechanical properties of short basalt fibre reinforced polypropylene and the effect of fibre sizing on adhesion. Compos Part B 2019;176. doi:10.1016/j.compositesb.2019.107260.

[92]   Colombo C, Vergani L, Burman M. Static and fatigue characterisation of new basalt fibre reinforced composites. Compos Struct 2012;94:1165–74. doi:10.1016/j.compstruct.2011.10.007.

[93]   Liu Q, Shaw MT, Parnas RS, Mcdonnell A. Investigation of Basalt Fiber Composite Mechanical Properties for Applications in Transportation *. Polym Compos 2006;27:41–8. doi:10.1002/pc.

[94]   Chairman CA, Palani S, Babu K. Mechanical and Abrasive Wear Behavior of Glass and Basalt Fabric-Reinforced Epoxy Composites. J Appl Polym Sci 2013:120–30. doi:10.1002/app.39154.

[95]   Sfarra S, Ibarra-castanedo C, Santulli C, Paoletti A, Paoletti D, Sarasini F, et al. Falling weight impacted glass and basalt fibre woven composites inspected using non-destructive techniques. Compos Part B 2013;45:601–8. doi:10.1016/j.compositesb.2012.09.078.

[96]   Lopresto V, Leone C, Iorio I De. Mechanical characterisation of basalt fibre reinforced plastic. Compos Part B 2011;42:717–23. doi:10.1016/j.compositesb.2011.01.030.

[97]   Dorigato A, Pegoretti A. Fatigue resistance of basalt fibers-reinforced laminates. J Compos Mater 2011;46:1773–85. doi:10.1177/0021998311425620.

[98]   Mingchao W, Zuoguang Z, Yubin L, MIN L, Zhijie S. Chemical Durability and Mechanical Properties of Alkali-proof Basalt Fiber and its Reinforced Epoxy Composites. J Reinf Plast Compos 2008;27. doi:10.1177/0731684407084119.

[99]   Wei B, Cao H, Song S. Degradation of basalt fibre and glass fibre / epoxy resin composites in seawater. Corros Sci 2011;53:426–31. doi:10.1016/j.corsci.2010.09.053.

[100]   Botev M, Betchev H, Bikiaris D, Panayiotou C. Mechanical Properties and Viscoelastic

Behavior of Basalt Fiber-Reinforced Polypropylene. J Appl Polym Sci 1999;74:523–31. doi:10.1002/(SICI)1097-4628(19991017)74:3<523::AID-APP7>3.0.CO;2-R.

[101] Czigany T. Special manufacturing and characteristics of basalt fiber reinforced hybrid polypropylene composites : Mechanical properties and acoustic emission study. Compos Sci Technol 2006;66:3210–20. doi:10.1016/j.compscitech.2005.07.007.

[102] Akinci A, Yilmaz S, Sen U. Wear Behavior of Basalt Filled Low Density Polyethylene Composites. Appl Compos Mater 2012;19:499–511. doi:10.1007/s10443-011-9208-9.

[103] Akinci A, Ercenk E, Yilmaz S, Sen U. Slurry erosion behaviors of basalt filled low density polyethylene composites. Mater Des 2011;32:3106–11. doi:10.1016/j.matdes.2010.12.029.

[104] Akinci A. Mechanical and morphological properties of basalt filled polymer matrix composites. Arch Mater Sci Eng 2009;35:29–32.

[105] Deák T, Czigány T, Tamás P, Németh C. Enhancement of interfacial properties of basalt fiber reinforced nylon 6 matrix composites with silane coupling. EXPRESS Polym Lett 2010;4:590–8. doi:10.3144/expresspolymlett.2010.74.

[106] Zhang Y, Yu C, Chu PK, Lv F, Zhang C, Ji J, et al. Mechanical and thermal properties of basalt fiber reinforced poly (butylene succinate) composites. Mater Chem Phys 2012;133:845–9. doi:10.1016/j.matchemphys.2012.01.105.

[107] Wang J, Chen B, Liu N, Han G, Yan F. Combined effects of fiber / matrix interface and water absorption on the tribological behaviors of water-lubricated polytetrafluoroethylene-based composites reinforced with carbon and basalt fibers. Compos Part A 2014;59:85–92. doi:10.1016/j.compositesa.2014.01.004.

[108] Zhang X, Pei X, Wang Q. Friction and Wear Properties of Polyimide Matrix Composites Reinforced with Short Basalt Fibers. J Appl Polym Sci 2008;111:2980–5. doi:10.1002/app.

[109] Tábi T, Zoltán A, Tamás P, Czigány T, Gábor J. Investigation of injection moulded poly (lactic acid) reinforced with long basalt fibres. Compos Part A 2014;64:99–106. doi:10.1016/j.compositesa.2014.05.001.

[110] Tábi T, Tamás P, Kovács JG. Chopped basalt fibres : A new perspective in reinforcing poly (lactic acid) to produce injection moulded engineering composites from renewable and natural resources. EXPRESS Polym Lett 2013;7:107–19. doi:10.3144/expresspolymlett.2013.11.

[111] Liu T, Yu F, Yu X, Zhao X, Lu A, Wang J. Basalt Fiber Reinforced and Elastomer Toughened Polylactide Composites : Mechanical Properties , Rheology , Crystallization , and Morphology. J Appl Polym Sci 2012;125:1292–301. doi:10.1002/app.

[112] Rosa IM De, Marra F, Pulci G, Santulli C, Sarasini F, Tirillò J, et al. Post-impact mechanical characterisation of E-glass / basalt woven fabric interply hybrid laminates. EXPRESS Polym Lett 2011;5:449–59. doi:10.3144/expresspolymlett.2011.43.

[113] Sarasini F, Tirillò J, Valente M, Valente T, Cioffi S, Iannace S, et al. Effect of basalt fiber hybridization on the impact behavior under low impact velocity of glass / basalt woven fabric / epoxy resin composites. Compos Part A 2013;47:109–23. doi:10.1016/j.compositesa.2012.11.021.

[114] Chikhradze NM, Marquis FDS, Japaridze L, Abashidze GS, Okujava LM. Polymer Based Composite and Hybrid Materials for Wind Power Generation. Mater Sci Forum 2010;654–

656:2612–5. doi:10.4028/www.scientific.net/MSF.654-656.2612.

[115] Ferrante L, Tirillò J, Sarasini F, Touchard F, Ecault R, Urriza MAV, et al. Behaviour of woven hybrid basalt-carbon / epoxy composites subjected to laser shock wave testing : Preliminary results. Compos Part B 2015;78:162–73. doi:10.1016/j.compositesb.2015.03.084.

[116] Subagia IDGA, Kim Y, Tijing LD, Sang C, Kyong H. Effect of stacking sequence on the flexural properties of hybrid composites reinforced with carbon and basalt fibers. Compos PART B 2014;58:251–8. doi:10.1016/j.compositesb.2013.10.027.

[117] Wang X, Hu B, Feng Y, Liang F, Mo J, Xiong J, et al. Low velocity impact properties of 3D woven basalt / aramid hybrid composites. Compos Sci Technol 2008;68:444–50. doi:10.1016/j.compscitech.2007.06.016.

[118] Sarasini F, Tirillò J, Valente M, Ferrante L, Cioffi S, Iannace S, et al. Hybrid composites based on aramid and basalt woven fabrics : Impact damage modes and residual flexural properties. Mater Des 2013;49:290–302. doi:10.1016/j.matdes.2013.01.010.

[119] Prasath KA, Krishnan BR. Mechanical Properties of Woven Fabric Basalt / Jute Fibre Reinforced Polymer Hybrid Composites. Int J Mech Eng Robot Res 2013;2.

[120] Pandian A, Vairavan M, Winowlin JT, Uthayakumar M. Influence of stacking sequence on mechanical properties of basalt-jute fiber-reinforced polymer hybrid composites. J Polym Eng 2012;32:547–54. doi:10.1515/polyeng-2012-0063.

[121] Fiore V, Scalici T, Badagliacco D, Enea D, Alaimo G, Valenza A. Aging resistance of bio-epoxy jute-basalt hybrid composites as novel multilayer structures for cladding. Compos Struct 2017;160:1319–28. doi:10.1016/j.compstruct.2016.11.025.

[122] Suresh Kumar C, Arumugam V, Dhakal HN, John R. Effect of temperature and hybridisation on the low velocity impact behavior of hemp-basalt/epoxy composites. Compos Struct 2015;125:407–16. doi:10.1016/j.compstruct.2015.01.037.

[123] Dhakal HN, Sarasini F, Santulli C, Tirillò J, Zhang Z, Arumugam V. Effect of basalt fibre hybridisation on post-impact mechanical behaviour of hemp fibre reinforced composites. Compos Part A Appl Sci Manuf 2015;75:54–67. doi:10.1016/j.compositesa.2015.04.020.

[124] Sarasini F, Tirillò J, Sergi C, Carolina M, Cozzarini L, Graupner N. Effect of basalt fibre hybridisation and sizing removal on mechanical and thermal properties of hemp fibre reinforced HDPE composites. Compos Struct 2018;188:394–406. doi:10.1016/j.compstruct.2018.01.046.

[125] Sergi C, Tirillò J, Seghini MC, Sarasini F, Fiore V, Scalici T. Durability of Basalt / Hemp Hybrid Thermoplastic Composites. Polymers (Basel) 2019;11:1–17.

[126] Almansour FA, Dhakal HN, Zhang ZY. Effect of water absorption on Mode I interlaminar fracture toughness of flax / basalt reinforced vinyl ester hybrid composites. Compos Struct 2017;168:813–25. doi:10.1016/j.compstruct.2017.02.081.

[127] Almansour FA, Dhakal HN, Zhang ZY. Investigation into Mode II interlaminar fracture toughness characteristics of fl ax / basalt reinforced vinyl ester hybrid composites. Compos Sci Technol 2018;154:117–27. doi:10.1016/j.compscitech.2017.11.016.

[128] Zivkovi I, Fragassa C, Pavlovi A, Brugo T. Influence of moisture absorption on the impact properties of flax , basalt and hybrid flax / basalt fiber reinforced green composites. Compos Part B 2017;111:148–64. doi:10.1016/j.compositesb.2016.12.018.

[129] Boria S, Pavlovic A, Fragassa C, Santulli C. Modeling of Falling Weight Impact Behavior

of Hybrid Basalt / Flax Vinylester Composites. Procedia Eng 2016;167:223–30. doi:10.1016/j.proeng.2016.11.691.

[130] Petrucci R, Santulli C, Puglia D, Nisini E, Sarasini F, Tirillò J, et al. Impact and post-impact damage characterisation of hybrid composite laminates based on basalt fibres in combination with flax, hemp and glass fibres manufactured by vacuum infusion. Compos Part B Eng 2015;69:507–15. doi:10.1016/j.compositesb.2014.10.031.

[131] Najafi M, Darvizeh A, Ansari R. Characterization of moisture effects on novel agglomerated cork core sandwich composites with fiber metal laminate facesheets. J Sandw Struct Mater 2018;0:1–34. doi:10.1177/1099636218789613.

[132] Scalici T, Fiore V, Valenza A. Experimental assessment of the shield-to-salt-fog properties of basalt and glass fiber reinforced composites in cork core sandwich panels applications. Compos Part B 2018;144:29–36. doi:10.1016/j.compositesb.2018.02.021.

[133] Fiore V, Scalici T, Valenza A. Evaluation of aging behavior under salt-fog spray conditions of green sandwich structures. J Nat Fibers 2018:1–10. doi:10.1080/15440478.2018.1444530.

[134] Daniel IM, Cho J-M. Strain-Rate-Dependent Behavior of Polymeric Foams. 52nd AIAA/ASME/ASCE/AHS/ASC Struct. Struct. Dyn. Mater. Conf., 2011, p. 1–8.

[135] Mines RAW. Strain rate effects in crushable structural foams. Appl Mech Mater 2007;7–8:231–6. doi:10.4028/www.scientific.net/AMM.7-8.231.

[136] Tagarielli VL, Deshpande VS, Fleck NA. The high strain rate response of PVC foams and end-grain balsa wood. Compos Part B Eng Part B 2008;39:83–91. doi:10.1016/j.compositesb.2007.02.005.

[137] Sasso M, Mancini E, Chiappini G, Sarasini F, Tirillò J. Application of DIC to Static and Dynamic Testing of Agglomerated Cork Material. Exp Mech 2018. doi:10.1007/s11340-017-0369-9 Application.

[138] Gameiro CP, Cirne Jo, Gary G. Experimental study of the quasi-static and dynamic behaviour of cork under compressive loading. J Mater Sci 2007;42:4316–24. doi:10.1007/s10853-006-0675-6.

[139] Thomas T, Mahfuz H, Carlsson LA, Kanny K, Jeelani S. Dynamic compression of cellular cores : temperature and strain rate effects. Compos Struct 2002;58:505–12. doi:10.1016/S0263-8223(02)00159-9.

[140] Wei Z, Nan Y. High strain rate and quasi-static compression behavior and energy absorption characteristic of PVC foam. Chall J Struct Mech 2016;2:212–5.

[141] Wouts J, Haugou G, Oudjene M, Coutellier D, Morvan H. Strain Rate effects on the compressive response of wood and energy absorption capabilities - Part A : Experimental investigations. Compos Struct 2016. doi:10.1016/j.compstruct.2016.03.058.

[142] Zhai X, Gao J, Liao H, Kirk CD, Balogun YA, Chen WW. Mechanical behaviors of auxetic polyurethane foam at quasi-static , intermediate and high strain rates. Int J Impact Eng 2019;129:112–8. doi:10.1016/j.ijimpeng.2019.03.002.

[143] Lu F De, Hua G, Wang L, Jiang H, Gao D. A phenomenological constitutive modelling of polyethylene foam under multiple impact conditions. Packag Technol Sci 2019;32:367–79. doi:10.1002/pts.2445.

[144] Fernandes FAO, Jardin RT, Pereira AB, Sousa RJA De. Comparing the mechanical performance of synthetic and natural cellular materials. Mater Des 2015;82:335–41.

doi:10.1016/j.matdes.2015.06.004.

[145] Sanchez-Saez S, Barbero E, Garcia-Castillo SK, Ivañez I, Cirne J. Experimental response of agglomerated cork under multi-impact loads. Mater Lett 2015;160:327–30. doi:10.1016/j.matlet.2015.08.012.

[146] Sarasini F, Tirillò J, Lampani L, Barbero E, Sanchez-Saez S, Valente T, et al. Impact behavior of sandwich structures made of flax / epoxy face sheets and agglomerated cork. J Nat Fibers 2020;17:168–88. doi:10.1080/15440478.2018.1477084.

[147] Sanchez-Saez S, Barbero E, Cirne J. Experimental study of agglomerated-cork-cored structures subjected to ballistic impacts. Mater Lett 2011;65:2152–4. doi:10.1016/j.matlet.2011.04.083.

[148] G M, D P, Tumino A. Using FEM simulation to predict structural performances of a sailing dinghy. Int J Interact Des Manuf 2018;12:811–22. doi:10.1007/s12008-017-0427-7.

[149] Potes FC, Silva JM, Gamboa P V. Development and characterization of a natural lightweight composite solution for aircraft structural applications. Compos Struct 2016;136:430–40. doi:10.1016/j.compstruct.2015.10.034.

[150] Fernandes FAO, Pascoal RJS, Sousa RJA De. Modelling impact response of agglomerated cork. J Mater 2014;58:499–507. doi:10.1016/j.matdes.2014.02.011.

[151] Pal A, Thu K, Mitra S, El-sharkawy II, Baran Saha B, Kil H-S, et al. Study on biomass derived activated carbons for adsorptive heat pump application. Int J Heat Mass Transf 2017;110:7–19. doi:10.1016/j.ijheatmasstransfer.2017.02.081.

[152] Martarelli M, Mancini E, Lonzi B, Sasso M. Sensor calibration of polymeric Hopkinson bars for dynamic testing of soft materials. Meas Sci Technol 2018;29. doi:10.1088/1361-6501/aa9136.

[153] Sasso M, Antonelli M, Mancini E, Radoni M, Amodio D. Experimental and numerical characterization of a polymeric Hopkinson bar by DTMA. Int J Impact Eng 2017;103:50–63. doi:10.1016/j.ijimpeng.2016.12.020.

[154] ADAMS D. Damage-resistance testing of composites 2016. https://www.compositesworld.com/articles/damage-resistance-testing-of-composites.

[155] Múgica JI, Aretxabaleta L, Ulacia I, Aurrekoetxea J. Impact characterization of thermoformable fibre metal laminates of 2024-T3 aluminium and AZ31B-H24 magnesium based on self-reinforced polypropylene. Compos Part A 2014;61:67–75. doi:10.1016/j.compositesa.2014.02.011.

[156] Sayer M, Bektaş NB, Sayman O, Topçu M. An Experimental Investigation on the Impact Behaviour of Glass / Epoxy and Hybrid Composite Plates. Adv Compos Lett 2009;18:113–22. doi:10.1177/096369350901800401.

[157] Ben-Dor G, Dubinsky A, Elperin T. On the Lambert – Jonas approximation for ballistic impact. Mech Res Commun 2002;29:137–9. doi:10.1016/S0093-6413(02)00246-X.

[158] Ramakrishnan KR, Shankar K, Viot P, Guerard S. A numerical study of the impact properties of sandwich panels with different cores. Proc. 7th Australas. Congr. Appl. Mech. (ACAM 7), 9-12 December 2012, Univ. Adelaide, 2012.

[159] Lim GT, Altstädt V. Understanding the Compressive Behavior of Linear and Cross-linked Poly(vinyl chloride) Foams. J Cell Plast 2009;45:419–39. doi:10.1177/0021955X09105372.

[160] Colloca M, Dorogokupets G, Gupta N, Porfiri M. Mechanical properties and failure mechanisms of closed-cell PVC foams. Int J Crashworthiness 2012;17:327–36. doi:10.1080/13588265.2012.661637.

[161] Abenojar J, Barbosa AQ, Ballesteros Y, del Real JC, da Silva LFM, Martınez MA. Effect of surface treatments on natural cork: surface energy, adhesion, and acoustic insulation. Wood Sci Technol 2014;48:207–24. doi:10.1007/s00226-013-0599-7.

[162] Gomes CMCPS, Fernandes AC, Saramago de Almeida B de JV. The Surface Tension of Cork from Contact Angle Measurements. J Colloid Interface Sci 1993;156:195–201. doi:10.1006/jcis.1993.1099.

[163] Mcginty KM, Brittain WJ. Hydrophilic surface modification of poly(vinyl chloride) film and tubing using physisorbed free radical grafting technique. Polymer (Guildf) 2008;49:4350–7. doi:10.1016/j.polymer.2008.07.063.

[164] Matias L, Santos C, Reis M, Gil L. Declared value for the thermal conductivity coefficient of insulation corkboard. Wood Sci Technol 1997;31:355–65. doi:10.1007/BF01159154.

[165] Limam A, Zerizer A, Quenard D, Sallee H, Chenak A. Experimental thermal characterization of bio-based materials (Aleppo Pine wood , cork and their composites) for building insulation. Energy Build 2016;116:89–95. doi:10.1016/j.enbuild.2016.01.007.

[166] Şen A, Van Den Bulcke J, Defoirdt N, Van Acker J, Pereira H. Thermal behaviour of cork and cork components. Thermochim Acta 2014;582:94–100. doi:10.1016/j.tca.2014.03.007.

[167] Shangguan W, Chen Z, Zhao J, Song X. Thermogravimetric analysis of cork and cork components from Quercus variabilis. Wood Sci Technol 2017. doi:10.1007/s00226-017-0959-9.

[168] Silvano TL, Vittorazzo Jr. AL, Araujo GR. Effect of Preparation Method on the Electrical and Mechanical Properties of PVC / Carbon Nanotubes Nanocomposites. Mater Res 2018;21. doi:10.1590/1980-5373-MR-2017-1148 Effect.

[169] Paiva D, Magalhães FD. Dynamic mechanical analysis and creep-recovery behavior of agglomerated cork. Eur J Wood Wood Prod 2017. doi:10.1007/s00107-017-1158-y.

[170] Khoshnoud P, Abu-zahra N. Effect of Cenosphere Fly Ash on the Thermal, Mechanical, and Morphological Properties of Rigid PVC Foam Composites. J Res Updat Polym Sci 2015;4. doi:10.6000/1929-5995.2015.04.01.1.

[171] Jiang Z, Du Z, Xue J, Liu W, Li M, Tang T. Hierarchical structure and properties of rigid PVC foam crosslinked by the reaction between anhydride and diisocyanate. J Appl Polym Sci 2018;46141:1–8. doi:10.1002/app.46141.

[172] Anjos O, Pereira H, Rosa ME. Effect of quality, porosity and density on the compression properties of cork. Holz Als Roh - Und Werkst 2008;66:295–301. doi:10.1007/s00107-008-0248-2.

[173] Anjos O, Rodrigues C, Morais J, Pereira H. Effect of density on the compression behaviour of cork. Mater Des 2014;53:1089–96. doi:10.1016/j.matdes.2013.07.038.

[174] Rosa ME, Fortes MA. Rate effects on the compression and recovery of dimensions of cork. J Mater Sci 1988;23:879–85. doi:10.1007/BF01153983.

[175] Jardin RT, Fernandes FAO, Pereira AB, Alves de Sousa RJ. Static and dynamic mechanical response of different cork agglomerates. Mater Des 2015;68:121–6.

doi:10.1016/j.matdes.2014.12.016.

[176] Avalle M, Belingardi G, Montanini R. Characterization of polymeric structural foams under compressive impact loading by means of energy-absorption diagram. Int J Impact Eng 2001;25:455–72. doi:10.1016/S0734-743X(00)00060-9.

[177] Barbenchon L Le, Girardot J, Kopp J, Viot P. Strain Rate Effect on the Compressive Behaviour of Reinforced Cork Agglom erates. EPJ Web Conf DYMAT 2018 2018;03018:1–6.

[178] Kanakkanatt S V. Mechanical Anisotropy of Open-Cell Foams. J Cell Plast 1972:50–3. doi:10.1177/0021955X7300900109.

[179] Tita V, Caliri Junior MF. Numerical simulation of anisotropic polymeric foams. Lat Am J Solids Struct · 2012;1:1–21. doi:10.1590/S1679-78252012000200005.

[180] Earl JS, Shenoi RA. Determination of the Moisture Uptake Mechanism in Closed Cell Polymeric Structural Foam During Hygrothermal Exposure. J Compos Mater 2004;38:1345–65. doi:10.1177/0021998304042736.

[181] Manujesh BJ, Vijayalakshmi R, Sham Aan MP. Moisture absorption and mechanical degradation studies of polyurethane foam cored E-glass-reinforced vinyl-ester sandwich composites. J Reinf Plast Compos 2013;33:479–92. doi:10.1177/0731684413503720.

[182] Rosa ME, Fortes MA. Water Absorption by Cork. Wood Fiber Sci 1993;25:339–48.

[183] May-Pat A, Avilés F. Long term water uptake of a low density polyvinyl chloride foam and its effect on the foam microstructure and mechanical properties. Mater Desig 2014;57:728–35. doi:10.1016/j.matdes.2014.01.042.

[184] Tanganov BB. About Sizes of the Hydrated Salt Ions- the Components of Sea Water. Eur J Nat Hist 2013;1:1–2.

[185] Rosa ME, Pereira H, Fortes MA. Effects of Hot Water Treatment on the Structure and Properties of Cork. Wood Fiber Sci 1990;22:149–64.

[186] Kaczynski P, Ptak M, Wilhelm J, Fernandes FAO, Sousa RJA De. High-energy impact testing of agglomerated cork at extremely low and high temperatures. Int J Impact Eng 2019;126:109–16. doi:10.1016/j.ijimpeng.2018.12.001.

[187] Kaczynski P, Ptak M, Fernandes FAO, Chybowski L, Wilhelm J, Alves de Sousa RJ. Development and Testing of Advanced Cork Composite Sandwiches for Energy-Absorbing Structures. Materials (Basel) 2019;12. doi:10.3390/ma12050697.

[188] Ptak M, Kaczynski P, Fernandes FAO, Alves de Sousa RJ. Assessing impact velocity and temperature effects on crashworthiness properties of cork material. Int J Impact Eng 2017;106:238–48. doi:10.1016/j.ijimpeng.2017.04.014.

[189] Saha MC, Mahfuz H, Chakravarty UK, Uddin M, Kabir E, Jeelani S. Effect of density , microstructure , and strain rate on compression behavior of polymeric foams. Mater Sci Eng A 2005;406:328–36. doi:10.1016/j.msea.2005.07.006.

[190] Long YAN, Zhang W, Peng L, Peng H, Li X, Huang X. Mechanical Behaviors of Ultrafine-Grained Ti-6Al-4V Alloy During Compression at Various Strain Rates. Metall Mater Trans A 2020;51:4765–76. doi:10.1007/s11661-020-05895-x.

[191] Buitrago BL, García-castillo SK, Barbero E. Experimental analysis of perforation of glass / polyester structures subjected to high-velocity impact. Mater Lett 2010;64:1052–4. doi:10.1016/j.matlet.2010.02.007.

[192] Lopez-Puente J, Zaera R, Navarro C. Experimental and numerical analysis of normal and oblique ballistic impacts on thin carbon / epoxy woven laminates. Compos Part A 2008;39:374–87. doi:10.1016/j.compositesa.2007.10.004.

[193] Amaro AM, Balbis Reis NP, Ivañez I, Sanchez-Saez S, Garcia-castillo SK, Barbero E. The High-Velocity Impact Behaviour of Kevlar Composite Laminates Filled with Cork Powder. Appl Sci 2020;10. doi:10.3390/app10176108.

[194] Khalfallah M, Abbès B, Abbès F, Guo YQ, Marcel V, Duval A, et al. Innovative flax tapes reinforced Acrodur biocomposites : A new alternative for automotive applications. Mater Des 2014;64:116–26. doi:10.1016/j.matdes.2014.07.029.

[195] Biagiotti J, Puglia D, Torre L, Kenny JM, Arbelaiz A, Cantero G, et al. A Systematic Investigation on the Influence of the Chemical Treatment of Natural Fibers on the Properties of Their Polymer Matrix Composites. Polym Compos 2004;25:470–9. doi:10.1002/pc.20040.

[196] Russo P, Vitiello L, Sbardella F, Santos JI, Tirillò J, Bracciale MP, et al. Effect of Carbon Nanostructures and Fatty Acid Treatment on the Mechanical and Thermal Performances of Flax / Polypropylene Composites. Polymers (Basel) 2020;12. doi:10.3390/polym12020438.

[197] Blaine RL. THERMAL APPLICATIONS NOTE Polymer Heats of Fusion. vol. TN048. n.d.

[198] Dong Z, Ding R, Zheng L, Zhang X, Yu C. Thermal Properties of Flax Fiber Scoured by Different Methods. Therm Sci 2015;19:939–45. doi:10.2298/TSCI130329005Z.

[199] Kiss P, Stadlbauer W, Burgstaller C, Archodoulaki V. Development of high-performance glass fibre-polypropylene composite laminates: Effect of fibre sizing type and coupling agent concentration on mechanical properties. Compos Part A 2020;138. doi:10.1016/j.compositesa.2020.106056.

[200] Watanabe R, Sugahara A, Hagihara H, Mizukado J, Shinzawa H. Insight into interfacial compatibilization of glass-fiber-reinforced polypropylene (PP) using maleic-anhydride modified PP employing infrared spectroscopic imaging. Compos Sci Technol 2020;199. doi:10.1016/j.compscitech.2020.108379.

[201] El-Sabbagh A. Effect of coupling agent on natural fibre in natural fibre / polypropylene composites on mechanical and thermal behaviour. Compos Part B 2014;57:126–35. doi:10.1016/j.compositesb.2013.09.047.

[202] Sergi C, Sbardella F, Lilli M, Tirillò J, Calzolari A, Sarasini F. Hybrid Cellulose – Basalt Polypropylene Composites with Enhanced Compatibility : The Role of Coupling Agent. Molecules 2020;25. doi:10.3390/molecules25194384.

[203] Chen J, Wang Y, Gu C, Liu J, Liu Y, Li M, et al. Enhancement of the Mechanical Properties of Basalt Fiber-Wood-Plastic Composites via Maleic Anhydride Grafted High-Density Polyethylene (MAPE) Addition. Materials (Basel) 2013;6:2483–96. doi:10.3390/ma6062483.

[204] Simeoli G, Sorrentino L, Touchard F, Mellier D, Oliviero M, Russo P. Comparison of falling dart and Charpy impacts performances of compatibilized and not compatibilized polypropylene / woven glass fibres composites. Compos Part B 2019;165:102–8. doi:10.1016/j.compositesb.2018.11.090.

[205] Sorrentino L, Simeoli G, Iannace S, Russo P. Mechanical performance optimization

through interface strength gradation in PP / glass fi bre reinforced composites. Compos Part B 2015;76:201–8. doi:10.1016/j.compositesb.2015.02.026.

[206] Boccardi S, Meola C, Carlomagno GM, Sorrentino L, Simeoli G, Russo P. Effects of interface strength gradation on impact damage mechanisms in polypropylene / woven glass fabric composites. Compos Part B 2016;90:179–87. doi:10.1016/j.compositesb.2015.12.004.

[207] Mehndiratta A, Bandyopadhyaya S, Kumar V, Kumar D. Experimental investigation of span length for flexural test of fiber reinforced polymer composite. J Mater Res Technol 2018;7:89–95. doi:10.1016/j.jmrt.2017.06.010.